

Osama Kabbashi M. Ibrahim

# Accidental release of liquid CO<sub>2</sub> from transport and storage

**Dissertation for the  
degree of Ph.D**  
Process, Energy  
and Automation

Faculty of Technology, Natural  
Sciences and Maritime Studies

---

Osama Kabbashi M. Ibrahim

# Accidental release of liquid CO<sub>2</sub> from transport and storage

A PhD dissertation in  
Process, Energy and Automation Engineering

© Osama Kabbashi M. Ibrahim, 2023

Faculty of Technology, Natural Sciences and Maritime Studies  
University of South-Eastern Norway  
Porsgrunn

**Doctoral dissertations at the University of South-Eastern Norway no. 174**

ISSN: 2535-5244 (print)  
ISSN: 2535-5252 (online)

ISBN: 978-82-7206-805-8 (print)  
ISBN: 978-82-7206-806-5 (online)



This publication is licensed with a Creative Commons license. You may copy and redistribute the material in any medium or format. You must give appropriate credit, provide a link to the license, and indicate if changes were made. Complete license terms at <https://creativecommons.org/licenses/by-nc-sa/4.0/deed.en>

Print: University of South-Eastern Norway

**F g f k e c v k q p "**

To the beloved people who have meant and continue to mean so much to me.

"

## Rt ghceg''

This dissertation is submitted to fulfill the requirements for the Ph.D. degree at the Faculty of Technology, Natural Sciences, and Maritime Sciences, The University of South-eastern Norway (USN). The research has been accomplished following Process, Energy, and Environmental Technology program and was carried out from 2020 to 2023 in Telemark Process Safety, Combustion, and Explosion Laboratory (TPSCEL). It is part of a project on the phase transition following the accidental release of liquid carbon dioxide during transport and storage. The thesis presents the research work and includes associated journal articles and conference contributions.

As a part of a continuous learning journey, the three years of my Ph.D. were full of surprising insights, acquiring new skills, and joyful moments. The contribution of many individuals through the course of this work is gratefully acknowledged. In particular, my heartfelt gratitude to my supervisor, Dr. Knut Vågsæther, for his excellent guidance, great thoughtfulness, and support. I am also profoundly grateful to my co-supervisors, Dr. Per Morten Hansen and Dr. Dag Bjerketvedt, for their expert help, constructive comments, patience, and encouragement. The fruitful discussions and suggestions through which all supervisors imparted their knowledge to me were greatly appreciated.

I sincerely thank Dr. André Vagner Gaathaug for his ingenious ideas during experiments and for editing assistance. Also, I want to express my eternal gratitude to the rest of the TPSCEL research group members: Drs. Joachim Lundberg, Mathias Henriksen, Agnieszka Lach, Prasanna Welahettige, and Raghav Sikka, for assistance and advice and for creating a cheerful atmosphere. Thanks to Øyvind Johansen, Fredrik Hansen, and Bjørn Vegard Tveraaen for masterly providing the necessary technical help. I am also grateful to the University of South-eastern Norway for supporting financially this Ph.D. research which enabled me to carry out essential work.

Finally, I would like to add personal thanks to all my friends and brother for their encouragement and support throughout this journey.

The journey continues

Porsgrunn, May 2023

Osama Kabbashi M. Ibrahim

\* The last submitted journal article "Release of liquid CO<sub>2</sub> from the bottom of a duct" is published after the thesis submission.



## Cduvtcev''

An unintended release of liquid CO<sub>2</sub> during transport by tanks or pipelines could result in instantaneous depressurization and rapid phase transition with explosive evaporation. Under certain conditions, it could lead to a boiling liquid expansion vapor explosion (BLEVE). This research project is concerned with the safety of CO<sub>2</sub> transport and storage facilities. It is a continuation of the prior research in the USN laboratory to investigate the rapid phase changes and the evolution of the evaporation and blast waves. Further, to evaluate the hazards that arise during the accidental release of liquid CO<sub>2</sub> into the environment. This experimental research expanded former studies to cover the effect of a diverging cross-sectional geometry on phase transition mechanism and expansion wave behavior during sudden depressurization. It investigated the effect of liquid volume fraction on the dynamic characteristics of rarefaction, evaporation, and blast wave in the existing setup. In addition, the research examined the phase transition mechanism during the CO<sub>2</sub> release from the bottom of a rectangular duct.

This research presents a new installation comprising a vertical high-pressure conical-shaped vessel with a double-membrane release process. A slip-on flange separates the two membranes, constituting a medium-pressure (MP) section. The experimental rig is instrumented with pressure transducers, temperature thermocouples, and a high-speed video camera. The vapor/liquid CO<sub>2</sub> could be depressurized by increasing or decreasing the pressure in the MP flange. Operational analyses based on the experimental results showed that increasing the pressure in the MP section is a more reliable method to run CO<sub>2</sub> depressurization tests on this installation. In contrast to decreasing the pressure in the MP section technique, its operation was more controllable, ensuring instantaneous membranes' rupture without reflecting waves affecting the evaporation process in the test section.

The dynamic evaporation characteristics were investigated by increasing pressure in the MP section. The results showed that the evaporation wave velocity increased downward with decreasing cross-sectional area and increased liquid volume fraction. The divergent cross-section led to a more significant fluid expansion as the rarefaction



wave propagated toward a smaller area. Simultaneously, the expanded two-phase mixture propagated toward a constantly increased cross-sectional area. In addition, the evaporation wave upstream state properties after the isentropic expansion in the metastable region were resolved by applying the Span-Wanger equation of state. Comparing the obtained results with former conclusions of CO<sub>2</sub> decompression from a constant cross-section rectangular duct demonstrated considerable differences in rarefaction and evaporation wave velocities. The waves' propagation speed was steady in the rectangular duct, but their velocities increased as they propagated towards a diminished cross-sectional area in the conical-shaped vessel. Besides, the liquid in the conical vessel had attained a higher degree of superheating at the metastable state.

Blastwave effects during CO<sub>2</sub> depressurization in the conical vessel have been studied experimentally. Overpressures and multiphase flow evolution have been recorded during CO<sub>2</sub> release through a polycarbonate tube with atmospheric conditions. Analysis of measured peak overpressures and calculated impulse indicated their increase as the liquid volume fraction increased. The results also demonstrated that the rapid liquid evaporation has substantially influenced the peak overpressure and impulse positive phases and durations. Additionally, the study examined the flying fragments' velocities and their kinetic energies based on the captured high-speed videos. Results also showed increased fragments' velocity and kinetic energy with increased liquid volume fraction. Fragment velocity and kinetic energy of about 121 m/s and 205 J, respectively, have been observed from a test with a liquid volume fraction of 73.6%. Such fragments involve a significant hazard.

A series of experiments were performed to release saturated liquid and vapor CO<sub>2</sub> below the liquid level in a rectangular duct."The study characterized the rarefaction and evaporation wave pattern and the evolution of the expanded two-phase flow inside the duct after the diaphragm ruptured at the bottom. Pressure and temperature records were analyzed simultaneously with high-speed shadowgraph images to gain insight into the phase transition mechanism."The results were also compared with previous top-release experiments. During bottom-release tests, the liquid evaporated two times

faster than in the top-release, but it attained a lower degree of superheating due to instant liquid outflow from the bottom. Shadowgraphs showed that the vapor expansion had an insignificant influence on the evaporation onset. The flow measurements and the visualized wave pattern demonstrated a unique evaporation mechanism during bottom-release experiments. This different fluid expansion behavior could potentially lead to a container's catastrophic failure and must be considered in risk analysis to prevent such accidental hazards.

**Key Words:**

Phase-transition, BLEVE, Rarefaction wave, Evaporation wave, Blastwave, Divergent cross-section.

## Nkuv'qhr cr gt u'

h

M Ibrahim, O., Hansen, P. M., Bjerketvedt, D., Vågsæther, K. (2022). Release mechanisms and waves interaction during liquified CO<sub>2</sub> depressurization in a double-membrane conical vessel. *oV'' o*, vol. 4, no. 4, p. 89.  
doi: 10.1007/s42452-022-04975-4.

h

M Ibrahim, O., Hansen, P. M., Bjerketvedt, D., Vågsæther, K. (2021). Evaporation characteristics during decompression of liquified CO<sub>2</sub> from a conical-shaped vessel. *k* - vol. 12, p. 100304.  
doi: <https://doi.org/10.1016/j.rineng.2021.100304>.

h

M Ibrahim, O., Gaathaug, A.V., Hansen, P. M., Bjerketvedt, D., Vågsæther, K. (2023). Release of liquid CO<sub>2</sub> from the bottom of a duct. This manuscript is under review in the *oV'' o* (submitted in April 2023).

## Nkuv'qh'E qphgt gpeg'eqpv t kd wkp pu'

h

M Ibrahim, O., Hansen, P. M., Bjerketvedt, D., Vågsæther, K. (2022). Blast Wave Overpressures from CO<sub>2</sub> Depressurization in a Conical-Shaped Vessel. 10<sup>th</sup> International Seminar on Fire and Explosion Hazards. Oslo, Norway. p. 86-94.  
<https://hdl.handle.net/11250/3030345>

h

M Ibrahim, O., Welahettige, P., Vågsæther, K., Lie, B. (2022). Modeling of the two-phase flow during depressurization of liquified CO<sub>2</sub> in a pipe. Proceedings of the 63rd International Conference of Scandinavian Simulation Society, SIMS, NTNU, Trondheim, Norway, No. 192 pp. 226. doi: <https://doi.org/10.3384/ecp192>.

h

M Ibrahim, O., Hansen, P. M., Bjerketvedt, D., Vågsæther, K. (2022). Expansion waves behavior during liquified CO<sub>2</sub> depressurization in a divergent cross-section vessel. Extended Abstract, Proceedings of the 28<sup>th</sup> International Colloquium on the Dynamics of Explosions and Reactive Systems (ICDERS), Napoli, Italy, June 2022.

h

Vågsæther, K., M Ibrahim, O., Hansen, P. M., Bjerketvedt, D. (2023). Modeling the effect of phase transition on the blast wave in BLEVEs. Extended Abstract, Submitted to the 29<sup>th</sup> International Colloquium on the Dynamics of Explosions and Reactive Systems (ICDERS), SNU Siheung, KOREA, July 2023.

## **Nku'qh'hi wt gu''**

- 7 · CO<sub>2</sub> storage tank BLEVE in Worms, Germany (1988), (a-c) Rocketed pieces of the tank and (d) the tank location after its failure .....
- 7 · Pressure-specific volume diagram illustrates the expansion of liquified CO<sub>2</sub> from the saturation point (1) to the metastable limit (2).....
- 7 · y-t diagram of wave patterns and state zones during the phase change following saturated liquid depressurization in a vertical vessel. Zones: A- Undisturbed air ahead of the shock wave, B- Air behind the shock, C-Two-phase mixture, D- Superheated liquid, and E- Undisturbed saturated liquid.....
- 7 · A drawing of the evaporation wavefront's zones as it moves through a superheated liquid.....
- 7 · Flow diagram showing the possible paths of a BLEVE incidence.....
- 7 · A photograph of the setup. 1- the conical-shaped vessel with the flanges. 2- An atmospheric chamber. 3- An auxiliary installation with a rectangular duct. 4- illuminating panels. 5- Data acquisition system (DAQ) .....
- 7 · Schematic of the HP vessel fixed to the MP and atmospheric flanges on the left-hand side; and a corresponding image on the right-hand side.....
- 7 · Schematic of the setup: 1. HP Conical-shaped vessel, 2. MP slip-on flange, 3. Chamber space, 4. Hub, 5. Triggering unit, 6. DAQ, 7. 3-way valve, 8. PC, 9. High-speed camera, 10. Illuminating panels.....
- 7 · Schematic drawing showing the diaphragms' rupture sequence; (a) increasing and (b) decreasing the pressure in the MP slip-on flange.....
- 7 · (b) Height-time diagram illustrating the expansion waves' paths along the vessel height (a). (c) an enlarged segment showing the time turning point on the pressure-time curve.....
- 7 · (a) Modified setup, (b) A drawing of the transparent tube with indicated distances between transducers, (c) A photograph of the excavated flange.....
- 7 · A sketch of the HP rectangular duct showing its dimensions and sensor positions.....
- 7 · A sketch and an image of the HP rectangular duct installation showing its

central parts and the locations of the sensors.....

7      Shadowgraph system configuration used in the experiments of Setup 3...

7      The pressure histories inside the conical vessel, from top to bottom (P1 to P4), during the CO<sub>2</sub> depressurization by increasing (Incr. P line) and decreasing (Drop. P line) the pressure in the MPS. Close-up plots (c), (e), and (h) show the oscillations resulting from HP diaphragm rupture, and (a), (b), (d), (f), (g) and (i) show fluctuations due to waves reflections.....

7      Pressure history in the MP section (PMPS) and the overpressure in the chamber space center (PCHS) during CO<sub>2</sub> depressurization by increasing (Incr. P line) and decreasing the pressure (Drop. P line) in the MP section.....

7      cropped images from the high-speed video from the CO<sub>2</sub> depressurization experiment with LVF of 52%. The small arrows in the upper series show the flying MP diaphragm position.....

7      Recorded pressure and temperature signals inside the HP vessel during 50 ms of liquid CO<sub>2</sub> depressurization for LVFs of 0% (a, d), 62.5% (b, e), and 96.4% (c, f).....

7      Pressure-time signals drawn on the vessel height-time during 20 ms of liquid CO<sub>2</sub> depressurization for LVF of 35.1% in (a), 62.5% in (b), and 96.4% in (c). (RWT) and (EWT) denote the rarefaction and evaporation waves' trajectories.....

7      Pressure histories during 50 ms of CO<sub>2</sub> depressurization in the RD and the CV for LVFs of 0% (a), 100 and 62, 5%(b), and 100 and 96.4% (c).....

7      Measured peak overpressures at the top and bottom of the tube during CO<sub>2</sub> depressurization in a conical vessel for LVFs of 15 (a), 35.2 (b), and 52.7% (c). Graphs (a'), (b'), and (c') are enlarged segments of the second peak during 40 ms.....

7      The correlations between measured peak overpressure at the top and bottom of the tube and the LVFs during CO<sub>2</sub> depressurization in the conical-shaped vessel.....

7      The resultant impulse from integrating the measured overpressure records at the bottom (a) and top (b) of the tube.....

7      Sequence of images processed from a high-speed video during 10.4 ms of

CO<sub>2</sub> depressurization with 35.2% LVF and synchronized pressure histories inside the vessel.....

7        Graphs (a-d) Pressure histories inside the rectangular duct during 40 ms as the liquid CO<sub>2</sub> released from the bottom for LVFs of 29, 53, 66, and 97%, respectively.....

7        Pressure records during 30 ms of liquid CO<sub>2</sub> release from the rectangular duct's top (a and b) and bottom (d and e). Graphs (c and f) are 3 ms close-ups of (b and e).....

7        Chronological sequence of processed frames from shadowgraph videos (a and c) and corresponding pressure records (b and d) during liquid CO<sub>2</sub> release from the bottom of a duct. LVFs were 35% in (a and b) and 58% in (c and d) .....

7        (a) Pressure transducers' records P1-P4 (top to bottom) in the HP vessel during 50 ms of CO<sub>2</sub> decompression. (b) the bottom transducer records for LVFs of 0, 62.5, and 96.4%.....

7        Pressure records inside the HP vessel during 14 ms of CO<sub>2</sub> depressurization for LVFs of 62.5% (a) and 96.4% (b). Fluctuations after the rarefaction wave, A, and after the evaporation wave, B.....

7        Images series of the HP diaphragm rupturing through a tube during CO<sub>2</sub> depressurization in a conical-shaped vessel; and corresponding measured overpressure at the top and bottom of the tube (180 and 650 mm from the hp diaphragm).....

7        Height-time diagram demonstrating pressure records on the height-axis during 4.5 ms of liquid CO<sub>2</sub> release from the duct's bottom side for LVF of 35%, and displaying synchronous shadowgraph images .....

## **Nkuv'qh'w dıgu'**

- u      rarefaction and evaporation wave velocities calculated at three vessel's height regions.....
- u      The pre-ruptured saturated state and calculated properties for superheated liquid after expansion to a metastable state.....
- u      The fragments calculated velocities and kinetic energy after the rupturing of the HP diaphragm.....



## Cddt gxk vqpu'

AUSM+-up	Advection Upstream Splitting Method
BLEVE	Boiling liquid expanding vapor explosion
BR	Bottom release
CCPS	Center for Chemical Process Safety
CCS	Carbon capture and storage
CFD	Computational Fluid Dynamics
CV	Conical-shaped vessel
DAQ	Data acquisition system
DOS	Degree of superheat
EOS	Equation of state
FLIC	Flux Limiter Centered Scheme
fps	Frames per second
HEM	Homogeneous equilibrium model
HFE	Helmholtz free energy
HLLC	Harten-Lax-van Leer Contact
HP	High-pressure
HRM	Homogeneous relaxation model
KSL	Kinetic superheat limit
LVF	Liquid volume fraction

MP	Medium-pressure
MUSTA	Multi-stage centered scheme
NIST	National Institute of Standards and Technology
SW-EOS	Span-Wagner equation of state
SLT	Superheat limit temperature
TFM	Two-fluid model
TR	Top release
TSL	Thermodynamic superheat limit
UDF	User-defined functions
#	
CO <sub>2</sub>	Carbon dioxide
R-11	Trichlorofluoromethane

## Appendix A

$k$	Thermal conductivity	W/m·K
$c_p$	Isobaric specific heat	J/kg·K
$k$	Kinetic energy	J
$m$	Mass	kg
$P$	Pressure	MPa
$Q_{ex}$	Excess heat	J
$R_{cr}$	Critical radius	m

$T$	Temperature	K
$t$	Time	s
$u$	Velocity	m/s
$V$	Volume	m <sup>3</sup>
$v_f$	Fragment velocity	m/s
$\delta$		
$\Pi$	Comparative degree of superheat	-
$\beta_T$	Isothermal compressibility	1/Pa
$\phi$	Liquid volume fraction	-
$v$	Molar volume	m <sup>3</sup> /kmol
$\rho$	Density	kg/m <sup>3</sup>
$\sigma$	Surface tension	N/m
$c$	Contact surface	
$E$	Evaporation wave	
$ms$	Metastable state	
$R$	Rarefaction wave	
$sat$	Saturated state	

## Vcdrg'qh'eqpvgrvu'

)		@
h		@
.		†
O	h	†@
O	7	CE
O	u	@
.		†@
V		CE
u		CE@
@		.
1.2	Thesis objectives and scope.....	4
1.3	Outline of the thesis.....	5
O	k k u	.
2.1	Superheated liquids .....	7
2.1.1	Thermodynamic aspects of superheated liquids.....	7
2.1.2	Degree of superheat (DOS) .....	8
2.1.3	Superheat limit temperature (SLT) .....	9
2.1.4	Kinetic superheat limit (KSL) .....	10
2.1.5	Equation of state (EOS) .....	11
2.2	Explosive evaporation .....	12
2.2.1	Waves configuration .....	12
2.2.2	Evaporation wavefront propagation.....	13
2.3	Description of the BLEVE incident .....	15
2.4	BLEVE: BLEVE Consequences .....	18
2.4.1	Overpressure and impulse .....	18
2.4.2	The blast released energy .....	19
2.4.3	Vessel Fragmentation (Fragment initial velocity) .....	21
2.5	BLEVE: experiments and modeling .....	22
2.5.1	Release mechanisms in BLEVE experiments.....	22

2.5.2	Experimental studies in CO <sub>2</sub> BLEVE.....	24
2.5.3	Modeling of CO <sub>2</sub> depressurization.....	27
<b>h</b>		
3.1	Setup 1: Double-membrane conical rig.....	30
3.1.1	HP and MP sections.....	32
3.1.2	Diaphragm description.....	33
3.1.3	CO <sub>2</sub> supply and filling procedure.....	33
3.1.4	Instrumentation.....	34
3.1.5	Release mechanisms.....	36
3.1.6	Experimental procedure.....	37
3.1.7	Determination of expansion waves' velocities.....	38
3.1.8	Image processing.....	40
3.2	Setup 2: modification for overpressure measurements.....	40
3.3	Setup 3: Release from the bottom of a rectangular duct.....	41
3.3.1	The HP test section.....	42
3.3.2	Control equipment and test procedure.....	43
3.3.3	Shadowgraph imaging.....	44
<b>h</b>		
4.1	Paper A: Release mechanisms and waves interaction during liquified CO <sub>2</sub> depressurization in a double-membrane conical vessel.....	46
4.1.1	Introduction.....	46
4.1.2	Results and Discussion.....	46
4.1.3	Conclusion.....	50
4.2	Paper B: Evaporation characteristics during decompression of liquified CO <sub>2</sub> from a conical-shaped vessel.....	52
4.2.1	Introduction.....	52
4.2.2	Results and Discussion.....	52
4.2.3	Conclusion.....	57
4.3	Paper C: Blast Wave Overpressures from CO <sub>2</sub> Depressurization in a Conical-Shaped Vessel.....	58

4.3.1	Introduction .....	58
4.3.2	Results and Discussion .....	58
4.3.3	Conclusion .....	63
4.4	Paper D: Release of liquid CO <sub>2</sub> from the bottom of a duct.....	64
4.4.1	Introduction .....	64
4.4.2	Results and Discussion .....	64
4.4.3	Conclusion .....	70
)		
5.1	Release mechanism in a conical-shaped vessel.....	71
5.2	Evaporation characteristics in a constantly reduced cross-sectional area..	73
5.3	Influence of phase transition on the blast wave .....	76
5.4	Release below the liquid level .....	79
o	#	
k		
h	@Published and submitted papers)	
Paper 1	.....	98
Paper 2	.....	111
Paper 3	.....	121
Paper 4	.....	141
Paper 5	.....	152
Proceeding A	.....	160
Proceeding B	.....	167
Errata	.....	177



### 3 Key of develop"

Carbon capture and storage (CCS) was proposed as a solution to reduce the escalating CO<sub>2</sub> emissions in recent years. The goal is to stabilize the atmospheric CO<sub>2</sub> concentrations and, in turn, alleviate climate change. CO<sub>2</sub> transport and storage processes have been utilized in food and medical industries and oil recovery practices for many years. Burning fossil fuels and chemical industries contribute significantly to CO<sub>2</sub> emissions, impacting Earth's temperature. According to the Paris climate agreement, about 94 Gt of CO<sub>2</sub> is estimated to be captured and stored by 2050. The target is to limit the average global temperature increase to 1.5°C [3, 4]. As large volumes of CO<sub>2</sub> must be captured and stored in upcoming years, CCS infrastructure requires progressive improvement and development. After capturing from power plants and CO<sub>2</sub>-intensive industries, CO<sub>2</sub> is dehydrated to prevent possible corrosion problems. Then it is compressed to high pressure and transported as a pressurized liquid phase. CO<sub>2</sub> is transported by ship and rail storage tanks or onshore/offshore pipelines to storage sites. Transportation of large CO<sub>2</sub> quantities raises safety concerns over accidental release.

A tank or pipe transporting liquid CO<sub>2</sub> could fail due to mechanical malfunctioning, projectile impact, corrosion, or overheating caused by outer fire. An accidental release from such a tank includes rapid phase change, leading to a massive fluid expansion and explosion. Such development may result in a highly hazardous incident in certain situations: boiling liquid expanding vapor explosion (BLEVE) [2]. The term BLEVE has various definitions in the published literature. For example, Birk et al. [3] defined it as "A BLEVE is the explosive release of expanding vapor and boiling liquid when a container holding a pressure liquified gas fails catastrophically.". Although BLEVE has many definitions, descriptions of the most important features can be extracted from them. These include a catastrophic failure of the container filled with pressurized liquified gas; and a rapid phase change with the eruption of a large volume of superheated liquid and vapor into the atmosphere [3, 4].



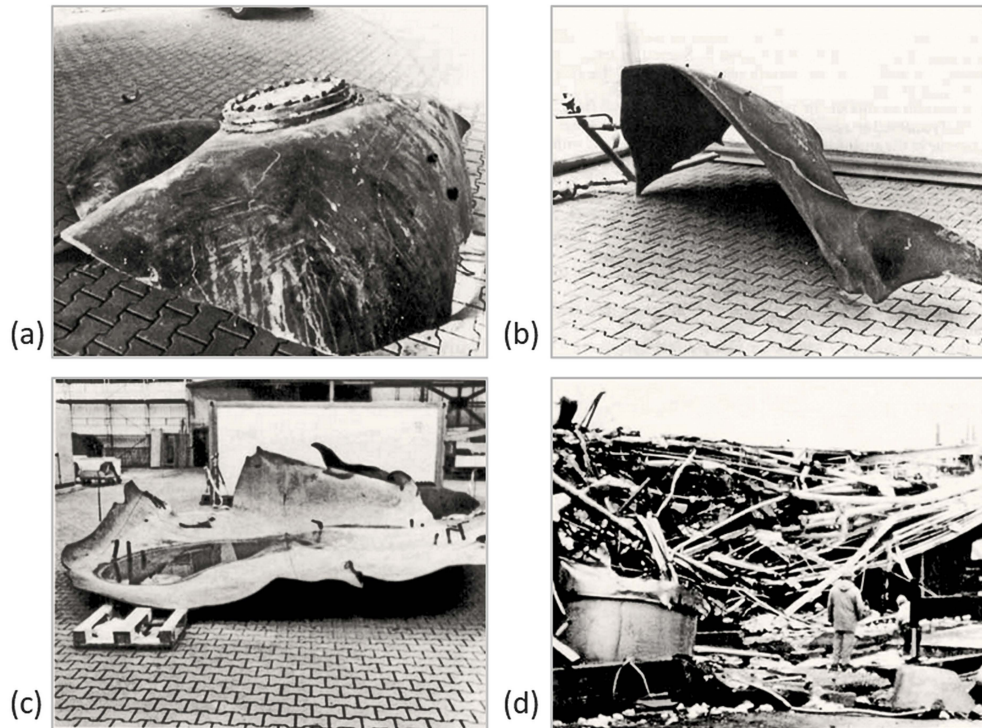
Although CO<sub>2</sub> is categorized as a non-flammable or mostly non-poisonous substance, a CO<sub>2</sub> BLEVE event involves extremely devastating effects. It generates powerful pressure waves with high-pressure loads on the vicinity surfaces. Furthermore, the rocketed fragments following the shattering of the container may have destructive consequences. Possible health and ecological hazards also arise from releasing sizable CO<sub>2</sub> volumes into the surroundings. Primary hazards for nearby humans include asphyxiation, poisoning at high concentrations, and frostbite injuries [5].

Many BLEVE accidents have occurred in the chemical process industry. Their devastating effects were demonstrated in the collected data for BLEVE accidents between 1940 and 2005, reported by Abbasi and Abbasi [6]. In these severe events, over a thousand people died, ten thousand were injured, and the explosions caused extensive property damage. A few CO<sub>2</sub> BLEVE accidents have also been described in the literature. Incidents that took place in Repcelak (Hungary), Worms (Germany), Zhejiang (China), and Satartia (USA) are presented in the following.

A CO<sub>2</sub> BLEVE event occurred in 1969 in Repcelak, Hungary. Four cascaded CO<sub>2</sub> storage vessels exploded in a domino effect manner, wherein nine people died. All vessels were shattered into pieces, and one weighing 2.8 tons was found 150 meters away. Another fragment of one ton flew 250 meters from the explosion site. One vessel had taken off its base and rocketed into a nearby laboratory. The first vessel with 35 tons of CO<sub>2</sub> at 1.5 MPa and -30°C burst during filling, and the sequential explosions were likely due to the fragments' impact. Overfilling was reported as a potential reason caused by level indicator malfunctioning [6, 7].

An incident of CO<sub>2</sub> storage tank BLEVE took place in Worms, Germany 1988, leaving behind three fatalities, eight persons experienced acute frostbites, and the adjacent buildings collapsed due to powerful pressure loads. The tank capacity was 30 tons at 2 MPa and -20 °C. According to the investigation team, exposure to higher temperatures with a frozen relief valve and brittle fractures were the reasons for the explosion [8]. Figure 1.1 (a-c) shows the fragments which flew approximately 300 meters away from

the tank's initial position after its shattering and (d) the scene behind the tank location after the explosion.



7 # "Qf- ‡ 8 k  
# 8

In 2008 a CO<sub>2</sub> ship storage tank violently exploded in Yuhang's pool in Zhejiang, China. The ship was destroyed due to the explosion of 130 m<sup>3</sup> CO<sub>2</sub> at 2.3 MPa and -15 °C. That caused two death casualties and three injured from fragments hit. In addition, two ships sunk carrying dangerous chemical substances (sulfuric acid and hydrogen peroxide). Overfilling and technical defects were potentially the leading causes. It has also been mentioned that the 16 MnR steel tank (-20-475°C) was inappropriate for operating at low temperatures [7].

A rupture of the CO<sub>2</sub> transport pipeline occurred in 2020 at about 1.6 km outside the village of Satartia, Mississippi. A massive cloud of CO<sub>2</sub> covered the region, resulting in the residents' evacuation of the village and around the area. Forty-five people were driven to the hospital because of asphyxiation and poisoning. The investigation report pointed out that heavy rains resulted in a landslide all over the pipe's failure location. And, in turn, led to an excessive axial strain on a pipeline weld [9].

These accidents show the severity and destructive power of CO<sub>2</sub> explosions in liquid storage tanks and pipelines. Therefore, carrying out a required risk assessment and safety management in constructing and handling CO<sub>2</sub> tanks and pipes is vital. Thus, this necessitates deep knowledge of the CO<sub>2</sub> phase transition mechanisms leading to the BLEVE incident. Considering these concerns, this research is within the process safety of CO<sub>2</sub> transport and storage and studies the processes involved in the BLEVE incidence. Its primary part intended to provide results and analyses of CO<sub>2</sub> depressurization from a newly designed experimental rig that combined a divergent cross-section vessel with double-membrane rupturing techniques. In particular, it investigated the rapid evaporation mechanisms, two-phase mixture evolution, and blast wave consequences. Additionally, it researched the phase transition underlying mechanisms during the release of liquid CO<sub>2</sub> from the bottom of a rectangular duct.

## u

Most experimental studies on phase transition during CO<sub>2</sub> depressurization found in the literature were performed in a constant cross-sectional shock tube type. Over recent years, the research group for process safety, combustion, and explosions at the University of South-Eastern Norway has studied rapid phase change in compressed liquid CO<sub>2</sub>. Earlier studies used different experimental setups but were primarily conducted in constant cross-section containers. Consequently, this research project stood as a continuation of these endeavors, and it sought to expand previous research with the following objectives:

- Investigate the release mechanisms of liquid CO<sub>2</sub> from a conical-shaped vessel using the double-diaphragm bursting technique and evaluate its operation under these mechanisms.
- Study the effect of the vessel's divergent cross-section on the rarefaction and evaporation wave velocity. As well as consider the influence of liquid volume fraction on expansion waves' behavior.
- Evaluate the effects of blast waves, including overpressure, impulse, and flying fragments during CO<sub>2</sub> depressurization in the conical-shaped vessel.

- Examine the phase transition characteristics and the evolution of expansion and evaporation waves during the release of liquid CO<sub>2</sub> from the bottom of a rectangular duct.

The analyses of the rarefaction, evaporation, and blast waves from different experimental setups should have been contrasted with the previous tests conducted in a constant cross-section container. Even though several kinds of research have offered various analyses on BLEVE, all aspects of CO<sub>2</sub> BLEVE mechanisms are not fully understood. Therefore, this study contributes to research on liquid CO<sub>2</sub> depressurization by (1) utilizing a high-pressure conical-shaped vessel and employing a double-diaphragm technique. (2) releasing liquified CO<sub>2</sub> below the liquid level. The hypothesis that has been examined was that the divergent cross-sectional area would lead to a significant fluid expansion and simultaneously avoid choking conditions in the test section. The conical-shaped vessel was designed to try to obtain a 2D/3D-shaped release, as the release from this geometry is more like a catastrophic failure of a tank than a 1D release with a constant area. The experimental setup should clarify whether the phase transition rate and metastable state following the rarefaction wave are independent of fluid expansion. Another question is whether the vapor expansion influences the evaporation mechanism during liquid CO<sub>2</sub> release at the bottom of a duct. The results and analysis from this experimental research were reported in three journal articles, a conference paper, and two conference contributions as extended abstracts. Another conference paper was intended to model a two-phase mixture's transient flow during the accidental release of liquid CO<sub>2</sub> in a pipe. This paper appears not to associate directly with the major thesis research. However, they are linked with a shared central thread. That is to study the dynamic features of phase transition in different geometries. The primary goal was to determine whether the constructed model successfully captures the rapid phase transition.

\ . . . .

This article-based thesis has been divided into two parts. The first part comprises six chapters, including this introductory chapter. Chapter two introduces the relevant

theoretical aspects of the research and presents their settings in the related literature. Selected works of experimental CO<sub>2</sub> depressurization and modeling have also been introduced. The third chapter involves the experimental installations and methodology used for this study. It depicts three setups' equipment, methods used to run the experiments, and the methods analysis to interpret the results. The fourth section encapsulates the produced papers, focusing on the research outcomes. Chapter five describes the main findings' analyses, and discussions were undertaken throughout the research. Finally, a summary and conclusions are presented in the sixth chapter, including suggestions for further research. The second part includes published and submitted journal articles and conference contributions.

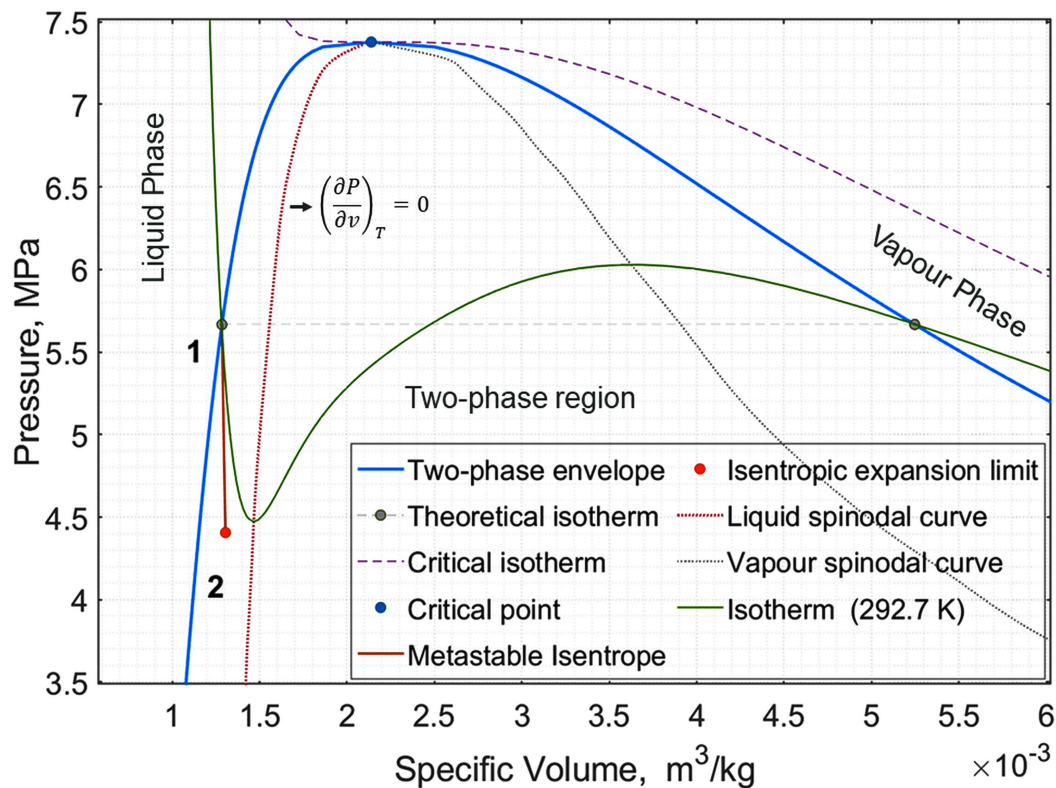
## 4 'Nkgt cwt g'Tgxky 'cpf 'Tgrgxcpv'Vj gqt { "

This chapter begins by laying out the theoretical perspectives relevant to the research's areas and reviewing their background in the corresponding literature. Primarily, it discusses the thermodynamic characteristics of superheated liquids, the phase transition process, and evaporation wave features. Besides, it considers the violent and rapid evaporation, the potential to induce a BLEVE, and the consequences following the catastrophic loss of containment. This section also presents experimental and modeling research on liquid CO<sub>2</sub> depressurization: background aspects and significant outcomes. Selected works exemplify the reviewed literature, but the studied field was not limited to those.

O

### 2.1.1.1 Thermodynamic aspects of superheated liquids

Description of the thermodynamic state is critical in the evaporation process analysis, as the substances' thermophysical properties change during the phase transition. CO<sub>2</sub> is transported and stored in containers as a pressurized liquid phase exceeding its atmospheric boiling temperature. The dense liquid phase is at thermodynamic equilibrium with the overhead vapor at saturated temperature and pressure. If such a container depressurizes, the liquid may expand beyond the saturation line without altering its phase. It temporarily undergoes isentropic expansion to a superheated state. The increased saturated liquid temperature above its boiling point at constant pressure can also expand it into superheated [10]. Figure 2.1 shows a diagram of CO<sub>2</sub> liquid expansion from saturated to metastable during isothermal depressurization. The liquid state after the expansion is described as metastable, and no phase transition occurs as long as it remains in this state between the saturation and spinodal curves. Between these two curves, the liquid is in an intermediate energetic state and sensitive to minor disturbances, which can lead to its vaporization. In Figure 2.1, the initial state is saturated temperature and pressure at point 1 on the liquid's saturated curve. Point 2 denotes superheated liquid at metastable state. The isentropic liquid expansion (1-2) occurs rapidly and characterizes the superheat's extent.



7 h

#A

The liquid spinodal curve specifies the thermodynamic stability limit beyond which the metastable liquid enters the unstable region. Moreover, all the points on the spinodal curve signify the thermodynamic stability wherein the condition  $(\partial P/\partial V)_T = 0$  is satisfied. At the intersection of the spinodal curve with the isotherm, its slope turns zero.

### 2.1.2 Degree of superheat (DOS)

DOS characterizes the measure by which the liquid has shifted from saturation to the metastable state. DOS is typically defined as a difference between the liquid temperature at the metastable state before the phase change occurs  $T_{ms}$ , and saturated temperature at metastable state's pressure  $T_{sat}(P_{ms})$ . Thus, the DOS measures the accessible thermal energy for vaporization. i.e., a higher DOS signifies more available energy for the boiling process. Simões-Moreira [11] estimated the DOS expressed in terms of pressure since the liquid is expanded by depressurization.

$$\Pi = \Delta P / P_{sat}; \quad \Delta P = P_{sat} - P_{ms}$$

where  $P_{sat}$  is saturated pre-rupture pressure, and  $P_{ms}$  is metastable limit pressure after the isentropic expansion.  $\Delta P$  represents DOS' fundamental concept, while  $\Pi$  comparatively assesses the extent of expansion into the metastable zone. Skripov [12] stated that the isentropic process response to slightly local perturbations is described by isothermal compressibility ( $\beta_T = -\frac{1}{V}(\partial V/\partial P)_T$ ) and isobaric specific heat ( $c_p = T(\partial s/\partial T)_p$ ). Hence, at metastable state, the liquid remains stable only if  $\beta_T > 0$ , and  $c_p > 0$  (i. e.  $(\partial P/\partial V)_T < 0$ , and  $(\partial T/\partial s)_p > 0$ ).

### 2.1.3 Superheat limit temperature (SLT)

The liquid temperature at the spinodal curve is referred to as the thermodynamic superheat limit (SLT). Reid [13] defined it as: "The maximum absolute attainable temperature, at some absolute pressure P, for a superheated liquid is often called the superheat-limit.". Determination of SLT is essential for secure design and control against explosive evaporation. Attempts have been made previously, for instance, by Ermakov and Skripov [14] and Blander et al. [15], to calculate SLT by applying different equations of state (EOS) and spinodal stability criterion. However, the outcomes created uncertainties because they were not correlated well with superheated liquid parameters P, V, and T [13].

Results from the thermodynamic stability method present considerable discrepancies when using different EOSs. Another approach based on energy balance in the initial liquid mass just before the explosion has been proposed by Salla et al. [16]. This method merely utilized the substance's properties to calculate the SLT. It indicated that every substance acted depending on its molecular structure. The analyses compared seven calculating methods on various substances; for CO<sub>2</sub>, based on energy balance, the suggested SLT was 7.05°C. Abbasi and Abbasi [17] offered SLT results from seven cubic EOS applying Maxwell transformation and SLT criteria. They also compared the calculated figures with the previous experimental results. For CO<sub>2</sub>, it has been found that the calculated SLT deviated in a range of 2 to 6 % (Redlich-Kwong to Soave- Redlich- Kwong EOS) from the experimental result of -6°C at 2,9 MPa.



#### 2.1.4 Kinetic superheat limit (KSL)

Several attempts have been made to determine the liquid superheat limit empirically. These include recognized bubble column experiments [18-22], wherein a droplet of immiscible liquid is heated in a column filled with a liquid with higher density. As the droplet ascends through the increasingly heated liquid, it explodes at a specified temperature termed kinetic superheat temperature. Reid [13, 23] and Xie [24] stated that the experimentally observed superheat limit temperatures constantly were KSL. The kinetic nucleation theory could also theoretically estimate the liquid superheat limit. It analyzes the liquid metastable state's thermal fluctuations and the probability of vapor nuclei creation. Based on the Boltzmann equation for nuclei distribution, vapor formation probability increases exponentially with an increase in liquid superheating [15, 25].

Hill [26] described the mechanisms of vapor formation during liquid decompression. Because the density randomly varies continuously on a molecular level of the liquid phase, its deficiency at some spots leads to nucleus formation. The superheated liquid has the strength to overcome the surface tension forces, which attempt to suppress nucleus growth to bubbles. The mechanical equilibrium of a typical vapor bubble is attained only at a critical radius ( $k$ ). This equilibrium can occur when the excess pressure inside the bubble equalizes the surface tension effect. So, this radius is proportional to the surface-tension coefficient ( $\sigma$ ) and inversely proportional to the excess pressure ( $\Delta P$ ):

$$R_{cr} = \frac{2\sigma}{\Delta P}$$

Formed bubbles with a radius  $R > R_{cr}$ , are most likely to grow, while those with a smaller radius condensate. At the early stage, the bubble's nuclei growth is induced by its movement speed through the surrounding liquid. Then, the process is controlled by heat transfer from superheated liquid to the bubble interface for vapor formation. Consequently, the vaporization speed depends on the bubble/liquid interface's temperature gradient, as Prosperetti and Plesset described [27].

### 2.1.5 Equation of state (EOS)

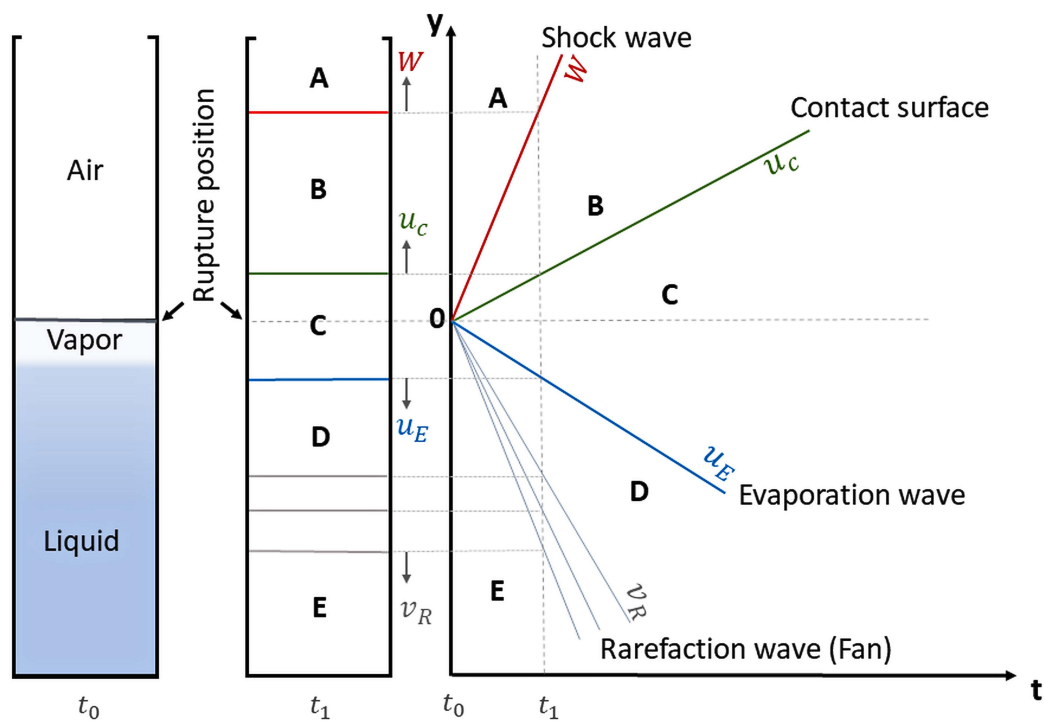
Using EOS to identify the flow thermodynamic properties is essential when obtaining them by experimental means is challenging. In the CO<sub>2</sub> phase transition analyses, the EOS determines the state properties and their relations, particularly in a metastable state. However, most calculations based on different EOSs are limited to equilibrium zones and require extrapolation from the saturation state to calculate the variables in the metastable state. These calculation precisions depend on the EOS application. Therefore, choosing an EOS that utilizes thermodynamic functions to facilitate reasonable extrapolation to a metastable state is crucial.

The Span-Wagner EOS (SW-EOS) [28] is considered the most accurate equation to compute thermodynamic variables for CO<sub>2</sub> phase transition." It is formulated in Helmholtz's free energy (HFE) as a function of temperature and molar volume,  $a(T, v)$ . All other thermodynamic properties can be expressed in terms of their partial derivatives. It covers the fluid region from the triple point temperature to 1100 K at pressures up to 800 MPa. The SW-EOS is worked out based on splitting the dimensionless HFE into two parts: one considering the ideal-gas behavior and the other the residual fluid behavior. The HFE dimensionless residual part is expressed as a function of the reduced value of these independent variables.

Recently, Harvey and Lemmon [29] from NIST have developed a replacement for SW-EOS to calculate CO<sub>2</sub> thermodynamical properties. The new equation utilized molecular calculations for the ideal-gas heat capacity and thermal virial coefficients to enhance accuracy for the gas phase and improve extrapolation to higher temperatures. The capability of the EOS has been adjusted to avoid erroneous behavior and challenges in mixture calculations. Therefore, the authors claimed it has better execution and reduced time calculation than SW-EOS. However, the calculations in this research are based on SW-EOS tabulated data [28] and its solution version introduced by Mjaavatten [30]. The new EOS by Harvey and Lemmon calculations could be explored in future work and compared with SW-EOS results.

### 2.2.1 Waves configuration

Figure 2.2 displays the configuration of waves and regions that developed during the depressurization of saturated liquid in a vertical vessel with an outlet on the top. Point 0 indicates the rupture position at time zero. The rupture of a vessel filled with pressurized liquified gas leads to a rapid pressure decrease. A rarefaction wave propagates throughout the saturated headspace vapor and then the liquid. Subsequently, the liquid expands, becomes superheated, and temporarily remains in the metastable state before evaporation onset. Many authors have previously studied this phenomenon; for instance, Simões-Moreira [11] and Hill [26].



The phase transition occurs as the evaporation wave propagates through the superheated liquid. The evaporation wavefront represents a narrow bubbly zone moving with nearly constant velocity behind the rarefaction wave [31]. Subsequently, a

large volume of the expanded two-phase mixture bursts out of the vessel owing to the rapid phase change. A shock wave is simultaneously generated due to the compression of the surrounding air ahead [32]. This wave propagates upwards to the surrounding area with supersonic speed, followed by the contact surface that initially was a liquid-vapor interface [31].

In Figure 2.2, once the vessel ruptures, a rarefaction wave travels into the saturated liquid with the local speed of sound ( $u_R$ ). Simultaneously, a shock wave propagates upward with supersonic velocity ( $W$ ). Behind the shock, moves the contact surface at ( $u_c$ ). An evaporation wave follows the expansion fan into the presently superheated liquid with a velocity ( $u_E$ ). The pressure and the flow velocity are constant in regions B and C.

### 2.2.2.2 Evaporation wavefront propagation

The phase transition occurs as the evaporation wave propagates through the superheated liquid. The phenomenon of propagation of the two-phase/liquid interface during boiling has been designated with several terms in the literature. Such expressions, for instance, but not limited, include the "flashing front" used by Das et al. [33], "boiling front" by Reinke et al. [34], "flashing boundary" by Fairuzov [35], and "evaporation wave" by Hill [26]. This dissertation uses the terms evaporation wave and -wavefront to refer to the abovementioned phenomenon. The wavefront represents a narrow zone of bubbles traveling with almost constant velocity [31]. High-speed photograph observations by Hill [26] showed that the evaporation wavefront had a thickness of several millimeters. Besides, its leading edge (upstream layer) is dominated chiefly by tiny bubbles with a minor diameter that could reach less than 100  $\mu\text{m}$ . This region implied rapid evaporation wherein a continuous bubble generation occurred. The wavefront's tail (downstream layer) is occupied with more giant continuously breaking bubbles within the fragmentation/acceleration region. Figure 2.3 illustrates the wave front's layers while propagating through a superheated liquid.

The DOS significantly influences the evaporation wavefront propagation velocity into the superheated liquid. Watanabe et al. [36] demonstrated that the DOS before evaporation starts substantially depends on the depressurization rate. The wavefront

propagation is initiated as the superheated liquid approaches KSL. At low superheat degrees, the evaporation rate is insufficient for producing severe explosions [37].

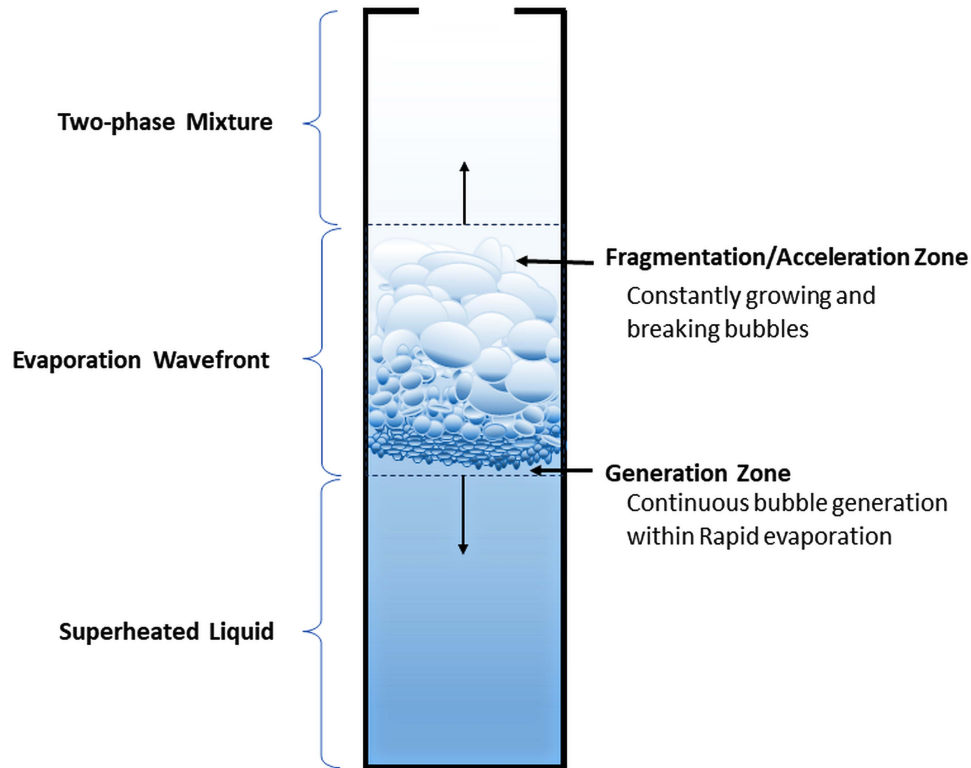


Figure 2.3: A drawing of the evaporation wavefront's zones as it moves through a superheated liquid.

Reid [13, 32] and Stutz and Simões-Moreira [38] described how the DOS influences the bubbles' formation, growth, and, subsequently, the blast intensity. At a low or moderate DOS, heterogeneous nucleation typically originates at the nucleation sites on the vessel's inner surface (pits and scratches) or/and particle impurities. As the pressure decreases, more bubble sites are activated, and the existing ones grow. Then, their speedy collisions, coalescence, and upward movement lead to powerful boiling developments. The DOS depends on the depressurization rate and the container's inner surface roughness. When the container has a smooth surface and a high depressurization rate, there is insufficient time to initiate heterogeneous nucleation on the wall surface. Consequently, homogeneous nucleation may originate throughout the liquid bulk.

Many noticeable studies have been done on evaporation wave features. Grolmes and Fauske [39] experimented on the evaporation rate during depressurization of subcooled water, R-11, and methyl alcohol in tubes with 2-50 mm diameters. High-speed images showed that Marangoni-type surface waves, as the authors called them, induced the evaporation wave's start. Also, the DOS was inversely proportional to the tube diameter. Hill [26] and later Reinke et al. [40] characterized the bubble formation and movement of the propagated wavefront utilizing optical techniques. Besides, they measured the velocities ahead of and behind the evaporation wavefront. Based on the flow form and heat transfer characteristics, Wu et al. [41] investigated the evaporation wave behavior in experiments of water depressurization in a chamber. The study distinguished between three evaporation stages: bubble production, evaporation acceleration, and evaporation deceleration stage.

) . . " Q † - . .

A high-energy content is released when a vessel with pressurized liquified gas ruptures, leading to explosive evaporation. Such instantaneous phase change typically results in rapid expansion and powerful pressure loads on the surroundings. A boiling Liquid Expanding Vapor Explosion ( BLEVE) is one of the most severe mechanical explosions following a vessel's failure containing liquified gas [42].

Several authors have approached the BLEVE term differently depending on what they considered essential factors and effects [24]. Birk et al. [3] have emphasized the importance of a container's catastrophic failure. Whereby the vessel is wholly broken and rapidly releases its contents. A further detailed description of BLEVE was introduced by Venart et al. [43, 44] for a choked expanded two-phase mixture during evaporation. Accordingly, the bubbles were compressed due to the pressure rebuild and then released their energy during the full container's disintegration. As BLEVE could originate from flammable and non-flammable liquids, Van der Berg et al. [45] indicated the ambiguity around the term when the explosion involves a fireball. They mentioned that the BLEVE definition must not include subsequent ignition and fire development. The Center for Chemical Process Safety (CCPS) [4] has given a definition restricted to

pressure-liquified gases as: "a sudden loss of containment of a pressure-liquified gas existing above its normal atmospheric boiling point at the moment of failure.". Though various definitions for BLEVE have been introduced in the literature, most include three aspects. First, an explosion of the vessel containing a liquid (or liquid and vapor) at a temperature much higher than its boiling point at atmospheric pressure. Second, a complete catastrophic loss of containment. Third, substantial amounts of superheated liquid are suddenly released into the surroundings. The fireball may also be included in a BLEVE for flammable liquids.

Several attempts have been made to identify the conditions that induce BLEVE. Reid's superheat limit theory [46, 47] specified the conditions for the BLEVE incident. Accordingly, the vessel rupture leads to a pressure decrease, and the liquid leaves behind the saturation line into the saturation dome. It becomes superheated in the metastable state until it reaches the SLT. BLEVE almost certainly occurs when the liquid temperature approaches the SLT at the liquid spinodal curve (see Figure 2.1). Additionally, the liquid should attain a high DOS, prompting homogeneous nucleation in the liquid bulk.

Investigating the influence of SLT on the BLEVE development, Abbasi and Abbasi [6, 48] noted that the boiling intensified when SLT approached the spinodal liquid curve. These results were verified later from experimental observations by Van der Voort et al. [49]. The results showed that as the superheated liquid state approached nearer the spinodal line, the evaporation wave more rapidly propagated through the entire liquid, and a large vapor volume instantaneously expanded. However, Birk et al. [3] pointed out that homogeneous nucleation may not be a strict condition to cause a BLEVE. Zhang et al. [7] and Bjerketvedt et al. [50] indicated that explosive evaporation could occur without the liquid temperature reaching the SLT. Aside from the liquid's thermodynamic state development, the BLEVE event also depends on the container's durability. Laurent et al. [51] stated that If the container's crack following the initial failure proceeds to total loss of containment and without the liquid reaching SLT, the explosion can be described as cold BLEVE. Ibarreta et al. [42] and Ibrahim [52] emphasized the dependence of the

BLEVE event on the liquid thermodynamic condition and the container's strength. They presented a flow diagram proposed by Birk et al. [53] demonstrating possible paths for BLEVE occurrence. It included the superheating limit theory. Figure 2.4 shows the flow diagram created by Birk et al. [53] for potential paths for BLEVEs. It also illustrates BLEVE consequences if the pressurized liquid is flammable.

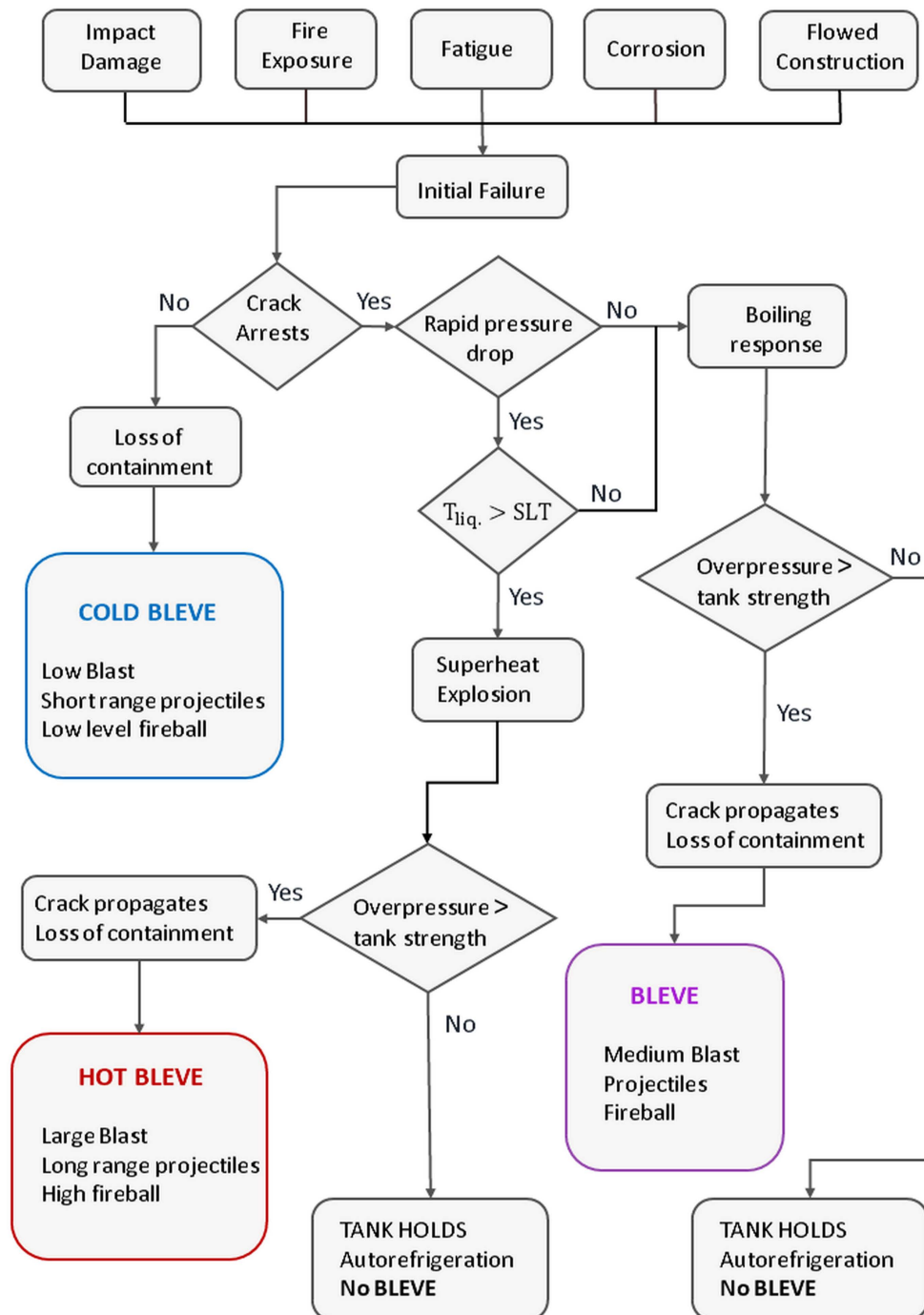


Figure 2.4. Potential paths for BLEVEs (Birk et al. [53]).



## "O†- "O†- '#

A container carrying pressurized liquified gas could be exposed to harmful conditions that eventually result in complete tank failure and loss of containment. These conditions include exposure to higher temperatures, projectile impact, "fatigue," or corrosion. The catastrophic failure of the container is a primary risk, wherein a substantial volume of multiphase mixture explodes into the surroundings. Such an explosion could, under certain conditions, be termed a BLEVE. It is among the highly hazardous explosions because it is characterized by the sudden generation of destructive pressure waves and dangerous flying fragments [4]. In addition, for CO<sub>2</sub>, a significant health risk arises from the ejection of large volumes of the multiphase mixture into the surroundings. It is toxic at high concentrations (above 5%) and can cause asphyxiation and frostbite injuries.

### 2.4.1 Overpressure and impulse

During the vessel explosion, the vapor and liquid's internal energy is partially converted into mechanical energy as it expands to atmospheric pressure. The mechanical energy release can be divided into (1) a blast wave and (2) propelled fragments that accelerate into the surroundings when the vessel shatters. Many factors influence the blast wave's intensity and structure, such as released energy rate, vessel geometry, expanded fluid properties, and rupture method. The blast waveform, denoted by the transient change in pressure, depends on the vapor/liquid expansion behavior. If the expansion is rapid, the waveform has a steep increase in pressure; otherwise, it increases gradually [54].

The peak overpressure and the positive phase impulse are the essential parameters that describe the strength of the shock wave and estimate its effect on the adjacent structures and living beings [45]. The positive impulse phase and its duration characterize the potential damage to the structure. It is calculated by integrating the pressure-time curve. Birk et al. [3] performed BLEVE experiments in containers with different levels of liquid propane to demonstrate the effect of liquid content on the resulting overpressure. The results showed that liquid energy content slightly affected the generated shock overpressure. Moreover, when the container shattered, intense

dynamic overpressure on the surfaces was observed due to the energy of the expanded multiphase flow.

Van der Voort et al. [49] have conducted experiments on 40-liter cylinders filled with pressure-liquified carbon dioxide to study overpressures during CO<sub>2</sub> BLEVE. The results showed good agreement with the inertia-limited prediction model offered by Van den Berg [55]. The effects of liquid content and the vent size on overpressures were studied experimentally by Hansen et al. [56]. The results from CO<sub>2</sub> depressurization in a rectangular duct were compared with simulations of single-phase gas dynamics in a confined chamber. They also demonstrated good correspondence. Other models have also intended to calculate the overpressures during the BLEVE based on the contained energy in the vessel and energy released during the explosion [55, 57, 58].

#### 2.4.2 The blast released energy

Estimating the transferred energy quantity during the blast is crucial to evaluate the blast strength and subsequent effects. The expansion energy is the total energy released during the isentropic expansion and the adiabatic evaporation. It signifies first from the initial saturated liquid state, then through the superheated (metastable state), and to the final equilibrium state [4]. The evaporation process is considered to occur adiabatically in most energy expansion models. Accordingly, the evaporation process is induced by enthalpy variation between saturated and final equilibrium states. During the vessel rupture, the multiphase mixture volume originated from the vapor headspace and rapid liquid evaporation. Therefore, the blast's extent also depends on the liquid's degree of superheat (DOS), and in turn, on the evaporated liquid fraction. The blast strength increases as the evaporated liquid fraction increase. The explosion's maximum possible work can be determined based on the description of the thermodynamic path or energy function built by initial and final states. Ibarreta and Biteau [59] and Casal [60] have demonstrated that the models proposed to calculate the explosion energy during the BLEVE incident can be divided into two approaches: Calculations based on the assumption that the released explosion energy is mainly generated due to the vapor

volume expansion. Other calculations are based only on the liquid's stored energy released during evaporation.

Crowl [61, 62] has presented calculations for determining the explosion energy of compressed gas using batch thermodynamic availability (exergy). This is the maximum potential work to bring the system into equilibrium with its environment. Crowl's calculation approach seemed similar to the energy released during explosive evaporation. Ogle et al. [63] have pointed to this analogy and modified Crowl's model to comply with the BLEVE case. The computation was based on the determination of thermomechanical exergy. That is the maximum accessible work to undergo the phase change by expanding from the saturated state to the final equilibrium state.

Prugh [57] has treated the explosion energy as the work done during the isentropic expansion of the vapor, which is assumed to behave as an ideal gas. The method calculates vaporized liquid fraction and total vapor volume for the BLEVE case. The overall exploded vapor volume includes the vapor volume initially being at a saturation state in the headspace and the vapor portion resulting from the liquid evaporation. Hansen [56] also applied this method to estimate the energy released during the expansion of CO<sub>2</sub> in the rectangular duct. The calculation was implemented using the vapor mass fraction determined by the Rankine-Hugoniot model.

Methods based mainly on the liquid stored energy in the metastable state assume that the expansion of the container's vapor is insignificant compared to liquid evaporation and can be neglected. Besides, these methods consider a high liquid volume fraction in the container. The energy release is estimated as the adiabatic expansion work during liquid evaporation. i.e., the change in energy amounts before and after the explosion. Casal et al. [64] have suggested that the work done to develop overpressure is the transformed part of the energy stored in superheated liquid, shifting the system to the final equilibrium state. In this calculating procedure, the superheating energy is determined as the difference in enthalpies at the superheated liquid and final states.

Genova et al. [65] suggested a different approach, assuming the expansion energy primarily originated from liquid evaporation. The model considered the expansion of liquid evaporation as a thermal incident induced by the excess heat stored in the liquid instantly before the explosion. The contribution of the vapor in the expansion work is neglected due to the mentioned earlier assumption of a high liquid filling degree. Laboureur et al. [66] have evaluated the calculation methods available in the literature with different experimental results. They utilized results from large-scale experiments conducted by Johnson et al. [67], mid-scale by Birk et al. [3], and small-scale by Stawczyk [68]. The minor inaccuracy approximation of overpressure was found to be the model with an irreversible expansion developed by Casal. It had an average error of 35% compared to all contrasted measurements. They also mentioned that this model could be applied to all compared BLEVE conditions and scales.

#### 2.4.3 Vessel Fragmentation (Fragment initial velocity)

During a BLEVE, the pressure vessel shatters and produces fragments that could rapidly travel a long distance from the explosion source. They are hazardous to surrounding living beings and structures and may trigger catastrophic secondary accidents. Analyzing flying fragments and missiles is vital to evaluate the BLEVE effects. Besides, knowing the consequences and impacts on the nearby structure provides necessary data for better safety management. As Kang et al. [69] mentioned, calculating the fragment's kinematic parameters is crucial for effectively setting protective fragmentation barriers. The fragments' velocity, trajectory, number, and shape determine their direct effects. Unlike detonations, BLEVE generates a few fragments but with different shapes, sizes, and initial velocities. The initial velocity is a critical parameter that characterizes the fragment's trajectory shape and range.

The energy released in an explosion is the total of the pressure wave's energy, the fragments' kinetic and potential energy, and the surrounding heating. According to Casal et al. [70], about 80% of the explosion energy is estimated to contribute to the pressure wave energy for the fragile vessel fracture, while it is 40% for the ductile fracturing.

Several techniques were suggested to quantify the fragments' hazard. Birk [71] has experimented with the risk of shattering a tank filled with pressurized propane. The results showed that the projectile impact expressed in mass x range (kg·m) increased with an increase in average liquid temperature before the explosion. Tebiét al. [72] have estimated fragments' kinematic parameters resulting from cylindrical tanks BLEVE. They introduced initial acceleration based on the geometry and type of the tank material. This approach allowed a consistent evaluation of the fragment release angle. The fragment trajectories were determined depending on the thrust acceleration coefficients, and fragment ranges probability distributions were presented. They also stated that fragments with high air resistance and low thrust could impact 15 m height surfaces and distances of over 200 m. In a series of studies, Baum [73-76] formulated a calculation procedure for determining the fragment's initial velocity. The model treated expanded two-phase mixture strain on the end-cap as like a missile propelled under the action of a persistent pressure gas jet. Then, the rocketed fragment velocities were estimated based on the impulse put on the closed inner side of the end cap. Parallel experiments with pressurized water BLEVE in a horizontal vessel have verified the model's validity, particularly for the defined maximum end-caps and missile velocities.

"Q†- · · · · ·

### 2.5.1 Release mechanisms in BLEVE experiments

Several experimental works have been performed on laboratory-scale test devices of shock tube type. They have been extensively used for researching pressure-driven transient phenomena involving considerable energy transformation due to pressure change. BLEVE experiments have been run in devices with different geometries, sizes, number of diaphragms and sections, and release mechanisms. For instance, studies by Simões-Moreira [11], Hill [26], Das et al. [33], Ren et al. [77], and Dewangan et al. [78] have been conducted on vertical test devices to describe the flow properties behind the incident shock and expansion waves' propagation. Horizontal tubes have also been

employed in large-scale experiments such as in [79-81]. Most studies applied the one-membrane burst method and constant cross-sectional vessels.

Constant and diverging cross-sectional ducts have been utilized in Chaves' [82] experiments of liquids with high specific heat. The study described the boiling process as a splitting of two expansion waves propagated in a superheated liquid. In addition, it found that the evaporation wave development during depressurization was a restricted thermodynamic incident independent of the geometry. Zabelinskii et al. [83] employed a horizontal shock tube of a variable cross-section between high and low-pressure parts to burst an explosive mixture diluted with cold hydrogen. The tests intended to study the effect of a divergent section and the driver diameter on the primary shock-front shape. They concluded that, unlike the constant cross-sectional device, the variable cross-section retained wavefront surface inhomogeneities.

Different release mechanisms have been used and established for sudden depressurization experiments in shock tubes. Thompson et al. [84] have applied a standard mechanical diaphragm rupturing method in experiments intended to study expansion waves in a fluid of high heat capacity. An expansion tube, including a rectangular high-pressure section with opposite walls of optical glass, was used in decompression tests. A sharp metallic arrow driven by a stretched spring ruptured the strengthened aluminum diaphragm. The experiments were initiated when an electromagnet device released the arrow.

Hill [26] employed a glass tube submerged in a liquid-filled jacket while observing evaporation waves propagating into superheated refrigerants R12 and R114. An aluminum foil diaphragm set between the tube and low-pressure reservoir was cut using knife blades triggered by a pneumatic cylinder. Das et al. [33] investigated boiling development during a column's depressurization of superheated liquid. A four-bladed cutter was set adjacent to the top of the plastic diaphragm and covered by an air chamber. When the pressure fell in the air chamber using a vacuum pump, The diaphragm bulged until it touched the blades and punctured.

A rupturing mechanism with a moveable disk was introduced by Reinke [34] to study the explosive evaporation of superheated liquids. A brass sheet diaphragm was installed on the test section flange and pressed from the top with two flanges different in inner diameter, one inside the other. The outer flange with the larger inner diameter had a sharp edge. The inner flange pressed the diaphragm in a smaller circle and could move up and down. Lifting the mobile flange off resulted in an increase in the diaphragm area under load. Subsequently, the tension at the circumference increased, leading to the diaphragm rupturing by the sharp-edged flange.

Dewangan et al. [78] recently presented a different rupturing technique in evaporation wavefront propagation research. They used a ring-shaped Nichrome heating wire to heat up and rupture the plastic diaphragm fixed between two flanges. Li et al. [85] examined the factors influencing the initiation of BLEVE. The experiments were run by heating dry ice in a cylindrical vessel sealed with a burst disc. The pressure increased as the dry ice melted until the disc could not withstand the increased pressure load and ruptured. Stotz et al. [79] constructed a double-diaphragm shock tube to study atomized liquids and the related combustion processes. It comprised three horizontally connected tubes with a total length of 12 m. Two aluminum diaphragms separated the driver and driven sections from the mid-pressure buffer zone. The diaphragms were ruptured following the rapid pressure drop in the buffer section.

### 2.5.2 Experimental studies in CO<sub>2</sub> BLEVE

In recent years, there has been an increasing amount of experimental research on CO<sub>2</sub> BLEVE. Quinn et al. [86] have depressurized Sub-cooled and supercritical CO<sub>2</sub> to explore the expansion waves of CO<sub>2</sub> BLEVE. The observations were carried out using a rectangular expansion tube with double-diaphragm chambers. Schlieren and standard high-speed photography were used to visualize the expansion and the phase transition zone during depressurization. The pressure measurements indicated the appearance of pressure plateaus below the saturation pressure. Indeed, it verified a delay of bubble nucleation related to the phase change during decompressing. Additionally, the degree

of superheating (as normalized pressure) increased as the saturation to critical temperature ratio decreased.

Jamois et al. [87] have developed an experimental setup for researching the scenario of CO<sub>2</sub> release resulting from a brittle fracture caused by temperature reduction. The tests run in a thermally insulated sphere vessel volume of 2 m<sup>3</sup> attached to a discharge pipe equipped with a control valve to adjust the depressurization rate. The release could be achieved at the vessel's mid-section, either on the vapor or liquid side at the bottom. Pressure and temperature records, as well as optic ports, were utilized to observe phase transitions. Analyses of temperature histories indicated a nearly adiabatic process producing high vertical temperature gradients in the gas phase. Also, the multiphase pressure plateau was detected at the triple point during CO<sub>2</sub> gas phase releases. Experiments on the identical setup have been conducted by Teberikler et al. [88], Drescher et al. [89], and Vaillant et al. [90]. Records of pressure, fluid mass, and temperature inside the vessel and at the wall have been analyzed. Then, these measured parameters were used to evaluate the capability of thermodynamic and transport models available in LedaFlow and UniSim Design software.

Through controlled BLEVE experiments, Shang et al. [91] investigated the risk of CO<sub>2</sub> explosion during fracturing in enhanced coalbed methane recovery technology. The liquid CO<sub>2</sub> was heated in a horizontal tube of 1.5 m, and three parameters monitored the phase change: release opening area, injection level, and blasting pressures. The results showed maximum explosion intensity at the highest blasting pressure, medium filling level, and maximum release orifice.

Li et al. [92] carried out CO<sub>2</sub> explosion experiments to study the container's resistance during different rupturing shapes and the intensity of the flying fragments. The tests were conducted in a cylindrical steel tube diameter of 80 mm and a wall thickness of 5 mm. To control the burst direction, the tubes' outer surfaces were grooved at a depth of 4 mm along the height, either with a V or X shape. A steel ball of 1 g was set into the grooved area to monitor the fragment path and speed. Pressurized CO<sub>2</sub> was injected into the tube until its failure. The results showed that the tube with a V-shaped groove held a higher resistance to the maximum and average bursting



pressure than that with an X-shaped groove. Besides, a fragment's initial velocity of about 272.8 m/s was observed with a flying distance of over 7 m.

Hansen et al. [93] investigated the rapid depressurization of CO<sub>2</sub> in a high-pressure duct. The setup comprised a stainless-steel rectangular duct filled with liquid CO<sub>2</sub> to a specified level. The sudden release was performed by rupturing a multi-layer aluminum diaphragm with a pneumatically driven cross-shaped knife. Pressure and temperature records inside the duct and high-speed Schlieren imaging were used to analyze the phase transition process. Processed schlieren images demonstrated an evaporation wave traveling downwards at 30-40 m/s. However, a heterogeneous nucleation on the wall was observed, descending at 240-260 m/s ahead of the evaporation wave. Consequently, it reduced the degree of superheat in the current setup and overshadowed the evaporation wavefront details.

Cicarelli et al. [94] studied the rapid boiling of CO<sub>2</sub> in a vertical shock tube. A transparent polycarbonate tube with aluminum covers was used as a driver section. The tube was set inside a channel with circulating water and separated from a steel pipe (driven section) by a thin aluminum diaphragm. The tube was filled with dry ice and heated until it melted. As the pressure inside the tube rose due to the contents' expansion, the diaphragm ruptured, leading to depressurization and rapid liquid boiling. Pressure and temperature histories and high-speed videos were used to describe the decompression and vaporization developments. The results showed that rapid evaporation did not influence the early phase of the tube expansion. However, it was controlled by the vapor expansion, maintaining a high pressure for a prolonged period.

Tosse et al. [95] have conducted experiments depressurizing liquid CO<sub>2</sub> in a transparent polycarbonate tube to analyze the phase change and evaporation wave progression. A two-layer Mylar sheet was employed as a membrane ruptured by a needle driven by a pneumatic linear actuator. In a series of tests, the diaphragm was placed on the tube's top and bottom in another series. The high-speed videos from top releases showed an evaporation wave moving downwards with a velocity of up to 30 m/s. The interface

vapor/two-phase mixture was also observed to accelerate outwards. The liquid side releases demonstrated that it evaporated as it flowed downwards from the tube vent with a significantly higher velocity than the evaporation wavefront speed inside the tube.

Bjerketvedt et al. [50] have conducted small-scale experiments on CO<sub>2</sub> BLEVE in cylindrical plastic tubes filled with dry ice. The test tube was sealed with two flanges utilizing a pneumatic cylinder. A phase change from solid to liquid occurred when the dry ice was heated, and the pressure developed to saturated. Then, the pressure was increased until the tube exploded. Analyzing pressure, temperature, and high-speed video recordings, they concluded that a violent boiling might proceed without reaching the spinodal temperature point. The experimental results indicated that the shock waves resulted from the vapor expansion before rupture. However, the numerical simulations employing Random Choice Method (RCM) demonstrated that the liquid evaporation had increased blast wave duration.

### 2.5.3 Modeling of CO<sub>2</sub> depressurization

Several models have been proposed to predict state properties and simulate the transient two-phase flow during pure or CO<sub>2</sub>-rich mixture depressurization in ducts or pipes. Some of these are presented here to exemplify their application in different fields. Brown et al. [96] have extended the AUSM+-up (Advection Upstream Splitting Method) scheme to resolve two-phase flow in ducts with cross-sectional area change. The scheme simulated saturated two-phase CO<sub>2</sub> and CO<sub>2</sub>-mixture in a shock tube test with rapid change in the cross-sectional area and demonstrated adequate robustness. Besides, the scheme computed both the reflected and transmitted shocks appropriately.

Log et al. [97] also modeled CO<sub>2</sub> two-phase flow in a discontinuous area duct, developing Harten-Lax-van Leer Contact (HLLC) approximate Riemann solver. The principal approach was discretizing the non-conservative term separately (termed HLLC+S) or including the non-conservative term in the Riemann solver (termed HLLCS). The evaluation has been done for a two-phase flow using a homogeneous equilibrium model

(HEM) combined with the Peng–Robinson equation of state. The methods were uniformly correct and more robust than those presented for non-resonant flow.

Relevant analogies of instability during the evaporation phase transition with that in deflagration gas explosion have been drawn in several studies [82, 84, 98-102]. Whereby the evaporation wave is considered a discontinuity in the flow field. As the evaporation wavefront propagates in a thin discrete region, it is demonstrated as a jump in flow properties up and downstream of the wavefront. Hansen et al. [93] researched the Rankine-Hugoniot relation across evaporation wavefront in superheated CO<sub>2</sub>. The evaporation wave was processed as a jump between two states, superheated liquid and two-phase equilibrium at adiabatic conditions. The model demonstrated excellent qualitative agreement with experimental measurements from three different setups.

Many models have been suggested to predict state properties during pure or CO<sub>2</sub>-rich mixtures depressurization in pipes. Munkejord et al. [81, 103] have employed HEM to capture the phase transition features during a pipe's CO<sub>2</sub> and CO<sub>2</sub>-rich mixture decompression. The studies focused on decompression-wave velocity for its significance in the ductile fracture of pipelines. The model was validated by comparing its results with measurements from large-scale experiments. The tests were executed in a pipe length of 61.67 m with high-resolution pressure and temperature recordings. The model agreed well with the decompression-wave velocity in single and two-phase flows. Additionally, the impurities substantially affected the pressure plateau, an essential measure for evaluating running-ductile fracture. Pressure plateaus were increased drastically for the CO<sub>2</sub>-rich mixtures.

Elshahomi et al. [104] used CFD ANSYS Fluent to develop a CO<sub>2</sub> decompression model. The objective was to predict state properties during the condensation phase transition. To determine the thermodynamic state properties of CO<sub>2</sub> mixtures, GERG-2008 EOS was integrated into the model using User Defined Functions (UDF). The results demonstrated fair accordance with previous shock tube experimental data. Munkejord et al. [105, 106] have studied the influence of impurities and the initial temperature on wave velocity during CO<sub>2</sub>-rich mixture decompression. Two models were developed: the

homogeneous equilibrium model (HEM) and the two-fluid model (TFM). They were formulated using the multi-stage centered scheme (MUSTA), Soave-Redlich-Kwon, and Peng-Robinson EOS to calculate the thermodynamical properties. The results were compared with measurements from shock tube tests and showed a slight improvement in TFM predictions compared to HEM.

Botros et al. [80] formulated different models based on three equations of state: GERG-2008, Peng-Robinson, and BWRS. The aim was to examine the capability of each model in predicting the state properties during CO<sub>2</sub> depressurization. They have also performed shock tube experiments on pure CO<sub>2</sub> and compared the results with models' estimations. Results illustrated that GERG-2008 matched well with experimental data, but the discrepancies enhanced as the temperature decreased. Brown et al. [107] have introduced a homogeneous relaxation model (HRM) to simulate the decompression of liquid CO<sub>2</sub> during pipe rupturing. The model was coupled with cubic EOS to describe the thermodynamic properties. Parallel, it was implemented by combining a semi-discrete Finite Volume Method and HLL (high-level language) approximate Riemann solver. The predictions were contrasted against experimental data from a CO<sub>2</sub> pipeline rupture for model validation. Outcomes showed a reasonable agreement with the data from the rupturing CO<sub>2</sub> pipeline.

The literature survey of the previous experimental and analytical studies demonstrated limited experimental data and analyses associated with the phase transition mechanisms during (1) the sudden release of liquid CO<sub>2</sub> from a container with a divergent cross-sectional area and (2) the release of CO<sub>2</sub> below the liquid level. Therefore, this experimental investigation seeks to quantify and gain better insight into explosive evaporation and its consequences by addressing these research gaps.

## 5 'Gzr gt lo gpvcnlugwr 'cpf 'b gj qf qm { "

The results and analyses presented in this thesis are based on the experiments performed on three setups. This chapter describes the research configurations and methods. Setup 1 is a double-membrane conical-shaped vessel installation for studying the release mechanism and the expansion wave behavior during liquid CO<sub>2</sub> depressurization. Setup 2 is a modified structure of Setup 1 to characterize the blast effects. A rectangular duct with the outlet pointing downwards represents a test section in Setup 3. It is intended to describe the phase transition mechanisms inside the duct as the liquid CO<sub>2</sub> is released from the bottom.

o . ) . . .

Most research in the published literature on the depressurization of liquified CO<sub>2</sub> was carried out in vessels with constant cross-sectional area, primarily using the one-membrane burst method. Unlike previous studies, the present work focuses on a divergent cross-sectional area and a double-diaphragm rupturing method. The double-membrane conical rig (see Figures 3.1 and 3.2) was designed for small-scale experiments investigating the sudden release of liquified CO<sub>2</sub> and the related rapid phase transition processes. It was a custom-made apparatus of a shock tube structure.

The double-membrane design comprised a high-pressure (HP) conical vessel and a medium-pressure (MP) slip-on flange. Two aluminum diaphragm sets with different thicknesses were used in this setup. One set was placed between the HP vessel and the MP flange. The other separated the MP flange from another slip-on flange on the top and opened to an atmospheric chamber. Besides, the conical vessel was fixed on t-slot framing aluminum construction and fastened with the two slip-on flanges and diaphragms by eight bolts.

The expanded mixture was released into an atmospheric chamber during CO<sub>2</sub> depressurization. It was an extension of aluminum bars above the test section covered with polycarbonate sheets on all six faces. Besides, it had a volume of 0.338 m<sup>3</sup> and a

one-side vent on the top. The polycarbonate sheets facilitated recording high-speed motion pictures for the flow evolution inside the chamber.

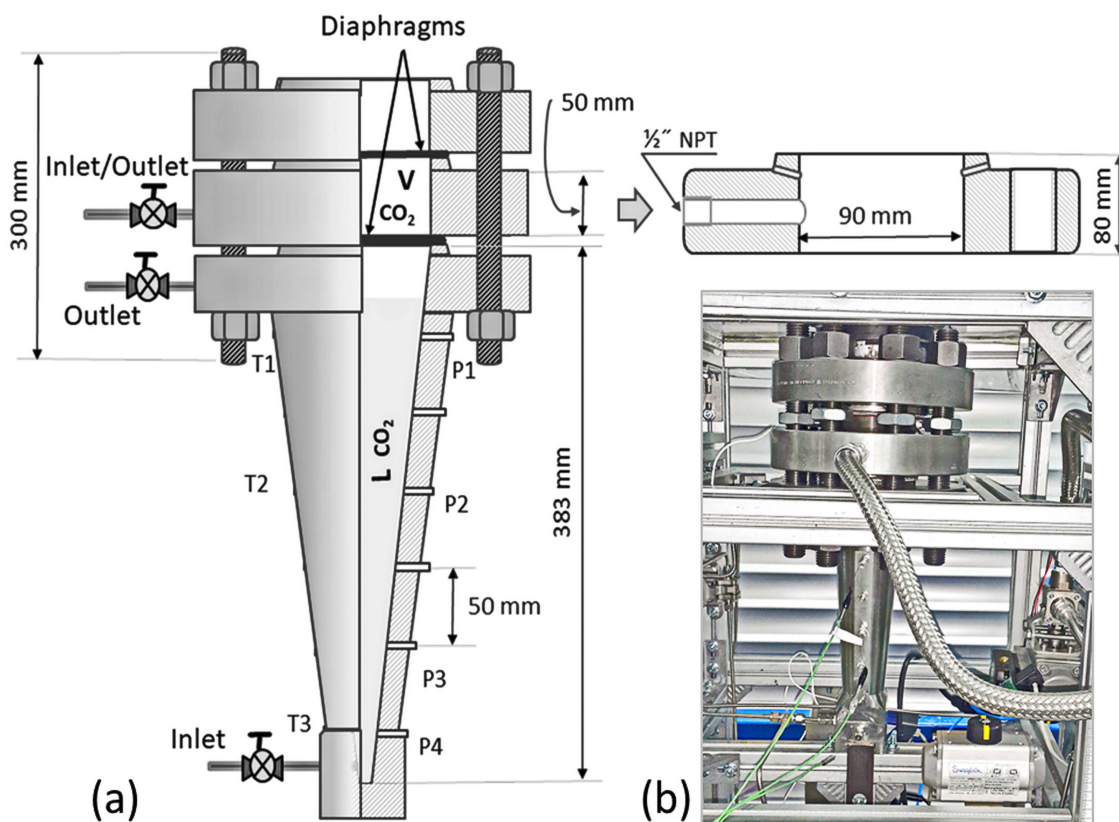
An auxiliary installation comprising a rectangular duct with a glass window was utilized as a level gauge to determine the liquid height in the solid walls HP vessel. The HP vessel and MP flange were filled separately from two industrial-graded gaseous and liquid CO<sub>2</sub> cylinders. One line supplied the vessel and the rectangular duct, and the other connected to the MP flange. The gaseous cylinder was outfitted with a regulator and a control valve, while the liquid CO<sub>2</sub> cylinder had a dip tube and two control valves. A photograph of the double-diaphragm conical arrangement is shown in Figure 3.1.



7 Figure 3.1: Double-diaphragm conical arrangement for the accidental release of liquid CO<sub>2</sub> from transport and storage.

### 3.1.1 AHP and MP sections

The HP vessel consisted of a stainless steel AISI 316 conical part and slip-on flange. The conical-shaped segment was welded to the flange to carry the diaphragm gaskets under load. The vessel had a volume of  $480 \cdot 10^3 \text{ mm}^3$  and a height of 383 mm. Its upper opening diameter was 90.7 mm, while the bottom diameter was 9.37 mm. The tapered bottom was reinforced with a cubic base to avoid excessive strain due to expansion waves propagating downwards. Also, the vessel had a wall thickness of 18,67 mm, an inclination of  $4^\circ$ , and an inner surface with an average roughness ( $R_a$ ) of  $3.2 \text{ }\mu\text{m}$ . It had a bottom inflow opening and outflow on the top. The vessel's sidewalls had twelve threaded holes, six for pressure sensors and another six on the opposite side for temperature sensors. Figure 3.2 shows the HP conical vessel and slip-on flanges shape and dimensions (a), and an image of the HP vessel fastened with the flanges (b).



7 0 =h Uh

The MP slip-on flange was fabricated from stainless steel ASME B 16.5 with a middle cylindrical section volume of  $510 \cdot 10^3 \text{ mm}^3$ . Additionally, it had an inlet/outlet opening equipped with a 1/2-inch flexible metallic hose attached to a pneumatic three-way valve. The hose enabled the mobilization of the slip-on flange for the diaphragm replacement. Two additional openings were machined to fit pressure and temperature sensors. The flange's upper and bottom surfaces had O-ring grooves to seal the diaphragms firmly. Another slip-on flange was placed on the top of the MP flange to press the MP diaphragm tightly. It was open to a chamber with atmospheric conditions.

### 3.1.2 Diaphragm description

Two diaphragm sets were firmly fastened between flanges to seal and separate the zones filled with CO<sub>2</sub> at different pressures. The diaphragm material and thickness are crucial features in shock tube functionality. In CO<sub>2</sub> depressurization experiments, aluminum has been used due to its quick crack propagation. The diaphragms were cut from blank aluminum sheets from Alfer Aluminum in circular shapes with three different thicknesses: 0.3, 0.5, and 0.8 mm. Depending on the operational conditions, the required diaphragm set was determined by an empirical procedure through a series of tests. The results demonstrated that the appropriate total thickness for the HP diaphragm should be 1.5-1.6 mm, while for the MP diaphragm, the thickness should be 1.4-1.5 mm. The diaphragm was set between two gaskets, categories of Tesnit BA-GL and Centurion, to seal the HP and MP sections firmly. The gaskets were made of glass, aramid fibers, and nitrile binders, certified for use with CO<sub>2</sub> at high pressure and temperature.

### 3.1.3 CO<sub>2</sub> supply and filling procedure

The high-pressure conical vessel and medium-pressure flange were separately filled from two industrial-graded cylinders containing gaseous and liquid CO<sub>2</sub>, respectively. The gaseous cylinder was equipped with a regulator and a control valve, while the liquid CO<sub>2</sub> cylinder had a dip tube and two control valves. The liquid volume fraction (LVF) was a crucial parameter for BLEVE analyses and can be calculated knowing the liquid level in



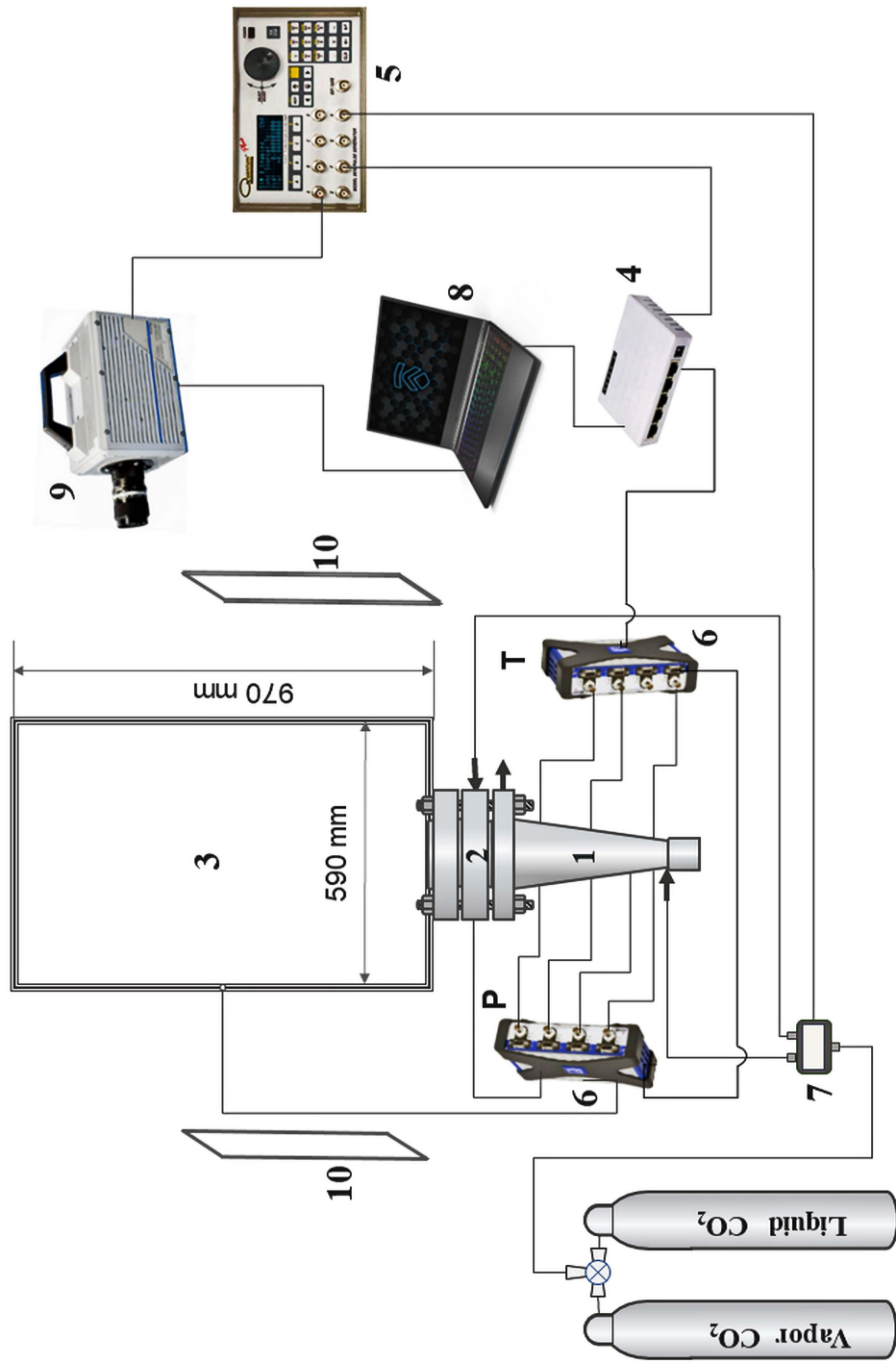
the conical vessel. As the conical vessel has a non-transparent wall, an auxiliary installation of a high-pressure rectangular duct with a glass window was employed as a level gauge. A pipe network connected the level gauge through four pneumatic valves. The first valve regulated the CO<sub>2</sub> flow from supply cylinders to the conical vessel's inlet. The second valve adjusted the flow between the conical vessel and the rectangular duct. The third and fourth valves controlled the vessel and duct outlet flow linked to a regulator and control valve before the CO<sub>2</sub> discharge.

### 3.1.4 Instrumentation

Four pressure transducers (Kulite XTM-190-2000G) were used to measure the pressure change inside the HP vessel. They were fitted on the vessel wall with distances between them 100, 100, and 50 mm from top to bottom. They have a pressure range of 0-14 MPa and a natural frequency of 410 kHz.

The pressure inside the MP flange was recorded using one sensor (Kulite XTM-190-1000G). It has an operating range of 0-7 MPa and the same natural frequency of 410 kHz. A (Kulite XTM-190-100G) sensor measured the overpressure after the release of CO<sub>2</sub> into the chamber. Besides, it was mounted in the middle of the vertical chamber's steel beam. It has a measuring pressure range of 0-0.7 MPa with a natural frequency of 95 kHz. All pressure transducers have a piezoresistive sensor as a sensing element and an accuracy of about  $\pm 1\%$ . An illustration of the setup showing all the described parts is presented in Figure 3.3.

Three K-type thermocouple temperature sensors were utilized to determine the temperature variations in the HP vessel during CO<sub>2</sub> decompression. They were installed on the opposite side of the pressure transducers. The thermocouples had a bead diameter of around 0.1 mm and a measuring accuracy of  $\pm 1$  K. The distance between two adjacent transducers was 150 and 100 mm from the bottom to the top. In addition, the data acquisition system (DAQ) included three HBM Quantum modules. Two HBM MX410 modules were used for pressure measurements and triggering, and one MX440B module was used for temperature measurements.



7 . . . 0 . . . =h# . . . Uh . . . # . . . = . . . U  
 . . . ="U) °j . . . h# . . . @ . . .

The modules transferred the sensors' recorded data through a hub to a computer.

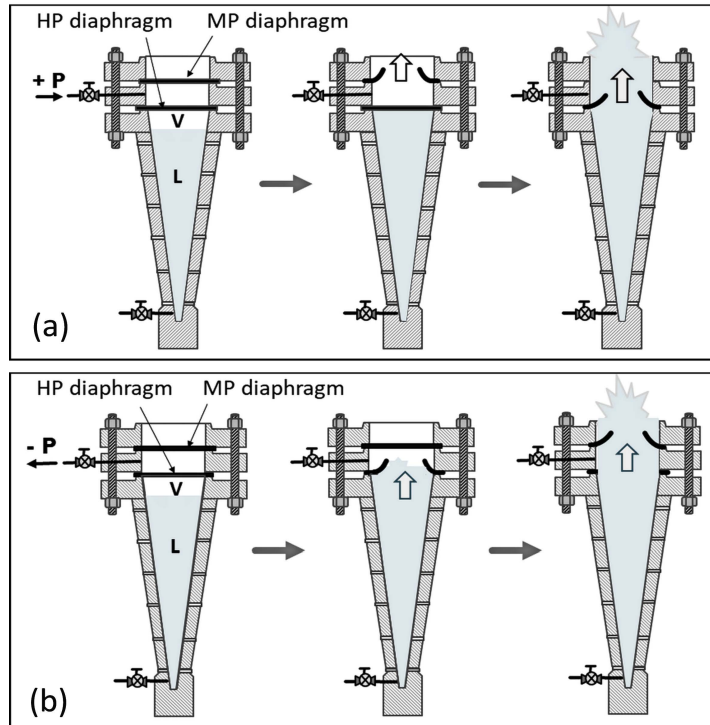
The development of the expanded mixture in the atmospheric chamber was captured using a Photron Fastcam SA-1 high-speed camera. The emergence and the evolution of multiphase release were captured with a sample rate of 5400 frames per second. Additionally, the chamber was illuminated from two opposite sides with three LED panels (one 80 W and two 38 W).

### 3.1.5 Release mechanisms

The experiments were carried out using two different opening methods. In turn, these methods resulted in different diaphragms' rupturing sequences. The diaphragms were ruptured by increasing or decreasing the pressure in the MP flange. Besides, the increase or decrease in the pressure was achieved by controlling the three-way valve for rapid pressure build-up or release from the MP flange. Figure 3.4 shows a drawing of the diaphragm rupture stages by increasing (a) and decreasing (b) the pressure in the MP section during CO<sub>2</sub> depressurization in the double-membrane arrangement.

The MP diaphragm ruptured when the pressure was increased in the MP flange, separating the MP and atmospheric flanges. Subsequently, the pressure inside the MP flange volume dropped rapidly to atmospheric. As a result, the HP diaphragm separating the MP flange and the HP vessel ruptured because of the increased pressure difference.

As the pressure decreased in the MP flange, the pressure rapidly reduced to atmospheric in the MP section. Consequently, the HP diaphragm ruptured. Then, the pressure built up again in the MP flange, and the MP diaphragm burst as the pressure difference between its sides increased.



7 drawing showing *Uh*

### 3.1.6 Experimental procedure

The experiments were conducted under the following conditions: the pressure inside the HP vessel ranged between 5.2 and 6.1 MPa, while the pressure in the MP flange was 2.5-2.9 MPa. The atmospheric chamber, HP vessel, and MP flange had identical initial temperatures varying between 16 and 23°C throughout the experimental campaigns.

The HP vessel was flushed three times with the gaseous CO<sub>2</sub> at 1 MPa before filling. The conical vessel and the rectangular duct were filled instantaneously with liquid CO<sub>2</sub> to a selected level pointed on the duct's glass window. Besides, the MP flange was mainly loaded with pressurized CO<sub>2</sub> gas. Then, the fluid inside the HP vessel was separated from the rectangular duct by closing the connecting control valve. Before the experiment started, a period of about 7 minutes was necessary for the liquid level to stabilize and reach liquid/vapor equilibrium in the test section.

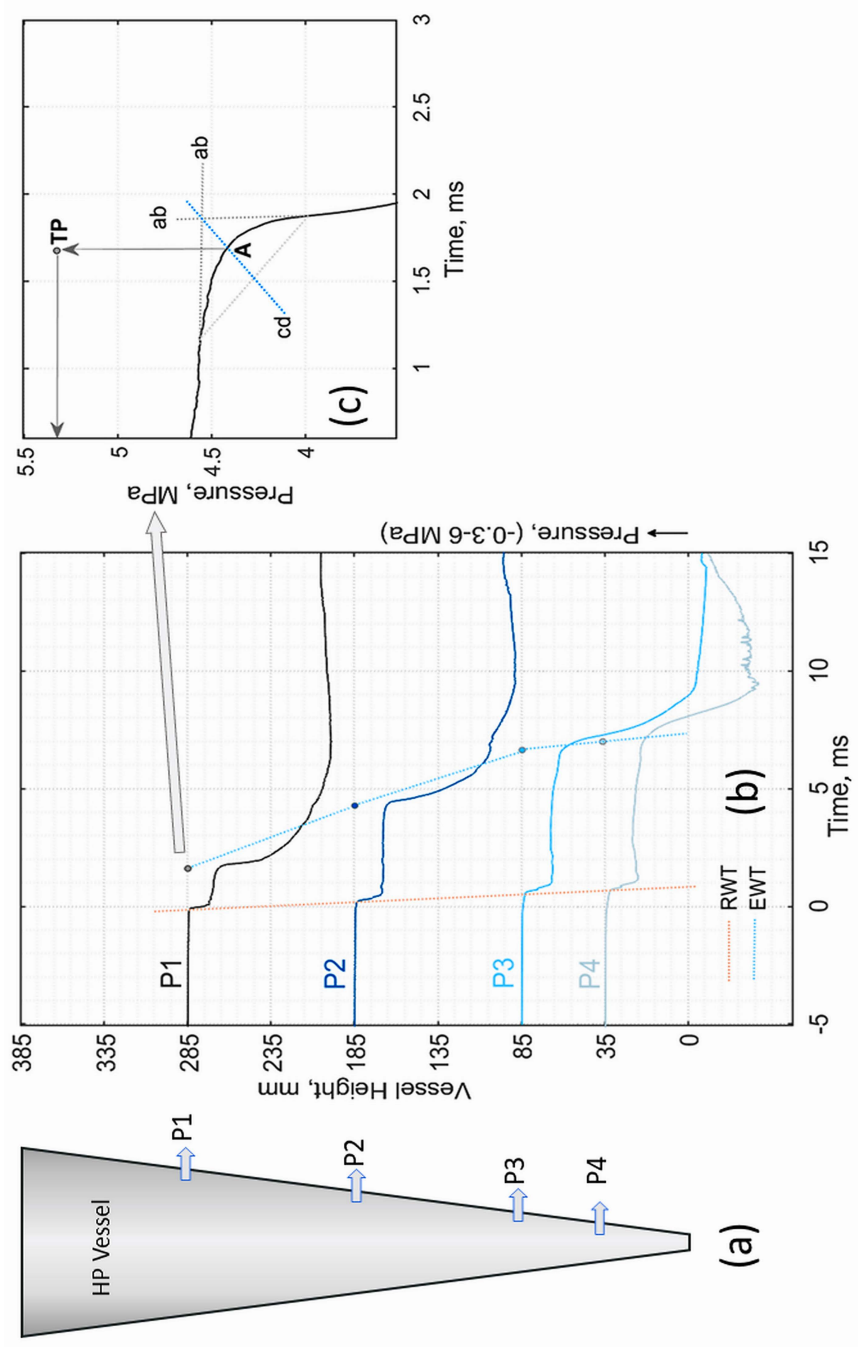
The experiments were initiated by concurrently triggering the 3-way valve, the DAQ system, and the high-speed camera. They were prompted by a transmitted signal of 5 V

from a Quantum (Composers 9500 series) pulse generator. After the diaphragms were ruptured by increasing or decreasing the pressure in the MP flange, an expansion wave traveled through the superheated liquid. Simultaneously, a shock wave propagated upwards into the chamber, followed by a multiphase mixture. The pressure and temperature recorded data were saved in appropriate formats and then analyzed in MATLAB. In addition, the high-speed videos were stored and processed in Photron FASTCAM Viewer Software and MATLAB.

### 3.1.7 Determination of expansion waves' velocities

The expansion waves' velocities were determined by a graphical method analyzing the pressure records at the specified position of each sensor. The pressure-time signals were drawn on the vessel's height-time scale, whereby each synchronized pressure-time line was started at the corresponding transducer position. The rarefaction wave trajectory passed through the location coincided with the first sudden pressure drop, while the evaporation wavefront corresponded with the second steep pressure drop. As shown in Figure 3.5, the evaporation wave route passed through the time points of the second sudden pressure change at a stationary height level.

The plateaus' duration on the initial pressure signals constantly changes along the vessel's height. So, a path-time diagram is established since all signals are synchronized. A close-up graph in Figure 3.5 (c) illustrates the time turning point on the pressure-time curve. The exact turning time point was found by drawing tangent lines on both sides of the curve's turn (lines ab). Then, the tangent lines' junction point was linked to the mid-point of the line connecting the tangency points (line cd). The time turning point (A) was specified as the intersection of this connecting line with the pressure-time curve. Then, point (A) moved to a stationary pressure transducer position to indicate the exact turning point (TP).



7

### 3.1.8 Image processing

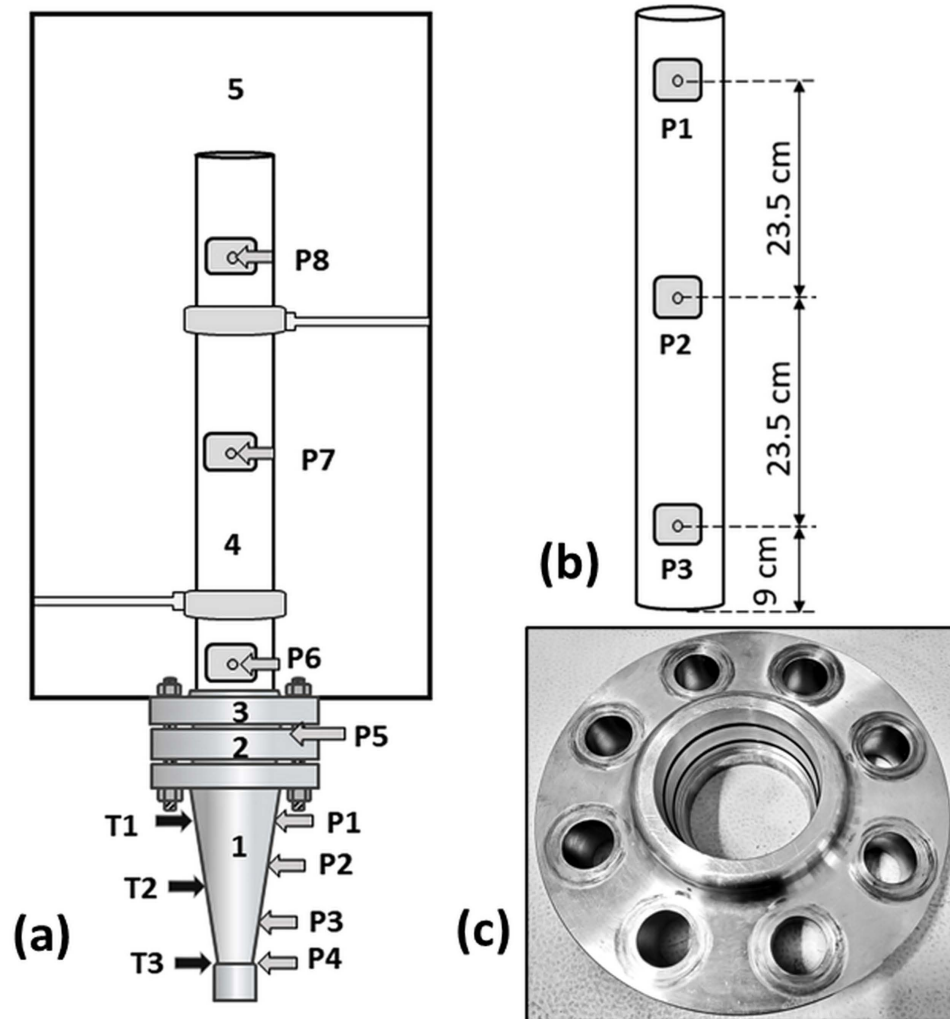
The fragments' velocities were calculated by processing the high-speed videos. The specified methodology is based on visually tracking the flying diaphragm locations along the chamber height. The velocity calculation started with determining the pixel-to-height conversion. Two measurements were required to resolve this ratio: pixel resolution and the chamber or tube dimensions in mm. In addition, video recordings speed in frames per second was needed to calculate the velocities. Diaphragm trajectory tracking was implemented at different heights using Photron FASTCAM Viewer Software. Pictorial schemes were produced by processing the video frames as cropped images with reduced resolution. For this purpose, the images of the video frames were transferred to MATLAB to be processed as a chronological sequence of cropped images, creating height-time plots.

○

For more accurate measurements and analysis, the blast wave overpressure should be determined side-on in the parallel direction of the shock and the released flow. Therefore, setup 1 was modified by adding a polycarbonate tube above the upper flange. The tube was the same diameter as the HP vessel opening and the MP flange's orifice. This design allowed the multiphase mixture to flow in a similar cross-section. The upper atmospheric flange was modified to avoid leakage between the flange opening and the tube's end and ensure a tight connection. Its cylindrical upper rim was machined as the tube could precisely fit in at a depth of 60 mm. Two O-ring grooves were machined into the flange's inner surface.

The transparent polycarbonate tube has a height of 650 mm and an inner diameter of 90 mm. It is equipped with three pressure transducers, which include Kulite XTM-190-100G and XTM-190-50G, to measure the blast wave overpressures during the explosion. The transducer Kulite XTM-190-50G has a pressure measuring range of 0-0.35 MPa and a natural frequency of 95 kHz. Figure 3.6 shows an illustrative drawing (a) of the setup

modified parts, a sketch (b) of the tube indicating the distances between transducers and an image (c) of the upper machined flange with side O-rings.



7. Figure 7. Schematic diagram of the experimental setup (a), sketch of the tube indicating the distances between transducers (b) and image of the upper machined flange with side O-rings (c).

The installation was intended for running CO<sub>2</sub> depressurization experiments on a rectangular duct pointing downwards. It comprised a rectangular duct fixed to the upper part of an aluminum structure. The contents were released into an atmospheric chamber placed directly below the duct. The chamber had dimensions of 0.50 m x 0.59



m x 0.97 m. It was covered with polycarbonate sheets to enable optical access. It has two vents on the top and bottom with a total area of about 0.01 m<sup>2</sup>.

### 3.3.1 The HP test section

The test section was a high-pressure rectangular duct made of stainless steel. It had a total volume of 191 cm<sup>3</sup>. Besides, the duct had borosilicate glass windows, enabling the capture of the boiling process inside. The duct opening incorporated a stainless steel tube height of 130 mm and was welded to a slip-on flange. The flange had an inner diameter of about 34 mm. Figure 3.7 shows a sketch of the test section with its dimensions and pressure and temperature sensors' locations.

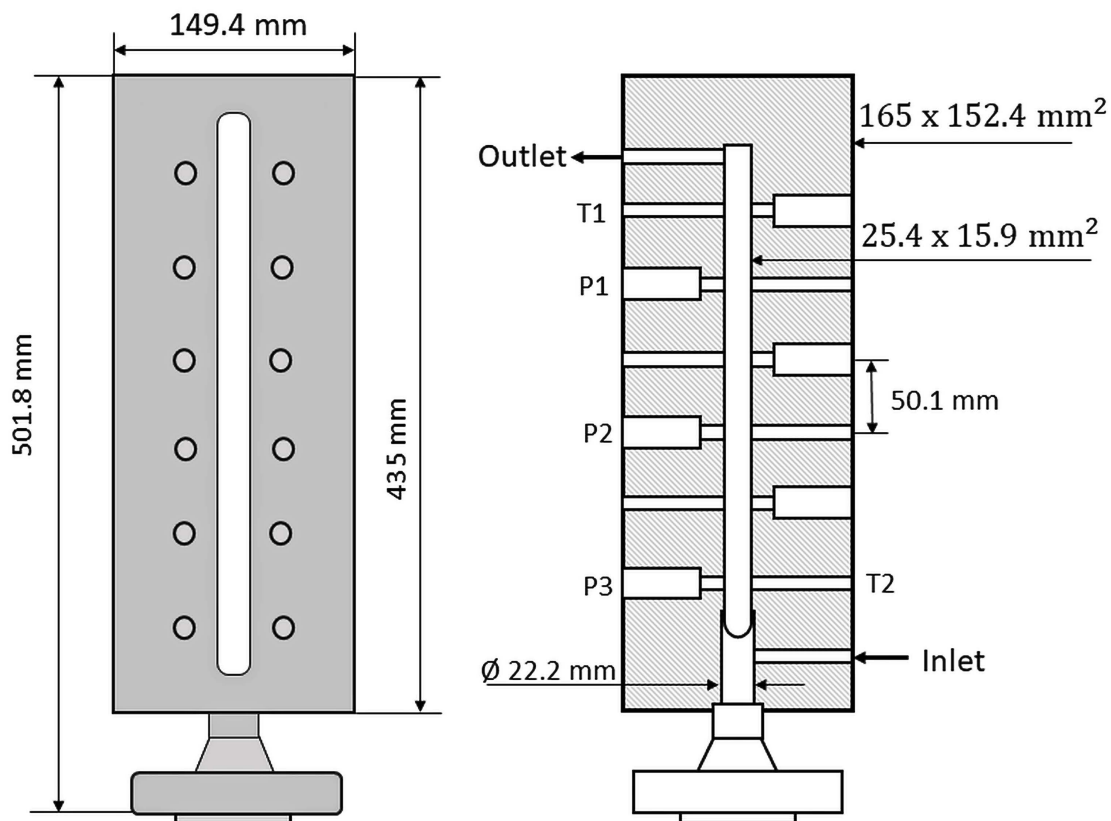


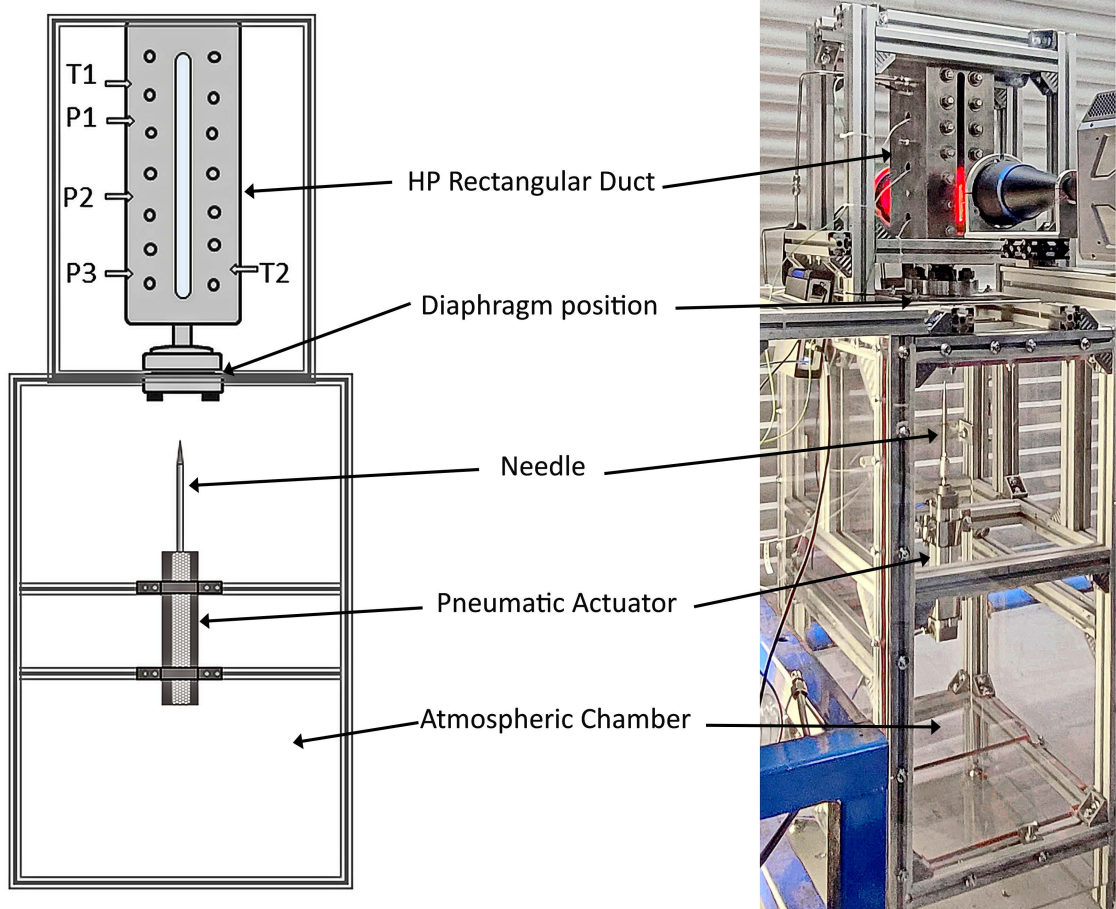
Figure 3.7. Sketch of the high-pressure test section with its dimensions and pressure and temperature sensors' locations.

The high-pressure duct was sealed with a diaphragm of eight circular aluminum foil slices. Each layer had a thickness of about 0.1 mm. Besides, the multi-layer diaphragm was set between two gaskets made of glass, aramid fibers, and nitrile binder. The

diaphragm with attached gaskets was tightly pressed at the duct's opening between two flanges with four bolts to avoid potential leakage.

### 3.3.2 Control equipment and test procedure

The duct was supplied from industrial-grade gaseous and liquid CO<sub>2</sub> cylinders outfitted with control valves, a dip tube for liquid, and a regulator for vapor. The duct was flushed with vapor CO<sub>2</sub> at 1 MPa before every experiment. It was then filled with liquid CO<sub>2</sub> to the desired level. The test was started about 10 minutes later to stabilize liquid/vapor equilibrium. A pneumatic cylinder actuator was affixed in the chamber's middle and precisely aligned with the duct's orifice. A sharp needle was fastened to a rod pneumatic cylinder actuator to puncture the diaphragm. Figure 3.8 shows a sketch and an image of the rectangular duct assembly defining its main parts and sensor positions.



Three Kulite XTM-190-2000G piezoresistive transducers were mounted alongside the duct sidewall to trace the pressure change during boiling in the duct. The transducers were positioned 100 mm from each other. Besides, they had a measuring range of 0-140 bar with a natural frequency of 410 kHz. Two K-type thermocouples were mounted on the top and bottom of the duct sides to measure the temperature. Overpressure in the chamber was traced utilizing Kulite XTM-190-1000G and Kulite XTM-190-100G piezoresistive transducers. They are mounted on the chamber's vertical side at 400 and 700 mm from the diaphragm location level. The data acquisition system (DAQ) consisted of three HBM Quantum module types, two MX410 and one MX440B, and connected to a hub. Figure 3.8 shows a photograph of the setup.

A Photron high-speed camera (Fastcam SA-1) captured the evolution of the multiphase jet emerging in the chamber space after the diaphragm ruptured. Two 80 W and 38 W LED panels were installed on the chamber's opposite sides to ensure sufficient lighting. The synchronous triggering of the pneumatic actuator, the DAQ system, and the high-speed cameras initiated the depressurization tests. A Quantum pulse generator composer 9500 was used to trigger the devices. The needle completely ruptured the diaphragm, and a multiphase flashing jet was observed in the chamber. The time histories of pressure and temperature and the captured high-speed videos were saved and then analyzed in MATLAB and Photron FASTCAM Viewer Software.

### 3.3.3 Shadowgraph imaging

The shadowgraph technique was applied to visualize the variation in the flow pattern during the phase transition inside the rectangular duct. This optical technique allows imaging changes in the refractive index according to the density variation of transparent media. The variations in the second derivative of the media's density govern the formed image. When the light rays pass through a test field, they are refracted, leading them to bend from their initial direction. Consequently, a characteristic lighting pattern is formed from the refractive deflection of a light ray, creating a light area on the captured plane, whereby the undeflected rays remain dark.

Shadowgraph installation incorporated Telecentric TC lenses and high-performance illuminator LTCLHP, fabricated by OPTO ENGINEERING. The illuminator and TC lenses were fastened on a metallic slap with clamps. Then, the illuminator was positioned on a plate attached to aluminum profiles. The illuminator's light beam covered the distance between pressure transducers P2 and P3 of the duct's height. It was an appropriate area (about 90 mm) to obtain a sharp image as the sharpness increased with a decrease in the beam's diameter. The TC lenses were installed on a 3D adjustable laboratory stand and aligned with the illuminator's focal point. Besides, Fastcam SA-Z high-speed camera was connected to the TC lenses for photography. An image of the shadowgraph arrangement is presented in Figure 3.9.

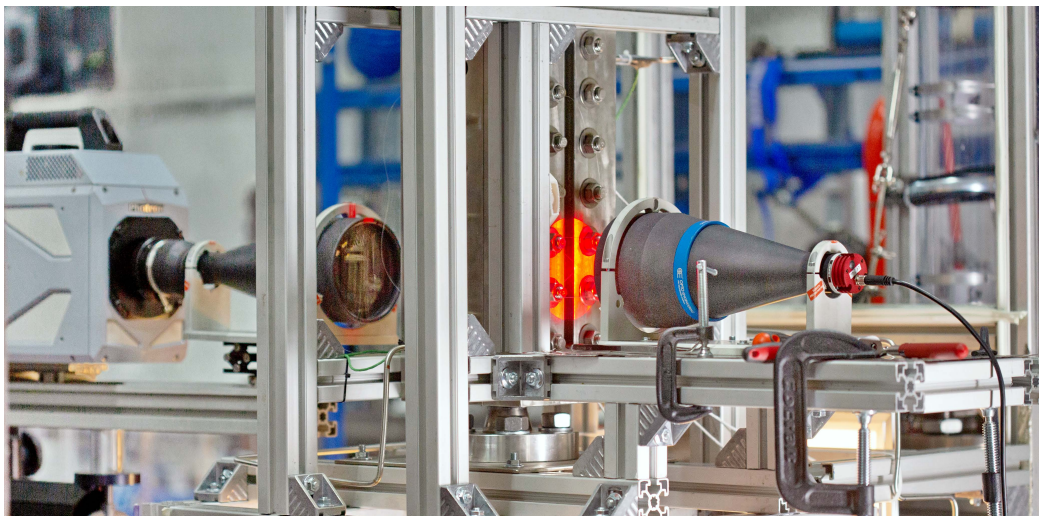


Figure 3.9. Shadowgraph arrangement for the experiment.

## 6 Reorganization of content

This chapter summarizes the most important results from four published and submitted papers comprising this research's fundamentals. The complete manuscripts of the journal articles and conference proceedings are included in Part 2.

h . . . k . . .

#\ . . .

### 4.1.1 Introduction

Depressurization of liquified CO<sub>2</sub> during a tank rupture is a major concern regarding the safe transport and storage of CO<sub>2</sub>. The failure of a container filled with liquified CO<sub>2</sub> could occur under different conditions, resulting in various explosion consequences. One of the critical issues is the container's rupturing method and position. This study describes a new experimental assembly wherein a high-pressure (HP) divergent cross-sectional vessel is sealed with double membranes. The membranes are separated by a slip-on flange, constituting a medium-pressure (MP) section. This design is intended for depressurization tests to investigate the waves' interaction with a constant area reduction in a vessel filled with CO<sub>2</sub> liquid in different contents. Even though a few studies have been performed with the double-diaphragm technique, the influence of rupturing method, i.e., increasing and decreasing the pressure in the MP section, has not been considered. The primary focus of this work is analyzing rupturing mechanisms and the resultant wave patterns to evaluate apparatus performance. It compares two membranes' rupturing techniques: Increasing and decreasing the pressure in the MP section and their effect on the waves' structures during phase transition.

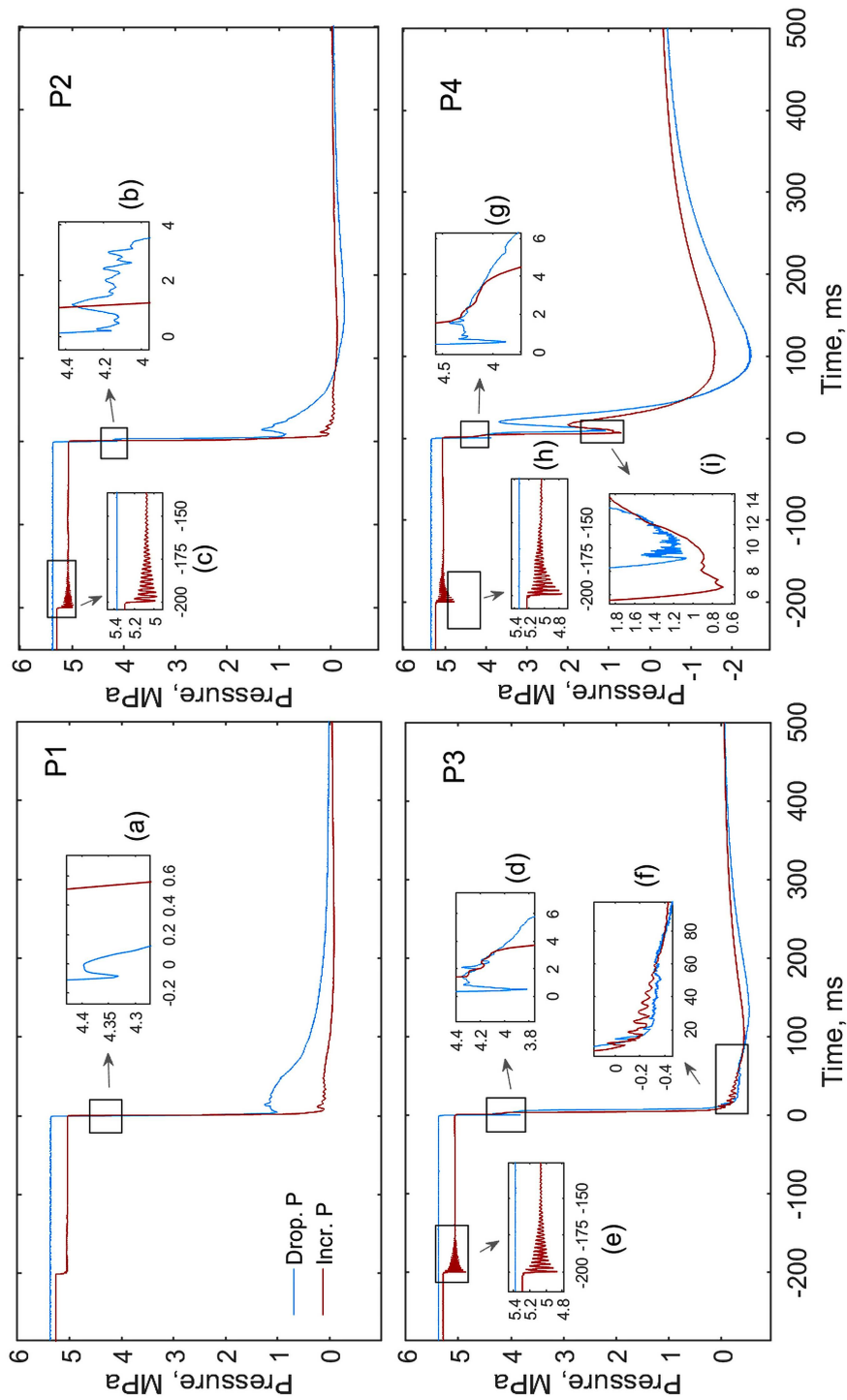
### 4.1.2 Results and Discussion

The experimental results were obtained using the setup described in section 3.1. This setup has three distinctive elements: A HP conical-shaped vessel, a slip-on flange that

signifies the MP section, and a double diaphragm rupturing technique whereby their burst could be done by increasing or decreasing the pressure in the MP section. The HP diaphragm separated the HP vessel from the MP flange, while the MP diaphragm separated the MP flange from atmospheric conditions. The experiments were conducted under the following requirements: the HP diaphragm set thickness was 1.5, and the MP diaphragm was 1.4 mm; Different liquid volume fractions (LVF) were 42 and 52%; the HP vessel's pressure was in the range of 5.2-5.5 MPa, and for MP flange was 2.6-2.8 MPa. The diaphragm rupturing mechanism and the wave patterns were analyzed based on the pressure histories and the high-speed video recordings of the released flow in the atmospheric chamber. The pressure measurements were collected from four positions inside the HP vessel, the MP flange, and the middle of the chamber.

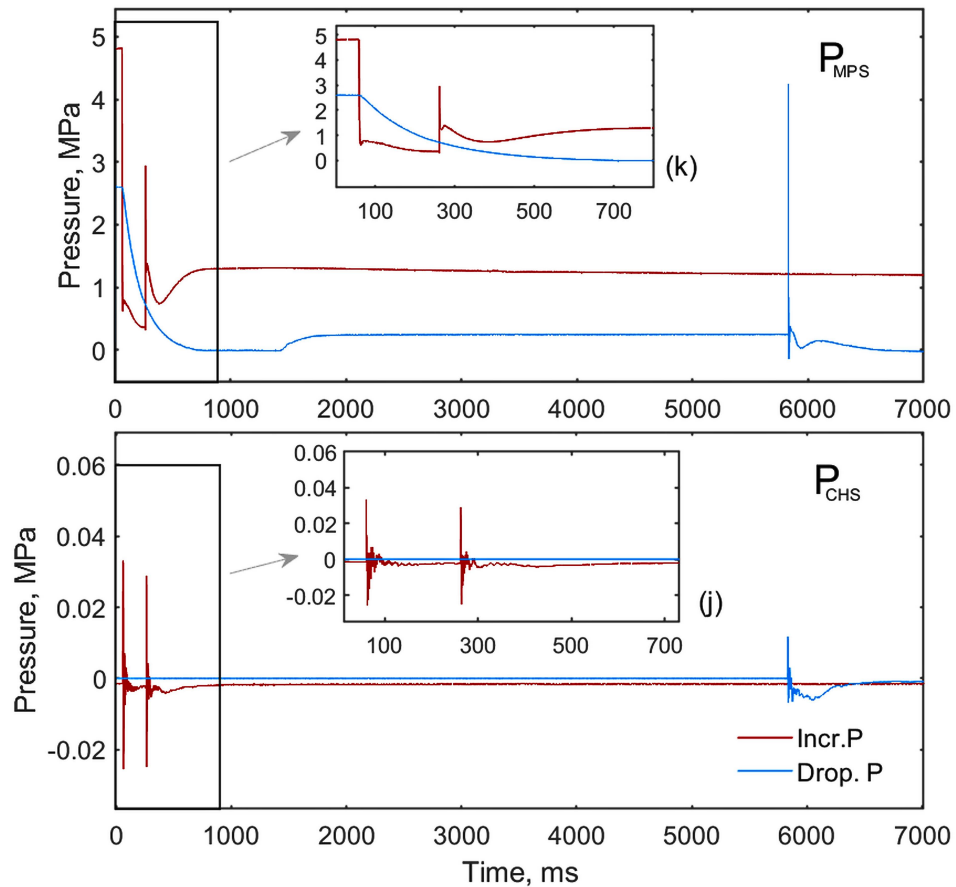
Figure 4.1 compares the effect of increasing and decreasing the pressure in the MP section on each pressure profile inside the HP vessel for LVF of 52%. As the pressure decreased in the MP section, the HP diaphragm ruptured because of the growth in the pressure difference between HP and MP sections. Subsequently, a shock wave moved upward, reaching the MP diaphragm, and reflected in the MP section. Meanwhile, the pressure in the MP section increased, leading to the rupture of the MP diaphragm. The decrease in pressure method is shown with a blue line (Drop. P). The shock wave reflection and the reflection from the expansion waves at the vessel's bottom as fluctuations can be observed in the close-up plots (a), (b), (d), (f), (g), and (i) in Figure 4.1.

The increase in the MP section pressure led to the rupture of the MP diaphragm, rapidly reducing the pressure to atmospheric. The HP diaphragm then burst due to the increased pressure difference between its sides. The oscillations in enlarged segments (c), (e), and (h) in Fig. 4.1 were due to the HP diaphragm's bulging after bursting the MP diaphragm. The increased pressure in the MP section led to the rupture of the MP diaphragm, rapidly reducing the pressure to atmospheric. The HP diaphragm then burst due to the increased pressure difference between its sides.



7 u @ 'h' . . . . . =h  
 . . . . . ) 'h' . . . . . Uho #  
 . . . . . 'h' 'h' 'h' 'h' '#'

The oscillations in enlarged segments (c), (e), and (h) in Fig. 4.1 were due to the HP diaphragm's bulging after bursting the MP diaphragm. The time delay between the bursting of HP and MP diaphragms was observed to be longer while applying the pressure decrease method. In this case, the reflected waves from the MP diaphragm impeded the incident shock progression and contact surface. Also, these reflections decelerated the pressure rebuild in the MP section. Figure 4.2 displays the MP section's pressure record and the overpressure at the middle of the chamber. It demonstrates the influence of two rupturing mechanisms on the duration between the diaphragm rupturing. The enlarged segments (k) and (j), in Figure 4.2, show the duration between diaphragm rupturing at the onset of the depressurization process.



7     h     U h     h<sub>Uho</sub>  
 h<sub>#=0</sub>     #\     @ h'  
 )     h'     U h'

The multiphase flow characteristics were dependent on whether the diaphragm was removed entirely. As the pressure difference between the diaphragm surfaces increased, it bulged, weakening the circular edge.



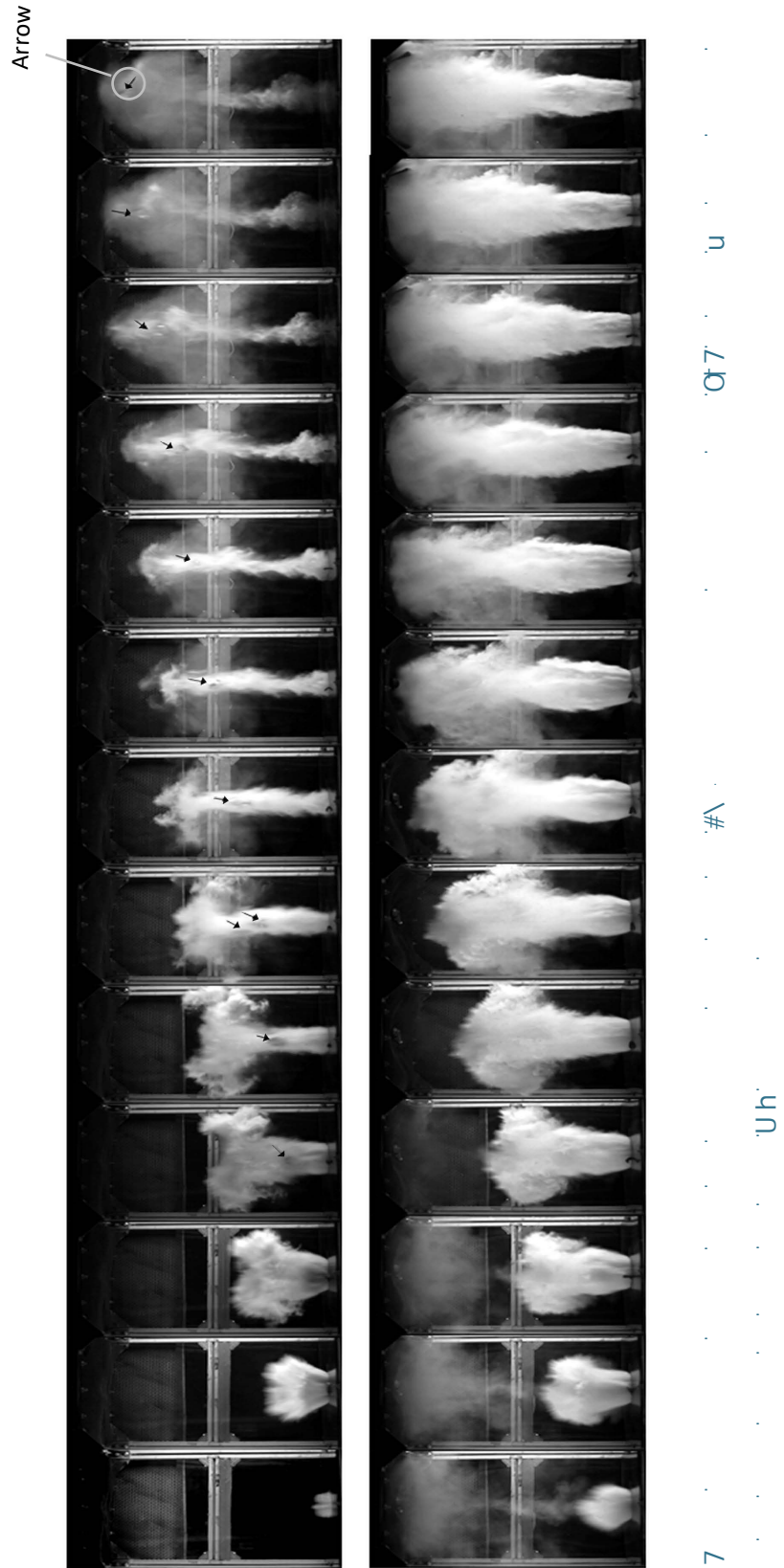
Consequently, it cracked in one location then the crack propagated further along the circumference. The circular under-pressure diaphragm part was wholly cut off when the increasing pressure method was used. In this case, the two-phase mixture was instantly released into the atmospheric chamber without hindrance. However, after decreasing the pressure method was applied, the diaphragm was cut circularly, but a small section was left. Accordingly, the multiphase mixture emerged inside the chamber as a thin jet increasingly developing to fill the entire outlet orifice. Figure 4.3 illustrates two series of cropped images from the high-speed video of CO<sub>2</sub> depressurization by increasing the pressure in the MP section for LVF of 52%.

The top images' sequence (a) shows the multiphase flow evolution and the flying MP diaphragm. The bottom series (b) display the multiphase flow development after the HP diaphragm ruptured. The time step between the frames in each series was 0.56 ms. The calculated MP diaphragm velocity from the captured videos was 118–123 m/s, while for HP diaphragm was 127–132 m/s.

#### 4.1.3 Conclusion

The experimental results demonstrated the followings:

- The vessel's rupture mechanism by increasing the pressure in the MP section showed no reflected compression wave that could cause complexities in the MP or HP sections.
- Decreasing the MP section pressure resulted in the compression waves being reflected into the vessel, slowing evaporation wave propagation. This behavior, in turn, reduced the phase transition rate.
- By increasing the MP section pressure, the rupturing mechanism demonstrated more reliability and simplicity than decreasing the pressure method. The wave pattern becomes clearer with fewer reflections into the HP section.



h " ' - . . . . .  
 . . . . . #\ . . . . .

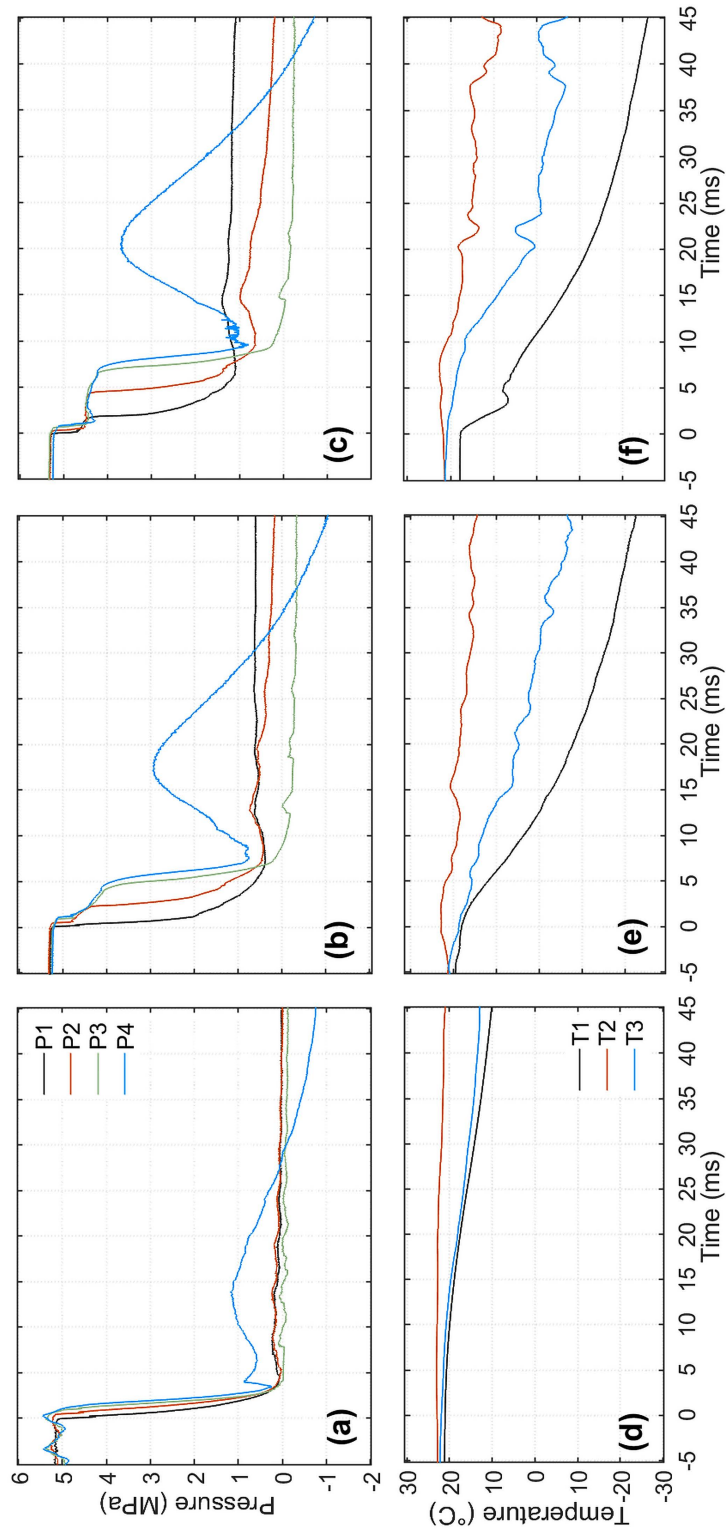
#### 4.2.1 Introduction

For setup 1, described in section 3.1, the increased MP section is established as a more controllable rupturing mechanism. This study presents experimental results and analyses of expansion waves' characteristics during liquid CO<sub>2</sub> depressurization in a divergent cross-sectional vessel. It focuses on the velocities of the rarefaction and evaporation waves and their interactions with conical-shaped geometry at different liquid volume fractions (LVF). Additionally, it discusses the divergent cross-section effect on evaporation wave characteristics by contrasting the results with previous results from tests in duct with a constant area. This research's approaches are analyzing the velocities along vessel three regions from the pressure records and defining the degree of superheat during isentropic expansion.

#### 4.2.2 Results and Discussion

Fig. 4.4 illustrates pressure and temperature histories inside the HP vessel during 50 ms of CO<sub>2</sub> depressurization. The experiments' temperature was (19–23 °C) in all sections, while the pressure was 2.6–2.9 MPa in the MP section, 5.3–5.6 MPa in the HP vessel, and atmospheric in the chamber. The rupture of the HP diaphragm is indicated by time 0. The LVFs were 0% in graphs (a, d), 62.5% in (b, e), and 96.4% in (c, f). The pressure sensor (P1–P4) are positioned at 285, 185, 85, and 35 mm from the vessel's bottom, and the temperature sensors (T1-T3) are 285, 185, and 35 mm.

Figure 4.4 shows that, after the HP diaphragm ruptured, a steep decline in the pressure was observed to the liquid's metastable state pressure. Except (a) with 0% LVF, this state is characterized by a steady pressure reduction that sharply decreased when the evaporation started. The lines' sudden turns signify the phase transition commencement, where the evaporation wavefront propagated downward, leaving behind a two-phase mixture moved upwards.



7 . . . k . . . . . =h . . . . . # . . . . . 07

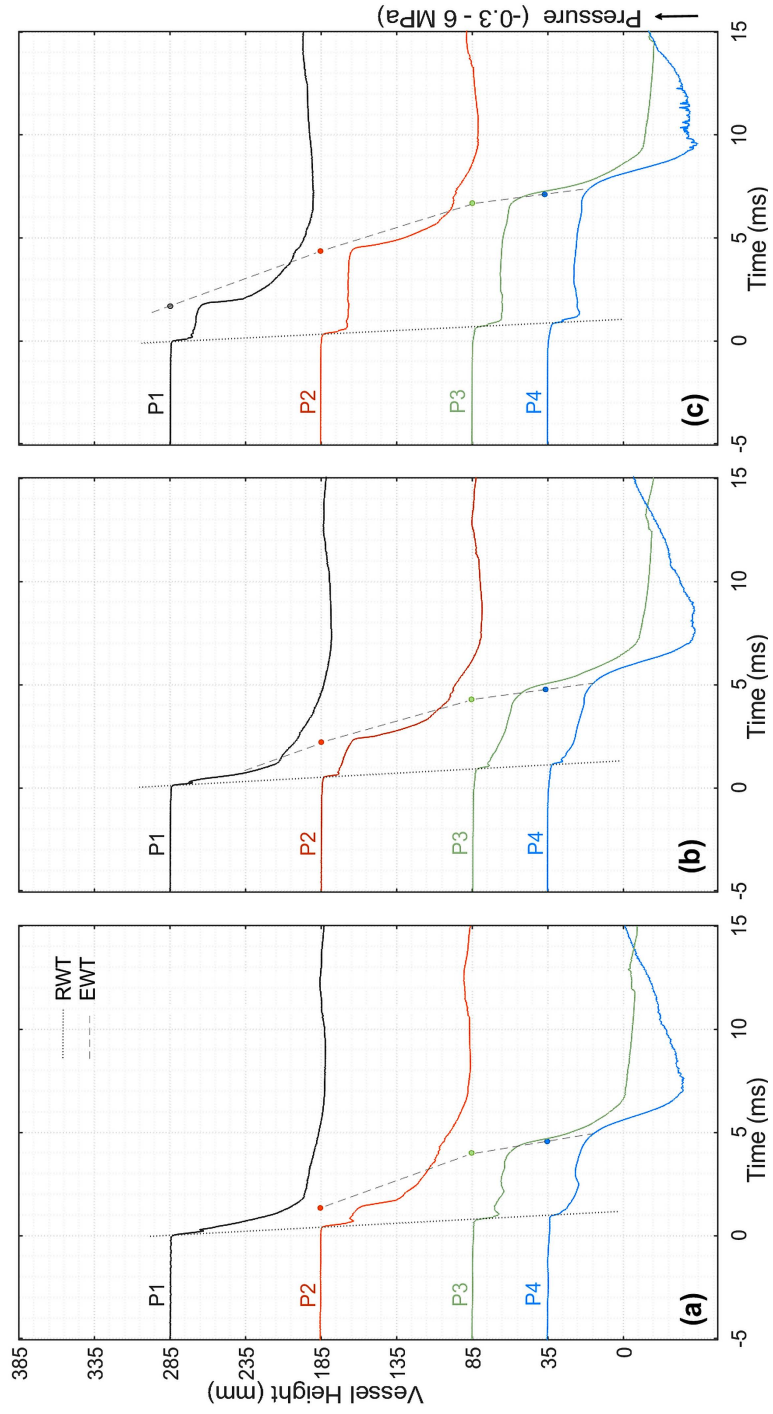
Chaves [81] and Simões-Moreira [11] have described analogous observations.

As the rarefaction wave moved through the vapor at about the local sound speed, it reached the vapor/liquid interface and was partially reflected. This behavior resulted in a minor pressure increase observed on the P1 lines. The duration of superheated liquid in a metastable state lengthened as the LVF increased. It can be observed in (b) and (c) Figure 4.4 that the pressure line profiles shift from a slight decrease (62.5% LVF) to almost plateaus (96.4% LVF).

A distinct behavior was seen in the bottom pressure line P4, whereby the rapid decline caused oscillations and a significant pressure increase. The curve P4 amplitudes increased with increasing the LVF from (a) to (c). This behavior could be due to the upward movement of the two-phase mixture's part after the sudden drop in the pressure. As a result, the pressure was rebuilt, then as the two-phase mixture propagated upwards again, the pressure peaked and gradually decreased.

The rarefaction and evaporation wave velocities were determined graphically by drawing the synchronized pressure-time signals on the vessel height-time scale. Thus, the pressure-time curves should start corresponding to the transducer positions. The detailed method description is given in section 3.1.7. Figure 4.5 exemplifies pressure-time traces drawn on the vessel height-time scale in 20 ms of liquid CO<sub>2</sub> depressurization for LVFs of 35.1, 62.5, and 96.4%.

Table 1 summarizes calculated rarefaction and evaporation wave velocities in the three vessel's height zones. It can be seen that the evaporation wavefront velocity increased as it moved toward the vessel bottom. The rarefaction wave velocity is dependent on the liquid height in the vessel. Its speed increased as it propagated through the vapor/liquid interface, and afterward, it was affected by the reflections from the vessel's bottom.



07

#

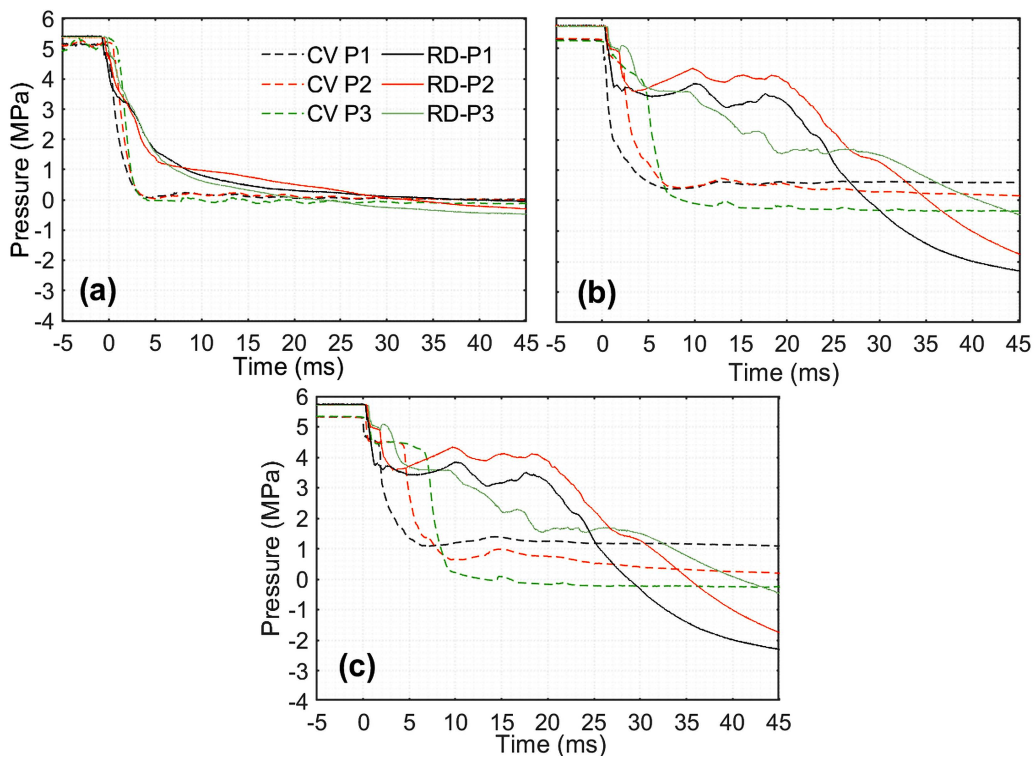
h  
k+u  
-+u

7

U

Liquid Height (mm)	Cross-section (mm <sup>2</sup> )	LVF (%)	Rarefaction Wave Velocity (m/s)				Evaporation Wave Velocity (m/s)		
			Height region (mm)						
			285-185	185-85	85-35	Average	285-185	185-85	85-35
134.1	277.5	35.1	199.4	291.6	249.1	246.7	–	37.6	88.9
239.4	880.4	62.5	244.3	293.2	245.3	260.9	46.3	47.6	107.1
369.2	2093.9	96.4	300.0	320.0	240.0	286.7	37.8	42.7	111.6

The influence of divergent cross-section geometry on evaporation wave characteristics was analyzed by comparing the recent results with the previous experiments in a rectangular duct with a constant area by Hansen [56]. Figure 4.6 compares the pressure records during liquid CO<sub>2</sub> depressurization in the rectangular duct (RD) and the conical vessel (CV). The RD and CV LVFs were equally 0% in (a), 100% and 62.4% in (b), and 100% and 96.4% in (c), respectively.



7

h

#\

k)

#1 07

Pressure sensors were at 31, 81.8, and 132.8 mm from the top of the RD. While in the CV, they were located at 98, 198, and 298 mm from the top. The pressure profiles show a more rapid evaporation process in the CV than in the RD. The pressure lines' fluctuations in the RD in Figure 4.6 (b, c) demonstrate that the two-phase mixture propagated non-spontaneously. As the expanded two-phase mixture moved toward the exit, this might imply choked flow due to the exit's small cross-section.

Because the evaporation wave velocity is influenced by the degree of superheating (DOS), a comparison was drawn between the DOS in RD and CV tests as specified by Simões-Moreira [11]. The calculated properties in the metastable state following isentropic expansion, the calculated velocities, and the pre-ruptured saturated state properties are shown in Table 4.2. The table compares the tests with LVFs of 100% for the RD with 96.4% for the CV. Calculations show that the liquid expanded with higher DOS in the CV tests than in the RD.

Table 4.2. Comparison of properties in the metastable state following isentropic expansion, the calculated velocities, and the pre-ruptured saturated state properties for the RD and CV tests.

Property		Rectangular Duct	Conical Vessel
Saturated State	Pre-rupture pressure $h_0$ / (Mpa)	5.8	5.4
	Temperature $\psi$ / (K)	294	290.3
	Density $\rho$ / (kg/m <sup>3</sup> )	764.4	801.3
Upstream Metastable State	Metastable limit pressure $h$ / (Mpa)	5.0	4.4
	Density $\rho$ / (kg/m <sup>3</sup> )	756.7	794.3
	Maximum EW velocity $u$ / (m/s)	38.1	111.6
	Minimum EW velocity $u$ / (m/s)	38.1	37.8
	Enthalpy $h$ / (kJ/kg)	257.6	245.4
	DOS	0.14	0.23

#### 4.2.3 Conclusion

- The analysis of rarefaction and evaporation wavefront velocities in the conical vessel was performed based on the pressure records at three different height zones. Results demonstrated that the evaporation wavefront velocity increased



as it propagated downward toward a reduced cross-sectional area. It also increased with an increase in LVF.

- A considerable difference in the behavior of the rarefaction and evaporation during CO<sub>2</sub> depressurization between the rectangular duct and conical vessel:

The rapidly expanded two-phase flow in the RD was choked due to a small exit cross-section. On the contrary, the two-phase flow in the CV propagated towards a constantly increased cross-sectional area.

The DOS after the isentropic expansion was higher in the CV experiments than in the RD, leading to significant differences in the properties of upstream flow.

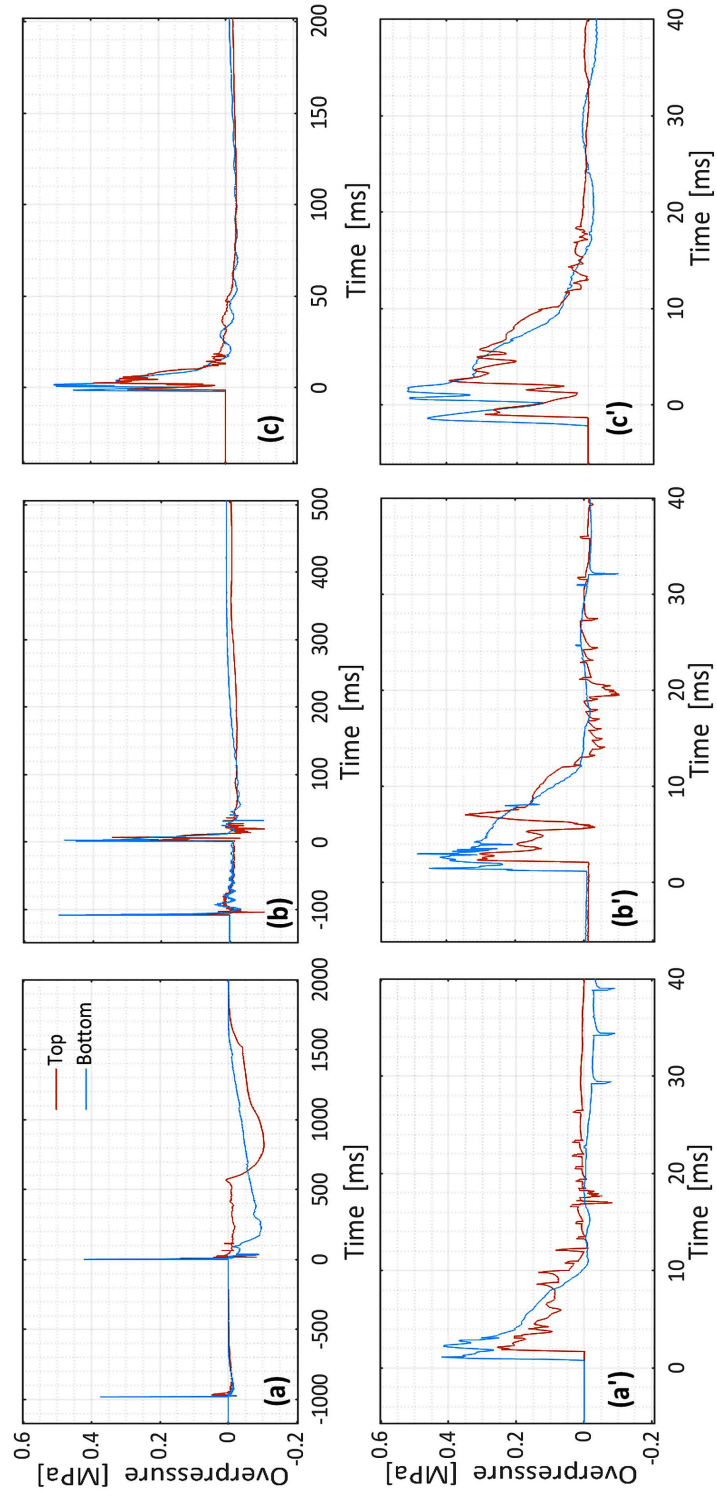
h # " W O #\ d  
 ) . . # o t .

#### 4.3.1 Introduction

This research deals with releasing liquid CO<sub>2</sub> from a double-membrane conical-shaped installation to a tube with atmospheric conditions. The aim was to characterize the blast wave consequences following CO<sub>2</sub> explosive evaporation. It focused on the measured peak overpressure, corresponding calculated impulse, and fragment velocity. Furthermore, the overpressures were measured alongside a polycarbonate tube attached to the top of the double-membrane conical apparatus. The setup description is given in section 3.2. A high-speed camera was utilized to capture the evolution of ruptured diaphragms and the released multiphase mixture inside the tube. The fragments' velocities and resultant kinetic energies were determined based on the recorded high-speed video analysis.

#### 4.3.2 Results and Discussion

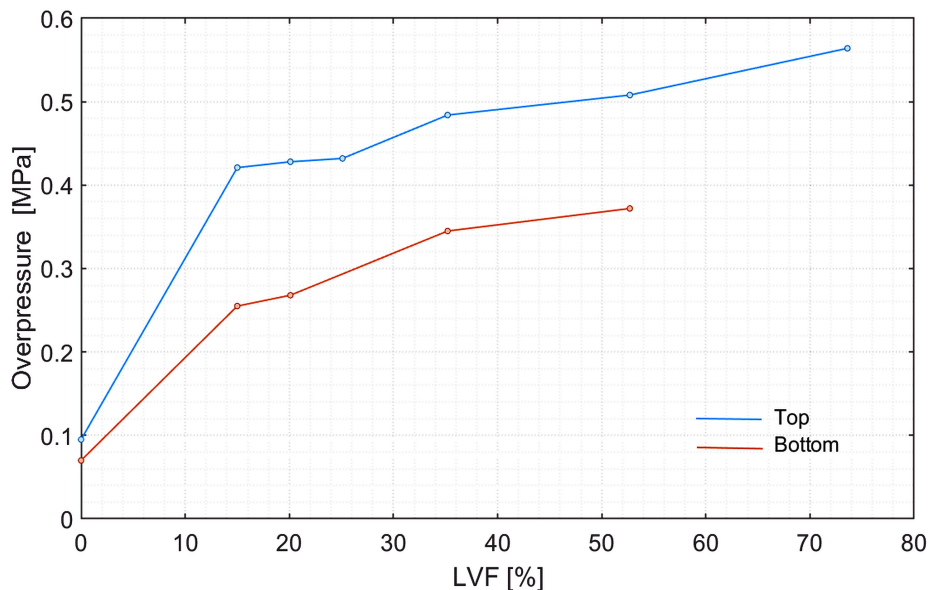
Figure 4.7 illustrates the measured peak overpressure in the tube for LVFs of 15, 35.2, and 52.7% in graphs (a), (b), and (c), respectively. The overpressures were measured at 180 mm (bottom sensor) and 650 mm (top sensor) from the HP diaphragm position.



7 . . . U . . . . . #\ . . . . . 8

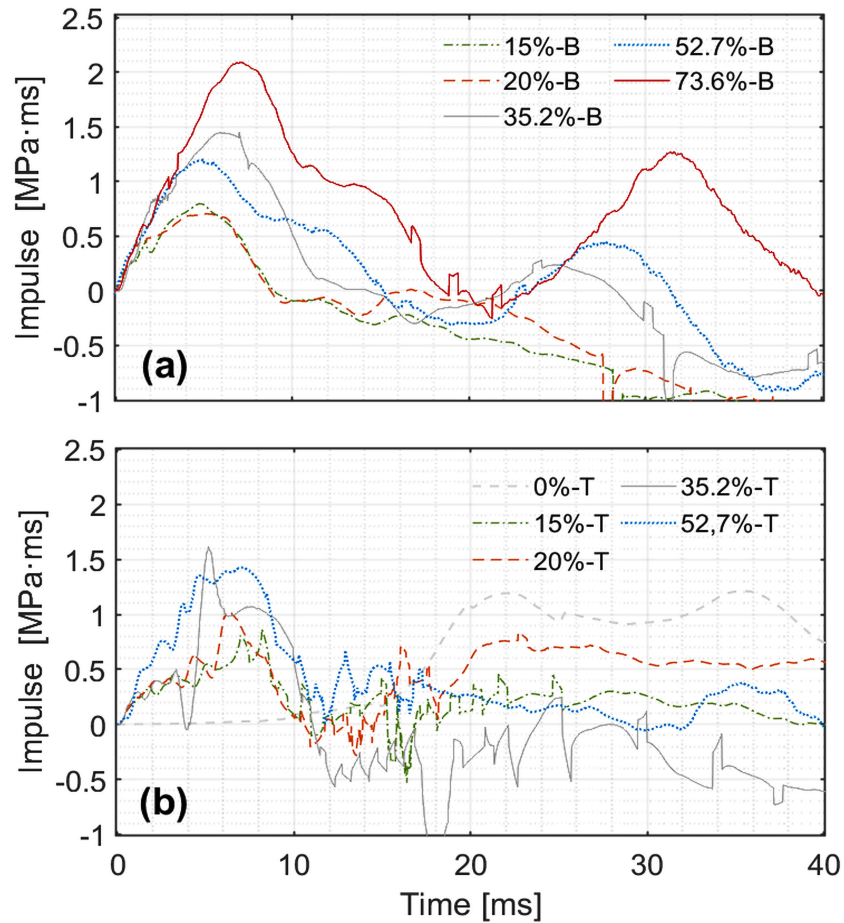
Time zero indicates the rupture of the HP diaphragm. The first peak overpressure is the blast wave following the MP diaphragm rupture, and the second is after the HP diaphragm rupture. Graphs (a'), (b'), and (c') are enlarged segments of the second peak overpressure during 40 ms.

In Figure 4.7 (a'), (b'), and (c'), the leading positive phase comprises two overpressure peaks. The first peak arose from expanded headspace vapor, while the subsequent higher peak was produced due to liquid evaporation. Additionally, as the LVF increased, the time interval between MP and HP diaphragms' ruptures decreased, and measured peak overpressure increased. Figure 4.8 presents the relationship between the measured overpressures and the LVFs.



7 u . . . . .  
 . . . . . #\ . . . . .

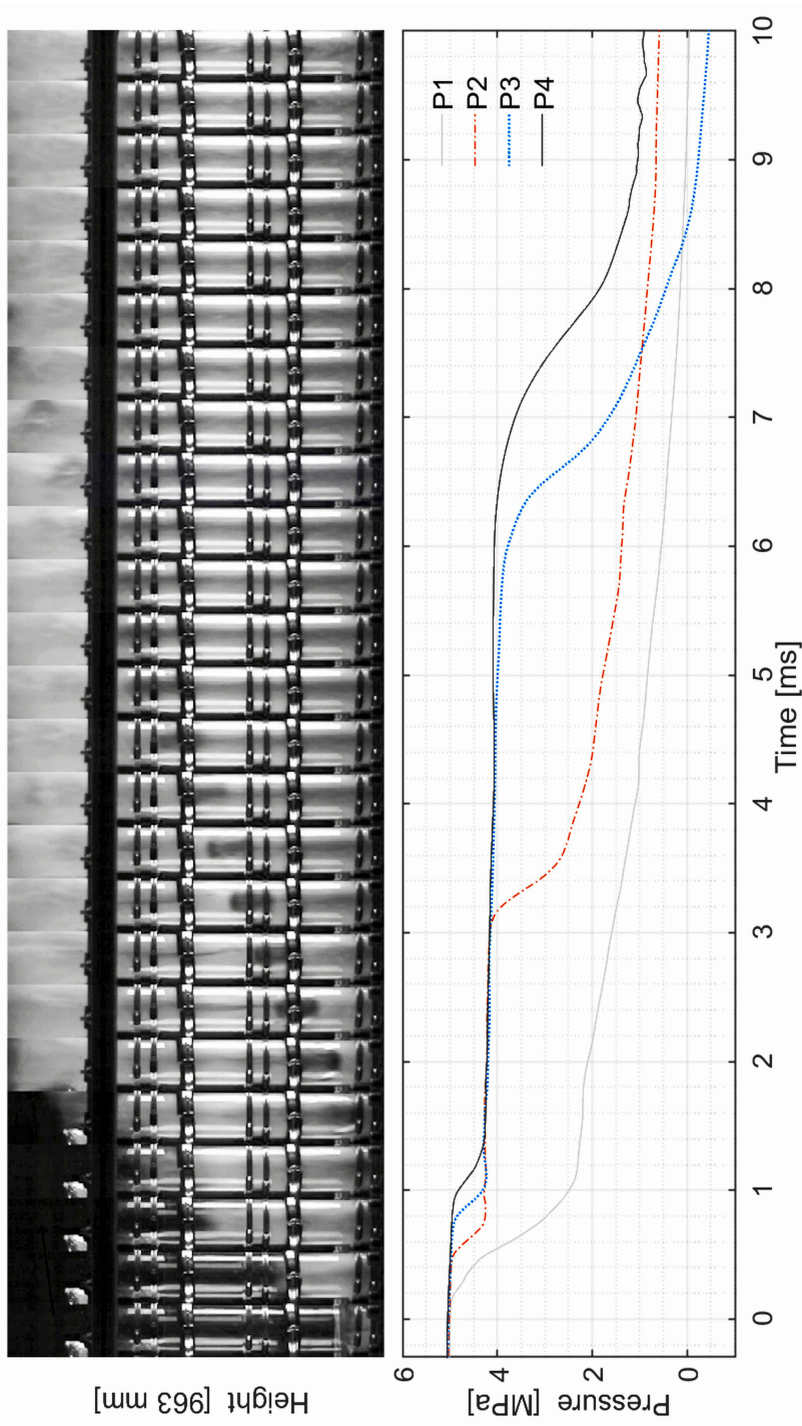
Figure 4.9 shows the calculated impulse over 40 ms. It demonstrates the explosion energy portion that could be transferred to the surrounding structures. Graphs a and b correspond to the impulse calculated from pressure records at the bottom and top transducers. Figure 4.9 (a) shows that the line with 35.2 % LVF has a higher peak than 52.7% in the first positive phase. However, they crossed each other, and the line with 52.7% peaked higher in the second positive phase.



7 Figure 4.10 Impulse histories for CO<sub>2</sub> depressurization with different LVFs

Opposite behavior was observed in the same figure graph (b), especially lines with 0% and 15% LVF. The fact that a larger volume of expanded vapor headspace with lower LVFs and the following rapid expansion of the multiphase mixture may have led to this behavior.

Fragments velocities were determined by analyzing the high-speed videos that captured the released multiphase flow and ruptured diaphragms in the tube. The videos were recorded at 7200 (fps) and a 256 x 1024 pixels resolution. The diaphragm paths were traced along the tube height with 0.94 mm/pixel. Fig. 4.10 displays a sequence of cropped images (top) during 10.4 ms CO<sub>2</sub> depressurization with LVF of 35.2 % and synchronous pressure histories (bottom). The images show the trajectory of the HP diaphragm inside the tube, and they have a time step of 0.42 ms.



7 "0 #\n07

The collected fragments were weighed to calculate the propelled diaphragms' kinetic energy. The results from velocities and kinetic energy calculation are presented in Table 4.3.

*u* = "u" =h

LVF, %	Weight, g	Velocity, m/s	Kinetic energy, J
73.6	27.9	121.1	204.9
52.7	28.2	109.3	168.6
35.2	28.5	112.0	177.1
25	28.5	94,6	127.4

As shown in the table above, the fragments' velocities and corresponding kinetic energy increased with an increase in LVF. In addition, fragment velocities were computed based on the formula suggested by Baum [73-76]. The equation offered the correlation between the fragment velocity and the excess heat stored in the liquid before the explosion. Comparing the results from Baum's calculation method with those based on the experiments demonstrates conservative discrepancies. For instance, for the rupture of a CO<sub>2</sub> vessel with 52.7% LVF and pre-ruptured conditions 5.58 MPa and 292 K, Baum's equation gave 93.4 m/s, less by 16 m/s than the value shown in Table 4.3. The obtained fragment velocities and kinetic energies from experimental results show that these fragments are hazardous.

#### 4.3.3 Conclusion

- Measured overpressure analysis demonstrated that the rapid evaporation considerably affected the leading overpressure positive phase. The overpressure's positive phase had two peaks: an early lower peak due to expanded headspace vapor and a second higher peak resulting from liquid evaporation.

- The peak overpressure, the propelled diaphragm's velocity, and the corresponding kinetic energy increased with increasing LVF.
- A comparison of the calculated velocities based on experiments with Baum's model for initial fragment velocity showed good agreement.

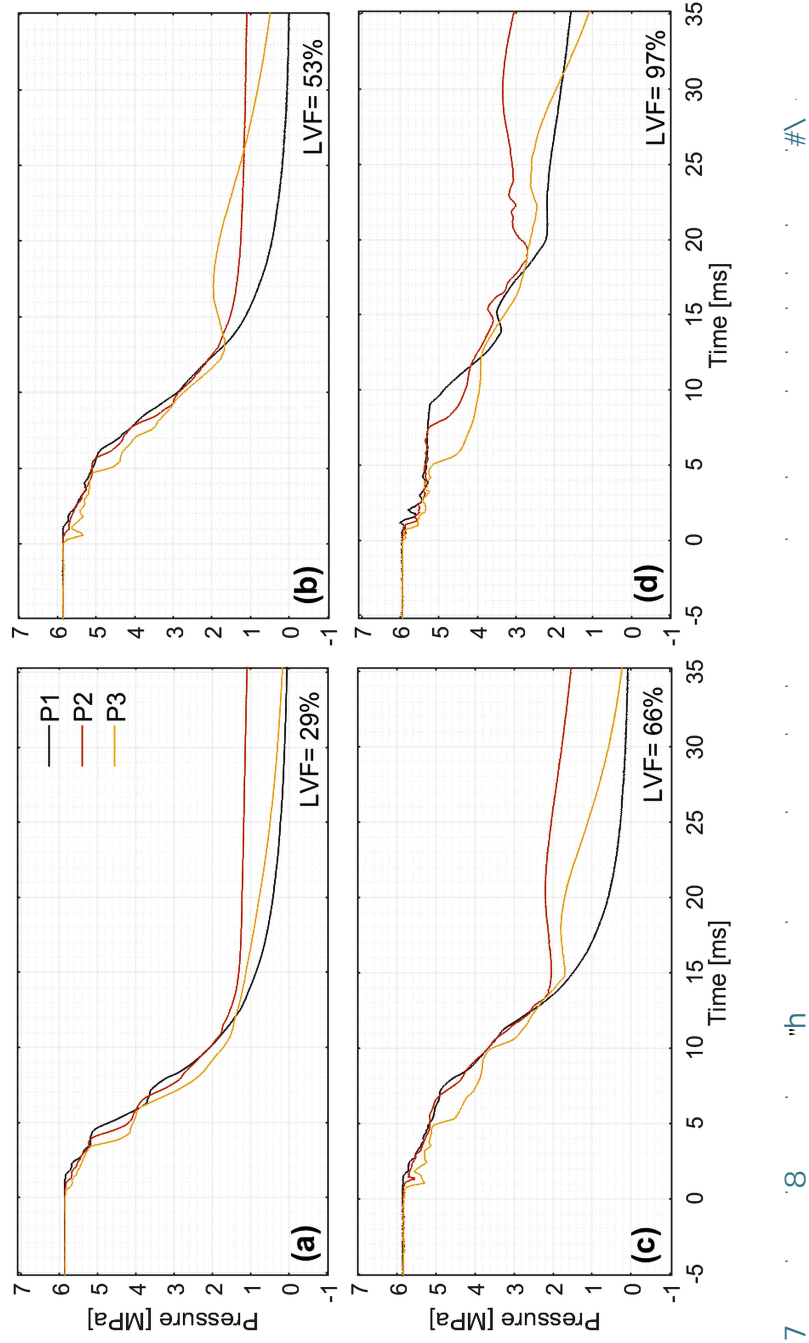
h ) 'k . . #\ . . . . .

#### 4.4.1 Introduction

This paper presents experimental results and analyses associated with phase transition characteristics during liquid CO<sub>2</sub> depressurization released from the bottom of a rectangular duct (BR). The motivation was to investigate the effects of bottom release (i.e., initial liquid at release area) on the behavior of rarefaction and evaporation waves inside a duct. A possible scenario of CO<sub>2</sub> BLEVE is a total catastrophic failure of a container ruptured below the liquid level. Therefore, the underlying phase transition processes should be considered. The experiments were conducted in a rectangular duct with the outlet pointing downwards. The soft aluminum diaphragm that sealed the HP section was ruptured by an arrow activated with a pneumatic actuator. Details about the setup are described in section 3.3. The analysis of phase transition characteristics was realized based on the pressure and temperature histories inside the duct. Besides, the shadowgraph technique captured the wave pattern inside the duct after rupturing. The results were contrasted with previous top-release tests (TR) in the same duct.

#### 4.4.2 Results and Discussion

Figure 4.11 shows pressure histories inside the duct during 35 ms of CO<sub>2</sub> liquid depressurization. Time 0 indicates the diaphragm rupture, and sensors (P1–P3) were arranged from top to bottom. The pre-ruptured pressure was 5.8–5.9 MPa. Figure 4.11 graphs (a–d) show that after the first pressure drop, the pressure profiles changed from steadily decreasing in (a) to about plateau in (d) as the LVF increased. This implies that the fluid stays in the metastable state for a longer period.



#A

"h

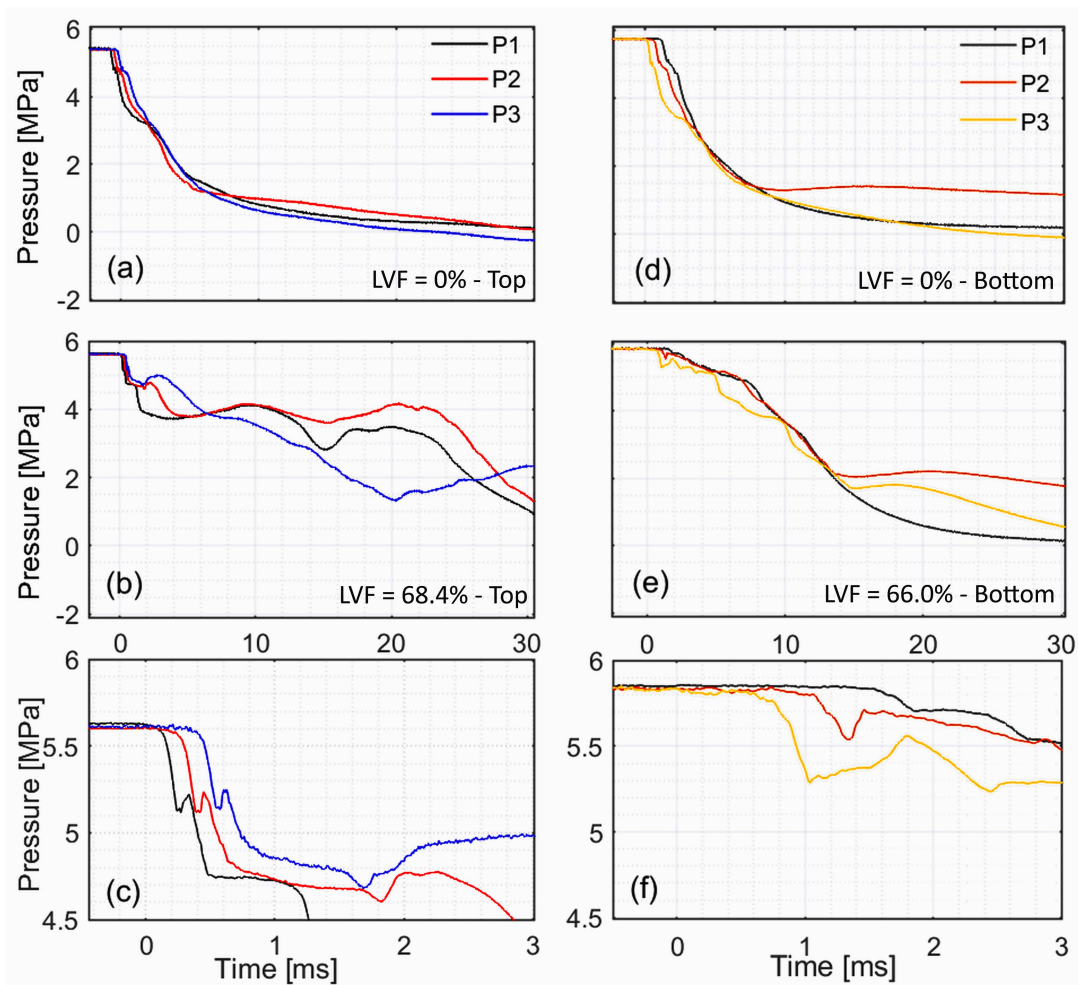
8

07



After the diaphragm rupturing, a slight decrease in pressure was observed, which signifies the first liquid and vapor expansion whereby the rarefaction wave propagated upward. Then the pressure gradually decreased, and the evaporation started. A steep decline in pressure with fluctuations characterized the expanded two-phase flow outwards.

The differences in the flow's dynamic characteristics between the bottom (BR) and top (TR) releases were identified by comparing the current results with previous TR tests in the same duct described by Hansen [56]. Figure 4.12 compares pressure histories inside the duct during TR (a and b) and BR (d and e) experiments. The (a and d) LVFs were 0, and (b and e) were 68.4, and 66%, respectively. Graphs (c and f) are corresponding close-ups of 3 ms.

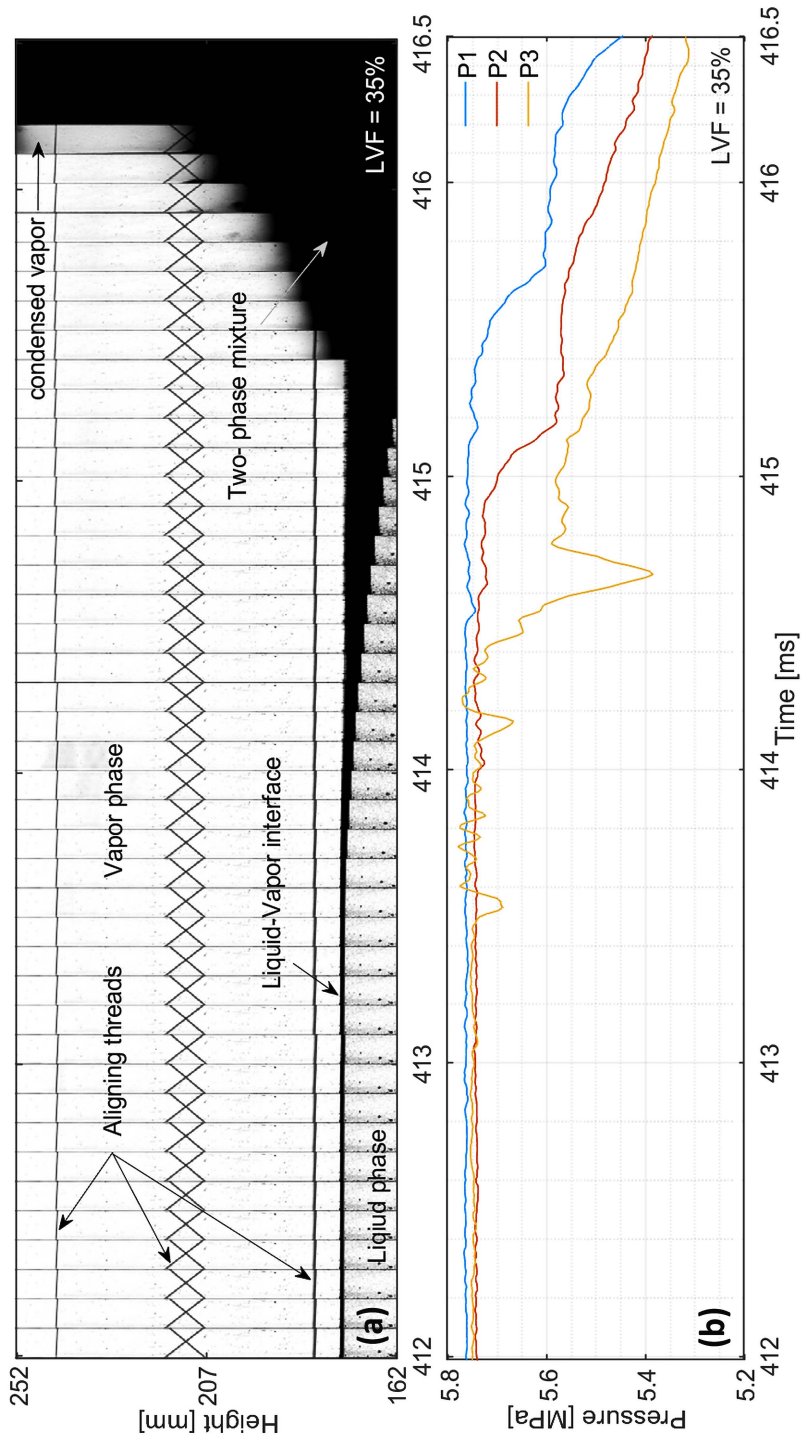


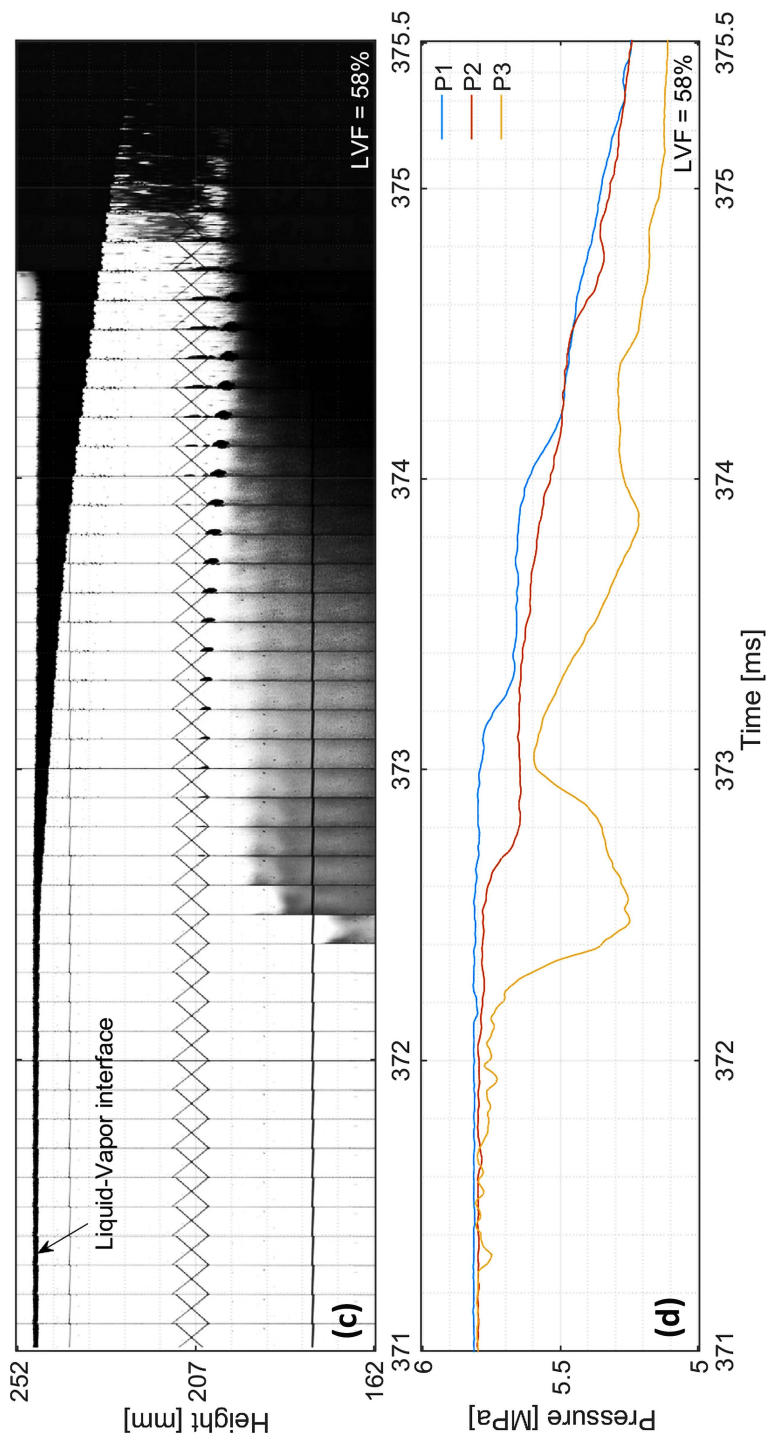
The graphs in Figure 4.12 show that during CO<sub>2</sub> depressurization, the pressure decreased more rapidly in BR tests than in TR. For P3 to drop to 2 MPa, it required about 26 ms in the TR test, while it was 13.7 ms in the BR tests. In addition, the DOS was higher in the TR tests than in the BR. The lesser DOS in the BR tests compared to the TR experiment is likely due to the large volume of the liquid rapidly flowing out of the duct after rupturing.

Figure 4.13 illustrates a sequence of images processed from shadowgraph video frames and corresponding pressure histories during 4.5 ms of CO<sub>2</sub> liquid release from the bottom of a rectangular duct for LVFs of 35 and 58%. The time step between two images is 0.1 ms.

The frames demonstrated the start of the boiling process at the liquid/vapor interface as a dark region of shadowgraphs expanded downwards. The expanded vapor rapidly moved into the liquid, forming a bubbly mixture propagating downwards. The two-phase mixture layer was also extended due to the bubbles developing by heterogeneous nucleation on the duct's wall. It gradually increased to cover the whole duct's volume.

As shown in Figure 4.13, the liquid/vapor interface developed into a two-phase mixture/vapor and was kept at an approximately constant level. Then the interface disintegrated, and the two-phase mixture traveled upward until it occupied the entire duct. This behavior is different from the evaporation mechanism during TR tests. The initial liquid/vapor interface moved upwards following the shock wave in TR experiments.





7 . . . . . # . . . . . \ . . . . . 07 . . . . .

#### 4.4.3 Conclusion

The experimental results demonstrated significant differences between the top-release and bottom-release tests in the evaporation mechanism and the flow characteristics:

- During BR tests, the evaporation rate inside the duct was faster, by a factor of two, compared to TR tests.
- The liquid expansion in BR tests attained a lower degree of superheat (DOS) than in the TR experiments.
- The shadowgraphs showed that during the boiling of liquid CO<sub>2</sub>, the liquid/vapor interface continued at a nearly constant level until it broke up. In the BR tests, the vapor had an insignificant effect on the early stages of the boiling process.

## 7 Framework

This chapter considers the research results and their implications, providing explanations and referring to contradictions to the previous research. It is divided into discussion parts according to the questions reflected in the summarized papers in section 4.

### k

The first part of the experimental work focused on the diaphragm rupturing mechanism. Characteristically, conducting the shock tube explosion tests with an instant release of exploded multiphase flow from the high-pressure test section is preferable. At the same time, the diaphragm rupture should be fast with a complete opening of the outlet cross-section. In addition, the two-phase mixture flow inside the vessel toward the exit should not be choked. Simultaneously, the exploded multiphase mixture into the atmosphere should not be disturbed by obstacles. During instantaneous depressurization, the liquid attains a degree of superheating due to rapid expansion. A higher expansion rate could also be considered as the rarefaction wave propagates through the liquid with area reduction in the vessel. Analyses of features such as overpressures, positive impulse, and multiphase mixture velocity and development depend on high-quality acquisition data and high-speed video recordings. This setup design is a proposed solution to the requests raised after evaluating the previous experimental works (for instance, Hansen [56]), especially for CO<sub>2</sub> release investigating two-phase mixture propagating in increased cross-sectional area and monitoring multiphase mixture movement without obstacles.

From the preceding, it is clear the necessity for a rupturing method that entirely removes the diaphragm from the release vent and, at the same time, avoids techniques using instruments above the test section, such as a pneumatically driven knife. Also, it should avoid complicated procedures with sensitive parts that can be damaged during the explosion test, such as electrical wires and heating devices. It has been found that a double-diaphragm method is controllable, simple, and satisfies the abovementioned

requirements. However, "during liquified CO<sub>2</sub> decompression, the double-membrane rupturing sequence affects the expansion wave pattern and evaporation rate. Therefore, by increasing or decreasing the pressure between the diaphragms considering the wave pattern in each application, the diaphragm's rupturing sequence became crucial.

The results of the diaphragm rupturing mechanism indicated that the change in the MP section pressure initially resulted in the diaphragm bulging and weakening the circular edge. Subsequently, the diaphragm layers began to rift at one point, and then the crack rapidly propagated on the circumference. The crack propagation speed depended on how fast the pressure difference between the diaphragm surfaces increased. When the pressure decreased in the MP section by decreasing pressure method, the crack propagation speed slowed due to the time taken for the pressure to reach the atmospheric one. As a result, the diaphragm was not fully circularly cut, but it opened and held with a small part to the remaining frame.

Analysis of the conical vessel experimental results showed that complicated wave patterns were created when decreasing the pressure method was used. In this case, the HP diaphragm ruptured first, leading to the reflection of the waves into the vessel. Additionally, this process had a prolonged period between the diaphragms rupturing and, even though the diaphragms were opened, not utterly removed. All these factors decelerated the evaporation wave propagation and reduced the phase transition rate.

In comparison, increasing the pressure between diaphragms led to the MP diaphragm rupture, followed by the HP diaphragm, and there were no reflection waves into the HP vessel. Also, the duration between the rupturing diaphragms was much less, about 28 times, and the diaphragms were wholly cut off.

On the question of how the change in MP section volume affects the experimental results, the study found that increasing the pressure in the MP section led first to the MP diaphragm rupturing. As a result, the MP section pressure rapidly dropped close to atmospheric pressure, followed by the HP diaphragm rupture. If so, it is thought that

the MP section volume has a minor effect on the subsequent process. However, when the pressure decreased in the MP section, the HP diaphragm ruptured, and the fluid expanded into the MP section before the MP diaphragm ruptured. In this case, the expansion process in the HP vessel depends on the MP section volume. The extended duration between HP and MP diaphragms' rupturing could affect the expansion wave behavior if the MP section volume is increased. Despite the change in the MP section volume, the time between diaphragms' rupturing is constantly higher when decreasing MP section pressure except when the opening orifice has an identical diameter as the flange's top outlet.

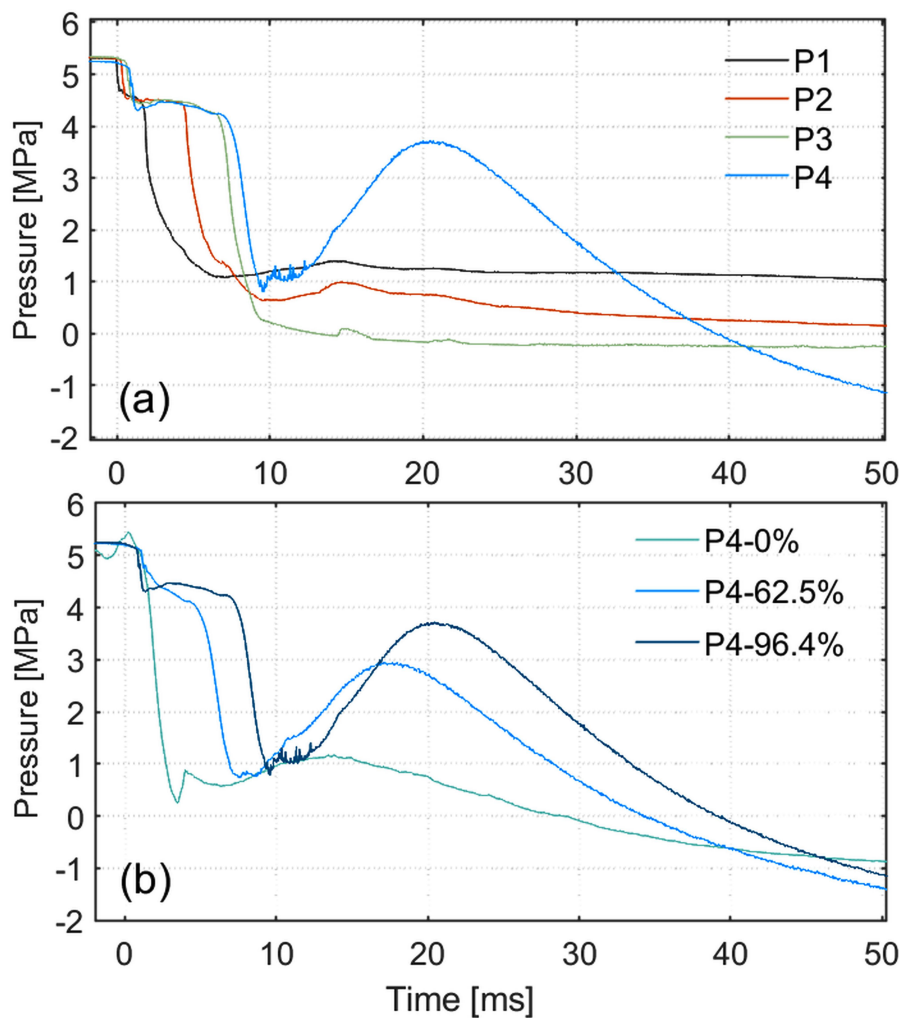
Based on the pressure records inside the HP vessel with constant area reduction, the rarefaction and evaporation wave velocities were calculated in the three vessel's height sections. The results showed increased evaporation wavefront velocity as it propagated downwards, i.e., as the cross-sectional area diminished. Also, as the liquid volume fraction (LVF) increased. The highest calculated velocity was 111.6 m/s at the vessel's bottom for LVF of 96.4%. These results differ from the previous experimental results from CO<sub>2</sub> depressurization in a constant cross-sectional area duct (Hansen [56]), wherein the rarefaction and evaporation wave velocities were found to be steady along the duct's height.

The most interesting finding was observed from the pressure history at the vessel's bottom. Figure 5.1 (a) shows the pressure transducer histories (P1-P4 top to bottom) inside the divergent cross-sectional area HP vessel during CO<sub>2</sub> depressurization for LVF of 96.4%. Graph (b) compares the bottom pressure transducer records for LVFs of 0, 62.5, and 96.4%.

The graphs in Figure 5.1 show that the P4 lines have distinct signal routes with oscillations followed by a significant pressure rise. The increase in pressure observed in the P4 after the primary evaporation wave had passed was most likely due to

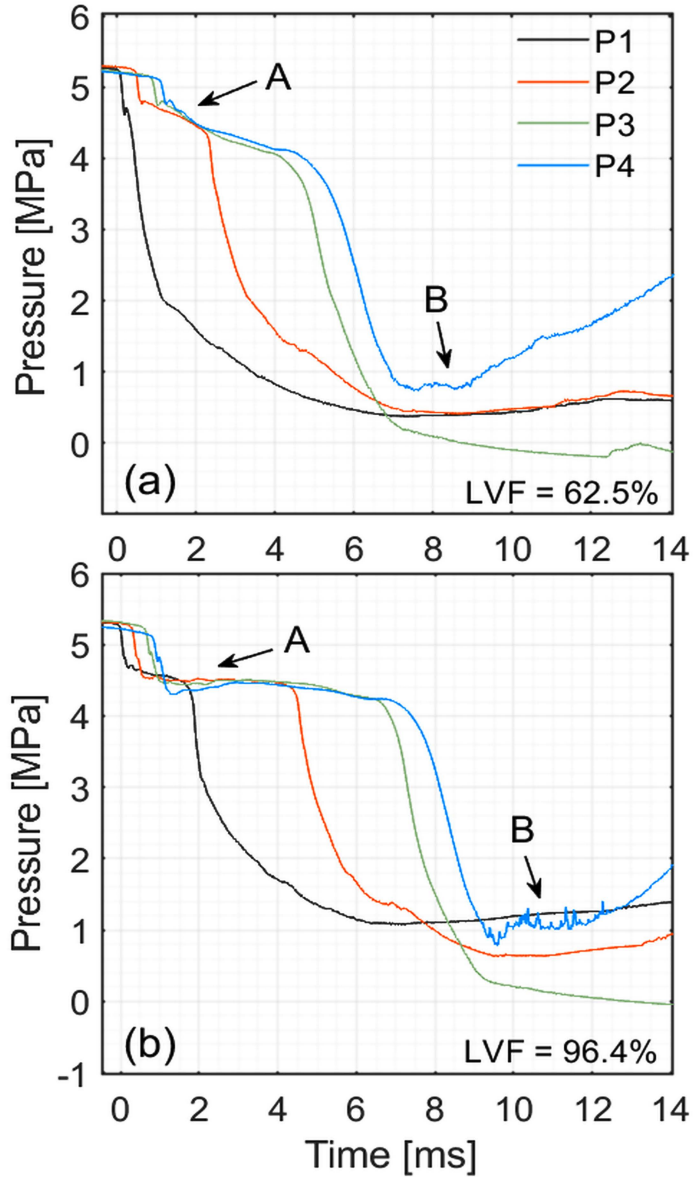


overexpansion. This effect is quite dramatic when the expansion waves interact with area reduction in a vessel. As the pressure at the P4 region runs to the trough, the rarefaction wave reflects, and the two-phase mixture flows upwards. The low pressure at the vessel's bottom has drawn the heavy two-phase mixture back downwards at relatively high velocities. Once it stagnates at the bottom, the pressure increases again (Figure 5.1). Then it decreases due to another rarefaction wave, and lighter gas follows the heavier one.



As mentioned above, the rarefaction wave velocity increases with an increase in LVF. Thus, its reflection from the vessel's bottom intensifies with higher liquid content. At the same time, with increased LVF, an extended period of superheated liquid remains in the

metastable state before evaporation occurs. The interaction of the reflected rarefaction waves with the propagated evaporation wave can be seen from the oscillations in P4 after the rarefaction wave, A, and after the evaporation wavefront propagation, B in Figure 5.2 (a, b).



P4 pressure records indicate faster evaporation at the vessel's bottom for LVF of 96.4% than for 62.5%. That is evident from the pressure drop duration on P4 lines in Figure 5.2,

and this may have accounted for the difference between 62.5 and 96,4% LVF in pressure rise amplitudes after the evaporation wave has passed.

@

A series of experiments were carried out in setup 2 (section 2.2), wherein the blast wave overpressures were measured at the top and bottom alongside a polycarbonate tube parallel to the generated waves and the released multiphase mixture. Results from measured peak overpressure showed two overpressure peaks in the leading positive phase. The initial peak corresponded to the headspace vapor expansion, while the following was from the expansion caused by the liquid evaporation. Interestingly, the second peak increased in height and duration with an increase in LVF, demonstrating that the rapid phase change significantly influenced the overpressure's positive phase. Also, the results indicate rapid phase transition in the conical-shaped vessel since the expanded two-phase mixture propagated in a constantly increased cross-sectional area. Therefore, it can be assumed that the explosion energy from this geometry is produced from the headspace vapor expansion and primarily from the liquid's stored energy released during evaporation.

The experimental results were used to validate a blast wave model of phase change during CO<sub>2</sub> depressurization in a conical-shaped vessel. The model is built of CFD simulations involving conservation equations for two immiscible fluids. The basis for calculation is the "Classical Nucleation Theory, focusing on the rate at which the number of critical-size bubbles per volume is produced." The phase transition mass rate (the source term in the two-fluid equation set) is modeled using the production rate of critical bubbles. The liquid state properties and the relationship between internal energy and the pressure were computed using stiffened gas equation of state. The equation set is solved using "the Flux Limiter Centered Scheme (FLIC) and Newton-Rhapson iterative solver. The simulations were performed for LVFs of 35 and 73% in 2D axis symmetry, and the geometry's center axis signifies the vessel's center axis. The simulation of blast overpressure for the bottom sensor (270 mm from the HP diaphragm) is overestimated because the modeled phase transition rate was too rapid. This inconsistency may be

because the influence of preceding nucleation at the wall was not considered. This explanation seems possible since the vessel's inner surface roughness average (Ra) was 3.2 μm. The simulation showed a closer blast overpressure for LVF of 35 % to the experimental results than for 73 %. It may be that the headspace vapor expansion drives the blast from the vessel with LVF of 35 %. However, for the LVF of 73 %, the blast wave originated mainly from liquid evaporation.

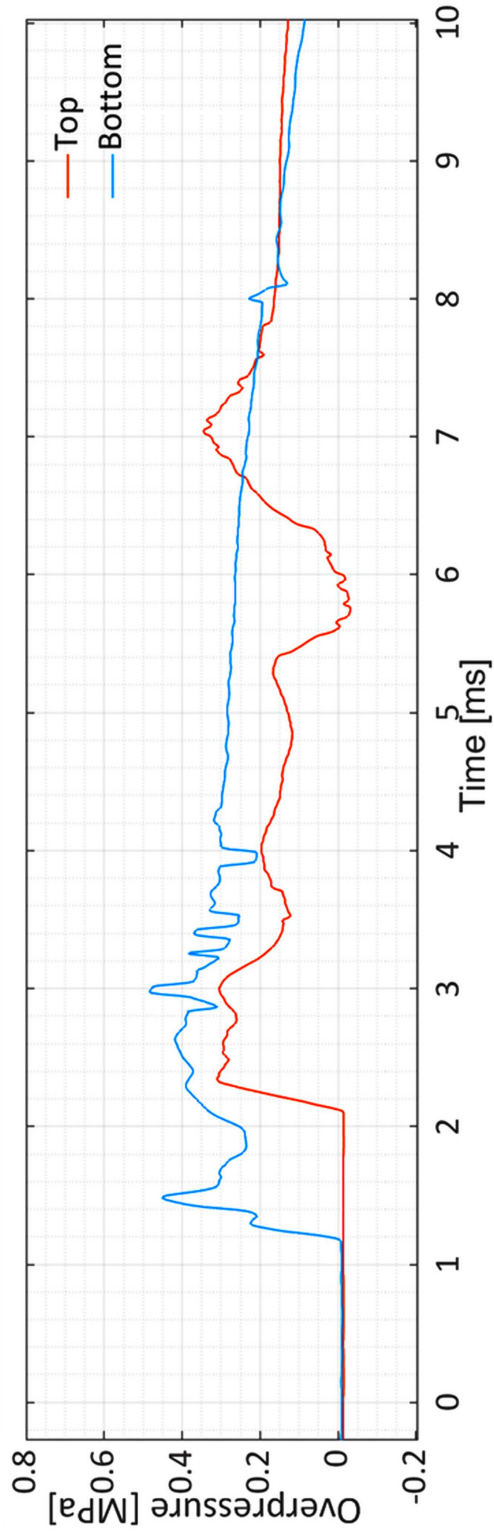
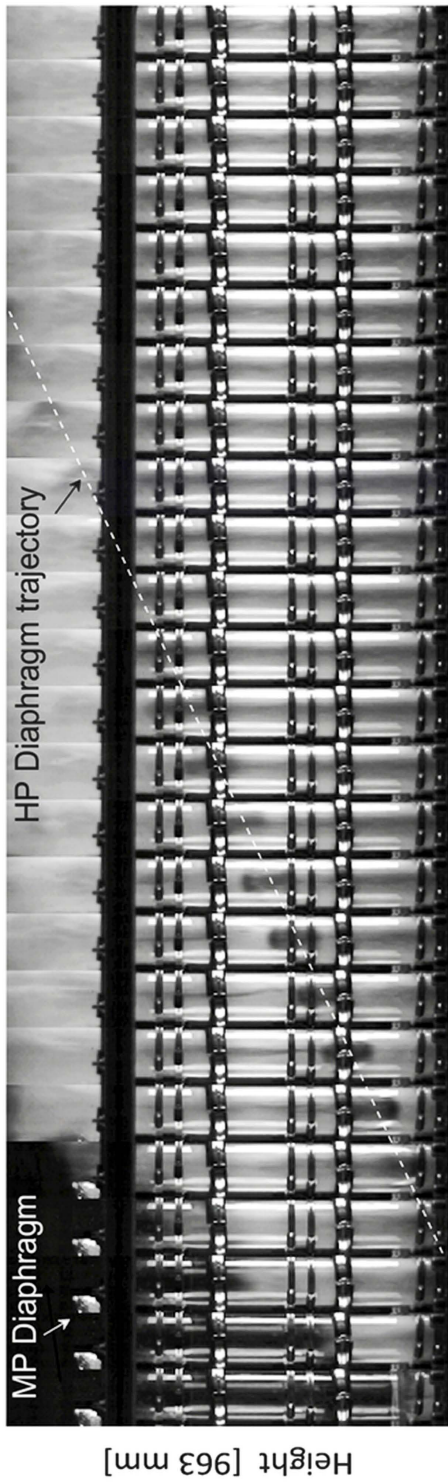
This study calculated the propelled diaphragms' velocities and kinetic energy based on the high-speed videos' analysis. Additionally, it compared these calculations with diaphragm velocity estimations based on the model for initial fragment velocity suggested by Baum [73-76] and modified later by Genova et al. [65]. The proposed model includes the following equations:

$$v_f = \left( \frac{2 \cdot k_q \cdot Q_{ex}}{m_f} \right)^{0.5}$$

$$Q_{ex} = m_l \cdot C_p \cdot (T_{rupt} - T_b) = (V_V \cdot \phi \cdot \rho_l) \cdot C_p \cdot (T_{rupt} - T_b)$$

where  $m_f$  is the fragment mass [kg],  $Q_{ex}$  is the excess heat stored in the liquid before the explosion [J], and  $k_q$  is the fraction of the excess heat transformed into the fragment kinetic energy.  $C_p$  is the pre-ruptured liquid's specific heat at constant pressure [kJ/kg·K],  $T_{rupt}$  is superheated liquid temperature [K],  $T_b$  is the liquid boiling temperature at atmospheric pressure [K].  $V_V$  is the vessel volume [m<sup>3</sup>].  $\phi$  is liquid volume fraction.  $\rho_l$  is the Liquid density at the superheated state [kg/m<sup>3</sup>].

The diaphragm velocity calculations were done by image processing of high-speed videos. The videos were captured at 7200 fps and a resolution of 256x1024 pixels. The height-to-pixel conversion was 0.94 mm/pixel. Figure 5.3 illustrates a sequence of images during the HP diaphragm rupturing through the tube and synchronously measured overpressure on the top and bottom of the tube (180 and 650 mm from the HP diaphragm). The duration between images is 0.42 ms, and the dashed line signifies the propelled diaphragm trajectory.



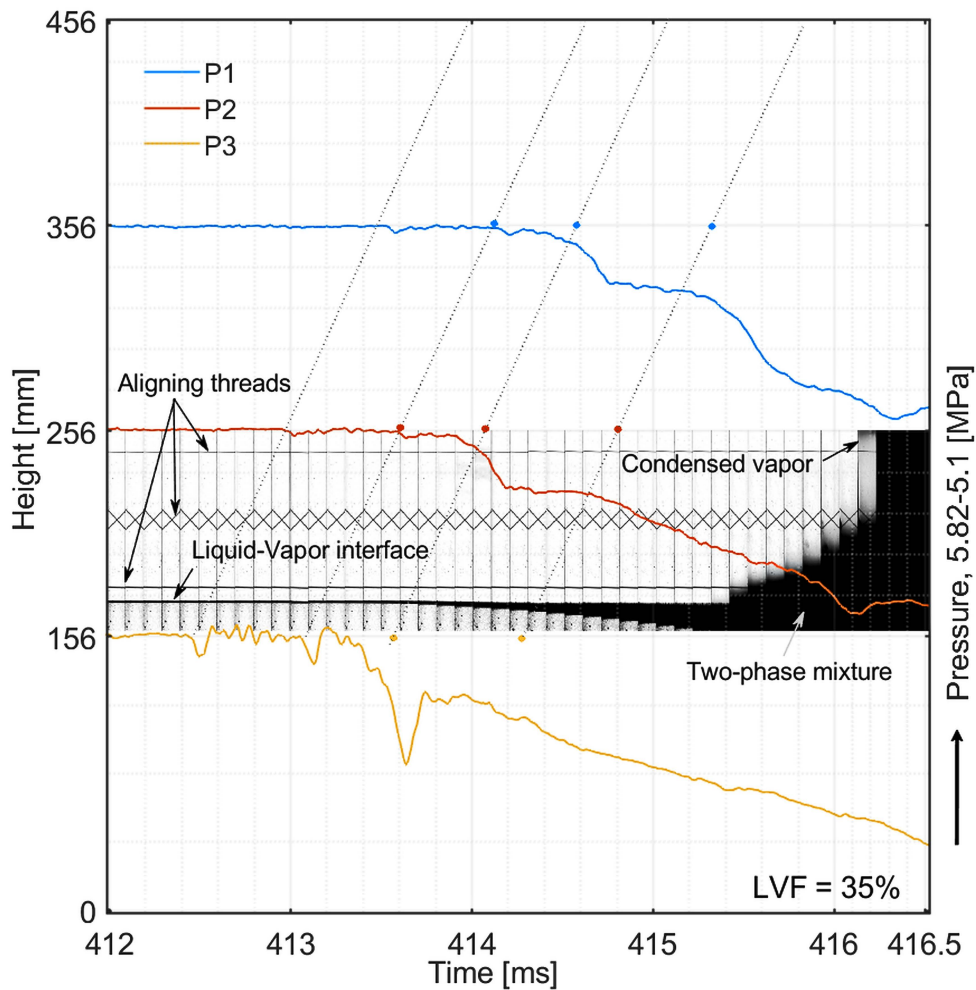
The calculation results showed increased diaphragms' velocity and kinetic energy as the LVF increased. Baum's model calculations demonstrated lower fragments' velocities with a difference of (15-23 m/s) from the experiments. A possible explanation for this might be the proposed value of the excess heat fraction ( $k_q$ ) by Genova et al. [65] ( $1.26 \cdot 10^{-3}$  as the best-fit coefficient). Besides, it could also be the computation of the excess heat stored in the liquid before the explosion. This computation depended on the pre-ruptured CO<sub>2</sub> saturated state properties, determined from SW-EOS and NIST tabulated data. The fragment velocity calculations from experimental results suggest a recent value of  $k_q$  to be  $1.73 \cdot 10^{-3}$ . According to the JRC European Commission's Science and Knowledge Service report [108], fragments are considered hazardous to incapacitation if their kinetic energy exceeds 80 J (80Joule-rule). Also, the report presents a fragment velocity-mass diagram of three models' curves, including the (80Joule-rule) to describe different fatality prospects. Based on this analysis, the fragments' velocities and kinetic energies from the experiments (shown in Table 4.3) demonstrate that these fragments imply great danger.

k . . . . .

Experiments carried out on Setup 3 (section 2.3) investigated the expansion and evaporation mechanisms inside a rectangular duct during the release of liquid CO<sub>2</sub> from the bottom. Comparing the experimental analyses with the previous results from experiments with top releases revealed a significant difference in evaporation mechanisms. The pressure histories demonstrated a faster pressure decrease during bottom release. It implies faster evaporation since the duct had less liquid volume to evaporate due to the liquid mass outflow from the bottom.

Analysis of the shadowgraph images displayed a flattened vapor/two-phase interface developed from the initial vapor/liquid interface after the evaporation onset. The expanded vapor penetrated this interface into the liquid, forming a bubble layer that expanded downwards. In this region, heterogeneous nucleation also contributed to an increased two-phase mixture. Simultaneously, a two-phase mixture descended from the duct's top due to the condensation resulting from the rarefaction wave propagation

through the vapor phase. Figure 5.4 shows pressure records (5.8 - 5.2 MPa) drawn on the duct height scale during 4.5 ms of liquified CO<sub>2</sub> depressurization for LVF of 35%. And including the corresponding shadowgraph images' sequence. The apparent inclines indicate waves' paths that follow the defined time points at the fixed pressure sensors' positions. Further evidence for the observed condensation was given from the vapor quality calculations based on the Span-Wagner EOS; it showed that the expanded fluid after the isentropic expansion had a vapor quality of 0.93. So, the evaporation mechanism during bottom release differs from top-release tests, wherein the liquid/vapor contact surface and two-phase mixture propagated upwards following expanded vapor ahead.



7

#\

07

## 8 Uwo o ct{ 'cpf 'Eqpenwukqp''

The presented work offers data and analysis concerning phase transition mechanisms and blast wave consequences during CO<sub>2</sub> depressurization in a vessel with a divergent cross-sectional area. In addition, the thesis discusses evaporation characteristics during CO<sub>2</sub> release from the bottom of a rectangular duct. The research's motivation was that the mechanisms of the rapid phase transition during CO<sub>2</sub> depressurization in divergent cross-section vessels and below the liquid level are not fully understood. So far, there have been few published studies on these processes, and the accessible experimental data are sparse. Therefore, this experimental work was undertaken to study the fluid expansion resulting from the rapid phase transition and subsequent generated blast wave as in a BLEVE scenario.

The first part of the experimental work was performed in setup 1 (section 3.1), where a double-membrane release system was attached at the top of the HP conical-shaped vessel filled with saturated liquid and vapor CO<sub>2</sub>. The rupture procedure either increased or decreased the pressure between the membranes (MP section). The study focused on the influence of the membranes' rupturing sequence on the wave pattern in the test section. Analysis of the pressure histories and the high-speed video recordings demonstrated that increasing the pressure between the membranes precluded the possibility of complex reflected wave interactions in the test section. It also minimized the extended duration between membranes rupturing, which was observed in decreasing the pressure procedure. Furthermore, the ease of control, the complete removal of the diaphragm, and instantaneous depressurization made the increasing pressure method a reliable and convenient operating technique.

A series of experiments investigated the dynamic characteristics of the expansion waves during CO<sub>2</sub> depressurization in the conical-shaped vessel. The rarefaction and evaporation wave velocities were determined based on analysis of the pressure records." The liquid's state properties in the metastable region following the isentropic expansion were determined by SW-EOS."The interactions of the expansion wave with the divergent cross-sectional geometry were described contrasting these analyses with the previous



conclusions from liquid CO<sub>2</sub> release in a constant cross-sectional rectangular duct. The study showed increasing rarefaction and evaporation wave velocities as they propagated downwards in the conical-shaped vessel and with an increase in liquid volume fraction. In contrast, these velocities were nearly constant in the rectangular duct tests.

The evaporation in the conical vessel was much faster than in the rectangular duct. That is because the two-phase flow behind the evaporation wave was choked, while the two-phase mixture in the conical vessel propagated through a constantly increased cross-sectional area. Furthermore, the degree of superheating was higher in the conical vessel than in the rectangular duct. Accordingly, in the conical-shaped vessel, the liquid's superheat following the isentropic expansion was high enough to release the contact surface explosively. It was a more intense eruption than observed in high-speed pictures from the rectangular duct releases. A significant finding to emerge from this study is the pressure rise at the vessel's bottom after the evaporation wavefront had passed. This phenomenon arises due to over-expansion when a portion of the two-phase mixture is drawn into the low-pressure bottom region.

The experiments carried out in setup 2 (section 3.2) sought to describe the consequences of the blast wave during liquid CO<sub>2</sub> depressurization in a divergent cross-sectional vessel. Measurements of peak overpressure (at the top and bottom of the polycarbonate tube) and the calculated impulse indicated a significant impact of rapid phase transition on their leading positive phase. The leading phase had two positive peaks, first lower and second higher, corresponding to the expanded headspace vapor, then the rapid evaporation. Besides, the second peak amplitude and duration increased as the liquid content increased in the vessel. These results suggest that the liquid's stored energy released during evaporation is the primary source of the blast wave energy in the presented geometry. Subsequently, it can be argued that this is a CO<sub>2</sub> BLEVE. According to the diagram shown in Figure 2.4, it can be described as hot BLEVE.

Calculations based on the analysis of high-speed videos and ruptured diaphragms demonstrated increased propelled diaphragm velocity and kinetic energy as liquid

volume fraction increased (up to 121 m/s and about 205 J for LVF of 73%). However, comparing these diaphragm velocity results with estimations based on the fragment's initial velocity model [65, 73-76] showed that the model had a lower slight difference in a range of 15-23 m/s. The study suggests a current value for a fraction of the excess heat transformed into the fragment kinetic energy to be  $k_q = 1.73 \cdot 10^{-3}$ . The experimental data from this study was employed to validate a blast wave model of CO<sub>2</sub> depressurization in identical geometry. The model is based on CFD simulations integrating conservation equations for two immiscible fluids, the Classical Nucleation Theory and the "stiffened gas equation of state. The numerical method involves the Flux Limiter Centered Scheme (FLIC) and Newton-Rhapson solver. The simulations of blast overpressure illustrated a higher phase transition rate than the experimental records. The reason is thought to be that the reducing impact of the wall nucleation at the earlier stages of expansion was undervalued in the model calculations.

The phase change during release below the liquid level was studied using setup 3 (section 3.3), wherein liquid CO<sub>2</sub> was released from the bottom of a rectangular duct. Interpreting the pressure and temperature histories in conjunction with high-speed shadowgraph images was the basis for analysis. The phase transition characteristics in these experiments differed from the previous top-release tests. The pressure records indicated faster evaporation during bottom-release tests than in top-release by a factor of two. However, during expansion in bottom-release tests, the liquid attained a lower degree of superheating due to liquid mass outflow from the bottom."

In top-release tests, the liquid-vapor interface propagated upwards following the vapor outflow as evaporation proceeded. Subsequently, the expanded gas/two-phase flow was choked at the outlet. Contrary to the top-release results, shadowgraph images showed that the initial contact surface remained flattened, almost horizontally, for a relatively extended duration before breaking up. Then, it increasingly developed into a two-phase mixture, covering the duct's upper section, trailing the expansion wave. Simultaneously (on the liquid side of the interface), another liquid/two-phase mixture

interface emerged at the contact surface, propagating downward. This progression signifies that the evaporation wave developed independently of the vapor expansion.

A homogeneous equilibrium model (HEM) was used to simulate transient CO<sub>2</sub> two-phase flow during CO<sub>2</sub> depressurization in a pipe. The liquid CO<sub>2</sub> depressurization was simulated in the middle of the pipe from the saturated pressure of 7.27 to 3.67 MPa. The structured model included central-upwind-weighted essentially non-oscillatory (CU-WENO) numerical schemes with a smoothness indicator instead of the limiter function. Besides, the Span-Wagner EOS calculated the thermodynamic properties. The model should determine whether employing SW EOS and an integrated CU-WENO scheme could capture rapid phase transition. The method simulation was able to describe the pressure, two-phase mixture density, and vapor volume fraction patterns during the phase transition. It also characterized the dynamics of rarefaction and evaporation waves and the CU-WENO scheme's convergence.

The current findings offer an enhanced understanding of CO<sub>2</sub> BLEVE mechanisms and possible consequences during depressurization in containers with a divergent cross-sectional area or release below the liquid level. The unique set of experimental data presented in this thesis can provide a basis for risk analyses that help safely construct and handle CO<sub>2</sub> tanks. It can also be utilized to validate or as inputs in the numerical models studying CO<sub>2</sub> depressurization in comparable geometry and positions.

k

- Even though the flow measurements provided significant observations on the evaporation wavefront propagation in the conical-shaped vessel, the waves' interaction with the divergent cross-sectional area is not fully revealed. The difficulty lay in the non-transparent walls of the stainless steel vessel, which could not enable optical observation inside the vessel. A simulation of waves and two-phase mixture flow interaction with the divergent cross-sectional area could offer additional data for phase transition characterization in this geometry.

- The study of releasing liquid CO<sub>2</sub> from the bottom of a rectangular duct has focused on the evaporation mechanism inside the test section. However, it would be interesting to study the phase transitions occurring in the outflowing flashing liquid jet and its effect on the blast wave intensity. Future research on the flashing jet would further analyze the explosive evaporation of outflowing liquid CO<sub>2</sub> during release from the bottom. Adding pressure sensors at fixed positions perpendicular to the duct outlet could give insight into shock wave pressures and impulses.
- All the experiments were conducted with saturated CO<sub>2</sub> at atmospheric temperature. However, certain CO<sub>2</sub> storage tanks are maintained at relatively low temperatures than the atmospheric. Experimenting with controlling liquid CO<sub>2</sub> temperature could help explore phase transition mechanisms during the release of saturated CO<sub>2</sub> at low temperatures.
- The simulation of the pressure inside the conical-shaped vessel illustrated probable bubble formation on the wall, reducing the superheated liquid's duration at the metastable state. Future research should therefore utilize refined inner surface walls to reduce the effect of heterogeneous nucleation on the phase transition rate.
- The diaphragm rupture of a container at a horizontal position filled with liquid CO<sub>2</sub> would lead to simultaneous liquid and vapor outflow. Instantaneously, the inside liquid evaporates while the vapor expands due to faster propagation of the rarefaction wave in the liquid phase than in the vapor. This would affect the evaporation wavefront velocity, shape, and subsequent behavior of the expanded two-phase flow inside the container. Further experimental investigation of liquid CO<sub>2</sub> release from a container at a horizontal or an inclined position close to the horizontal would be recommended.



## Tghgt gpegu'

- [1] IEA (2016). "20 Years of Carbon Capture and Storage: Accelerating Future Deployment." Paris, International Energy Agency. <https://www.oecd-ilibrary.org/content/publication/9789264267800-en>.
- [2] M. Xie (2013). "Thermodynamic and Gasdynamic Aspects of a Boiling Liquid Expanding Vapour Explosion." Ph.D. doctoral thesis, Multi-Scale Physics, Technische Universiteit Delft S-Hertogenbosch, The Netherlands. <https://doi.org/10.4233/uuid:37dc661e-ce11-4e67-a670-2d6d066ee548>.
- [3] A. M. Birk, C. Davison, and M. Cunningham (2007). "Blast overpressures from medium scale BLEVE tests." *K O h h @* vol. 20, no. 3, pp. 194-206, doi: <https://doi.org/10.1016/j.ilp.2007.03.001>.
- [4] CCPS (2010). "Guidelines for Vapor Cloud Explosion, Pressure Vessel Burst, BLEVE, and Flash Fire Hazards," C. f. C. P. Safety, Ed. NY: Center for Chemical Process Safety, AIChE-Wiley, 2010, pp. 311-360.
- [5] EIGA "SAFE HANDLING OF LIQUID CARBON DIOXIDE CONTAINERS THAT HAVE LOST PRESSURE" European Industrial Gases Association, Brussels. <https://www.eiga.eu/?s=SAFE+HANDLING+OF+LIQUID+CARBON+DIOXIDE+CONTAINERS+THAT+HAVE+LOST+PRESSURE>.
- [6] T. Abbasi and S. A. Abbasi (2007). "The boiling liquid expanding vapour explosion (BLEVE): Mechanism, consequence assessment, management." *K* vol. 141, pp. 489-519, doi: 10.1016/j.jhazmat.2006.09.056.
- [7] Y. Zhang, J. Schork, and K. Ludwig (2013). "Revisiting the conditions for a CO<sub>2</sub> tank explosion." in *# - o U 8 # h o*, San Antonio, Texas, 109-120. <https://www.aiche.org/conferences/aiche-spring-meeting-and-global-congress-on-process-safety/2013/proceeding/paper/43c-revisiting-conditions-and-consequences-co2-tank-explosions-2>.
- [8] W. E. Clayton and M. L. Griffin (1994). "Catastrophic failure of a liquid carbon dioxide storage vessel." *h o h* vol. 13, no. 4, pp. 202-209, doi: <https://doi.org/10.1002/prs.680130405>.
- [9] U. D. o. Transportation (2022). "Failure Investigation Report – Denbury Gulf Coast Pipelines LLC" Pipeline and Hazardous Materials Safety Administration. <https://www.phmsa.dot.gov/sites/phmsa.dot.gov/files/2022-05/Failure%20Investigation%20Report%20-%20Denbury%20Gulf%20Coast%20Pipeline.pdf>.
- [10] P. G. Debenedetti (1996). "Metastable Liquids: Concepts and Principles." Princeton, New Jersey USA, Princeton University Press. <https://books.google.no/books?id=tzvsltE6Y8C>.
- [11] J. R. Simões-Moreira (1994). "Adiabatic evaporation waves". Ph.D. Dissertatioin, Department of Mechanical Engineering, Rensselaer Polytechnic Institute, Troy, N.Y. <https://books.google.no/books?id=mJigtgAACAAJ>.

- [12] V. P. Skripov (1990). "Behavior of liquid thermodynamic stability under superheating and supercooling." *Kolloidnyi Zhurnal* vol. 59, no. 3, pp. 1135-1140, doi: <https://doi.org/10.1007/BF00870507>.
- [13] R. C. Reid (1976). "Superheated Liquids." *Journal of Applied Physics* vol. 64, no. 2, pp. 146-156. Available: <http://www.jstor.org/stable/27847154>.
- [14] G. V. Ermakov and V. P. Skripov (1970). "Equation of state and stability boundary of a metastable liquid." *Journal of Applied Physics* vol. 8, no. 5, pp. 916-21.
- [15] M. Blander and J. L. Katz (1975). "Bubble nucleation in liquids." *Journal of Applied Physics* vol. 21, no. 5, pp. 833-848, doi: <https://doi.org/10.1002/aic.690210502>.
- [16] J. M. Salla, M. Demichela, and J. Casal (2006). "BLEVE: A new approach to the superheat limit temperature." *Journal of Applied Physics* vol. 19, no. 6, pp. 690-700. doi: <https://doi.org/10.1016/j.jlp.2006.04.004>.
- [17] T. Abbasi and S. A. Abbasi (2007). "Accidental risk of superheated liquids and a framework for predicting the superheat limit." *Journal of Applied Physics* vol. 20, no. 2, pp. 165-181. doi: <https://doi.org/10.1016/j.jlp.2005.11.002>.
- [18] H. Wakeshima and K. Takata (1958). "On the Limit of Superheat." *Journal of Applied Physics* vol. 13, no. 11, pp. 1398-1403. doi: <https://doi.org/10.1143/JPSJ.13.1398>.
- [19] G. R. Moore (1959). "Vaporization of superheated drops in liquids." *Journal of Applied Physics* vol. 5, no. 4, pp. 458-466, doi: <https://doi.org/10.1002/aic.690050412>.
- [20] M. Blander, D. Hengstenberg, and J. L. Katz (1971). "Bubble nucleation in n-pentane, n-hexane and n-pentane + hexadecane mixtures and water." *Journal of Applied Physics* vol. 75, no. 23, pp. 3613-3619. doi: <https://doi.org/10.1021/j100692a022>.
- [21] J. E. Shepherd and B. Sturtevant (1982). "Rapid evaporation at the superheat limit." *Journal of Applied Physics* vol. 121, pp. 379-402. doi: <https://doi.org/10.1017/S0022112082001955>.
- [22] H. C. Park, K. T. Byun, and H. Y. Kwak (2005). "Explosive boiling of liquid droplets at their superheat limits." *Journal of Applied Physics* vol. 60, no. 7, pp. 1809-1821, doi: <https://doi.org/10.1016/j.ces.2004.11.010>.
- [23] R. C. Reid (1979). "Possible Mechanism for Pressurized-Liquid Tank Explosions or BLEVE's." *Journal of Applied Physics* vol. 203, no. 4386, p. 1263. doi: 10.1126/science.203.4386.1263.
- [24] X. Mengmeng (2013). "Thermodynamic and gas dynamic aspects of a BLEVE." Ph.D. Thesis, Delft University, The Netherlands. <http://resolver.tudelft.nl/uuid:a3514a6a-49d8-41b3-ada5-7a7dccb376ea>.
- [25] P. Reinke (1997). "Surface boiling of superheated liquid." PhD Dissertation, Mechanical Engineering, ETH Zurich, Switzerland, PSI--97-01. [http://inis.iaea.org/search/search.aspx?orig\\_q=RN:28030620](http://inis.iaea.org/search/search.aspx?orig_q=RN:28030620).
- [26] L. G. Hill (1991). "An experimental study of evaporation waves in a superheated liquid". PhD Dissertation. California Institute of Technology. California IT, USA. <https://resolver.caltech.edu/CaltechETD:etd-10242005-103224>.

- [27] A. Prosperetti and M. Plesset (1978). "Vapor-Bubble Growth in a Superheated Liquid." *K* *7* *U* vol. 85, no. 2, pp. 349-368. doi:10.1017/S0022112078000671.
- [28] R. Span and W. Wagner (1996). "A New Equation of State for Carbon Dioxide Covering the Fluid Region from the Triple - Point Temperature to 1100 K at Pressures up to 800 MPa." *K* *h* *#* *k* *)* vol. 25, no. 6, pp. 1509-1596, doi: <https://doi.org/10.1063/1.555991>.
- [29] Allan H. Harvey and E. W. Lemmon (2022). "New Reference Equation of State for Carbon Dioxide." in *u* *@* *o* *#* *h* *#* *o* , San Antonio, Texas USA, No.14. <https://sco2symposium.com/proceedings.shtml>.
- [30] A. Mjaavatten. "Thermodynamic models and tools for H<sub>2</sub>O, H<sub>2</sub>, CO<sub>2</sub> and Air." GitHub. <https://github.com/are-mj/thermodynamicsGitHub>. (accessed 2021).
- [31] J. R. Simões Moreira and J. E. Shepherd (1999). "Evaporation waves in superheated dodecane." *K* *7* *U* vol. 382, pp. 63-86. doi: 10.1017/S0022112098003796.
- [32] R. C. Reid (1979). "Possible Mechanism for Pressurized-Liquid Tank Explosions or BLEVE's.", *o* vol. 203, pp. 1263-5. doi: 10.1126/science.203.4386.1263.
- [33] P. K. Das, G. S. Bhat, and V. H. Arakeri (1987). "Investigations on the propagation of free surface boiling in a vertical superheated liquid column." *@* *K* *=* *U* *u* vol. 30, no. 4, pp. 631-638. doi: [https://doi.org/10.1016/0017-9310\(87\)90193-1](https://doi.org/10.1016/0017-9310(87)90193-1).
- [34] P. Reinke (1997). "Surface boiling of superheated liquid". Ph.D., Mechanical Engineering, ETH Zurich, Switzerland, PSI--97-01. [http://inis.iaea.org/search/search.aspx?orig\\_q=RN:28030620](http://inis.iaea.org/search/search.aspx?orig_q=RN:28030620).
- [35] Y. V. Fairuzov (1998). "Blowdown of pipelines carrying flashing liquids." *@* *-* *K* vol. 44, no. 2, pp. 245-254, doi: <https://doi.org/10.1002/aic.690440203>.
- [36] T. Watanabe, H. Maehara, M. Nakamura, H. Ohta, and S. Itoh (2015). "Flashing Phenomena of Liquid Nitrogen in a Pressure Vessel Under Rapid Depressurizations." in *o* *U* *-* *h* *t* *h* *#* , <https://doi.org/10.1115/PVP2015-45976>.
- [37] Center for Chemical Process Safety (1994). "Guidelines for Evaluating the Characteristics of VaporCloud Explosions, Flash Fires, and BLEVEs." New York, Wiley. pp. 69-160, <https://books.google.no/books?id=vYF9QgAACAAJ>.
- [38] B. Stutz and J. R. Simões-Moreira (2013). "Onset of boiling and propagating mechanisms in a highly superheated liquid - the role of evaporation waves." *@* *K* *=* *U* *u* vol. 56, no. 1, pp. 683-693, doi: <https://doi.org/10.1016/j.ijheatmasstransfer.2012.08.057>.
- [39] M. A. Grolmes and H. K. Fauske (1974). "Axial propagation of free surface boiling into superheated liquids in vertical tubes." in *@* *=* *u* *#* , Tokyo, Japan, pp. 30-34. <https://www.osti.gov/servlets/purl/4267547>.



- [40] P. Reinke and G. Yadigaroglu (2001). "Explosive vaporization of superheated liquids by boiling fronts." *Journal of Loss Prevention in the Process Industries* vol. 27, pp. 1487-1516, doi: 10.1016/S0301-9322(01)00023-4.
- [41] H. Wu, W. Liu, X. Li, F. Chen, and L. Yang (2019). "Experimental Study on Flash Evaporation under Low-pressure Conditions." *Journal of Loss Prevention in the Process Industries* vol. 22, no. 2, pp. 213-220, doi: 10.6180/jase.201906\_22(2).0002.
- [42] A. Ibarreta, H. Biteau, and J. Sutula (2016). "BLEVES and Fireballs," in *Handbook of Hazardous Materials*, M. J. Hurley Eds. New York, NY: Springer New York, 2016, pp. 2792-2816.
- [43] J. E. S. Venart, G. A. Rutledge, K. Sumathipala, and K. Sollows (1993). "To BLEVE or not to BLEVE: Anatomy of a boiling liquid expanding vapor explosion." *Journal of Loss Prevention in the Process Industries* Article vol. 12, no. 2, pp. 67-70, doi: 10.1002/prs.680120202.
- [44] J. E. S. Venart and C. M. Yu (1996). "The boiling liquid collapsed bubble explosion (BLCBE): A preliminary model." *Journal of Loss Prevention in the Process Industries* vol. 46, no. 2, pp. 197-213, doi: [https://doi.org/10.1016/0304-3894\(95\)00071-2](https://doi.org/10.1016/0304-3894(95)00071-2).
- [45] A. C. Van den Berg, M. M. Van der Voort, J. Weerheijm, and N. H. A. Versloot (2006). "BLEVE blast by expansion-controlled evaporation." *Journal of Loss Prevention in the Process Industries* vol. 25, no. 1, pp. 44-51, doi: 10.1002/prs.10116.
- [46] R. C. Reid (1976). "Superheated Liquids: Liquids in the superheated state, far from being a laboratory curiosity, occur more often than thought and may cause industrial accidents." *Journal of Loss Prevention in the Process Industries* vol. 64, no. 2, pp. 146-156. doi: <http://www.jstor.org/stable/27847154>.
- [47] R. C. Reid (1980). "Some Theories on Boiling Liquid Expanding Vapour Explosions." *Journal of Loss Prevention in the Process Industries* pp. 525-26.
- [48] T. Abbasi and S. A. Abbasi (2007). "Accidental risk of superheated liquids and a framework for predicting the superheat limit." *Journal of Loss Prevention in the Process Industries* vol. 20, pp. 165-181. doi: <https://doi.org/10.1016/j.jlp.2005.11.002>.
- [49] M. M. van der Voort, A. C. van den Berg, D. J. E. M. Roekaerts, M. Xie, and P. C. J. de Bruijn (2012). "Blast from explosive evaporation of carbon dioxide: experiment, modeling and physics." *Journal of Loss Prevention in the Process Industries* vol. 22, no. 2, pp. 129-140, doi: 10.1007/s00193-012-0356-0.
- [50] D. Bjerketvedt, K. Egeberg, W. Ke, A. Gaathaug, K. Vaagsaether, and S. H. Nilsen (2011). "Boiling liquid expanding vapour explosion in CO<sub>2</sub> small scale experiments." *Journal of Loss Prevention in the Process Industries* vol. 4, pp. 2285-2292. doi: <https://doi.org/10.1016/j.egypro.2011.02.118>.
- [51] A. Laurent, L. Perrin, and O. Dufaud (2016). "Consequence Assessments of a Cold BLEVE. Can We Do It Better?," *Journal of Loss Prevention in the Process Industries* vol. 48, pp. 211-216, doi: <https://doi.org/10.3303/CET1648036>.
- [52] M. S. Ibrahim (2007). "An overview on BLEVE." *Journal of Loss Prevention in the Process Industries* vol. 16, no. 5, pp. 740-54, doi: 10.1108/09653560710837037.
- [53] A. M. Birk, Z. Ye, J. Maillette, and M. H. Cunningham. (1993) "Hot and cold BLEVES : observation and discussion of two different kinds of BLEVEs." in *Proceedings of the 1993 AIChE Symposium Series*, Atlanta, GA, A. NY, Ed., vol. 89: AIChE Symposium Series, pp. 119-30.

- [54] J. C. A. M. v. Doormaal and R. M. M. v. Wees (2005). "Rupture of vessels." in *U* The Hague: Min. VROM, 2005, ch. 7, pp. 7.1 -7.78.
- [55] A. C. van den Berg (2008). "Blast charts for explosive evaporation of superheated liquids." *h o h* vol. 27, no. 3, pp. 219-224. doi: <https://doi.org/10.1002/prs.10252>.
- [56] P. Hansen (2018). "Experimental and theoretical studies of rapid phase transitions in carbon dioxide". PhD dissertation, Process, Energy and Automation Engineering, University of South-Eastern Norway. <https://openarchive.usn.no/usn-xmlui/handle/11250/2587457?show=full>.
- [57] R. W. Prugh (1991). "Quantitative Evaluation of "BLEVE" Hazards." *K* '7 *h* - vol. 3, no. 1, pp. 9-24, doi:10.1177/104239159100300102.
- [58] E. Planas-Cuchi, J. M. Salla, and J. Casal (2004). "Calculating overpressure from BLEVE explosions." *K O h h @* vol. 17, no. 6, pp. 431-436, doi: <https://doi.org/10.1016/j.jlp.2004.08.002>.
- [59] A. Ibarreta and H. Biteau (2016). "BLEVES and fireballs." Springer, pp. 2792-2816.
- [60] J. Casal (2008). "Evaluation of the Effects and Consequences of Major Accidents in Industrial Plants." Elsevier. <https://books.google.no/books?id=L5gJxo1jkhAC>.
- [61] D. A. Crowl (1992). "Using thermodynamic availability to determine the energy of explosion for compressed gases." *h \ h* vol. 11, no. 2, pp. 47-49, doi: <https://doi.org/10.1002/prsb.720110206>.
- [62] D. A. Crowl (1991). "Using thermodynamic availability to determine the energy of explosion." *h \ h* vol. 10, no. 3, pp. 136-142, doi: <https://doi.org/10.1002/prsb.720100306>.
- [63] R. A. Ogle, J. C. Ramirez, and S. A. Smyth (2012). "Calculating the explosion energy of a boiling liquid expanding vapor explosion using exergy analysis." *h o h* vol. 31, no. 1, pp. 51-54, doi: 10.1002/prs.10465.
- [64] J. Casal and J. M. Salla (2006). "Using liquid superheating energy for a quick estimation of overpressure in BLEVEs and similar explosions." *K = U* vol. 137, no. 3, pp. 1321-1327. doi: <https://doi.org/10.1016/j.jhazmat.2006.05.001>.
- [65] B. Genova, M. Silvestrini, and F. J. Leon Trujillo (2008). "Evaluation of the blast-wave overpressure and fragments initial velocity for a BLEVE event via empirical correlations derived by a simplified model of released energy." *K O h h @* vol. 21, no. 1, pp. 110-117. doi: <https://doi.org/10.1016/j.jlp.2007.11.004>.
- [66] D. Laboureur, F. Heymes, L. Aprin, J.-M. Buchlin, and P. Rambaud (2012). "BLEVE Overpressure: Small Scale Experiments and Multi-Scale Comparison with Literature Survey of Blast Wave Modeling." in *8 # h o*, Houston, TX.
- [67] D. M. Johnson, M. J. Pritchard, B. G. p. Research, and T. Division (1991). "Large Scale Experimental Study of Boiling Liquid Expanding Vapour Explosions (BLEVEs)." British Gas plc, Research and Technology Division. <https://books.google.no/books?id=CvcDMwECAAJ>.

- [68] J. Stawczyk (2003). "Experimental evaluation of LPG tank explosion hazards." *K = U* vol. 96, no. 2-3, pp. 189-200. doi: 10.1016/s0304-3894(02)00198-x.
- [69] J. Kang, J. Zhang, and J. Gao (2016). "Analysis of the safety barrier function: Accidents caused by the failure of safety barriers and quantitative evaluation of their performance." *K O h h @* vol. 43, pp. 361-371, doi: <https://doi.org/10.1016/j.jlp.2016.06.010>.
- [70] J. Casal, J. Arnaldos, H. Montiel, E. Planas-Cuchi, and J. A. Vi'lchez (2002). "Modeling and understanding BLEVEs." in *U = U* *O u*. NY: McGraw-Hill, 2002, pp. 22.1-22.27.
- [71] A. M. Birk (1996). "Hazards from propane BLEVEs: An update and proposal for emergency responders." *K O h h @* vol. 9, no. 2, pp. 173-181, doi: [https://doi.org/10.1016/0950-4230\(95\)00046-1](https://doi.org/10.1016/0950-4230(95)00046-1).
- [72] L. B. Tepić G, Tanackov I, Sremac S, Milisavljević S, Kostelac M. (2019). "Numerical Model of Fragmentation Hazards Caused by a Tank Explosion." *U 7 U - V* vol. 43, pp. 27-41, doi: <https://doi.org/10.21278/TOF.43403>.
- [73] M. R. Baum (1991). "Rupture of a gas-pressurized cylindrical pressure vessel: The velocity of rocketing fragments." *K O h h @* vol. 4, no. 2, pp. 73-85, doi: [https://doi.org/10.1016/0950-4230\(91\)80011-1](https://doi.org/10.1016/0950-4230(91)80011-1).
- [74] M. R. Baum (1993). "Velocity of a single small missile ejected from a vessel containing high pressure gas." *K O h h @* vol. 6, no. 4, pp. 251-264, doi: [https://doi.org/10.1016/0950-4230\(93\)80007-9](https://doi.org/10.1016/0950-4230(93)80007-9).
- [75] M. R. Baum (1995). "Rupture of a gas-pressurized cylindrical vessel: the velocity of a detached end-cap." *K O h h @* vol. 8, no. 3, pp. 149-161, doi: [https://doi.org/10.1016/0950-4230\(95\)00017-U](https://doi.org/10.1016/0950-4230(95)00017-U).
- [76] M. R. Baum (1999). "Failure of a horizontal pressure vessel containing a high temperature liquid: the velocity of end-cap and rocket missiles." *K O h h @* vol. 12, no. 2, pp. 137-145, doi: [https://doi.org/10.1016/S0950-4230\(98\)00051-5](https://doi.org/10.1016/S0950-4230(98)00051-5).
- [77] J. Ren, B. Zhao, C. Wang, and M. Bi (2020). "Experimental study on the characteristics of the explosive boiling induced by the pressure relief at the top of vertical vessels." *K O h h @* p. 104181, doi: <https://doi.org/10.1016/j.jlp.2020.104181>.
- [78] K. K. Dewangan and P. K. Das (2020). "Experimental analysis of flashing front propagation in superheated water—Effects of degree of superheat, tube inclination, and secondary nucleation." *h 7* vol. 32, no. 7, p. 073311. doi: 10.1063/5.0006840.
- [79] I. Stotz, G. Lamanna, H. Hettrich, B. Weigand, and J. Steelant (2008). "Design of a double diaphragm shock tube for fluid disintegration studies." *k O @* vol. 79, no. 12, p. 125106, doi: 10.1063/1.3058609.
- [80] K. K. Botros, J. Geerligs, B. Rothwell, and T. Robinson (2015). "Measurements of Decompression Wave Speed in Pure Carbon Dioxide and Comparison With

- Predictions by Equation of State." *K* *h* *t* *u* vol. 138, no. 3, doi: 10.1115/1.4031941.
- [81] S. T. Munkejord, A. Austegard, H. Deng, M. Hammer, H. G. J. Stang, and S. W. Løvseth (2020). "Depressurization of CO<sub>2</sub> in a pipe: High-resolution pressure and temperature data and comparison with model predictions." - vol. 211, p. 118560, doi: <https://doi.org/10.1016/j.energy.2020.118560>.
- [82] H. Chaves (1984). "Changes of phase and waves on depressurization of liquids with high specific heat." PhD Dissertation, Max-Planck-Institut für Strömungsforschung, Göttingen, Germany.
- [83] I. E. Zabelinskii, I. M. Naboko, M. V. Tarasenko, and O. P. Shatalov (1991). "Distortion of the shock front in a shock tube with a divergent conical transition section." *7* ) vol. 26, no. 4, pp. 593-598, doi: 10.1007/BF01050323.
- [84] P. A. Thompson, H. Craves, G. E. A. Meier, Y.-G. Kim, and H. D. Speckmann (1987). "Wave splitting in a fluid of large heat capacity." *K* *7* *U* vol. 185, pp. 385-414, doi: 10.1017/S0022112087003227.
- [85] M. Li, Z. Liu, Y. Zhou, Y. Zhao, X. Li, and D. Zhang (2018). "A small-scale experimental study on the initial burst and the heterogeneous evolution process before CO<sub>2</sub> BLEVE." *K* = *U* vol. 342, pp. 634-642, doi: <https://doi.org/10.1016/j.jhazmat.2017.09.002>.
- [86] D. Quinn, D. Stannard, J. Edwards, K. K. Botros, and C. Johansen (2021). "Experimental visualization and characteristics of bubble nucleation during rapid decompression of supercritical and subcooled carbon dioxide." @ *K* *h* *t* *h* p. 104569. doi: <https://doi.org/10.1016/j.ijpvp.2021.104569>.
- [87] D. Jamois, C. Proust, L. Teberikler, and A. Fahmi (2022). "A Specific Device to Investigate and Monitor the Blowdown of Liquid CO<sub>2</sub> in Realistic Conditions (Including Cryogenic)." *oK V* - *K* doi: <http://dx.doi.org/10.2139/ssrn.4250904>.
- [88] L. Teberikler (2022). "Simulation of a CO<sub>2</sub> vessel blowdown with LedaFlow software " in @ # 8 8 # *u* 8=8*u* Lyon, France, <https://ssrn.com/abstract=4292071>
- [89] M. Drescher (2022). "Blowdown of CO<sub>2</sub> Vessels at Low and Medium pressure conditions: Experiments and Simulations " in @ # 8 8 # *u* 8=8*u* Lyon, France, <https://ssrn.com/abstract=4292065>
- [90] G. Vaillant, L. Teberikler, A. Fahmi, F. Garcia, C. Merat, and M. Drescher (2021). "Vessel Blowdown of CO<sub>2</sub>-Rich Fluids: Experiments and Simulations " in 8 8 # *u* # ,
- [91] Z. Shang (2021). "Experimental investigation of BLEVE in liquid CO<sub>2</sub> phase-transition blasting for enhanced coalbed methane recovery." *7* vol. 292, p. 120283, doi: <https://doi.org/10.1016/j.fuel.2021.120283>.
- [92] X. Li, Z. Liu, M. Li, P. Li, Y. Zhao, and S. Wan (2020). "Experiments on burst pressure and fragment dispersion effects of small-sized pressure vessel BLEVE." *7* vol. 277, p. 118145, doi: <https://doi.org/10.1016/j.fuel.2020.118145>.

- [93] P. M. Hansen, A. V. Gaathaug, D. Bjerketvedt, and K. Vaagsaether (2019). "Rapid depressurization and phase transition of CO<sub>2</sub> in vertical ducts – Small-scale experiments and Rankine-Hugoniot analyses." *K* vol. 365, pp. 16-25, doi: <https://doi.org/10.1016/j.jhazmat.2018.10.092>.
- [94] G. Ciccarelli, J. Melguizo-Gavilanes, and J. E. Shepherd (Year) "Pressure Field Produced by the Rapid Vaporization of a CO<sub>2</sub> Liquid Column." in *@* ; Cham, 2017 2017, vol. 2: Springer International Publishing, pp. 1293-1297, doi: [https://doi.org/10.1007/978-3-319-44866-4\\_87](https://doi.org/10.1007/978-3-319-44866-4_87).
- [95] S. Tosse, K. Vaagsaether, and D. Bjerketvedt (2015). "An experimental investigation of rapid boiling of CO<sub>2</sub>." *o* vol. 25, no. 3, pp. 277-282, doi: 10.1007/s00193-014-0523-6.
- [96] S. Brown, S. Martynov, and H. Mahgerefteh (2015). "Simulation of two-phase flow through ducts with discontinuous cross-section." *#* vol. 120, pp. 46-56, doi: <https://doi.org/10.1016/j.compfluid.2015.07.018>.
- [97] A. M. Log, S. T. Munkejord, and M. Hammer (2021). "HLLC-type methods for compressible two-phase flow in ducts with discontinuous area changes." *#* vol. 227, p. 105023. doi: <https://doi.org/10.1016/j.compfluid.2021.105023>.
- [98] H. Chaves, H. Lang, G. E. A. Meier, and H. D. Speckmann (1985) "Adiabatic phase transitions and wavesplitting in fluids of high specific heat." in *7* *k* , Berlin, Heidelberg, G. E. A. Meier and F. Obermeier, Eds., Springer Berlin Heidelberg, pp. 115-124.
- [99] D. L. Frost, J. H. S. Lee, and G. Ciccarelli (1991). "The use of Hugoniot analysis for the propagation of vapor explosion waves." *o* vol. 1, no. 2, pp. 99-110, doi: 10.1007/BF01414905.
- [100] J. R. Simões-Moreira (2000). "Oblique evaporation waves." *o* vol. 10, no. 4, pp. 229-234, doi: 10.1007/s001930000050.
- [101] Edvaldo Angelo, José Moreira, and D. Barrios (2005). "THEORY AND OCCURRENCE OF EVAPORATION WAVES." in *@* *#* *U* , Ouro Preto MG , Brazil. <https://www.abcm.org.br/anais/cobem/2005/PDF/COBEM2005-0475.pdf>.
- [102] A. A. Avdeev (2016). "Theory of Boiling Shock," in " : Springer 2016, pp. 265-273.
- [103] S. T. Munkejord, H. Deng, A. Austegard, M. Hammer, A. Aasen, and H. L. Skarsvåg (2021). "Depressurization of CO<sub>2</sub>-N<sub>2</sub> and CO<sub>2</sub>-He in a pipe: Experiments and modelling of pressure and temperature dynamics." *@* *K* *8* *8* *#* vol. 109, p. 103361. doi: <https://doi.org/10.1016/j.ijggc.2021.103361>.
- [104] A. Elshahomi, C. Lu, G. Michal, X. Liu, A. Godbole, and P. Venton (2015). "Decompression wave speed in CO<sub>2</sub> mixtures: CFD modelling with the GERG-2008 equation of state." *°* vol. 140, pp. 20-32. doi: <https://doi.org/10.1016/j.apenergy.2014.11.054>.
- [105] S. T. Munkejord, J. P. Jakobsen, A. Austegard, and M. J. Møltnvik (2010). "Thermo- and fluid-dynamical modelling of two-phase multi-component carbon dioxide

- mixtures." @ *Journal of Loss Prevention in the Process Industries* vol. 4, no. 4, pp. 589-596, doi: <https://doi.org/10.1016/j.ijggc.2010.02.003>.
- [106] S. T. Munkejord and M. Hammer (2015). "Depressurization of CO<sub>2</sub>-rich mixtures in pipes: Two-phase flow modelling and comparison with experiments." @ *Journal of Loss Prevention in the Process Industries* vol. 37, pp. 398-411. doi: <https://doi.org/10.1016/j.ijggc.2015.03.029>.
- [107] S. Brown, S. Martynov, H. Mahgerefteh, and C. Proust (2013). "A homogeneous relaxation flow model for the full bore rupture of dense phase CO<sub>2</sub> pipelines." @ *Journal of Loss Prevention in the Process Industries* vol. 17, pp. 349-356. doi: <https://doi.org/10.1016/j.ijggc.2013.05.020>.
- [108] G. Solomos, M. Larcher, G. Valsamos, V. Karlos, and F. Casadei (2020). "A survey of computational models for blast induced human injuries for security and defence applications." JRC European Commission's science and knowledge service, Luxembourg. doi:10.2760/685.



## **'Rct v'KK'**

Published and submitted papers



## Regrt '3'

k . . . . . #\ . . . . .

Published in the Journal of . . . . . , vol. 4, no. 4, p. 89.

doi: <https://doi.org/10.1007/s42452-022-04975-4>




## Research Article

# Release mechanisms and waves interaction during liquified CO<sub>2</sub> depressurization in a double-membrane conical vessel

Osama M. Ibrahim<sup>1</sup>  · Per Morten Hansen<sup>1</sup> · Dag Bjerketvedt<sup>1</sup> · Knut Vågsæther<sup>1</sup>

Received: 12 March 2021 / Accepted: 3 February 2022

Published online: 02 March 2022

© The Author(s) 2022  OPEN

## Abstract

An unintended release of liquid CO<sub>2</sub> during its transport results in depressurization with rapid phase transitions, evaporation, and expansion. Such progression may lead to catastrophic container failure with boiling liquid expanding vapor explosion (BLEVE). Therefore, to design safe CO<sub>2</sub> transport structures, it is essential to investigate the processes associated with CO<sub>2</sub> depressurization. This paper presents a new test rig combining a divergent cross-sectional test vessel with a double-membrane rupturing system. The rig is designed to study the effect of diverging cross sections on phase transition rates and wave propagation during liquid CO<sub>2</sub> depressurization. The apparatus has a high-pressure (HP) conical-shaped vessel and a medium-pressure slip-on flange section (MPS) that separates two membranes. The main contribution is examining rupturing methods and subsequent generated waves behavior to evaluate the installation performance. Pressure histories and high-speed video recordings were utilized to analyze the wave pattern and membrane rupturing mechanisms by increasing or decreasing the MPS pressure. A comparison of these two techniques demonstrates that decreasing the MPS pressure requires an extended period between diaphragms rupture and has a lower evaporation wavefront velocity than increasing the MPS pressure. Increasing the MPS pressure method has better reliability and simplicity and provides a more controllable operating system. Increasing the MPS pressure avoids a complicated wave pattern in the test section and prolonged rupturing time.

## Article Highlights

- The conical vessel with a double membrane shows the wave structure during saturated liquid CO<sub>2</sub> depressurization.
- During liquified CO<sub>2</sub> decompression, the double-membrane rupturing sequence affects the expansion wave pattern and evaporation rate.
- By decreasing the medium-section pressure, slower wave propagation and complex reflected waves are observed in the test section.

**Keywords** Liquid CO<sub>2</sub> depressurization · Double-membrane · Increasing/ · Decreasing pressure method · Evaporation wave · Rarefaction wave

✉ Osama M. Ibrahim, Osama.K.Ibrahim@usn.no; Per Morten Hansen, per.m.hansen@usn.no; Dag Bjerketvedt, Dag.Bjerketvedt@usn.no; Knut Vågsæther, Knut.Vagsather@usn.no | <sup>1</sup>Faculty of Technology, Natural Sciences, and Maritime Sciences, Department of Process, Energy and Environmental Technology, The University of South-Eastern Norway, Kjølnes Ring 56, 3918 Porsgrunn, Norway.



SN Applied Sciences

(2022) 4:89

| <https://doi.org/10.1007/s42452-022-04975-4>

## 1 Introduction

Carbon capture and storage (CCS) technologies have been developed as an exceptional solution to reduce CO<sub>2</sub> emissions from fossil fuel utilization, especially CO<sub>2</sub> emissions from power plants and industrial processes. The transportation of liquid CO<sub>2</sub> is a fundamental stage of the CCS technological processes [1]. The decompression of liquified CO<sub>2</sub> from tanks or pipelines is a continuing concern in terms of the safe transport and storage of CO<sub>2</sub>. A container filled with liquified CO<sub>2</sub> may fail due to projectile impact, corrosion, or overheating. Under some circumstances, liquid CO<sub>2</sub> depressurization may lead to rapid phase change with explosive boiling and the creation of blast waves. If the container fails catastrophically with a sizable multiphase mixture rapid outburst to the environment, it can be characterized as boiling liquid expanding vapor explosion (BLEVE) [2]. In such explosions, serious hazards arise from generated pressure loads and discharge of considerable CO<sub>2</sub> volume to the surroundings, in addition to dangerous flying fragments [3]. Therefore, there is a need for profound insights into process safety and risk assessment to protect against, avoid, and mitigate such devastating incidence. It is crucial to study the fundamental processes of rapid phase transition and evaporation, estimate the strength of the generated pressure waves, and determine the factors that affect these processes.

Attempts to specify the conditions promoting a BLEVE incident have been proposed in the published literature. Reid's superheat limit theory [4, 5] suggested the factors that produce BLEVE. According to this theory, a liquid crossing the saturation line after the decrease in pressure becomes superheated in the metastable state. It remains in this state between saturation and spinodal curves until it reaches the superheated limit temperature (SLT). BLEVE is more likely to occur whenever the liquid temperature exceeds the SLT and approaches the spinodal line. Depending on the depressurization rate, the liquid attains a high degree of superheating (DOS). In addition, evaporation must be rapid and induced by homogeneous nucleation in the liquid bulk. However, other studies have mentioned that explosive evaporation could occur even when the liquid temperature has not exceeded the SLT [6, 7]. When a liquid CO<sub>2</sub> depressurizes, a rarefaction wave propagates through the liquid, followed by an evaporation wave. The two-phase mixture formed behind the evaporation wave flows toward the atmospheric pressure side. As a result, it compresses the gas ahead and, in certain conditions, produces a shock wave. The vapor/liquid contact surface moves behind the shock wave into the surroundings [8, 9].

Different types of shock tubes have established their capability and effectiveness in small-scale experiments to measure the properties related to analogous phenomena. Such devices are used to study pressure-driven transient phenomena that involve considerable energy transformation due to pressure change. Several experimental studies aiming to describe the front propagating behind the incident shock or evaporation waves have been carried out on vertical laboratory-scale test devices with various fluids [10–14]. Several tests have been performed on larger horizontal tubes and pipes [15–17]. Almost all of these studies were conducted in constant cross-sectional vessels and mainly used the one-membrane burst method. This paper emphasizes experiments that include decompression from the top of vertical containers, divergent cross-sectional vessels, and double-diaphragm bursting mechanisms.

Chaves [18] performed experiments on two ducts with a constant and diverging cross-section to study the evaporation wave evolution during the depressurization of liquids with high specific heat. The study found that the splitting of the expansion wave is a restricted thermodynamic incident and is not dependent on the geometry. Zabelinskii et al. [19] tested the leading shock front shape in a gas (explosive mixture diluted with cold hydrogen) employing a horizontal shock tube with a conical passage between high and low-pressure parts. According to the study's outcome, the diverging cross-sectional passageway resulted in the retention of heterogeneities on the wavefront surface.

Various diaphragm rupturing methods have been developed and introduced to examine sudden decompression procedures in shock tubes. Hill [10] implemented a typical rupture method using knife blades prompted by a pneumatic cylinder to cut aluminum foil diaphragm sets between low- and high-pressure reservoirs. In the study on boiling development during the depressurization of superheated liquid in a column, Das et al. [13] employed a four-bladed cutter placed adjacent to and over a plastic diaphragm and covered by an air chamber. The diaphragm swells to touch the blades and is punctured when the pressure falls due to a vacuum pump in the air chamber. A remarkable study on explosive vaporization of superheated liquids was introduced by Reinke [20]: the moveable flange method. A brass sheet was pressed between the flanges from the bottom side and the two-ring flange from the top. The outer flange had a sharp edge, and the diaphragm was fixed to the next bottom flange. An inner ring, which could move up and down, pressed the diaphragm in a smaller circle. Lifting the mobile flange's ring increased the force on the diaphragm surface due to the increased area under load, and subsequently, the diaphragm ruptured.

Recently, a different method presented by Dewangan et al. [14] applied a Nichrome heating wire to heat and rupture the plastic diaphragm fixed between two flanges. Li et al. [21] questioned which factors influenced the promotion of boiling liquid expanding vapor explosion (BLEVE) by heating dry ice in a cylindrical vessel sealed with a burst disk. The container's pressure increased as the dry ice liquefied and evaporated until the point where the disk exploded. Stotz et al. [16] demonstrated a double-diaphragm shock tube to investigate atomized liquids and the associated combustion processes. The 12-m long horizontal installation consisted of three tubular parts: driver, driven, and buffer zones. The two diaphragms ruptured by the pressure quickly decreasing in the buffer section.

Over recent years, the depressurization of liquified CO<sub>2</sub>, the associated evaporation, and the developed pressure waves have been studied at the University of South-Eastern Norway (USN). Wei Ke [22] conducted experiments on BLEVE by using cylindrical plastic tubes filled with dry ice. The pressure rose by heating the test tube. Then, the pressure was vented with the help of a pneumatic piston. The tube exploded when it could not withstand the increasing pressure, and CO<sub>2</sub> splashed out. The progression of the evaporation waves during the decompression of liquid CO<sub>2</sub> was analyzed by Tosse et al. [23]. A transparent polycarbonate tube was utilized as a high-pressure unit, and Mylar sheets were utilized as a membrane ruptured by a pneumatically driven needle. Hansen et al. [24] broadly studied the rapid depressurization of CO<sub>2</sub> utilizing three different vertical apparatuses, two of which were described above. The third setup consisted of a stainless steel rectangular duct filled with liquid CO<sub>2</sub> to a specified level. Sudden decompression was performed by rupturing the aluminum diaphragm with a pneumatically driven cross-shaped knife.

One major issue in the previous CO<sub>2</sub> depressurization experiments was that the two-phase flow behind the evaporation wave was not instantaneously released from the test section. This is because the ducts' constant cross-sectional area, especially with more minor opening exits, did not allow the prompt release of the rapidly expanded two-phase mixture. In turn, the analysis of the evaporation process was complicated, and there may have been shock attenuation effects. In addition, the decompression in the previous test sections was performed by rupturing the diaphragms with an actuated knife or needle, which was fixed above the test duct. This arrangement disturbed the exploded multiphase flow and subsequently imprecisely captured its behavior. As a continuation of this research activity, this project seeks to expand prior research by providing results and analysis of expansion wave dynamics in a new vessel design.

The present work focuses on a divergent cross-sectional area, as opposed to previous work. The divergent cross-section will significantly enhance fluid expansion as the rarefaction wave propagates toward a smaller area. The experimental setup should identify whether the phase transfer rate and the metastable state following the rarefaction wave are independent of fluid expansion (the degree of superheating). This setup has three characteristic features. The vessel test section has a conical-shaped body (i.e., divergent cross section). The test section is sealed by a double-membrane, where a slip-on flange positioned between the two membranes constitutes a medium-pressure section (MPS). The rupturing of membranes could either be achieved by increasing or decreasing the pressure in the MPS. Although few types of research with rapid phase transition have been carried out on double-membrane apparatus, the difference in rupturing mechanisms by increasing and decreasing the MPS has not been discussed. This paper compares these two methods of rupturing membranes and how the rupture mechanism influences the waves. The focus here is on the rupture stages, the wave pattern, and the device performance.

## 2 Design description of the double-membrane test rig

The double-membrane conical rig is designed to carry out small-scale experiments to investigate the sudden release of liquified CO<sub>2</sub> and the associated underlying processes of rapid phase transition. It is a modified apparatus of shock tube type. The existing double-membrane system consists of two pressurized CO<sub>2</sub> sections: a high-pressure conical vessel (i.e., test section) and a medium-pressure slip-on flange. The conical vessel is reinforced on the aluminum structure and fastened together with the two slip-on flanges. The two aluminum diaphragms have different thicknesses. Figure 1 shows a sketch and an image of the rig.

### 2.1 High-pressure conical vessel

The conical part of the vessel was made of stainless steel AISI 316 and was welded to a slip-on flange (pressure class 1500 lb) with a full penetrating weld. The flange facilitates carrying the diaphragm gaskets underneath the load and firmly attaches the other parts to the vessel. The vessel has a total height of 383 mm, a volume of 480·10<sup>3</sup> mm<sup>3</sup>, and solid sidewalls with a thickness of 18.67 mm. The vessel wall is inclined at an angle of 4° and has an inner surface with an average roughness (Ra) of 3.2 μm. The conical

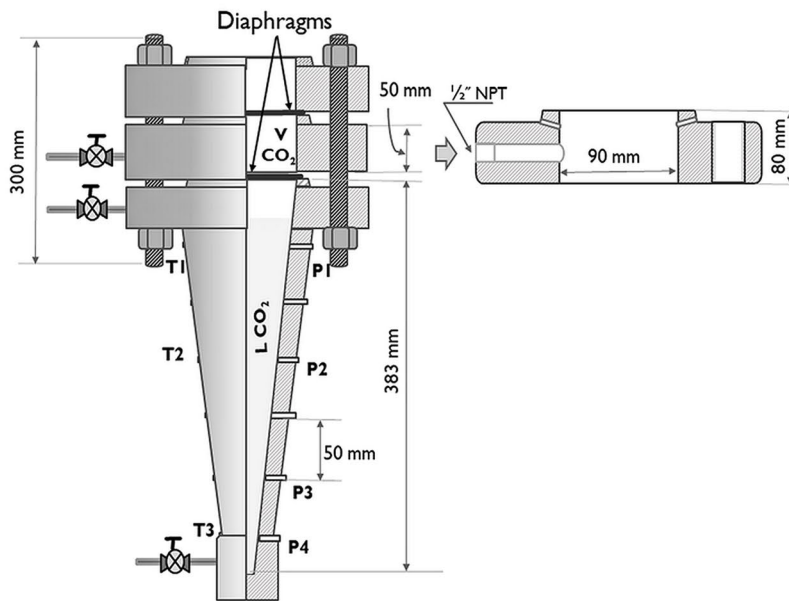


**Fig. 1** Schematic drawing of the double-diaphragm conical arrangement, its main dimensions, and a magnified MPS sketch on the left-hand side. An image of the conical vessel fastened with the two flanges on the right-hand side

vessel's upper orifice has a diameter of 90.7 mm. The vessel has a flat surface circular bottom (diameter 9.37 mm) to avoid excessively high stress that could arise from evaporation waves that descend just after the diaphragm ruptures. The tapered vessel bottom was strengthened with a cube-shaped block from the same material with a side of 70 mm. There are two openings for  $\text{CO}_2$ . Inflow in the bottom and outflow from the top of the vessel's wall, and each opening equipped with  $\frac{1}{4}$ " NPT fittings. Additionally, there are 12 threaded holes, six for pressure sensors on one vessel's side and the other six for temperature sensors on the opposite side. The distance between the sensors' holes is 50 mm.

## 2.2 Medium-pressure section

A slip-on flange is utilized as a medium-pressure section installed above the vessel. The MPS has a cylindrical cross section with a diameter of 90 mm, a depth of 80 mm, and a volume of  $510 \cdot 10^3 \text{ mm}^3$ . The slip-on flange is fabricated from stainless steel ASME B 16.5 (pressure class 1500 lbs). It is modified by drilling an inlet/outlet opening through its thick-disk sidewall. Additionally, two additional openings were drilled for fitting pressure and temperature sensors. O-ring grooves were machined to guarantee tight sealing. The inlet/outlet opening is equipped with a  $\frac{1}{2}$ " NPT fitting and connected to a pneumatic three-way valve by

a  $\frac{1}{2}$ " flexible metal hose that facilitates the slip-on flange's movement to replace the diaphragm. This arrangement enabled a controlled pressure relief unit. Another slip-on flange is positioned on the top of the MPS flange and opens to atmospheric conditions. This flange is used to keep the diaphragm pressed between the two flanges. The pressurized sections, the diaphragms, and the second slip-on flange are tightly held together by eight bolts. Figure 1 is a diagram of the double-diaphragm conical arrangement with a magnified MPS schematic, its main dimensions, and sensor positions used in the experimental setup on the left-hand side. Figure 1 also includes an image of the conical vessel fastened with the two flanges on the right-hand side.

## 2.3 Diaphragm material and employment

Two thin diaphragm sets are tightly attached to separate the high-pressure conical vessel from the MPS flange bottom opening (high-Pressure diaphragm / HP diaphragm) and the MPS flange top opening from the surrounding atmosphere (medium-Pressure diaphragm / MP diaphragm). The diaphragm is critical in shock tube employment, so the material and thickness are central features to consider. Aluminum has proven its compatibility in shock tube  $\text{CO}_2$  tests due to fast crack propagation, and aluminum does not create small and diverse fragments during rupturing.

The diaphragms were designed as circular pieces cut from blank, natural smooth aluminum sheets. In addition, the sheets have different thicknesses and were manufactured by Alfer Aluminium (manufacturer art. number: 4001116382741). Three plate thicknesses of 0.3, 0.5, and 0.8 mm were used to form diaphragm sets. An empirical method was applied to determine the optimal combination of thicknesses for the operating conditions (pressure difference between HPS, MPS, and atmospheric pressure section). A series of tests were conducted for this purpose. The tests demonstrated that the best thickness combination for the diaphragm separating the conical vessel from the MPS flange (HP diaphragm) is 1.5–1.6 mm. For the diaphragm between the MPS and atmospheric flanges (MP diaphragm), 1.4–1.5 mm is best. Two gaskets are applied to each diaphragm to prevent any leaks from the membrane. The gasket types are Tesnit BA-GL and Centurion. Both are made of glass, aramid fibers, and nitrile binder. The gaskets are approved for use with CO<sub>2</sub>, pressure up to 30 MPa, and temperatures up to 450 °C.

### 3 Diaphragms rupturing methods and wave patterns

In this double membrane arrangement, the diaphragms rupture either by increasing or decreasing the pressure in the medium-pressure section. Therefore, the pneumatic three-way valve has a prime role in controlling the swift pressure build-up or release in the MPS. Increasing or decreasing the pressure in the MPS occurs by triggering the three-way control valve, adjusting the opening-closing duration, and regulating the necessary amount of CO<sub>2</sub> entering or evacuating from the MPS.

#### 3.1 Diaphragm rupture induced by increasing the pressure in MPS

An increase in the MPS pressure higher than the bursting pressure (the maximum pressure that the diaphragm can withstand) results in the upper diaphragm rupture, which first separates the two flanges. By opening the first diaphragm, pressure in the flange section falls to atmospheric in milliseconds. Then, the second diaphragm ruptures following the increased pressure difference. Figure 2a shows the shape of the conical vessel and the two slip-on flanges fastened to the top of the vessel. Additionally, the steps of diaphragm rupture occur by increasing the pressure in the MPS during the decompression of gaseous and liquid CO<sub>2</sub>.

When the MP diaphragm ruptures, and due to the sudden air compression in the section with atmospheric pressure, a shock wave is generated and propagates outward in the chamber's space. Simultaneously, a rarefaction wave travels downward until it hits the second diaphragm, and then the wave is reflected upwards. Rupture of the diaphragm separating the conical vessel from the mid-section flange generates a second shock wave that propagates through the MPS toward the chamber space, followed by the vapor/liquid interface. A rarefaction wave moves downward through the liquid to the vessel's bottom side, while an evaporation wave travels behind it in the downward direction. Figure 3a shows a graphical representation of the wave pattern in the depressurization sections of liquified CO<sub>2</sub> from the conical vessel caused by increasing the pressure in the MPS.

#### 3.2 Diaphragm rupture prompted by decreasing the pressure in the MPS

When the pressure promptly falls to atmospheric pressure in the MPS, the diaphragm separating the conical

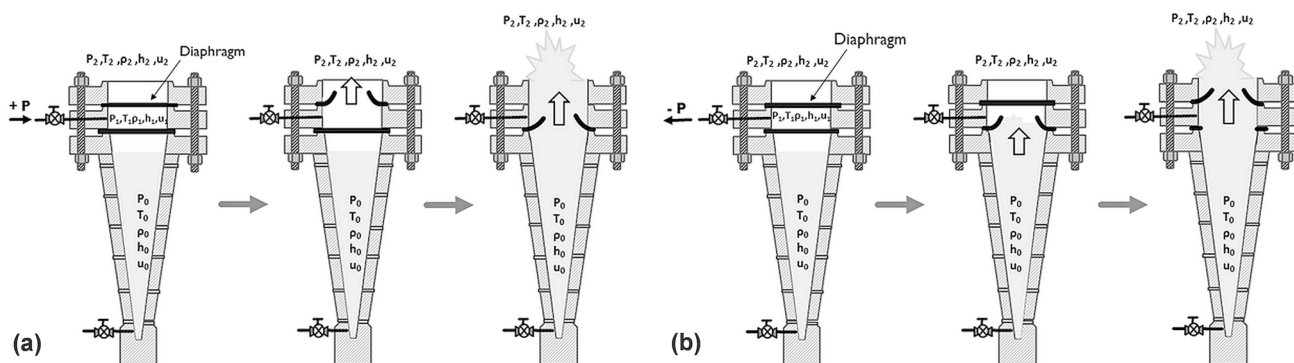


**Fig. 2** Schematic drawing of the structure and stages of diaphragm rupture during the depressurization of liquified CO<sub>2</sub> from the conical vessel. Increasing **a** and decreasing **b** the pressure in MPS

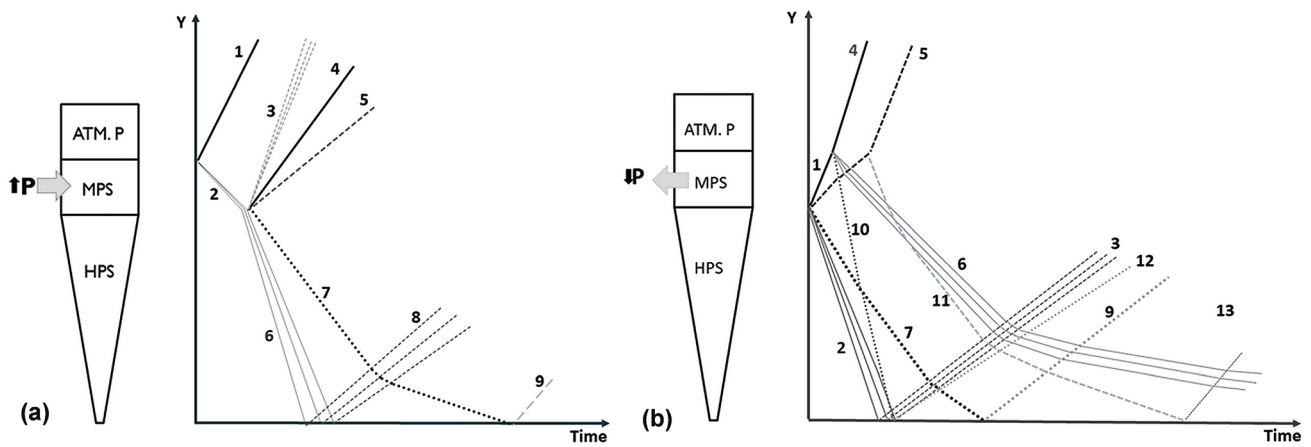


**Fig. 3** Illustrative graph of wave patterns in the vertical y-axis of the conical vessel during liquified CO<sub>2</sub> depressurization caused by increasing pressure in the MPS (a), and decreasing (b) the pressure in the MPS: 1- first shock wave; 2-first rarefaction wave (Fan); 3-first rarefaction wave (fan) reflection; 4-s shock wave; 5-contact surface;

6-s rarefaction wave (fan); 7-evaporation wave; 8-rarefaction wave (fan) reflection; 9-bottom evaporation waves reflection; 10-first shock wave reflection; 11-contact surface reflection; 12-first shock wave reflection's bottom reflection; 13- bottom wave reflection

vessel from the mid-flange ruptures first due to its failure to withstand the higher pressure difference. Then, the diaphragm between the flanges ruptures following the continuous higher difference in pressure. Figure 2 (b) shows the stages of diaphragm rupture in the double-membrane scheme by decreasing the MPS pressure and during CO<sub>2</sub> depressurization in the conical vessel.

Once the diaphragm placed between the vessel and the flange ruptures, a shock wave is formed and moves upward in the MPS. Concurrently, a rarefaction wave emerges and travels down through the liquid CO<sub>2</sub>, followed by an evaporation wave. The shock wave and the contact surface propagating behind it hit the upper diaphragm and are then reflected downward. Consequently, the rupturing of the HP diaphragm generates

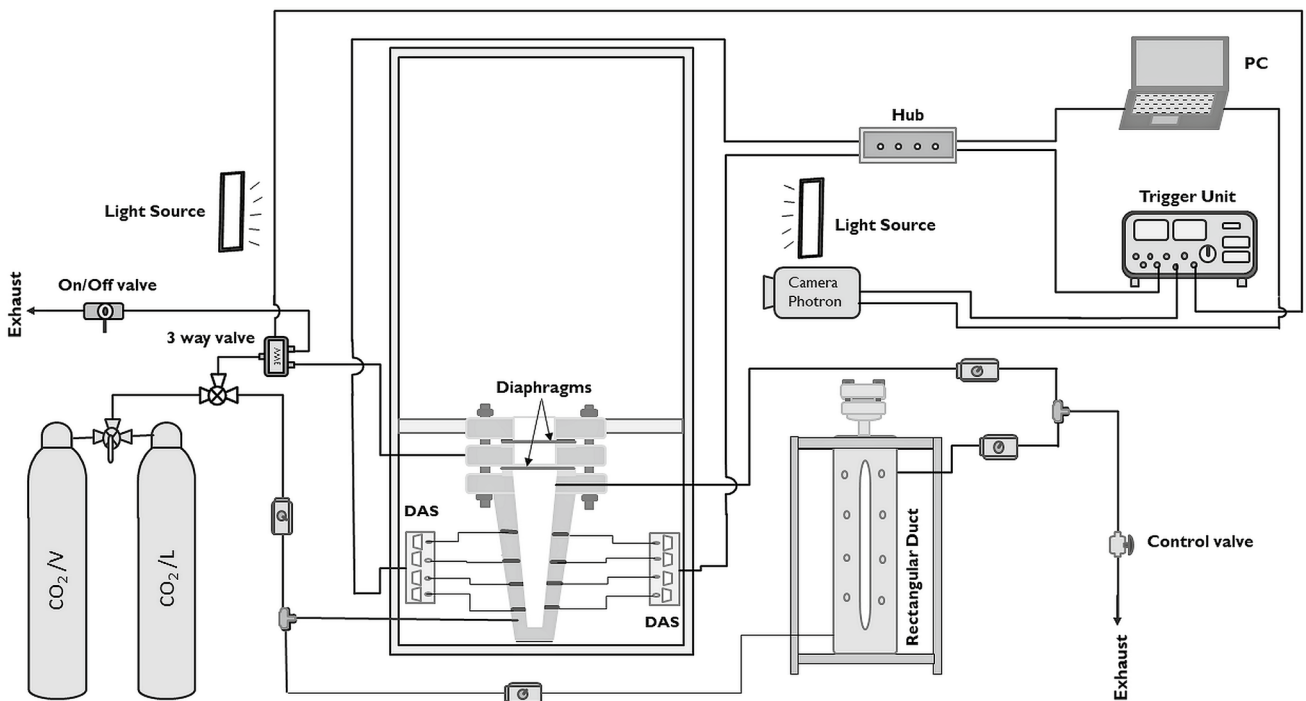


**Fig. 4** Graphical illustration of the constituent components of the experimental installation

a new shock wave that propagates outward toward the chamber's space together with the vapor–liquid contact surface moving behind it. Figure 3b illustrates the waves' pattern for the decreasing pressure method during the depressurization of the liquified CO<sub>2</sub> in the conical vessel.

## 4 Experimental setup and procedure

The experimental system consists of three components. (1) the conical vessel and its accessories in the double-membrane composition; (2) the auxiliary rectangular duct installation; and (3) the control, supply, and data acquisition systems. The double-diaphragm configuration is fixed on an aluminum structure. Above it, there is an atmospheric chamber with a volume of 0.338 m<sup>3</sup>. The chamber's space is covered by polycarbonate sheets on all six faces, with a vent from one side on the top. Figure 4 shows a sketch of the experimental setup.

Industrial-grade two cylinders gaseous and liquid CO<sub>2</sub> supply the HP and MP sections separately. One line supplies the conical vessel and the rectangular duct, and the second line connects to the medium-pressure flange. The gaseous cylinder is equipped with a regulator and a control valve, while the cylinder that supplies liquid CO<sub>2</sub> is equipped with a dip-tube and two control valves.

One of the vital parameters to know in the conical vessel experiments is the volume liquid fraction (LVF). An auxiliary structure is constructed to observe the liquid height in the opaque conical vessel. This structure includes a high-pressure rectangular duct with a glass window connected by a pipe net to the HP vessel, and CO<sub>2</sub> is supplied to the cylinders through four pneumatic valves. The first valve connects the CO<sub>2</sub> cylinders to the conical vessel inlet, and the second controls the flow between the conical vessel and the rectangular duct. The other two valves control the CO<sub>2</sub> flow to the conical vessel and duct outlet pipe, which is connected to a regulator and control valve before CO<sub>2</sub> exhaust. Before filling, the vessel is flushed two or three times with pressurized CO<sub>2</sub> gas at 10 bars. The MPS is primarily filled with CO<sub>2</sub> gas until the pressure reaches 26–28 bar, which is approximately half the pressure in the conical vessel (approximately 52–56 bar). The conical section is filled with liquid CO<sub>2</sub> to a selected level by viewing the rectangular duct's liquid height. It takes 5–7 min to stabilize the liquid level and obtain liquid/vapor equilibrium in the conical vessel. Then, the conical vessel is disconnected from the rectangular duct by closing the control valve between the vessel and the duct.

Four Kulite (XTM-190-2000G) pressure transducers are mounted on the vessel wall. The distances between these transducers are 50, 100, and 100 mm from the bottom.

Besides, these transducers have a pressure range of 0–70 bar and a natural frequency of 410 kHz. A sensor of the same type is attached to the MPS wall to measure the MPS pressure. A Kulite (XTM-190-100G) sensor is mounted in the middle of the vertical chamber's side to measure the overpressure after diaphragm rupture. This sensor has a pressure range of 0–3.5 bar, measuring the overpressure up to 7 bars, and has a natural frequency of 95 kHz. Both transducer types have a piezoresistive sensor as a sensing element and accuracy of approximately ± 1%. To determine the temperature variations in the vessel during CO<sub>2</sub> decompression, three K-type thermocouple temperature sensors were installed on the vessel wall. These temperature sensors are on the side opposite the pressure transducers. The spacing between two adjacent transducers was 150 and 100 mm measured from the bottom to the top. A Photron Fastcam SA-1 high-speed camera, which has a sample rate of 5000 frames per second, captures the emergence and evolution of multiphase release after diaphragm rupture. The illumination system installed on the chamber's opposite sides consists of three LED panels (CE & RoHS, one 80 W, and two 38 W).

## 5 Results and discussion

A series of tests were conducted by opening then closing the three-way valve for various time durations. The times were 0.3, 0.5, 0.8, 1, and 1.5 s. The objective was to draw a comparison between the rupture methods. In addition, two sets of diaphragm thickness combinations (MP/HP diaphragms), 1.5/1.6 and 1.4/1.5 mm, and different liquid volume fractions (LVFs), 42 and 52%, were used. The experiments were carried out under identical initial conditions in the chamber where the temperature and pressure were atmospheric ( $T = 19\text{--}23\text{ }^{\circ}\text{C}$  and  $P$  approximately 0.1 MPa), and the same atmospheric temperature range was maintained in the vessel and MPS. However, the pressure inside the conical vessel was 5.2–5.5 MPa, and the pressure in the MPS was 2.6–2.8 MPa.

### 5.1 Comparison of rupturing methods

Figure 5 shows the pressure readings in the conical vessel for i) increasing and ii) decreasing the MPS pressure. The conditions for the two diaphragms to rupture when decreasing the MPS pressure were the following: diaphragm thickness combination 1.4/1.5, 52% LVF, and valve opening/closing duration of 0.8 s. When the HP-diaphragm ruptured, i.e., a decrease in MPS pressure, a primary shock wave propagated upward followed by the contact surface. When the shock wave reached



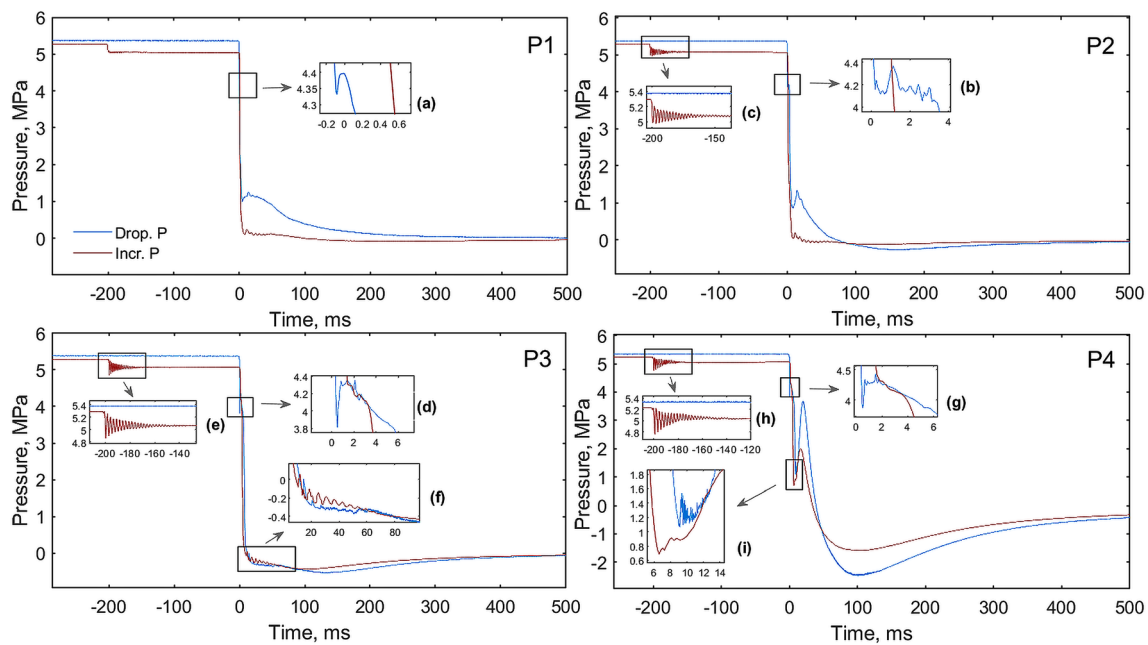


**Fig. 5** Change in pressure transducer recordings inside the conical vessel, from top to bottom (P1 to P4), during the CO<sub>2</sub> depressurization by increasing (Incr. P line) and decreasing the pressure in

the MPS (Drop. P line). Enlarged segments (c), (e) and (h) show the oscillations due to HP diaphragm rupture, and (a), (b), (d), (f), (g) and (i) show fluctuations due to wave reflection

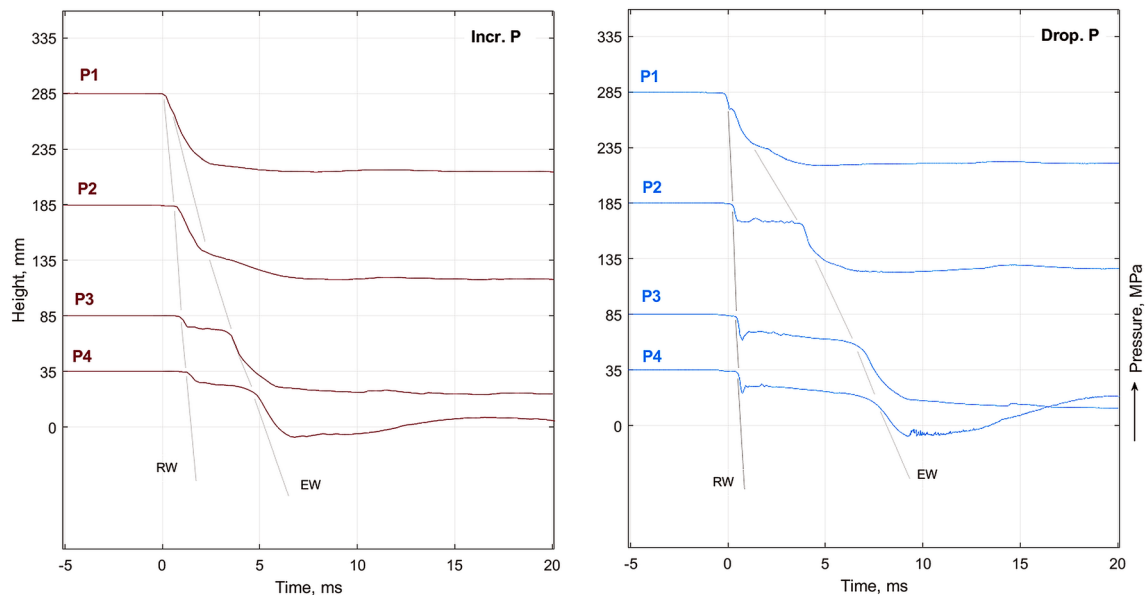


**Fig. 6** Diagram vessel height vs. time for pressure readings during 25 ms of liquified CO<sub>2</sub> depressurization by increasing (left) and decreasing (right) the pressure in the MPS. This shows the wave trajectories of rarefaction (RW) and evaporation (EW)

the MP diaphragm, the wave was reflected, resulting in an increased pressure difference. This pressure difference consequently caused the MP-diaphragm to rupture. The reflection of the first shock wave is shown in the enlarged sectors a, b, d, f, g, and i in Fig. 5 (the blue curves). The fluctuations that were observed on

the MPS pressure fall lines can also be explained as the effect of the reflections of the compression waves hitting the MP diaphragm and the reflections of the expansion waves propagating downwards through the liquid. In the enlarged sectors c, e, and h in Fig. 5, the first pressure drop is due to increasing the pressure in the lines, and

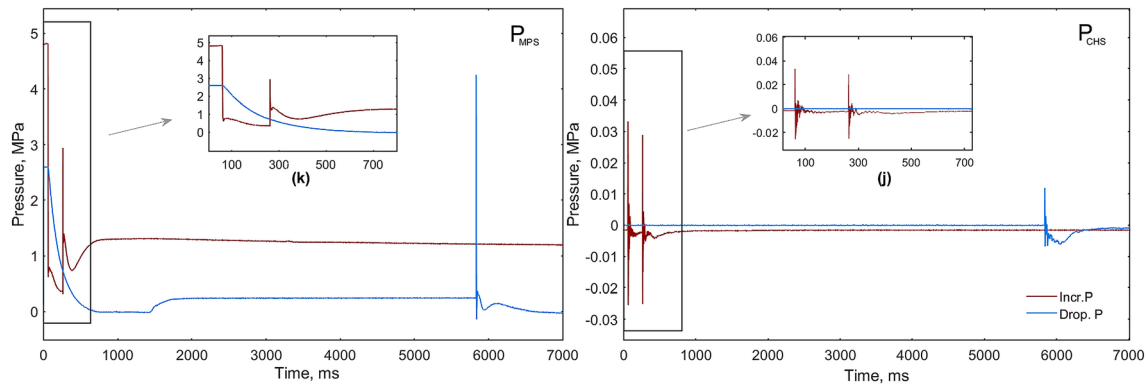


**Fig. 7** Pressure variation in the MPS ( $P_{MPS}$ ) and overpressure variation in the chamber space ( $P_{CHS}$ ) during the time of  $CO_2$  depressurization by increasing (Incr. P line) and decreasing the pressure (Drop. P line) in the MPS

the following oscillations are due to HP diaphragm bulge after MP diaphragm rupturing.

The pressure histories were drawn with reference to the vessel height to clarify the effect of the mentioned wave reflections on the rarefaction and evaporation wave propagation inside the vessel. Every synchronized pressure–time line starts at the corresponding transducer location, as shown in Fig. 6. The pressure–time lines' first and second pressure drop trajectories correspond to the rarefaction and evaporation wave paths, respectively. On the decreasing pressure in the MPS lines, the observed slight fluctuations on the second plateaus were caused by the reflected waves from the MPS. This process slows evaporation wave propagation, as seen from the comparison of the plateau time durations in Fig. 6. The evaporation wavefront velocities were calculated along two height regions (185–85 mm) and (85–35 mm), as shown in Fig. 6. The results indicate that for increasing pressure in the MPS method, the evaporation wavefront propagated with a mean velocity of  $59.98 \pm 0.4$  m/s, while for the decreasing pressure method, the wave's mean velocity was  $39.92 \pm 2.56$  m/s.

Figure 7 illustrates the pressure change in the MPS ( $P_{MPS}$ ) and overpressure generated in the chamber space ( $P_{CHS}$ ) during  $CO_2$  decompression from the conical vessel after the pressure surged in the MPS (Incr. P line), and the pressure fell (Drop. P line). Overpressure was measured, appointing atmospheric pressure as the reference pressure.

The time duration between diaphragm ruptures in the bursting method when increasing the MPS pressure is shorter than that when decreasing the pressure. A possible explanation is that in the former technique, due to the extended pressure variation between the HP diaphragm sides, only this diaphragm needs to burst as the MP diaphragm is already ruptured by a sudden MPS pressure increase. However, in the latter technique, rupturing both

diaphragms is required. Two reflection waves are propagated in the opposite direction of the incident shock and contact surface. Subsequently, the travel of these waves through the MPS slowed down, as shown in magnified parts (j) and (k) in Fig. 7. The time duration between the pressure drop in the MPS and the HP diaphragm rupture is 200.5 ms for the increasing pressure test and 5740 ms for the decreasing pressure test.

The effect of reflected compression waves and encountered reflection of the expansion waves when decreasing the MPS pressure slowed the diaphragm rupture. It also weakened the intensity of the generated shock wave after the MP diaphragm ruptured. This behavior can be observed from the overpressure peaks in Fig. 7, which were 12 kPa after the MP diaphragm ruptured by decreasing the MPS pressure. Furthermore, they were 33 and 29 kPa after the MP and HP diaphragms ruptured, respectively, when increasing the MPS pressure.

When increasing the pressure in the MPS, the MP diaphragm ruptures before the HP diaphragm. Then, the MPS gas expands rapidly close to atmospheric pressure before the HP diaphragm rupture initiates the depressurization process inside the HP vessel. The volume of the MPS is thought to have an insignificant effect on the consequent process. When lowering the pressure in the MPS, the bottom diaphragm will rupture and cause an expansion of fluid from the HP vessel into the MPS before the top diaphragm ruptures. In this case, the state in the HP vessel will depend on the MPS volume. Moreover, an increase in the MPS volume results in a prolonged time between diaphragm rupture and subsequently influences the expansion wave behavior. Regardless of the MPS volume, the duration between diaphragm rupture is still higher for the decreasing MPS pressure technique than for the increasing MPS pressure technique unless the vented opening has the same diameter for both methods.



**Fig. 8** The left and middle images show circular tracks on the bulged diaphragm circumference after the HP diaphragms were ruptured by MPS pressure relief. The right image shows the remain-

ing ring after the bulged loaded section was entirely removed by the HP diaphragm rupturing when increasing MPS pressure

### 5.2 Rupturing mechanism

The diaphragm rupture mechanism depends on considerations such as the pressure required for prompt rupturing, the time duration of the gas entering or leaving the MPS, and the diaphragm disk layer durability and hardness. However, to regulate these factors, it is essential to completely open the diaphragm area under load and prevent multiphase flow disturbance. Regardless of the rupturing method, the bursting mechanism was initiated when the diaphragm layers began bulging due to CO<sub>2</sub> filling. Subsequently, the circular cross-sectional edge weakens due to the maximum strain applied. By increasing the pressure difference between its surfaces, the diaphragm starts to crack in one spot along the circumference and then stretches to remove the entire underloaded cross-section in the case of increasing the pressure in the MPS. In the case of pressure decrease in MPS, a cut is made circularly while leaving a small portion on one side. The images in Fig. 8 show the crack trajectory on the loaded diaphragm circumference after rupturing by decreasing pressure

in the MPS. Furthermore, the residual ring after the diaphragm loaded area was removed because of increased pressure in the MPS. This rupturing mechanism emphasizes that diaphragm bursting does not occur immediately [25], making the multiphase flow start as a jet and grow until it occupies the vessel orifice cross section.

Figure 9 shows cropped images from the high-speed video captured during the experiment with LVF of 52% and 1.5/1.6 diaphragm sets. It shows the development of the multiphase flow and rocketed diaphragm parts after bursting due to the increasing pressure in the MPS. The top series illustrates the MP diaphragm rupture and release from the MPS, whereas the bottom series displays the HP diaphragm rupture and the release from the HP vessel.

As the upper diaphragm bursts first by increasing the MPS pressure and its cross-section under the increased pressure is entirely broken and opened, there is a free path for the upcoming shock wave and multiphase flow. No reflection occurs. This implies that the reflected

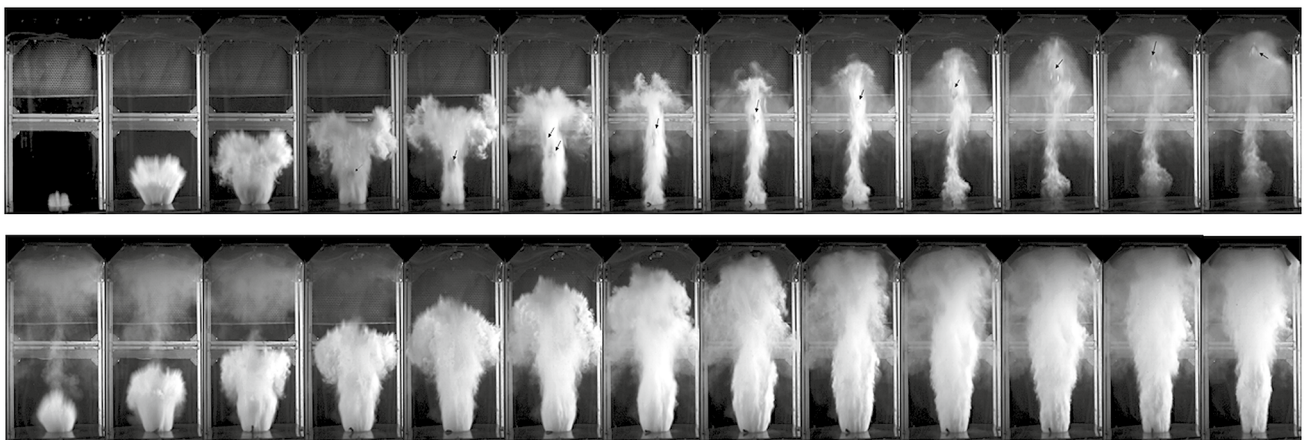


**Fig. 9** High-speed images of the evolution of multiphase flow and the ruptured diaphragm fragments after diaphragm bursting. The time step between two images was 0.56 ms in both sequences

compression wave does not influence the processes inside the conical vessel.

The velocity of the ruptured diaphragms in the chamber is estimated by processing the high-speed videos. The designated approach was to visually track the rocketed diaphragm positions upward after rupturing for 860 mm (the inner vertical distance in the chamber space).

All videos were recorded within 1.79 s at 5400 frames per second (fps) and a resolution of 576 × 1024 pixels. Trajectory tracking was performed with a 0.91 mm/px pixel height conversion. Calculating the velocity of the ruptured slices from the MP diaphragm gives 118–123 m/s, and for the HP diaphragm, it gives 127–132 m/s. As shown in Fig. 9, the ruptured diaphragm fragments, indicated by small arrows on the upper image sequence, proceed with nearly identical velocity as the multiphase flow proceeds. The time step between the pictures on each line is 0.56 ms, and the time between the upper and lower image sequences is 1.68 ms.

## 6 Conclusions

A double-diaphragm vertical conical rig for studying decompression of liquified CO<sub>2</sub> from a diverging cross-sectional vessel is described. The paper also highlights the characteristic features of the test setup. This setup includes a slip-on flange as a medium-pressure section, and the method of rupturing the diaphragms is either a pressure increase or decrease in the medium-pressure section (MPS). A series of experiments were carried out on this setup to compare its performance when applying the two diaphragm rupturing methods.

This paper focuses on the sequence and mechanism of diaphragm rupturing and the generated wave pattern. The conditions included different liquid volume fractions in the conical vessel, different three-way valve opening/closing durations (this valve controls the entry or evacuation of gas in the MPS), and different diaphragm thicknesses.

The experimental results indicate that the rupture caused by increasing the MPS pressure has no reflected compression wave complications in the MPS or test vessel. This is because the MP diaphragm ruptures firstly, the underloaded diaphragm sections are entirely removed. When the pressure in the MPS decreases, the compression waves are reflected back into the vessel, which slows evaporation wave propagation. This evaporation wave slowing, in turn, reduces the phase transition rate. Furthermore, the time between diaphragm bursting when increasing the MPS pressure is shorter than that when decreasing the pressure. In addition, increasing the pressure in the MPS offers more operating simplicity and reliability.

These operational analyses suggest that increasing the MPS pressure is a more feasible technique to conduct CO<sub>2</sub> depressurization tests on this installation for the conditions compared.

Finally, a potential weakness to consider is that the pressure drop in the MPS was performed by evacuating the gas from the MPS through a ½" opening. The evacuation rate could be too slow to attain a higher pressure difference between the vessel and the MPS. The limited dimensions of the slip-on flange used as the MPS excluded a larger opening.

**Authors' contribution** OMI modification of the double-membrane installation, the experimental work, prepared the results and analysis, and wrote the manuscript's first draft. Discussion and editing manuscript. KV Design of experimental setup, geometry, and shape of the conical vessel. Part of discussion and preparation of results. PMH Part of experimental setup assembly, discussion, and preparation of results and manuscript editing. DB discussion of the experimental setup. Discussion and preparation of results and manuscript editing.

**Funding** The funding for the presented work was granted by the University of South-Eastern Norway, USN.

## Declarations

**Conflict of interest** The authors declare there are no conflicts of interest relevant to the content of this article.

**Availability of data and material** The data are not open at the moment but will be made available in the future.

**Code availability** Not applicable.

**Open Access** This article is licensed under a Creative Commons Attribution 4.0 International License, which permits use, sharing, adaptation, distribution and reproduction in any medium or format, as long as you give appropriate credit to the original author(s) and the source, provide a link to the Creative Commons licence, and indicate if changes were made. The images or other third party material in this article are included in the article's Creative Commons licence, unless indicated otherwise in a credit line to the material. If material is not included in the article's Creative Commons licence and your intended use is not permitted by statutory regulation or exceeds the permitted use, you will need to obtain permission directly from the copyright holder. To view a copy of this licence, visit <http://creativecommons.org/licenses/by/4.0/>.

## References

1. Salvi BL, Jindal S (2019) Recent developments and challenges ahead in carbon capture and sequestration technologies. *SN Appl Sci* 1(8):885. <https://doi.org/10.1007/s42452-019-0909-2>
2. Mengmeng X (2013) Thermodynamic and gas dynamic aspects of a BLEVE. Delft University, The Netherlands
3. CCPS (2010) Guidelines for vapor cloud explosion, pressure vessel Burst, BLEVE, and flash fire hazards. American Institute of Chemical Engineers, New York

4. Reid RC (1976) Superheated Liquids. *American Scientist* 64:146–156. <https://www.jstor.org/stable/27847154>.
5. Reid RC (1980) Some theories on boiling liquid expanding-vapour explosions. *Fire* 3:525–526
6. Birk AM, Davison C, Cunningham M (2007) Blast overpressures from medium-scale BLEVE tests. *J Loss Prevent Process Ind* 20(3):194–206. <https://doi.org/10.1016/j.jlp.2007.03.001>
7. Zhang Y, Schork J, Ludwig K (2013) Revisiting the Conditions and Consequences of CO<sub>2</sub> Tank Explosions. 9th G. C. on Process Safety, San Antonio, Texas.
8. Reid RC (1979) Possible mechanism for pressurized-liquid tank explosions or BLEVE's. *Science* 203:1263–1265. <https://doi.org/10.1126/science.203.4386.1263>
9. Simões-Moreira JR, Shepherd JE (1999) Evaporation waves in superheated dodecane. *J Fluid Mech* 382:63–86. <https://doi.org/10.1017/S0022112098003796>
10. Hill LG (1991) An experimental study of evaporation waves in a superheated liquid. Dissertation, California Institute of Technology. <https://resolver.caltech.edu/CaltechETD:etd-10242005-103224>
11. Ren J, Zhao B, Wang C, Bi M (2020) Experimental study on the characteristics of the explosive boiling induced by the pressure relief at the top of vertical vessels. *J LP Process Ind*. <https://doi.org/10.1016/j.jlp.2020.104181>
12. Simões-Moreira J, Shepherd J (1994) Adiabatic evaporation waves. *J Braz Soc Mech Sci* 16(4):445–451
13. Das PK, Bhat GS, Arakeri VH (1987) Investigations on the propagation of free surface boiling in a vertical superheated liquid column. *I J Heat and Mass Trans* 30(4):631–638. [https://doi.org/10.1016/0017-9310\(87\)90193-1](https://doi.org/10.1016/0017-9310(87)90193-1)
14. Dewangan KK, Das PK (2020) Experimental analysis of flashing front propagation in superheated water—Effects of degree of superheat, tube inclination, and secondary nucleation. *Phys Fluids* 32(7):073311. <https://doi.org/10.1063/5.0006840>
15. Munkejord ST, Austegard A, Deng H, Hammer M, Stang HGJ, Løvseth SW (2020) Depressurization of CO<sub>2</sub> in a pipe: high-resolution pressure and temperature data and comparison with model predictions. *Energy* 211:118560. <https://doi.org/10.1016/j.energy.2020.118560>
16. Stotz I, Lamanna G, Hettrich H, Weigand B, Steelant J (2008) Design of a double diaphragm shock tube for fluid disintegration studies. *Rev Sci Instrum* 79(12):125106. <https://doi.org/10.1063/1.3058609>
17. Botros KK, Geerligs J, Rothwell B, Robinson T (2015) Measurements of Decompression Wave Speed in Pure Carbon Dioxide and Comparison With Predictions by Equation of State. *J Pressure Vessel Technol* 10(1115/1):4031941
18. Chaves H (1984) Changes of phase and waves on depressurization of liquids with high specific heat. Dissertation. Max-Planck-Inst. für Stroemungsforschung, Goettingen.
19. Zabelinskii IE, Naboko IM, Tarasenko MV, Shatalov OP (1991) Distortion of the shock front in a shock tube with a divergent conical transition section. *Fluid Dyn* 26(4):593–598. <https://doi.org/10.1007/BF01050323>
20. Reinke P (1997) Surface boiling of superheated liquid. PhD Thesis. ETH Zurich, Switzerland. [http://inis.iaea.org/search/search.aspx?orig\\_q=RN:28030620](http://inis.iaea.org/search/search.aspx?orig_q=RN:28030620)
21. Li M, Liu Z, Zhou Y, Zhao Y, Li X, Zhang D (2018) A small-scale experimental study on the initial burst and the heterogeneous evolution process before CO<sub>2</sub> BLEVE. *J Hazardous Mater* 342:634–642. <https://doi.org/10.1016/j.jhazmat.2017.09.002>
22. Ke W (2009) CO<sub>2</sub> BLEVE (Boiling Liquid Expanding Vapor Explosion). Thesis, Telemark University College. Norway. <http://hdl.handle.net/11250/2439029>
23. Tosse S, Vaagsaether K, Bjerketvedt D (2015) An experimental investigation of rapid boiling of CO<sub>2</sub>. *Shock Waves* 25(3):277–282. <https://doi.org/10.1007/s00193-014-0523-6>
24. Hansen PM (2018) Experimental and theoretical studies of rapid phase transitions in carbon dioxide. Dissertation. The University of South-Eastern Norway. <https://openarchive.usn.no/usn-xmlui/handle/11250/2587457?show=full>
25. Davis HJ, Curchack HD (1969) Shock tube techniques and instrumentation. Harry Diamond Laboratories. Washington D. C.

**Publisher's Note** Springer Nature remains neutral with regard to jurisdictional claims in published maps and institutional affiliations.

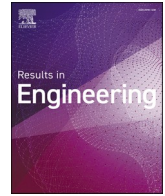
## Rcr gt '4''

- . . . . . #\ . . . . .

Published in the Journal *k* . . . . . , vol. 12.

doi: <https://doi.org/10.1016/j.rineng.2021.100304>.





# Evaporation characteristics during decompression of liquified CO<sub>2</sub> from a conical-shaped vessel

Osama M. Ibrahim<sup>\*</sup>, Per Morten Hansen, Dag Bjerketvedt, Knut Vågsæther

The University of South-Eastern Norway, Faculty of Technology, Natural Sciences, and Maritime Sciences, Department of Process, Energy and Environmental Technology, Kjolnes Ring 56, 3918, Porsgrunn, Norway

## ARTICLE INFO

### Keywords:

CO<sub>2</sub> depressurization  
Divergent cross-section  
Evaporation wave  
Isentropic expansion  
Metastable state

## ABSTRACT

Safe transport of pressurized CO<sub>2</sub> requires a profound knowledge of the processes' effect during the phase transition on catastrophic failure of a tanker filled with liquid CO<sub>2</sub>. This study presents experimental results and analyses associated with the characteristics of expansion waves during depressurization of liquified CO<sub>2</sub> in a divergent cross-section vessel. It explores the rarefaction and evaporation waves velocities analyzed in different three vessel's regions based on the pressure records. Results showed that the evaporation wave velocity increased downward with decreasing cross-section and increased liquid volume fraction. Also, the upstream state properties after the isentropic expansion in the metastable region were determined. The results were compared with previously achieved outcomes of CO<sub>2</sub> decompression from a constant cross-section rectangular duct.

Comparisons indicated significant differences in the wave pattern. So, expansion waves velocities varying in different vessel regions while they were nearly constant for the duct. The evaporation wave velocities were nearly identical for the duct and the upper conical vessel's regions. But their divergence increased as the evaporation wave propagated downwards. Furthermore, the downstream two-phase flow in the conical vessel propagated in an increased cross-section toward the exit. In comparison, there was non-spontaneous two-phase propagation behind the evaporation wave due to the small exit cross-section in the rectangular duct. Additionally, during the isentropic expansion, the degree of superheat was higher for the conical vessel than the duct, resulting in significant discrepancies in the upstream flow properties.

## 1. Introduction

Climate change and global warming are now affecting almost every part of the world due to the augmented greenhouse consequences. The CO<sub>2</sub> emissions from human activities are the primary cause, whereby the burning of fossil fuels like gas, oil and coal are significant contributors. To achieve the Paris climate agreement goal of keeping the rising temperature below 1.5 °C, around 94 Gt CO<sub>2</sub> is projected to be captured and stored by 2050 [1]. Carbon capture and storage (CCS) systems have become a pivotal solution to create carbon-neutral sound technologies. There are other supplemented techniques utilized to ease CO<sub>2</sub> reduction and capturing. These include gasification, conventional combustion, fuel cells, and fuel efficiency enhancement. For instance, upgrading lignite by flotation enhances its heat content and reduces CO<sub>2</sub> releases during combustion [2,3].

Transport of a large amount of captured CO<sub>2</sub>, as a part of carbon

capture and storage systems (CCS), necessitates a deep understanding of associated hazards. Serious safety concerns emerge from an unexpected failure of a tank carrying pressurized-liquified CO<sub>2</sub> caused by external fire overheating, mechanical failure, or corrosion. The rapid release of CO<sub>2</sub> from such a container could lead to an explosive boiling and vaporization and may be described as a boiling liquid expanding vapour explosion (BLEVE). The suddenly freed energy from depressurization initiates strong pressure waves. That potentially promote devastating effects caused by missiles from container fragmentation. Additionally, a considerable amount of CO<sub>2</sub> discharges to the surroundings.

BLEVEs tend to occur as an outsized volume of liquid and vapour expanded in a short time (milliseconds). Consequently, the container walls cannot withstand the grown stress resulting in an explosion [4,5]. Initially, the pressurized liquified CO<sub>2</sub> is at equilibrium with the vapour phase above it and has a temperature higher than its atmospheric boiling point. Its temperature can far surpass its boiling point at a specified

<sup>\*</sup> Corresponding author.

E-mail addresses: [osama.k.ibrahim@usn.no](mailto:osama.k.ibrahim@usn.no) (O.M. Ibrahim), [per.m.hansen@usn.no](mailto:per.m.hansen@usn.no) (P.M. Hansen), [dag.bjerketvedt@usn.no](mailto:dag.bjerketvedt@usn.no) (D. Bjerketvedt), [knut.vagsaether@usn.no](mailto:knut.vagsaether@usn.no) (K. Vågsæther).

<https://doi.org/10.1016/j.rineng.2021.100304>

Received 20 July 2021; Received in revised form 8 September 2021; Accepted 17 October 2021

Available online 11 November 2021

2590-1230/© 2021 The Authors. Published by Elsevier B.V. This is an open access article under the CC BY license (<http://creativecommons.org/licenses/by/4.0/>).



pressure. When the pressure drops rapidly, the liquid's state changes to superheated. The superheated liquid temperature would lay at any point in the metastable liquid region between the saturation and spinodal curves. However, the condition  $(\partial P/\partial V)_T = 0$  is satisfied along the spinodal lines. This line signifies a limit temperature for the thermodynamic degree of superheating (SLT), and the liquid is unstable beyond it. The degree of superheat depends upon the depressurization rate, which, in turn, influences the bubbles' forming and developing mechanisms [6]. In general, at a low/medium degree of superheat, heterogeneous nucleation starts at the wall's surface or on particle impurities. The bubbles develop gradually in size resulting in a violent boiling process. During rapid depressurization and smooth wall's surface, homogeneous nucleation could occur in the liquid bulk. Moreover, the degree of superheat is high, which causes an intense spurt of multiple-phase flow [7].

Several models have suggested that explosion occurs when the liquid that entering the saturation dome becomes superheated. The earliest attempts made by Reid [7] to set the conditions under which BLEVE could arise mentioned that the liquid's temperature should reach the superheat limit temperature (SLT). Thus, the temperature should approach the spinodal curve, and the vapour's expansion occurs promptly due to the evaporation throughout the whole liquid [8]. Additionally, depressurization must be very rapid so that there is not enough time for heterogeneous nucleation to start on the container's walls. Conversely, other experimental studies denoted that it is not strictly necessary for BLEVE incidence to occur that the liquid temperature surpasses the SLT [9,10]. Explosive vaporization of CO<sub>2</sub> could also occur before it reaches SLT as CO<sub>2</sub> changes to the solid phase at atmospheric pressure by originating nuclei which promote liquid flashing [6]. Abbasi and Abbasi [11] reported results from previous experiments where SLT for CO<sub>2</sub> at 2.9 MPa was  $-6^\circ\text{C}$ .

When a rapid decompression of pressurized liquified CO<sub>2</sub> occurs inside a vertical vessel with smooth walls, the superheated liquid in the metastable region attains a high degree of superheating. The homogeneous nucleation proceeds in the liquid bulk during the evaporation process, and the liquid suddenly liberates its stored internal energy. The evaporation process initiates in a part of the liquid, and heat amount is extracted from it. So, the liquid's temperature and vapour pressure drop. The liquid temperature keeps dropping until it reaches boiling temperature. Simultaneously, the vapour pressure reduces towards atmospheric pressure. The rapid phase change with expanded vapour's volume results in multiple-phase bursting out of the vessel, and subsequently, generates a shock wave due to compression of the surrounding air [7]. This wave propagates upwards to the surrounding area with supersonic speed, followed by a primarily created vapour-liquid contact surface. As a subsequent response to the pressure drop, a rarefaction wave propagates with sonic speed downwards inside the vessel, followed by an evaporation wave. The evaporation wave could exemplify a limited zone where the phase transitions occur and travelling with almost constant velocity [12]. The propagation of the evaporation wave into a metastable liquid depends on superheat degree, and it is potentially promoted when the temperature approaches the superheat limit. When the superheat degree is low, the subsequent evaporation rate is insufficient to generate a severe explosion [13]. Noticeable studies on evaporation waves features have been done by Hill [14] and later Reinke et al. [15]. They characterized the bubble formation and movement of the propagated boiling front (photographically). Besides, they measured the velocities ahead of and behind the evaporation wavefront.

The difficulties of full-scale experiments involving phase transition and explosion to provide typical results necessitate numerical models computation. Published literature describes several models to estimate the two-phase flow properties behind the evaporation or condensation waves and the multi-phase flow behind the shock waves. The issued studies described either the two-phase flow dynamics or the shock wave and thermodynamic properties [16–19].

A model describing the phase transition process identifies flow

thermodynamic properties by including an equation of state (EOS). Its function is to determine the state properties and the relation between them in the metastable region. Most EOS calculations are restricted to the equilibrium regions and need to extrapolate from the saturation properties to compute metastable state variables. Various EOSs have been used in depressurization and phase change models for different substances. However, Span-Wagner EOS (SW-EOS) [20] claimed to be the most accurate equation for CO<sub>2</sub> phase transition models. It is used in several types of research, for instance, by Giljarhus et al. [21] and Hansen [22]. SW-EOS has many solution versions, and this work uses the version presented by Mjaavatten [23]. SW-EOS is explicit in the Helmholtz free energy, whereby the thermodynamic properties are calculated as a function of temperature and molar volume.

Although some publications describe experimental work on CO<sub>2</sub> depressurization, very few of them have utilized a double-diaphragm rupturing mechanism with high-pressure or divergent cross-section vessels. Therefore, this study's originality provides new data and analysis of the evaporation characteristics during CO<sub>2</sub> decompression from a double-diaphragm conical rig compared with constant area containers. It focuses on two features: First, the rarefaction and evaporation waves' velocities, and waves propagation interaction during the phase transition. Second, the influence of the divergent cross-section on evaporation wave characteristics by drawing a comparison with previous results from constant cross-section tests.

## 2. Description of experimental arrangements and procedure

Small-scale experiments were carried out on a vertical double-diaphragm conical rig. This installation shows similarities with a shock tube. The main conical rig assembly is stainless steel (AISI 316) and comprises three parts, a conical vessel and two slip-on flanges. The conical vessel functions as a high-pressure section (HPS), while the middle flange operated as a medium-pressure section (MPS). The additional upper flange opens to an atmospheric chamber. It also holds the diaphragm that separates the MPS and atmospheric conditions under load. The conical vessel was securely fixed on the t-slot framing aluminium construction and tightly fastened with the flanges and diaphragms by eight bolts. The conical vessel has a volume of  $480 \cdot 10^3 \text{ mm}^3$  and an inside height of 383 mm. It has solid steel walls with an inclination of  $4^\circ$ , a thickness of 18,67 mm, and an inner surface roughness average of 3.2. The vessel has a bottom diameter of 9.37 mm and is strengthened with a cubic base to hold possible excess strain due to expansion waves propagating through the liquid to the bottom. It has two openings for inflow on the bottom and outflow on the top. Twelve holes for sensors are drilled on the vessel's sidewalls. There are six holes for pressure sensors on one side and six for temperature sensors on the opposite side.

The medium-pressure slip-on flange has a cylindrical middle-section with a diameter of 90.3 mm, a height of 80 mm, and a volume of  $510 \cdot 10^3 \text{ mm}^3$ . Also, it has an inlet/outlet opening fitted with a flexible metallic hose and connected to a three-way valve. Its function is to fill or evacuate the vapour CO<sub>2</sub> in/from the medium-pressure section (MPS). Besides, the slip-on flange is sealed with O-rings on both sides to ensure firmly pressing of the diaphragms, and in turn, to avoid any potential leaks. Fig. 1 illustrates schematic drawing (a) with a close-up of the conical vessel and an image (b) of the experimental set-up.

There are two aluminium diaphragm sets tightly fixed between flanges. One set between the high-pressure conical vessel (HPS) and MPS. Another diaphragm is set between the MPS and the atmospheric flange. The diaphragms are cut from Alfer aluminium blank sheets with three different thicknesses 0.3, 0.5, and 0.8 mm. Based on the results from a series of implemented tests, the diaphragms' combination was designated to be 1.4–1.5 mm for medium-pressure diaphragm (MP) and 1.5–1.6 mm for high-pressure one (HP). Gaskets made mainly of glass, aramid fibres, and nitrile binder were added to the diaphragms' two sides to seal the MPS properly. They were compactly pressed between

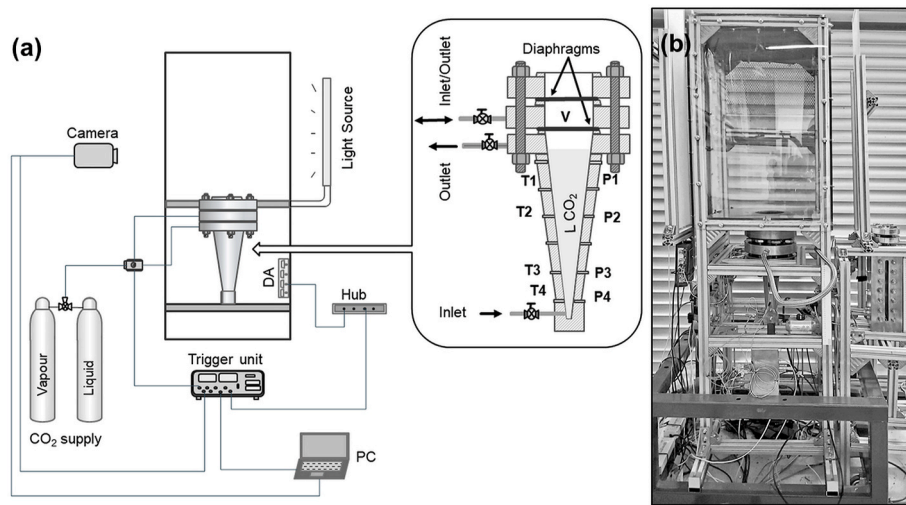


Fig. 1. (a) Set-up schematic drawing including an enlarged segment of the conical vessel details. (b) Installation image showing the conical rig and an auxiliary equipment.

the flanges.

The conical vessel (HPS) and medium-pressure flange (MPS) were separately filled from two industrial graded gaseous and liquid CO<sub>2</sub> cylinders until the pressure reached 5.2–5.6 and 2.6–2.8 MPa, respectively. Because the conical vessel’s walls were untransparent, an additional rectangular duct with a glass window was used as a level gauge. The conical vessel and the rectangular duct connected through a control valve, and they were filled simultaneously to determine the liquid level. The MP diaphragm ruptured following an increase in the MPS pressure by opening the three-way valve. It was triggered through its connection with Quantum pulse generator composers 9500. Subsequently, the MPS pressure swiftly fell to the atmospheric, and the HP diaphragm ruptured due to the growth of pressure difference. The pressure inside the HP vessel was recorded using four Kulite XTM-190-2000G transducers attached on one side of the vessel wall. For temperature recording, three K-type thermocouples were fixed on the opposite sidewall. The same type of transducer is mounted on the MPS’ cylindrical section to record the MPS pressure. Likewise, a Kulite XTM-190-100G measured the overpressure generated after diaphragms’ rupturing in the atmospheric chamber covered from all sides with polycarbonate sheets. These

transparent sheets allowed to capture multi-phase development by high-speed camera Photron Fastcam SA-1. Also, to illuminate the chamber space with three 80 and 38 W LED panels. Besides a high-speed camera, the three-way valve and the data acquisition system were triggered concurrently by the Quantum generating unit.

### 3. Experimental results and discussion

A series of experiments were conducted for the following liquid volume fractions (LVF): 96.4, 83, 73, 62.5, 52, 35.1, and 0%. The initial conditions were the same for all tests with atmospheric temperature in the three sections (19–23°C). While it was 2.6–2.9 in the MPS and 5.3–5.6 MPa in the conical vessel, the chamber pressure was atmospheric (0.1 MPa).

#### 3.1. Features of explosive evaporation from the conical vessel

Fig. 2 shows the variation in pressure sensors records over a 50 ms period of CO<sub>2</sub> decompression. The LVF for (a) was 0, (b) 62.5, and (c) 96.4%. Correspondingly, the temperature change (d), (e), and (f). The

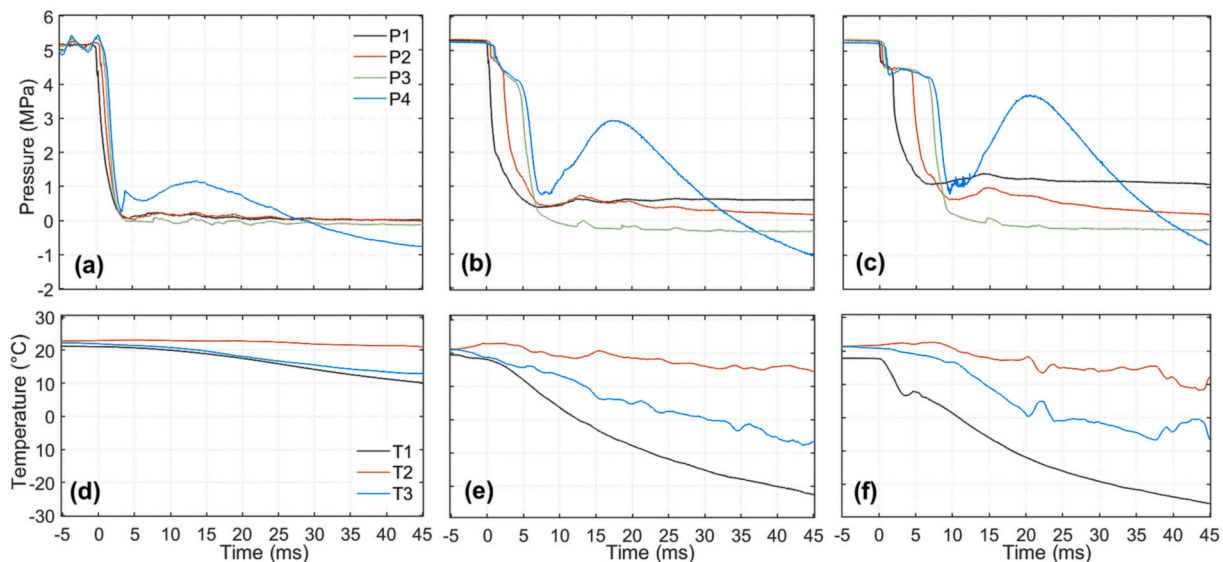


Fig. 2. Graphs from the pressure and temperature sensors’ records P1–P4 and T1–T3 (top to bottom) during 50 ms of CO<sub>2</sub> decompression. For LVF 0% (a, d), 62.5% (b, e), and 96.4% (c, f).

pressure sensors (P1–P4) are positioned at 285, 185, 85, and 35 mm from top to bottom, and the temperature sensors (T1–T3) at 285, 185 and 35 mm. Time 0 indicates the diaphragm rupture and the first pressure drop.

From the data in Fig. 2, when the HP diaphragm ruptured, the pressure fell sharply to temporary metastable liquid pressure. It is about 4.7 for (b) and 4.5 MPa for (c). Subsequently, it either declined steadily (b) or plateaued (c) until the liquid superheated and entered into the metastable state then started to evaporate. This behaviour was not observed in (a) as the LVF was 0%. The turns of the second rapid pressure drop corresponding to the onset of change in the density. Also, indicate a locus of the propagated front where a significant part of phase transition followed behind it. Similar behaviour has been reported by Chaves [24] and later by Simões-Moreira [25]. The pressure steeply fell until it reached between 0.3 and 1 MPa and then gradually decreased to atmospheric. Tiny fluctuations were observed during the latter pressure decrease on lines P1–P3. However, a characteristic development was observed in the bottom pressure transducer P4 signals. It had different record trails with intense oscillations followed by a considerable increase in pressure. As seen in Fig. 2 (a,b, and c), the pressure curve P4 amplitudes increase with increasing the LVF from (a) to (c). The pressure rise depends on the liquid fraction that these reflected waves pass through. So, the pressure curve peaked at 1.1 for (a), 2.9 for (b), and 3.7 MPa for (c). And at the time about 14, 17.6 and 20.4 ms respectively. Unsurprisingly, the temperature decreases during the evaporation process with increasing LVF. The readings from the top temperature sensor for 0–96.4% LVF show a decrease in about 35 °C after 45 ms (see above Fig. 2 (d,e, and f)). The observed pressure change in the P4 curve could be attributed to the expansion wave reflection on the vessel bottom. Which essentially affected the nearest transducer (P4). The compression is most likely caused by the rapid increase of vapour volume above the pressure transducer site. It might also be the damping effect of heterogeneous nucleation and the consequence of multiple reflections of the rarefaction wave from the vessel's bottom. The latter is explained in the next section.

The rarefaction wave propagated downwards through the vapour phase at the sound speed of the gas. A part of this wave reflected on the vapour/liquid contact surface and directed back into the vapour phase. Subsequently, a slight pressure rise (0.01–0.07 MPa) due to the compression observed on the P1-lines in (b and c) Fig. 2. As the LVF increased in the vessel, the liquid prolonged its state as superheated. Subsequently, the pressure indicated a nearly steady profile. For example, this trend can be seen on P2 lines with plateaus for 96.4% LVF and a slight decline for 62.5% LVF (see Fig. 3 below).

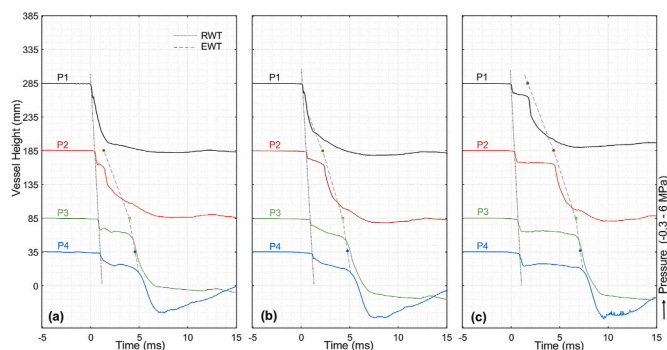


Fig. 3. Pressure transducers readings on vessel height-axis during 20 ms of depressurization of liquid CO<sub>2</sub>. For LVF of 35.1% in (a), 62.5% in (b) and 96.4% in (c). The liquid height in the vessel was 134.1, 239.4 and 369.2 mm, correspondingly. The graph also shows the trajectories of rarefaction waves (RWT) and evaporation waves (EWT).

### 3.2. Dynamic characteristics of the expansion waves

The pressure-time readings were drawn on vessel height versus time scale to measure the characteristic velocities of expansion waves. Wherein the synchronized pressure-time lines begin at the corresponding transducer position and the initial pressure value. Fig. 3 illustrates pressure records on vessel height scale during 25 ms of liquified CO<sub>2</sub> depressurization. For LVF of 35.1, 62.5, and 96.4%.

The curve's points where the first and the second pressure sharply fell represent a trajectory-time for rarefaction wave and evaporation wavefront. The evaporation wave path passes through the time points of pressure change at a stationary height level. As seen in Fig. 3, the evaporation wavefront path is not linear. That is, it propagates with non-constant velocity. As the LVF increases, its propagation starts to delay. As a result, the evaporation wavefront speeds up as it propagated downwards. The rarefaction wave and evaporation wavefront velocities were analyzed graphically based on the time between the turns in pressure sensors readings. Tangent lines were drawn for each pressure reading on the two sides of the curve. Then the tangents' crossing point was connected to the centre point on the line linking the tangency points. This line crossed the curve at a point that allocated the pressure change time.

The results obtained from velocities calculation in the three vessel's height regions are set out in Table 1. The uncertainty in velocities calculation was due to measurement errors of turning points where the pressure fell. The calculation errors were estimated to be between  $\pm 0.4$  and  $\pm 0.6$  m/s for rarefaction waves,  $\pm 1.3$  and  $\pm 3.5$  m/s for evaporation wavefront. The Mjaavatten version of SW-EOS [23] and tabulated data from SW-EOS [20] were used to compute the speed of sound based on the experimental range of saturated CO<sub>2</sub> temperatures 19.5–17.2°C. The average sound speed was 267.2–266.2 m/s. Correspondingly, it was 342.6–370.5 m/s for the liquid phase and 196.6–199.2 m/s for the vapour phase. It is apparent from this table that the evaporation wavefront speeds up as it propagated downwards. The highest speed is in the region between the vessel's height of 85 and 35 mm.

The Pressure-Time-Height graph and velocity calculations were plotted on the height-time diagram to clarify the expansion waves movement and possible reflections interactions. Fig. 4 shows the difference between rarefaction (RW) and evaporation (EW) waves trajectories and their propagation speed. The LVF for (a) is 62.5% and for (b) is 96.4%. In addition, the grey lines show possible reflections after the RW hit the vessel bottom. The liquid height in the vessel substantially influenced those velocities.

After the first pressure drop, the rarefaction wave swiftly pass-through. Depending on the liquid height in the vessel (or LVF), its acceleration intensifies. (see Table 1). That implies it reached the vessel's bottom and reflected faster with increasing LVF. As the LVF increases, a prolonged time is expected for the liquid to stay in the metastable state. That leads to many rarefaction wave reflections between the vessel's bottom and the propagated evaporation wave, as in Fig. 4. It is also seen from the fluctuations just after the rarefaction wave passage, Fig. 2 (b and c). From these fluctuations, some rarefaction wave reflection velocities have been approximated between 192 and 222 m/s.

The fluctuations that emerged from wave reflections in this region were probably comparable to those developed after the evaporation wave has passed. P4 pressure records, Fig. 2 (b and c), required 2.31 ms to drop from 4.01 to 0.83 MPa, and 1.87 ms from 4.08 to 0.89 MPa, for 62.5% and 96.4% LVF, respectively. These numbers explain the disparity in the pressure rise amplitudes after the evaporation wave has passed between 62.5 and 96.4% LVF. The rapid evaporation due to the pressure fall to very low, relative to metastable state one, about 0.9 MPa, indicates a sizeable two-phase volume downstream travelling upwards. Simultaneously, as the pressure P4 run to the trough, a part of an upwards moving two-phase flow changes direction towards the bottom. Subsequently, the pressure increases again and peaks before the two-phase travelling upwards. Then the pressure continues its fall to the

**Table 1**  
Calculated velocities for rarefaction wave and evaporation wavefront in the conical vessel's three regions.

Liquid Height (mm)	Cross-section (mm <sup>2</sup> )	LVF (%)	Rarefaction Wave Velocity RWV/(m/s)				Evaporation Wave Velocity EWW/(m/s)		
			Height region (mm)				285–185	185–85	85–35
			285–185	185–85	85–35	Average			
134.1	277.5	35,1	199.4	291.6	249.1	246.7	–	37.6	88.9
239.4	880.4	62.5	244.3	293.2	245.3	260.9	46.3	47.6	107.1
369.2	2093.9	96,4	300	320	240	286.7	37.8	42.7	111.6

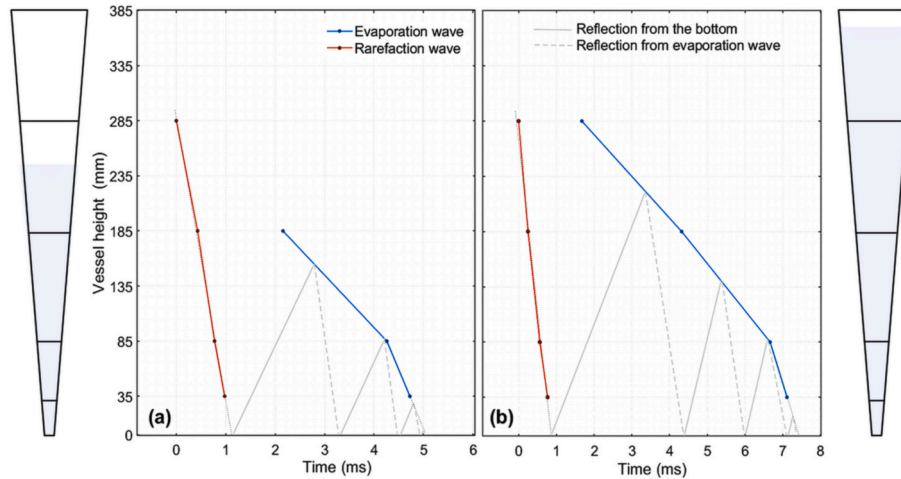


**Fig. 4.** Height-time graph demonstrating the rarefaction and evaporation wave propagation speed for 62.5 and 96.4% LVF, (a) and (b), respectively. Besides, the potential reflections between the vessel's bottom and the descended evaporation wave. Vessels sketches on the sides show the liquid level. The split lines signify the pressure transducers positions.

atmospheric pressure.

The thermodynamic state after the HP diaphragm rupture is traced by isentropic expansion. From the pre-ruptured saturated liquid to the superheated liquid in the metastable state. The thermodynamic properties in the metastable state were determined by applying the Mjåavatten version SW-EOS [23]. Fig. 5 presents pressure-specific volume *P-v* (a) and pressure-temperature *P-T* (b) phase diagrams. Wherein the former, an isentropic expansion performed by SW-EOS is presented on the *P-v* plane. In the latter, a possible path through the states is plotted based on experimental data, LVF of 96.4%.

The isentrope from 5.36 to 4.4 MPa is shown as a line connected states 0 to 1, Fig. 4 (a). The density correspondingly decreased to about 7 kg·m<sup>-3</sup>. Besides, the calculated speed of sound at the metastable

boundary at point 1 was 341.3 m/s. Fig. 5, (b) shows a similar expansion on the possible track line in the *P-T* graph. On the continuous states' development, point 2 denotes the conditions immediately after the second pressure drop. But not at the vessel's exit. The expansion rate (*R<sub>exp</sub>*) was determined from the density decrease during the isentropic expansion and the wave velocity at the metastable limit. The estimated *R<sub>exp</sub>* was 2389.1 kg·m<sup>-2</sup>·s.

### 3.3. Comparison with CO<sub>2</sub> depressurization results from a constant cross-section test device

According to Reinke [26] and Chaves [24], contrary to the current study results, the test device geometry does not influence the

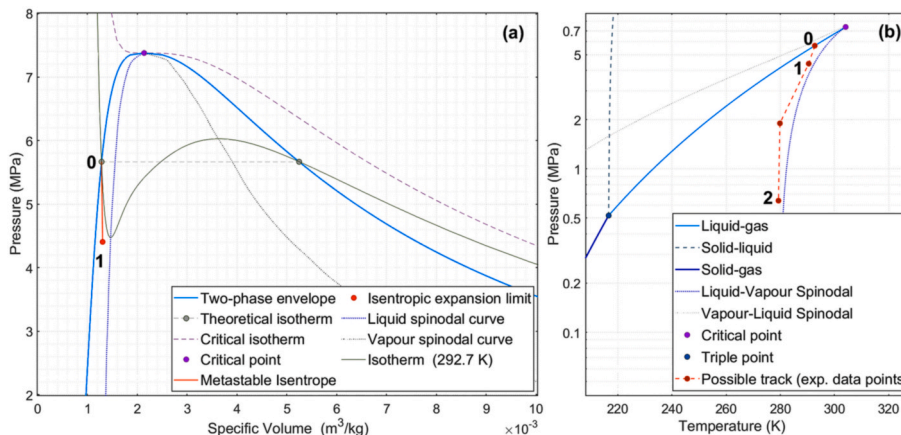


**Fig. 5.** (a) Pressure-specific volume phase diagram shows an isentropic expansion from saturated liquid state 0 to metastable state 1. (b) Pressure-temperature phase diagram displaying potential trajectory through the experimental states data P4 in Fig. 2-c.

evaporation wave movement and velocity. However, in the Reinke et al. study [15], the boiling front velocity was observed in different diameter tubes inserted into the test tube. They noticed that the front movement is affected by the tube wall. Subsequently, the velocity increased slightly with the decrease in tubes' diameter. But they mentioned that there was no significant effect of the cross-section area on the front velocity. At this juncture, the above velocity calculations are partly agreed with this observation. However, as stated earlier, the evaporation wave propagation speeded up considerably downwards (see Table 1). The different results from the mentioned studies were probably due to the decompression of other substances than CO<sub>2</sub> (Perfluoro-n-hexane, butane, propane, Refrigerant-134a, and water). It is also possible dissimilar details in the test device geometry.

Comparing the above-calculated velocities and those obtained from CO<sub>2</sub> depressurization in constant cross-section in previous research indicates notable differences in evaporation wave behaviour. In their studies, Hansen [19] and Tosse [27] described an evaporation wave propagated at a nearly constant velocity between 20 and 42 m/s. Whereas in the conical vessel, it travels at a higher speed in varied regions. Particularly in the zone close to the bottom (107,1–111.6 m/s), see Table 1.

### 3.3.1. Comparison of pressure profiles

The pressure records shown in Fig. 2 (b and c) were compared to those achieved by Hansen [21]. To capture detailed differences, CO<sub>2</sub> depressurization was conducted on a rectangular duct with a constant cross-section for 0 and 100% LVF. (the 100% is a possible visual height which corresponds to 68% of the duct's volume). Fig. 6 compares the pressure histories in the rectangular duct (D) and the conical vessel (CV). The corresponding contrasted LVF are both 0% in (a), 100% and 62.4% in (b), and 100% and 96.4% in (c). Pressure sensors were positioned on the upper part of the rectangular duct at 31, 81.8, and 132.8 mm from the top. In comparison, they sited at 98, 198, and 298 mm on the conical vessel from the top. The conical vessel has an extra 59 mm in inner height compared to the rectangular duct.

The pressure drop required more time in the rectangular duct during the evaporation process than the conical vessel. As seen in Fig. 6 (b, c), the additional time was about 21 ms to approach atmospheric pressure. It signifies that the two-phase flow downstream in the rectangular duct was not moving spontaneously. Instead, it probably choked or was disturbed due to a small cross-section in the exit for expanded two-phase flow. On the other hand, the two-phase flow in the conical vessel was propagating in a gradually increasing cross-section towards the exit.

The data in Fig. 6 shows considerable fluctuations in the rectangular duct's pressure lines. In contrast, no such pattern is related to the

pressure records from the conical vessel upper part. There are two likely explanations for the former behaviour. First, the rapid expansion of vapour/liquid phases develops a sizable two-phase flow, which is temporarily trapped before its exit from the duct. Besides, the bubbles' size growth caused by heterogeneous nucleation represses the evaporation process continuation. With the help of high-speed video recordings, Hansen [24] observed heterogeneous wall nucleation in front of the evaporation wave. He mentioned that it led to the reduction in the degree of superheat in the rectangular duct set-up. After the first drop in pressure and initiation of the rarefaction wave, the liquid in the conical vessel had remained longer in the metastable state than in the duct before the evaporation wave started its propagation. This difference is between the first and the start of the second pressure drop (see Fig. 8 below).

### 3.3.2. Clarifications about initial conditions

The pre-rupture pressure in the conical vessel experiments varied from those conducted in the rectangular duct. However, the conical vessel is a part of an arrangement that has a double-diaphragm rupturing mechanism. The medium-pressure diaphragm ruptured first due to increased pressure in the medium section. As a result, the high-pressure (HP) diaphragm bulged. Subsequently, the pressure inside the conical vessel became unsteady and reduced. Then it stabilized again before the

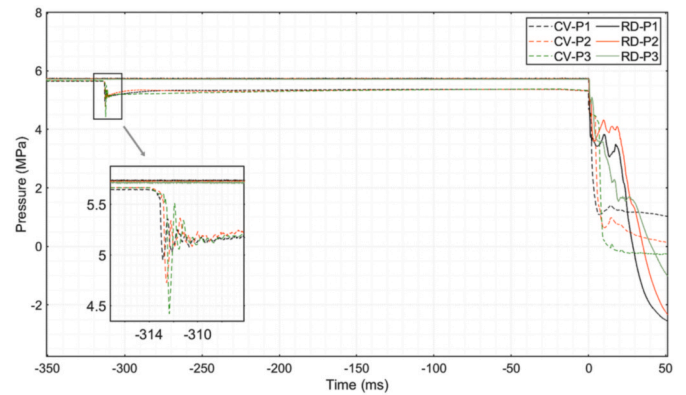


Fig. 7. Pressure signals recorded in the experiments shown in Fig. 6 (c), including 350 ms before the HP-diaphragm ruptured in the rectangular duct and conical vessel. The close-up section shows the pressure response to the MP-diaphragm rupturing in the conical rig.

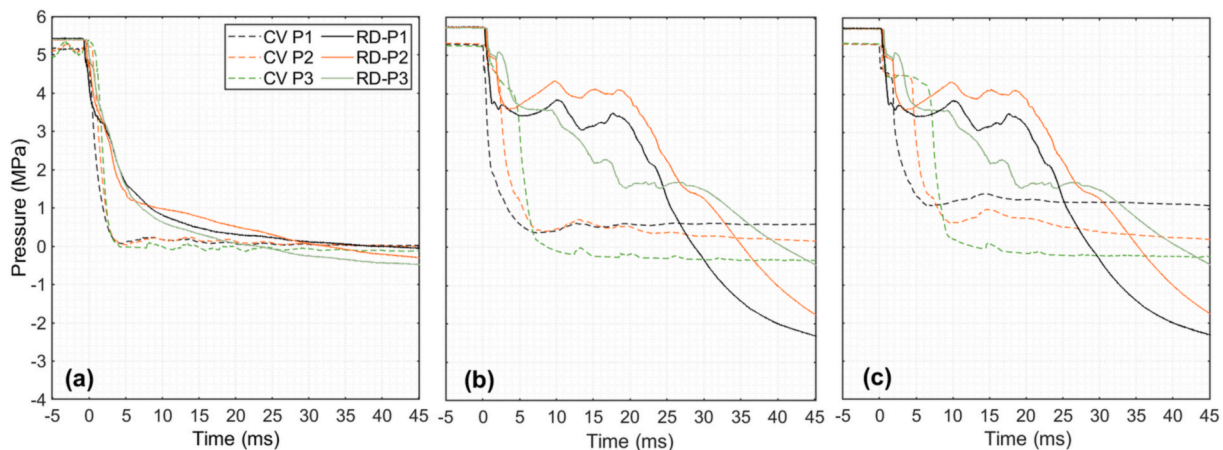


Fig. 6. Comparison of Pressure sensors readings over 50 ms of CO<sub>2</sub> depressurization from the rectangular duct and the conical vessel. (a) for 0%, (b) for 100 and 62, 5%, and (c) for 100 and 96.4% LVF.

HP-diaphragm has ruptured. The difference in pre-ruptured pressure between the two devices is about 0.36 MPa. Pressure records from the experiments displayed above in Fig. 6 (c) are compressed to cover 350 ms before the HP-diaphragm ruptures. It is illustrated in Fig. 7 for both rectangular duct and conical vessel. The graph contains an enlarged segment showing the MP-diaphragm rupturing at about 313 ms before the HP-diaphragm ruptured. The initial temperature was 292.7 K. After the MP-diaphragm rupturing in the conical vessel, the observed temperature change was minimal, about 3 K.

3.3.3. Comparison of expansion flow characteristics

The evaporation wave speed mostly depends on the degree of superheating (DOS) [14]. Which is defined as the maximum expansion in the metastable region and expressed by Simões-Moreira [25] as  $(P_s - P_m)/P_s$ . Where  $P_s$  is saturated pre-rupture pressure, and  $P_m$  is metastable limit pressure after the isentropic expansion (at state 1 in Fig. 5 (a)).

Fig. 8 represents enlarged segments comparing the pressure profiles shown in Fig. 6 during 10 ms of liquified CO<sub>2</sub> decompression in the conical vessel and the rectangular duct. The LVFs were 0% in (a), 62.5 and 100% in (b), 96.4 and 100% in (c), correspondingly.

For the duct's experiments with 100% LVF, the pressures dropped during isentropic expansion from 5.84 to 5.50 MPa. The corresponding DOS was about 0.14. On the other hand, during isentropic expansion in the conical vessel experiments (62.5 and 96.4% LVF), the

pressures fell from 5.36 to 4.40 MPa and 5.28 to 4.05 MPa. The resultant DOS were 0.18 and 0.23, respectively. Other experimental results done by Hansen [28] on the rectangular duct demonstrated much lower DOS (0.11). It is noticeable from these numbers that the DOS was higher in the experiments conducted in the conical vessel than those in the duct. Moreover, this also explains why the evaporation wave velocities were higher in the conical vessel than in the duct. Table 2 below compares the pre-ruptured saturated state and calculated properties for supersaturated liquid after isentropic expansion in the metastable region.

This table is quite revealing in several ways. First, the differences in upstream properties between the conical vessel and the rectangular duct were caused by the variation in DOS at the metastable state. There is a difference in the DOS of about 0.09 between the vessel and duct. This variation could have led to the mentioned disparity of the other properties (density and enthalpy). Second, the difference between calculated evaporation wave velocities grew as the conical vessel's cross-section decreasing. The difference was 73.5 m/s in the region close to the bottom and 0.3 m/s at the upper zone. The velocity is nearly constant for the rectangular duct. Third, since the evaporation wave velocity increased downward and the cross-section upward in the conical vessel, further discrepancies are expected to detect in downstream properties.

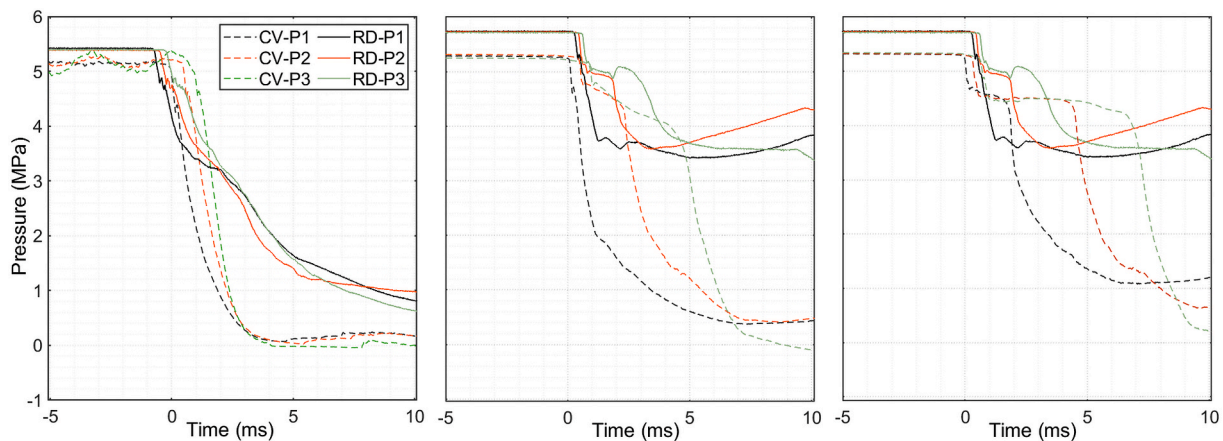


Fig. 8. Comparison of Pressure sensors readings over 10 ms of CO<sub>2</sub> depressurization from the rectangular duct and the conical vessel. (a) for 0%, (b) for 100 and 62, 5%, and (c) for 100 and 96.4% LVF.

Table 2

Pre-ruptured at the saturated state and calculated metastable upstream properties. The experiments were performed in the rectangular duct (100% LVF) and conical vessel (96.4% LVF).

Property		Rectangular Duct	Conical Vessel
Saturated State	Pre-rupture pressure $P_0'$ (Mpa)	5.8	5.4
	Temperature $T'$ (K)	294	290.3
	Density $\rho'$ (kg/m <sup>3</sup> )	764.4	801.3
Upstream Metastable State	Metastable limit pressure $P_f'$ (Mpa)	5.0	4.4
	Density $\rho'$ (kg/m <sup>3</sup> )	756.7	794.3
	Maximum EW velocity $v_{max}'$ (m/s)	38.1	111.6
	Minimum EW velocity $v_{min}'$ (m/s)	38.1	37.8
	Enthalpy $h_f'$ (kJ/kg)	257.6	245.4
	DOS	0.14	0.23

#### 4. Conclusion

Laboratory-scale experiments were conducted in a double-diaphragm installation that comprises a divergent cross-section vessel as a high-pressure section. The rarefaction and evaporation wavefront velocities were analyzed in three vessel's regions lengthwise based on the pressure histories. Results indicated that the evaporation wavefront velocity increased with decreased cross-section area and increasing liquid volume fraction (LVF). The calculated highest and lowest velocities were 111.6 and 37.8 m/s in the region close to the vessel's bottom and upper region, respectively, for 96.4% LVF. Besides, the thermodynamic properties of superheated CO<sub>2</sub> in the metastable state were determined utilizing the Span-Wagner equation of state. The obtained results were compared with previous experimental results from CO<sub>2</sub> depressurization in a vertical rectangular duct.

There are notable differences in expansion wave features in the two cases. First, the duct's exit cross-section did not allow instantaneous passage of rapidly expanded two-phase flow. In comparison, it moved in an increased cross-section towards the exit in the conical vessel. Second, the evaporation wave velocity was steady in the constant cross-section devices. In contrast, it increased in the conical vessel as the cross-section area shrank. Third, significant disparities in the upstream properties were caused by corresponded variation in the degree of superheating during the isentropic expansion in the metastable region. These differences are anticipated to influence downstream properties significantly.

#### Funding

This research did not receive any specific grant from funding agencies in the public, commercial, or not-for-profit sectors.

#### Credit Author Statement

**Osama M.Ibrahim:** Conceptualization, Methodology, Investigation, Writing – original draft, Visualization, Formal analysis. **Per Morten Hansen:** Methodology, Conceptualization, Resources, Writing-Reviewing and editing, Supervision. **Dag Bjerketvedt:** Conceptualization, Formal analysis, Writing- Reviewing and editing, Supervision. **Knut Vågsæther:** Conceptualization, Methodology, Validation, Resources, Writing- Reviewing and editing, Supervision, Project administration.

#### Declaration of competing interest

The authors declare that they have no known competing financial interests or personal relationships that could have appeared to influence the work reported in this paper.

#### References

- [1] I.E. Agency, 20 Years of Carbon Capture and Storage, 2016.

- [2] G. Cheng, M. Zhang, Y. Cao, Y. Lu, Y. Feng, S. Zhao, Preparation and evaluation of lignite flotation collector derived from waste hot-pot oil, *Fuel* 267 (2020) 117–138.
- [3] G. Cheng, Z. Li, Y. Cao, Z. Jiang, Research progress in lignite flotation intensification, *International Journal of Coal Preparation and Utilization* 40 (1) (2020) 59–76.
- [4] A.C. Van den Berg, M.M. Van der Voort, J. Weerheijm, N.H.A. Versloot, BLEVE blast by expansion-controlled evaporation, *Process Saf. Prog.* 25 (1) (2006) 44–51.
- [5] CCPS (Center for Chemical Process Safety), Guidelines for Vapor Cloud Explosion, Pressure Vessel Burst, BLEVE, and Flash Fire Hazards, second ed., Process Safety Progress, Wiley, New York, 2010, pp. 311–336.
- [6] R.C. Reid, Superheated liquids, *Am. Sci.* 64 (2) (1976) 146–156.
- [7] R.C. Reid, Possible mechanism for pressurized-liquid tank explosions or BLEVE's, *Science* 203 (4386) (1979) 1263–1265.
- [8] M.M. van der Voort, A.C. van den Berg, D.J.E.M. Roekaerts, M. Xie, P.C.J. de Bruijn, Blast from explosive evaporation of carbon dioxide: experiment, modeling and physics, *Shock Waves* 22 (2) (2012) 129–140.
- [9] Y. Zhang, J. Schork, K. Ludwig, Revisiting the conditions for a CO<sub>2</sub> tank explosion, in: Proceedings of the Ninth Global Congress on Process Safety, AIChE, San Antonio, Texas, 2013.
- [10] D. Bjerketvedt, K. Egeberg, W. Ke, A. Gaathaug, K. Vaagsaether, S.H. Nilsen, Boiling liquid expanding vapour explosion in CO<sub>2</sub> small scale experiments, *Energy Procedi* 4 (2011) 2285–2292.
- [11] T. Abbasi, S.A. Abbasi, Accidental risk of superheated liquids and a framework for predicting the superheat limit, *J. Loss Prev. Process. Ind.* 20 (2007) 165–181.
- [12] J.R. Simões Moreira, J.E. Shepherd, Evaporation waves in superheated dodecane, *J. Fluid Mech.* 382 (1999) 63–86.
- [13] CCPS (Center for Chemical Process Safety), Guidelines for Evaluating the Characteristics of Vapor Cloud Explosions, Flash Fires, and BLEVEs, Wiley, New York, 1994, pp. 60–160.
- [14] L.G. Hill, An Experimental Study of Evaporation Waves in a Superheated Liquid, PhD Thesis, California Institute of Technology, USA, Pasadena, California, 1991.
- [15] P. Reinke, G. Yadigaroglu, Explosive vaporization of superheated liquids by boiling fronts, *Int. J. Multiphas. Flow* 27 (2001) 1487–1516.
- [16] S. Gourari, F. Mebarek-Oudina, O. Makinde, M. Rabhi, Numerical investigation of gas-liquid two-phase flows in a cylindrical channel, *Defect Diffusion Forum* 409 (2021) 39–48.
- [17] A.M. Nagib Elmekawy, M.E.H.H. Ali, Computational modeling of non-equilibrium condensing steam flows in low-pressure steam turbines, *Result. Eng.* 5 (2020) 100065.
- [18] G. Pinhasi, A. Ullmann, A. Dayan, Numerical model for boiling liquid-vapour explosion (BLEVE), *Int. J. Heat Mass Tran.* 50 (2007) 4780–4795.
- [19] P.M. Hansen, A.V. Gaathaug, D. Bjerketvedt, K. Vaagsaether, Rapid depressurization and phase transition of CO<sub>2</sub> in vertical ducts – small-scale experiments and Rankine-Hugoniot analyses, *J. Hazard Mater.* 365 (2019) 16–25.
- [20] R. Span, W. Wagner, A new equation of state for carbon dioxide covering the liquid region from the triple-point temperature to 1100 K at pressures up to 800 MPa, *J. Phys. Chem. Ref. Data* 25 (6) (1996) 1509–1596.
- [21] K.E.T. Giljarhus, S.T. Munkejord, G. Skaugen, Solution of the Span-Wagner equation of state using a density-energy state function for fluid-dynamic simulation of carbon dioxide, *Ind. Eng. Chem. Res.* 51 (2012) 1006–1014.
- [22] P. Hansen, Experimental and Theoretical Studies of Rapid Phase Transitions in Carbon Dioxide, PhD Thesis, Process, Energy and Automation Engineering, University of South-Eastern Norway, Porsgrunn, Norway, 2018.
- [23] A. Mjaavatten, Thermodynamic Models and Tools for H<sub>2</sub>O, H<sub>2</sub>, CO<sub>2</sub> and Air, GitHub, 2020. <https://github.com/are-mj/thermodynamics/releases/tag/v2.1.1>.
- [24] H. Chaves, Changes of Phase and Waves on Depressurization of Liquids with High Specific Heat, PhD Thesis, Max-Planck-Institut für Strömungsforschung, Göttingen, Germany, 1984.
- [25] J.R. Simões-Moreira, J.E. Shepherd, Adiabatic Evaporation Waves, PhD Thesis, Department of Mechanical Engineering, Rensselaer Polytechnic Institute, Troy, N. Y., 1994.
- [26] P. Reinke, Surface Boiling of Superheated Liquid, PhD Thesis, Paul Scherrer Inst. (PSI), Villigen, Switzerland, 1997.
- [27] S. Tosse, K. Vaagsaether, D. Bjerketvedt, An experimental investigation of rapid boiling of CO<sub>2</sub>, *Shock Waves* 25 (3) (2015) 277–282, 2015.
- [28] P.M. Hansen, A.V. Gaathaug, D. Bjerketvedt, K. Vaagsaether, Blast from pressurized carbon dioxide released into a vented atmospheric chamber, *Shock Waves* 28 (5) (2018) 1053–1064.

## Reprint '5'

### Release of liquid CO<sub>2</sub> from the bottom of a duct.

This paper is under review and was submitted to *Journal of Loss Prevention in the Process Industries* in April 2023.





.....Tgrgcug'qhlhls wkf 'EQ4'ht qo 'vj g'dqvwqo 'qhl'c'f wev'

"

Quco c'O0Klctj ko "c."Cpft2 "Xci pgt'I ccyj cwi "c."Rgt'O qtvgp"J cpugp"c."Fci "Dlgtngxgf v"c.".....  
Mpw'X"i uâ vj gt"0'

"

c"Vj g'Wpkkgtuk{ "qh'Uqwj /Gcungtp" P qty c{ ." "  
"HcewM{ "qh'Vgej pqmji { ."P cwten'Uekpegu."cpf 'O ctkko g'Uekpegu." "  
"F gr ctvo gpv'qh'Rtqegu."Gpgti { "cpf 'Gpxkqpo gpvcn'Vgej pqmji { ." "  
"Mlãmpgu"Tkpi "78."5; 3: "Rqtui twpp."P qty c{0'  
.....

'Quco c0MKlctj ko B wup0q="Cpftg0KI ccyj cwi B wup0q="Mpw0Xci ucyj gtB wup0q="....."

'r gt0 0 cpugpB wup0q="Fci (Dlgtngxgf vB wup0q0"....."

'Quco c'O0Klctj ko \*Eqtgur qpf kpi "cwj qt+<QTEKF <2222/2225/4843/34340"

"

"

"

"

"

"

"

"

"

"

"

"

"

"

"

**Cduwcev''**

Vj ku'r cr gt'r t gugpu'g zr g tlo g pvcn't guwmu'qh'vj g'tcr kf 'r j cug'vcpukqap'qh'iks wkf 'EQ4'tgrgcugf 'htqo " vj g'dqwqo "qh'c"uo cm'tgevcpi wrc't f wev'\*DT-0'Vj g'cko "ku'vq"eqpukf gt'vj g'hcevqtu'kphwgpelpi "vj g" r j cug'vcpukqapu'cpf "vj g'tgrgcug'tcvg'kh'vj g'twr wtg'ctgc'ku'dgrny "vj g'iks wkf "rgxgr0'Vj g'vguu'y gtg" kpkkcvgf "d{ "twr wtkpi "vj g'f kcr j tci o "ugr ctcvki "vj g'vguv'ugevkap'htqo "cp"cw qur j gtle"ej co dgt0' Rt guuwg'cpf "vgo r gtcwtg'o gcuwtgo gpu'y gtg'wugf "vq"cpcn| g'vj g'r j cug'vcpukqap0'Cnuq."c"j ki j / ur ggf "uj cf qy i tcr j "vej pls wg'y cu'wugf "vq"xkuwrk| g'vj g'y cxgu0'Vj g't guwmu'y gtg'eqo r ctgf "y kj " gctrkgt "vqr /tgrgcug'vguu"\*VT +y j gtg'vj g'twr wtg'ctgc'y cu'cdqyg'vj g'iks wkf "rgxgr0'Vj g'f wevu'qwrpv" i culy q/r j cug'hmj "y cu'ej qngf "lp'vj g'VT"vguu0'Vguv't guwmu'uj qy gf "c'f khgtgpv'dgj cxkqt "hqt"vj g" DT0' Vj g'uj cf qy i tcr j "ko ci gu" f go qputcvgf "vj cv" y j gp" vj g" rks wkf ly q/r j cug" hmj gf "qww." vj g" rks wkf lcr qt "kpvthceg"tgo clpgf "pgctn| "hz gf "wpki'k" dtqng"wr 0'Vj ku'dgj cxkqt "kpf kcvgu"vj cv'vj g" j gcf ur ceg'xcr qt'j cf "ikwrg'kphwgp'ep'qp'vj g'kpkcn'gxcr qtcvkap'lp'vj g'DT"vguu0'Vj g't guwmu'htqo "vj g" ewtgpvDT"vguu'kpf kcvgf "c'hmj gt'f gi tgg'qhlwr gtj gcvki "vj cp'lp'vj g'VT"vguu."cpf "vj g'gxcr qtcvkap" tcvg'y cu'v|r kcm| "vy q'vko gu'hcuvgt0"

"

**Mg{y qtf u'**

Dqwqo 'tgrgcug.'Tctghcevkap'y cxg.'Gxcr qtcvkap'y cxg.'Rj cug'vcpukqap.'Vy q/r j cug'hmj 0'

"

**Ct veng'J hi j hi j vu'**

- Á Vj g'tgrgcug'dgrny "vj g'iks wkf 'EQ4'rgxgr'uj qy u'c'f kwp'ev'g zr cpukap'y cxg'ut wewtg"
- Á Hcuvt'gxcr qtcvkap'f wtkpi "dqwqo /tgrgcug'vguu"vj cp'lp'vqr 'tgrgcug"
- Á Uj cf qy i tcr j u'uj qy "vj g'iks wkf lcr qt'kpvthceg'u'gxqnwkap'f wtkpi "dqwqo /tgrgcug'vguu"

"

"

"

"

"

### 30 Kpvt qf wevkqp"

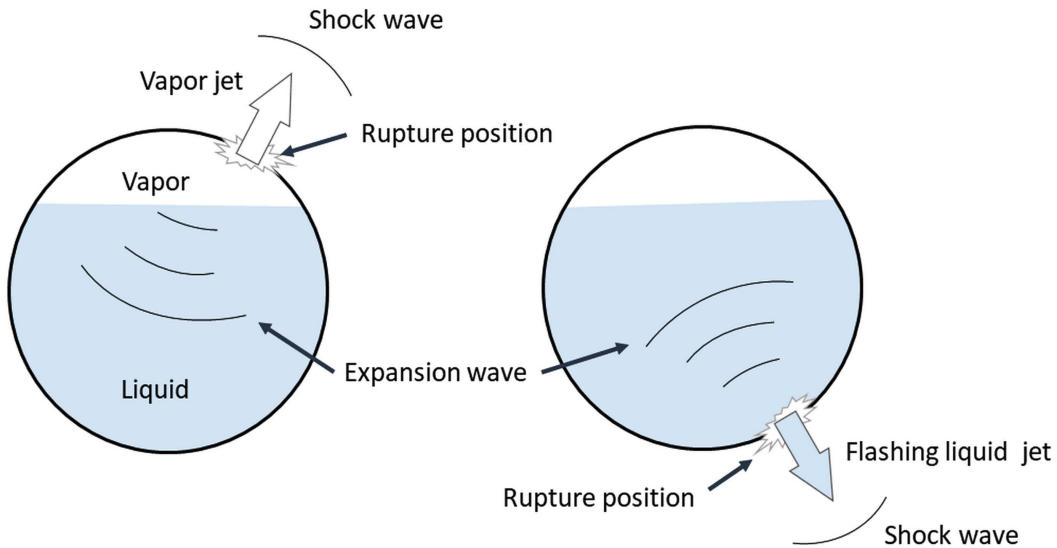
Ecvcutqr j le"hcwmg"qh"e"r tguuwtk gf "EQ4"xguugn'o c{ "ngcf"v"dqkiki "rks wkf" gZR cpf kpi "xcr qt" gZR mUKqp "DNGXG-0Qxgthkiki . "qxgtj gcvkpi . "h{ kpi "htci o gpw. "hwi wg. "qt"eqttukqp"o c{ "ecwug" uwej "gxgpw0Vj g"eqpugs wgegu"kpemf g"f co ci kpi "druv'y cxgu."j c| ctf qwu"m{ kpi "htci o gpw. "cpf" vj g"f kiej cti g"qh"hwkf u"kvq"vj g"uwttqwpf kpi u"]3\_0K"ku"etwekri"kp"f guki plki "cpf"qr gtcvki "EQ4" kphcutwewt g"v"wpf gtucpf "vj g"r tgeguugu"kpqxrgf "kp"vj g"ceekf gpwnt grgcug"qh'rks wkhgf "EQ40Vj ku" mpqy rgi g"ku'tgs wkt gf "v"r tgf kev."eqpvtqn"cpf "r tngxpvr"qvwpknj" c| ctf u0"

Cp"gzco r ng"qh"uwej "c"DNGXG"gxgpv"ku"vj g"EQ4"ceekf gpv"kp"Tr egrcm"J wpi ct{ ."kp"3; 8; 0Vj g" ceekf gpv'y cu"ecwugf "d{ "qxgtHkiki "c"xguugn"eqpcklki "57"vqu"qh"EQ4"cv"307"O Rc."cpf "/52A0Vj cv" xguugn'tw wtgf . "etgcvki "c"m{ kpi "htci o gpv"vj cvj k'cpf "dwtu'cpvj gt"xguugn'wpf gt"vj g'rks wkf "rgxgn0 Vj cv"xguugn'y cu'r wngf "htqo "ku"hwpf cvkqp"cpf "tqengvf "v"c"r tgegu"rdqtcvt{ "f kucpeg"cy c{ 0' P kg'r gtuqu'f kgf "f wg"v"vj g"gzr mUKqp"u"eqpugs wgegu"]4\_0'

Y j gp"vj g"xguugn'tw wtu'dgmj "vj g'rks wkf "rgxgn"vj g"gzr cpukqp"y cxg'r tqr ci cvgu'w y ctf u'vj tqwi j " vj g'rks wkf "cpf" "xcr qt. "cu'uj qy p"qp"vj g'tki j v'ukf g"qh"Hi 030C u'c'tguwn."vj g'rks wkf "ku'f kgev{ "r wuj gf" qw"kvq"vj g"uwttqwpf kpi u0'F wg"v"vj g"hw'r j cug"tcpuukqp."c"uj qem'y cxg"ku'i gpgtcvgf "kp"vj g"ck" qwukf g" vj g" xguugn' Xcr qtcvki "qewtu" cv" vj g" uco g" wo g" kpkf g" cpf "qwukf g" vj g" xguugn' Vj g" xcr qt k cvkqp"r tgegu"kpukf g"vj g" xguugn'ku"o ckn{ "kphwpegf "d{ "vj g"xcr qt"j gcf ur ceg"gzr cpukqp" hqmj gf "d{ "ku"eqpf gpucvki 0Vj g"gzr cpf gf "xcr qt"eqpf gpugu'f wg"v"vj g"gzr cpukqp"y cxg"htqo "vj g" tw wtg"xgpv"cpf "gzr cpukqp"y cxg"tghgevkqp"qp"vj g"xguugn'u"vqr 0'Y j gp"vj g"xguugn'tw wtu."vj g" qwhmj kpi "rks wkf "kpucpvn{ "gxcr qtcvku"]5\_0"

Y j gp"c"xguugn'tw wtu"cdqvg"vj g'rks wkf "rgxgn"vj g"xcr qt"r tguuwtg"kp"vj g"xguugn'tcr kn{ "f getgcugu0 Uko wncpgqwan{ ."c"tctghcevkqp"y cxg'r tqr ci cvgu'f qy py ctf u'vj tqwi j "vj g"xcr qt"j gcf ur ceg"cpf "vj g" rks wkf 0'Cu"vj g"xcr qt" gZR cpf u."ku"vgo r gtcwtg"f getgcugu"cpf "o c{ "r ctvn{ "eqpf gpug"cpf "htggj g0 O qtgqxt." f wtkpi " vj g" gZR cpukqp" y cxg" r tqr ci cvkqp." vj g" rks wkf " vgo r gtcwtg" tkugu" cdqvg" ku" cvo qur j gte" r tguuwtg" dqkiki " r kpv" cpf " dgeqo gu" uwrgtj gcvgf 0' K' tgo ckpu" vgo r qtctkn{ " kp" c" o gvcucdng"ucvg"dghqtg"vj g'r j cug"tcpuukqp"qewtu0Vj g"gxcr qtcvki"y cxg"htqpv'r tqr ci cvgu'cu'c"vj kp" | qp"qh"v{ "dwddrgu0Vj g'tgs wkt gf "rvgpvj" gcv'ht"xcr qt k cvkqp"ku"ces wkt gf "htqo "vj g"uwrgtj gcvgf " rks wkf " ]6\_0' Uwdugs wgpvn{ ." cp" gZR cpf gf " y q/r j cug" o kzwtg" r tqr ci cvgu" f qy puatgco " qh" vj g" y cxg"htqpv."cpf "vj g'tgo ckpki "rks wkf"u"xcr qt"r tguuwtg"cpf "vgo r gtcwtg"f getgcugu0K"vj g"rvgpvj" gcv' r tqxkf gf "d{ "vj g'rks wkf"u"ugpukdng"j gcv'ecppqv"gxcr qtcvg"vj g'y j qng'rks wkf . "vj g'tgukf wcnrks wkf "r qt vki"

ku'tgrgcugf "cu'c'hcuj kpi 'lqv'qwukf g"17\_0Vj g'f tcy kpi 'kp'Hki 03'uj qy u'vj g'f khgt gpegu'kp'vj g'utwewt g' dgwy ggp"vqr /ukf g'cpf "dqwqo /ukf g'tgrgcugu0""



**Hki 03** < Uej go c'le'f tcy kpi "uj qy kpi "vj g'tgrgcug"qh'r tguuwt k' gf "rks wkhgf "i cu'htqo "c"xguugn'f wtkpi " twr wtkpi 'htqo "vj g'vqr "rghv'cpf "vj g'dqwqo "t'ki j v0"

J ki j /ur ggf 'hkm kpi 'ku'y gml'uwk'gf "v'uwwf { kpi "vj g'ej ctcevgt'uwk'eu'qh'vj g'g'zr cpuk'qp'y cxgu'f wtkpi "vj g' tgrgcug" qh' uwr gtj gcvgf " rks wkh u0' J cpugp" gv' cr0' ]8\_ "gzco kpgf "vj g'r j cug" 't'cpuk'kqp" f wtkpi "vj g' f gr tguuwt k' c'kqp"qh'rks wkh "EQ4"kp" c'tgevcpi wrt "f wev'htqo "vj g"xguugn'u"vqr 0'C"ugt'k'gu'qh'uej r'kgt'gp" ko ci gu" f go qpux'cvgf " vj g' gctn' " uci gu" qh' tct'gh'c'v'kqp" cpf " g'xcr qtc'v'kqp" y cxg" r tqr ci c'v'kqp'0' Ceeqtf kpi n' . " vj g' g'xcr qtc'v'kqp" y cxg" r tqr ci cvgf " f qy py ctf " cv' 52/62" o lu0 Vj g' g'xcr qtc'v'kqp" y cxg'ht'qp'v'x'gm'ek'k'gu'cv'f khgt'gp'v'eq'p'v'k'p'gt' k'p'ek'p'c'v'k'qp"r qu'k'k'qp'u'j cxg'dggp" g'zr g'tko gp'v'cm' { "uwwf k'gf " d' { "F gy cpi cp"gv'cr0' ]9\_0Vj g'v'guu'y gtg'eqpf wevgf "kp"t'cpur ct'gp'v'wd'gu."ngpi vj "qh'20'o . "h'kmgf "y kj " y cvgt'0Vj g'wdg'y cu'ug'c'ngf "y kj "c'r' n'uwk'f k'cr j tci o "cpf "uwo gti gf "kp" c'eq'pu'v'cp'w' { "j gcvgf "rks wkh " eq'p'v'k'p'gt'y kj "t'cpur ct'gp'v'y cm'0Vj g't'guu'u'uj qy gf "cp"kp'v'k'c'v'g't'gr'v'k'qp'uj k' "dgwy ggp" g'xcr qtc'v'kqp" y cxg'ht'qp'v'x'gm'ek'k' { "cpf "wdg'k'p'ek'p'c'v'k'qp" cpi ng'0C'u'vj g'cpi ng'k'p'ek'p'c'v'k'qp" k'p'et'gcugf "kp"vj g'7/52Å"vj g' y cxg'ht'qp'v'x'gm'ek'k' { k'p'et'gcugf "f wg"v'q'vj g'x'cr qt'r j cug'u'hc'v'gt'o q'xgo gp'0C'p'k'p'uki p'k'k'c'p'v'y cxg'ht'qp'v' x'gm'ek'k' { "ej cpi g'y cu'q'dugt'x'gf "kp" c"t'cpi g'qh'52/67Å'0'J qy g'x'gt. "k'p'ek'p'c'v'k'qp" dgwy ggp"67"cpf " ; 2Å' i tcf wcm' { k'p'et'gcugf "vj g'y cxg'ht'qp'v'x'gm'ek'k' { 0Q'v'j gt'qr'w'c'n'v'ej' p'ks w'gu'y gtg'c'nu'q'w'k'k' gf "kp"ug'x'gt'c'n' uwwf k'gu'0Vj g'j ki j /ur ggf 'r j q'v'qi t'cr j u'vj c'v'k'nu'wt'cv'gf "vj g'g'xcr qtc'v'kqp"y cxg'utwewt g'cpf "f g'v'gt'o k'pgf " ku'x'gm'ek'k' { "y gtg'w'k'k' gf "kp"uwwf k'gu'uwej "cu"Uko ; gu/O qt'g'k'c": . "T'g'k'p'ng" ]4\_ "cpf "J k'n'i"; 0'

Uq'ht' . "vj gt'g'j cu'dggp"r'kw'g'f k'ue'w'uk'qp"cd'q'w'vj g'r j cug"t'cpuk'k'qp"o ge'j c'p'k'uo u'f wtkpi "vj g'tgrgcug" dg'ny "vj g'rks wkh "h'g'x'g'ri'kp" c'eq'p'v'k'p'gt'0X'gp'ct'v'gv'cr0' ]32\_ "f k'ue'w'ugf "vj g'gh'ge'v'q'h'vj g'rks wkh "eq'p'v'p'v'qp"

vj g"gxqrwkp"qh'c'xguugn'g'zr m'ukqp'f w'g'v'q'qxgtj g'c'v'p' 0'K'v'j g'vgo r gtcwtgu'tkug'kp'c'xguugn'hkmgf " vq'v'j g'o gf kwo 'h'xgn'v'j g'y cmi'eqwf 't'wr wt g'cv'v'j g'xcr qt'j gcf ur ceg'y kj 'cp'g'rcu'kcm' 'r' tqr ci cv'kpi " etcen'0Cu'v'j g'etcen'ut'gvej gu'dgm'y 'v'j g'rs w'k'f 'h'xgn'v'j g'xguugn'eqp'v'kpo gpv't'cr k'f n' 'h'cku' 't'gr'cukpi " v'j g'eqp'v'p'u'k'p'v'q'v'j g'uwtt'q'w'p'f k'pi u'0'E'q'p'ugs w'gp'v'w'f . "v'j g'eqp'v'p'u'g'zr cp'uk'qp' 'h'q'm'y u'cp' 'k'ug'p't'qr k'e" h'rcuj "g'xcr q't'c'v'k'p'0'V'j g't'gu'w'k'p'i "d'rc'u'v'g'h'g'ew'y g't'g'h'q'w'p'f "v'q'd'g'o q't'g'u'g'x'g't'g'k'p'v'j g'D'N'G'X'G'g'x'g'p'u' y kj "j k'j g't'h'k'p'i "h'x'g'n'0'V'ã'u'ug'g'v'c'f'0' ]33\_ "g'z'c'o k'p'g'f "v'j g'g'x'c'r q't'c'v'k'p'p'y c'x'g'c'p'f "e'q'p'v'c'ev'uw't'h'c'eg" uw't'w'ew't'g'f g'x'g'n'r o gp'v'k'p'c'x'g't'k'ec'n'r q'n'f'c't'd'q'p'c'v'g'w'd'g'f w't'k'p'i "r's w'k'f "E'Q'4'f g'eq'o r t'g'u'k'p'0'V'j g' r'c'r g't'eq'o r c't'g'f "y c'x'g'uw't'w'ew't'g'u'f w't'k'p'i "y'q'w'd'g'o go d't'c'p'g'd'w't'w'k'p'i "t'g'i k'o gu'q'p'v'j g'v'q'r "x'c'r q't" u'k'f g'+c'p'f "d'q'w'o "r's w'k'f "u'k'f g'0'Y j g'p'v'j g'w'd'g'o go d't'c'p'g'd'w't'w'q'p'v'q'r ."c'p'g'x'c'r q't'c'v'k'p'p'y c'x'g'y c'u' q'd'ug't'x'g'f "v'q'r t'q'r ci c'v'g'k'p'v'q'v'j g'r's w'k'f "y kj "c'x'g'm'ek'f "q'h'42/52"o l'u'y j k'g'v'j g'e'q'p'v'c'ev'uw't'h'c'eg" x'c'r q't' h'y q/r j c'ug'o k'z'w't'g'r t'q'r ci c'v'g'f "w'r y c't'f 0'J q'y g'x'g't. "y j g'p'v'j g'o go d't'c'p'g'd'w't'w'q'p'v'j g'd'q'w'o . " v'j g'k'p'v'g't'h'c'eg'x'c'r q't' h'y q/r j c'ug'o k'z'w't'g'y c'u'c'ee'g'n't'c'v'g'f "f'q'y p'y c't'f "c'u'g'x'c'r q't'c'v'k'p'p'r t'q'eg'g'f g'f "c'v'v'j g' w'y q/r j c'ug'o k'z'w't'g'r's w'k'f "uw't'h'c'eg'0'C'n'q. "v'j g'r's w'k'f "g'x'c'r q't'c'v'g'f "q'p'v'j g'd'q'w'o "u'k'f g.'d'w'v'j g'h'm'y k'p'i " q'w'y c't'f u'x'g'm'ek'f "y c'u'o w'ej "i t'g'c'v'g't'v'j c'p'v'j g'g'x'c'r q't'c'v'k'p'p'y c'x'g'r t'q'r ci c'v'k'p'p'k'p'k'f g'v'j g'w'd'g'o"

Uj c'p'i "g'v'c'f'0' ]34\_ "t'g'eg'p'w'f "r'g't'h'q't'o g'f "g'z'r g't'k'o g'p'u'y k'j "g'z'r m'uk'x'g'g'x'c'r q't'c'v'k'p'p'k'p'c'ew'd'g'x'g'u'gn'q'h' 39" f'o "v'q'g'x'c'n'c'v'g'v'j g't'w'r w't'g'r q'uk'k'p'k'o r c'ev'q'p'v'j g'g'z'r m'uk'p'p'k'p'v'p'uk'f 0'K'p'c' "u'g't'k'g'u'q'h'v'g'u'u. "v'j g' x'g'u'gn'y k'j "r t'g'u'uw't'k' g'f "y c'v'g't'y c'u't'w'r w't'g'f "c'd'q'x'g. "d'gm'y "v'j g'r's w'k'f "h'x'g'n'q't'c'v'v'j g'x'c'r q't' h'r's w'k'f " k'p'v'g't'h'c'eg'0'C'p'c'n'f' u'g'u"q'h'v'j g'r t'g'u'uw't'g'o g'c'u'w't'g'o g'p'u'f go q'p'ut'c'v'g'f "v'j c'v'v'j g't'w'r w't'g'f k'ue"n'q'ec'v'k'p'p' u'k'i p'k'h'k'ec'p'v'f "k'p'h'w'g'p'eg'f "v'j g'g'z'r c'p'uk'p'p'q'h'v'j g'v'y q/r j c'ug'h'm'y "q'w'c'p'f "k'p'uk'f g'v'j g'x'g'u'gn'0'C' "t'w'r w't'g' k'p'v'j g'i c'u'r j c'ug'r t'q'o q'v'g'f "g'z'r m'uk'x'g'g'x'c'r q't'c'v'k'p'p'q'h'v'j g'r's w'k'f "y kj "u'w'd'uc'p'v'k'n'v'y q/r j c'ug'q'w'h'm'y 0' V'j g'w'y q/r j c'ug'q'w'h'm'y "f g'et'g'c'ug'f "k'p'uk'f g'y j g'p'v'j g't'w'r w't'g'f k'ue"y c'u'q'ec'v'g'f "c'v'v'j g'i c'u'r's w'k'f " k'p'v'g't'h'c'eg'0'J q'y g'x'g't. "v'j g'r t'g'u'uw't'g'e'q'p'uk'f g't'c'd'n'f "t'g'd'q'w'p'f g'f 0'Y j g'p'v'j g't'w'r w't'g'y c'u'd'gm'y "v'j g'r's w'k'f " h'x'g'n'v'j g'r's w'k'f "r j c'ug'j c'f "p'q'v'g'z'r c'p'f g'f "g'p'q'w'i j =k'v'j c'f "d'g'eq'o g'k'p'u'w'h'h'k'ec'p'v'f "u'w'r g't'j g'c'v'g'f "v'q'ec'w'ug" u'k'i p'k'h'k'ec'p'v'f t'g'u'uw't'g't'g'd'q'w'p'f 0"

H'g'y "g'z'r g't'k'o g'p'c'n'uw'f k'g'u"j c'x'g'd'g'g'p'ect't'k'g'f "q'w'q'p'r's w'k'f "E'Q'4'f g'r t'g'u'uw't'k' c'v'k'p'p'd' { "t'w'r w't'k'p'i "v'j g' e'q'p'v'k'p'g't'd'gm'y "v'j g'r's w'k'f "h'x'g'n'0'J g'p'eg. "v'j g'r t'g'ug'p'v'uw'f { "f go q'p'ut'c'v'g'u'p'q'x'g'n'r j { u'k'ec'n'c'ur g'ew'q'h' r j c'ug'v't'c'p'uk'k'p'p'f w't'k'p'i "E'Q'4't'g'rc'ug'd'gm'y "v'j g'r's w'k'f "h'x'g'n'0'V'j k'u'y q't'n'h'q'ew'ug'u'q'p'v'j g't'c't'g'h'c'ev'k'p'p' c'p'f "g'x'c'r q't'c'v'k'p'p'y c'x'g'e'j c't'c'ev'g't'k'ue'u'k'p'uk'f g'c't'g'ev'c'p'i w'rc't'f w'ev'y k'j "v'j g'q'w'w'g'v'r q'k'p'v'k'p'i "f'q'y p'y c't'f u'0' V'j g'g'z'r g't'k'o g'p'c'n't'g'u'w'u'uj q'w'f "e'r'c't'k'h'f "y j g'y j g't'v'j g't'g'rc'ug'v'c'v'g'c'p'f "v'j g'd'g'j c'x'k'q't'q'h'g'z'r c'p'uk'p'p' y c'x'g'u'f w't'k'p'i "d'q'w'o "t'g'rc'ug'f'k'h'g't'u'f'q'o "r t'g'x'k'q'w'u'f "t'g'r q't'v'g'f "t'g'u'w'u'f'q'o "v'q'r /t'g'rc'ug'v'g'u'u" ]37\_0

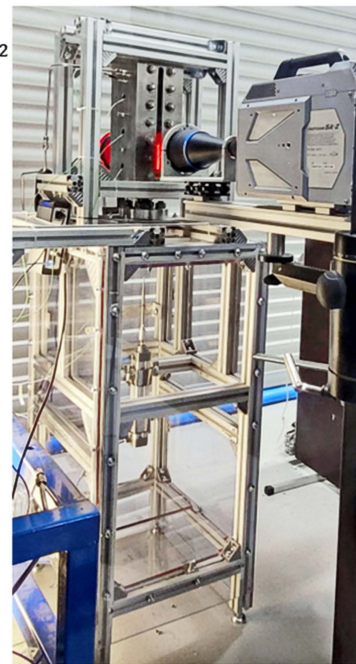
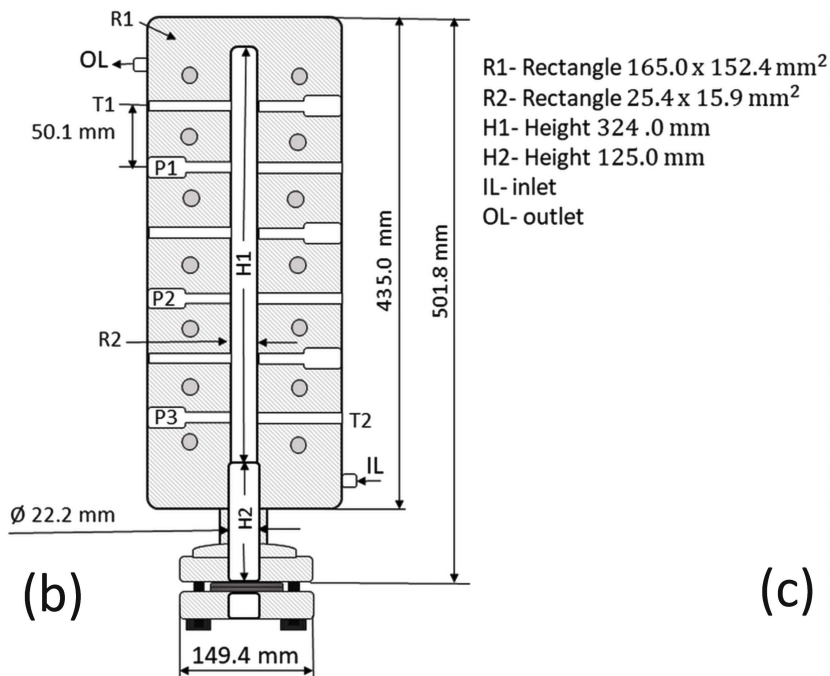
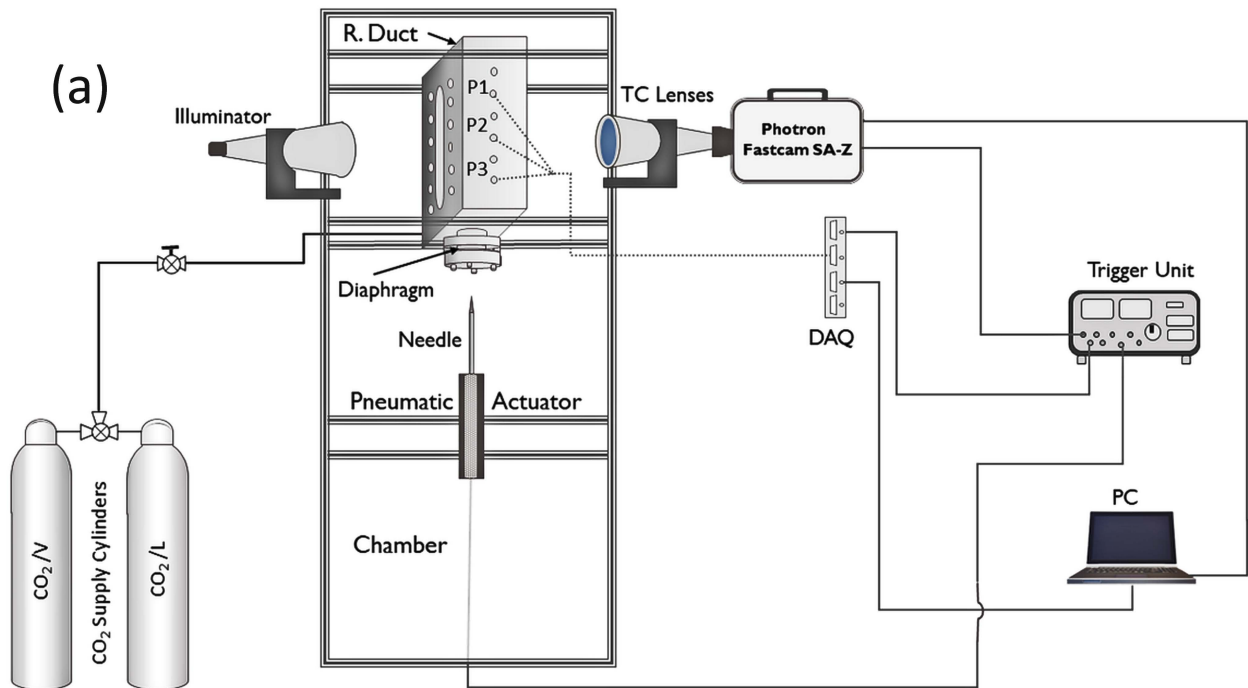
#### 40 Ugwr 'ēpf 'gZR gt ko gpwcnlt qegf wt g

Vj g'vuv'ugwr 'y cu'cuugo dnrf 'vq'r gthqto 'rcd/uecrg'gZR gt ko gpw'htq'uwwf {kpi 'tr kf 'r j cug'vcpukkkp" f wtkpi 'vj g'tgrcug'qhlks wghkf 'EQ4'vq'cvo qur j gtle'r tguuwtg0Hki 04'kmwutcvu'vj g'o ckp'eqo r qpgpw" qh'vj g'gZR gt ko gpwcnlpwcnr'vq'0Vj g'ugwr 'kpenmf gu'c'tgevcpi wrct 'f wev'hzgf 'vq'vj g'wr r gt'r ctv'qh'cp" cno kpw "utwewtg0K'ku'c'j ki j /r tguuwtg'xguugn'o cf g'qh'uvckprguu'uvgn'y kj "c'vqcn'xqno g'qh'3; 3" eo 50Vj g'f wev'j cu'qr r qukv/ukf g'dqtquk'ecvg'i rnu'y kpf qy u.'hcekrkcvkpi "qr v'ecn'ceegu0Vj g'f wev'u" qt'kleg"ku"qr gpgf "vq"vj g'cvo qur j gtle"ej co dgt "cv"vj g"dqwqo "qh"vj g'cno kpw "utwewtg"y kj " f ko gpukqpu'2072'z'207; 'z'20 9'o 50Vj g'ej co dgt 'ur ceg'ku'eqxgtgf 'htqo 'cmlkf gu'y kj 'r qn'ectdqpcvg" uj ggw0K'j cu'vy q'xgpw'qp'vj g'vqr 'cpf "dqwqo 'y kj "c'vqcn'ctgc'qh'cdqw'2023'o 40Vj g'vuv'ugev'kqp" ku'ugcrgf "y kj "c'o wnk/rc{gt'f kr j tci o "eqpukv'kpi "qh'gki j v'ektewrct"cno kpw "hqn'r kgegu'y kj "c" vqcn'vj kempguu'qh'cdqw'20 "o o 0Vy q'i cunwv.r tko ctkf "hcdt'ecvgf "qh'i rnuu.'ctco kf "hkdgtu.'cpf " pkt'krg"dkpf gt."y gtg"cwcej gf "vq"dqj "ukf gu'qh"vj g'f kr j tci o "vq"r t'gxgpv'r quukdrg" r'cnu0 Vj g' f kr j tci o "y kj "ch'kzgf "i cunwv'ku'ht'o n{ 'r t'guugf "cv'vj g'f wev'u'qr gpkpi "dgy ggp"vy q'h'ncpi gu'y kj " hqwt "dqnu0"

Vj g'i cugqwu'cpf 'vj g'rhs wkf 'EQ4'ctg'uw r r'kfg 'vq'vj g'f wev'htqo 'kpf wutkn'i tcf g'e{ r'kpf gtu'gs wkr r gf " y kj "eqpvtqn'xcrk'gu.'c'f kr 'wdg'ht'rhs wkf . 'cpf "c'tgi wrcvt'htq'i cugqwu0Vj g'f kr j tci o 'ku'r wpewtgf " y kj "cp"cttqy /uj cr gf "pggf ng'hcuvgpgf "vq"c'tqf "r pgwo c'ke"e{ r'kpf gt'cewcvqt'y j k'ej "ku'ceewtcvgn{ " crki pgf "y kj "vj g'f wev'u'qt'kleg0Vj g'r t'guuwtg'kp'vj g'f wev'ku'tgeqtf gf "wukpi 'vj tgg'Mw'krg'Z VO /3; 2/ 4222I "r kgl qt'guk'v'xg"v'cpuf wegtu'o qwpv'gf "crqpi ukf g'vj g'f wev'ukf gy cnu0Vj g'f kucpeg"dgy ggp"c" v'cpuf wegt'cpf 'vj g'cf l'ceg'v'qpg'ku'322'o o 0Vj gug'v'cpuf wegtu'j cxg'c'o gcuwtkpi 't'cpi g'qh'2/362'dct." c'pcwcn'ht'gs wpe{ 'qh'632'nd | . 'cpf "c'o gcuwtgo gpv'ceewtce{ 'qh'0306'dct0"

Hwt'j gto qtg.'vj g'f wev'ku'kputwo gpv'gf "qp'vj g'vqr 'cpf "dqwqo 'y kj "vy q'M'v{r g'vj gto qeqw r'gu'y kj " cp"ceewtce{ 'qh'03' 0Vj g'o qxkpi "cxgtci g'h'kngt"y cu'wugf "vq"uo qqj "vj g'tgeqtf gf "f cvc0Vj g'f cvc" ces wukkkp'u'ug'o "FCS +kpenmf gu'vj tgg'J DO 'S wcpwo 'o qf wrgu.'vy q'O Z632.'cpf "qpg'O Z662D0 Vj gkt'tgeqtf gf "f cvc'cv"; 8'nd | "ctg'v'cpuhgttgf "vq"c'eqo r wgt'vj tqwi j "c'j wd0""

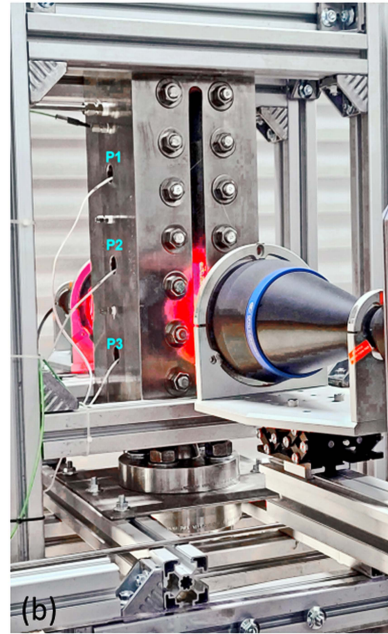
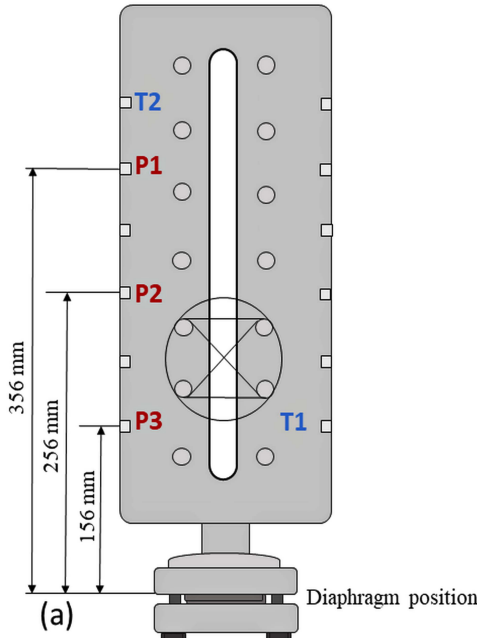
Vj g'r j cug'v'cpukkkp'r tqegu'f wtkpi 'f gr t'guuwtk'cv'kqp'k'pukf g'vj g'f wev'ku'xkuwcnk'gf "d{ 'uj cf qy i tr j " ko ci kpi 0Vj ku'vej pl'k'wg'xkuwcnk' gu'vj g'f gpukv{ 'i tcf k'gpw'0C'f k'ht'g'gpv'rk'j v'kpi "r cwgt'p'ku'r tqf wegf " f w'g"vq"vj g'tgh'ce'v'xg" f gh'ng'ev'kqp" qh'c" rki j v' t'c{ " hqto kpi "c" rki j v' ctgc" qp"vj g'ecr wtgf "r r'cpg0 Uj cf qy i tr j " eqph'ki w'cv'kqp" k'pxqrx'gu" Vgr'ge'gp'tle" VE" ngpugu" o cpw'ceewtgf " d{ " QRVQ" GPI KGGT'KI 'cpf "j ki j /r gthqto c'peg'k'no k'pcvqt'NVENJ R0"



Hi 04<\*c+Uej go ckle"ftcy lpi "qh"ugwr "hqt"EQ4"f gr tguwtk cvkqp"lp"ctgevcpi wrt"f wev'y kj "yj g" qr gplpi "r qlp"lpi "f qy py ctf u0\*d+"Vj g"j ki j /r tguwtg"f wev'u"fk gpukqu0\*e+"Rj qvqi tcr j "qh"yj g" gzr gtko gpvcn'ttcepi go gpw0'



Vj g'kmo kpcvt'y cu'kpuvcngf 'r gtr gpf kewct'v'j' g'y kpf qy u.'cpf 'ku'dgco 'eqxgtu'cdqw'; 2'o o 'qh' vj g'f wev'u'j gki j v'dgy ggp'r tguwtg'tcpuf wegtu'R4'cpf 'R50'Cuq.'''vj g'ko ci gu'y gtg'ecr wtgf 'd{ 'c' j ki j /ur ggf 'eco gtc'Rj qvtqp'UC/\ 'cv'72222'lr u'cpf 'c'tguqnwkqp'qh'478z3246'r kzgn0'Hi vtg'5''c+' uj qy u'c'ungvej 'f ghk'kpi 'vj g'ugpuqt'r qukk'qpu.'y j kg'\*d+'ku'c'r j qvqi tcr j 'kmuwtcvkpi 'vj g'mqecv'kqp'qh' vj g'uj cf qy i tcr j 'ngpugu'cpf 'r tguwtg'tcpuf wegtu'k'p'\*d-0''



**Hi 05<'c+'Ungvej 'qh'vj g'vuv'ugev'kqp'uj qy kpi 'vj g'r tguwtg'tcpuf wegt'r qukk'qpu'cpf 'vj g'f kuv'peg' htqo 'vj g'f kcr j tci o 'r qukk'k'p'\*d+'r j qvqi tcr j 'qh'vj g'f wev'uj qy kpi 'vj g'r qukk'qpu'qh'vj g'uj cf qy i tcr j 'ngpugu'cpf 'r tguwtg'tcpuf wegtu'0''**

Vj g'f wev'y cu'hwuj gf 'y kj 'EQ4'xcr qt 'cv'3'O Rc'dghqtg'gxgt { 'gZR gtko gpv.'vj gp'hkngf 'y kj 'rks wkf ' EQ4'v'j' g'tgs wktgf 'ngxgr0'K'tgo clpgf 'hqt'cdqw'32'o kpwgu'v'ucdkrk'g'dghqtg'y'j'v'g'v'uv'uctv'gf 0'Vj g' vgo r gtcwtg'i cxg'vj g'gs wkrkdkwo 'ucv'g'cv'c'r ct'vewct'vko g0'Vj g'S wcpwo 'r wug'i gpgtcvqt'kpk'cv'gf ' vj g'f gr tguwtk'cvkqp'v'g'uu'd{ 'u{pej tqpwun{ 'vki i gtlpi 'vj g'r pgwo cvk'cewcvqt.'vj g'F CS 'u{ ugo . ' cpf 'vj g'j ki j /ur ggf 'eco gtcu'0'F w'g'v'j' g'cewcvqt'u'r kuv'p'o qxgo gpv.'vj g'pggf ng'r wpewtgf 'vj g' f kcr j tci o 'gpvtgn{ 'y kj 'c'vko g'f grc{ 'qh'cdqw'622'o u00 CVNCD'cpf 'Rj qvtqp'HCUECO 'Xkgy gt' Uqhy ctg'y gtg'wugf 'v'cpcn| g'r tguwtg'cpf 'vgo r gtcwtg'tgeqt'f kpi u'cpf 'j ki j /ur ggf 'ko ci gu'0'Vj g' tguwnu'y gtg'eqo r ctgf 'y kj 'r tgxk'qwa'tguwnu'y j gp'vj g'f kcr j tci o 'y cu'qp'vqr 0''

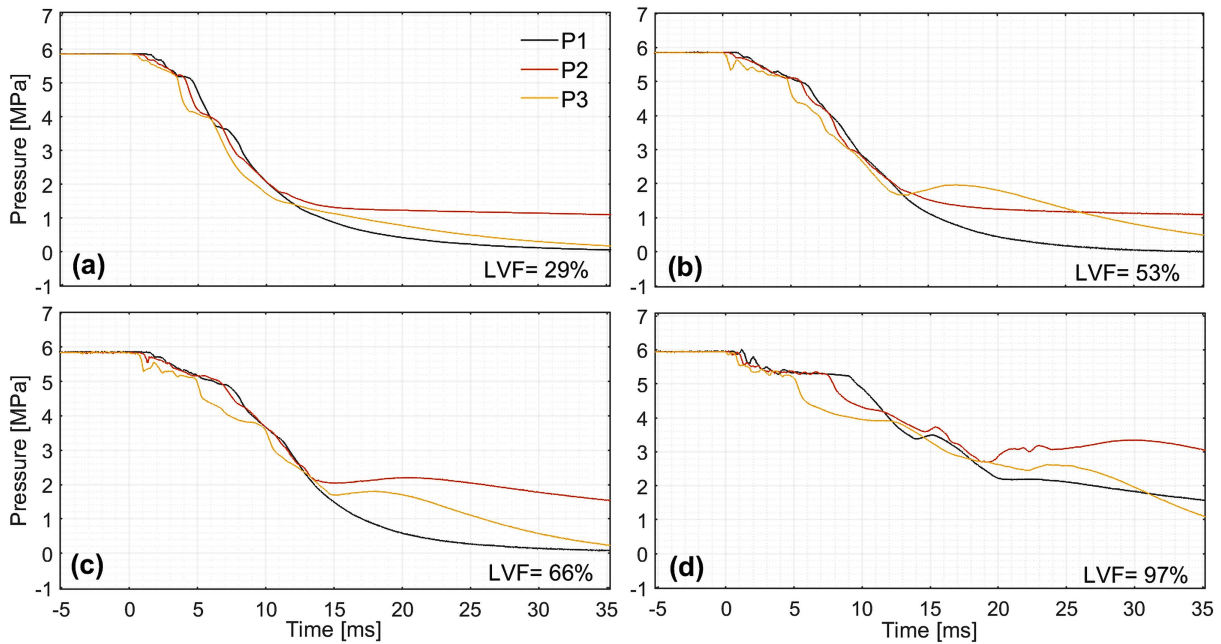
**50 Tguwnu'cpf 'F'kewuk'qpu**

C'ugt'k'gu'qh'v'g'uu'y gtg'r gthqto gf 'v'tgrgcug'r tguwtk'gf 'EQ4'htqo 'vj g'tgev'cpi wct'f wev'u'dqwqo ' kpv'vj g'cwo qur j gtg'0'Vj g'gZR gtko gpw'uctv'gf 'd{ 'twr wtk'pi 'vj g'f kcr j tci o 0'Vj g'kpk'kcn'eqpf k'k'qpu''

y gtg"rks wkf lker qt"cv"ucwtcvgf "r tguuwtg"xct { lpi "dgy ggp"79"cpf "83"O Rc."eqttgur qpf lpi "vq"vj g" ucwtcvgf "r tguuwtg"cv"co dlkpv\go r gtcwtg0Vj g'f wev\y cu'hkmgf "y kj "EQ4"cvf khgtgpv'rks wkf "xqmo g" htcevkpu"NXH"2."4; .57."63."75."7: .88."99."; .: "cpf "; 9' "qh'vj g"vqcn'xqmo g0

500A cxgu'Ej ctcevgtk cvkqp"

Hki 06"uj qy u'vj g'r tguuwtg"tgeqtf u'hqt "vj g'htuv"57"o u'chgt"twr wtkpi "vj g'f ker j tci o 0Vko g"2"ku"vj g" vko g'qh'vj g'f ker j tci o 'twr wtg'cpf "vj g'f gr tguuwtk cvkqp"qpug0Ugputu"R36R5+'ctg'r qukvkqpgf 'htqo " vqr "vq"dqwqo ."cu'uj qy p'lp'Hki 050Vj g'NXH"lp'Hki 06"e+y cu'4; .%d+75."e+88."cpf "f +; 9' ""qh'vj g" vqcn'xqmo g0Cu'uggp"lp'Hki 06."cm'NXHu"j cxg"e'htuv'f gerkp'lp'r tguuwtg'ecwugf "d{ "cp"gzr cpukqp" y cxg"htqo "vj g'f ker j tci o "twr wtkpi 0'Chgt"vj g'htuv"gzr cpukqp."vj g'rks wkf "ku"o gvcucdrng0 Vj g" o gvcucdrng"ucvg"f wtcevkqp"f gr gpf u"qp"vj g'NXH0Vj ku'f wtcevkqp"lpetgcugf "cu"vj g'NXH"lpetgcugf ."cu" uj qy p'lp"i ter j u"e/f +."Hki 060Nqy "NXH"uj qy u'c"i tcf wcn'r tguuwtg'f getgcug'f wtkpi "vj g'o gvcucdrng" ucvg."y j kg"vj g"j ki j guv'NXH"uj qy u'c"pgct/equpcv'r rvcgw'qh'r tguuwtg0"



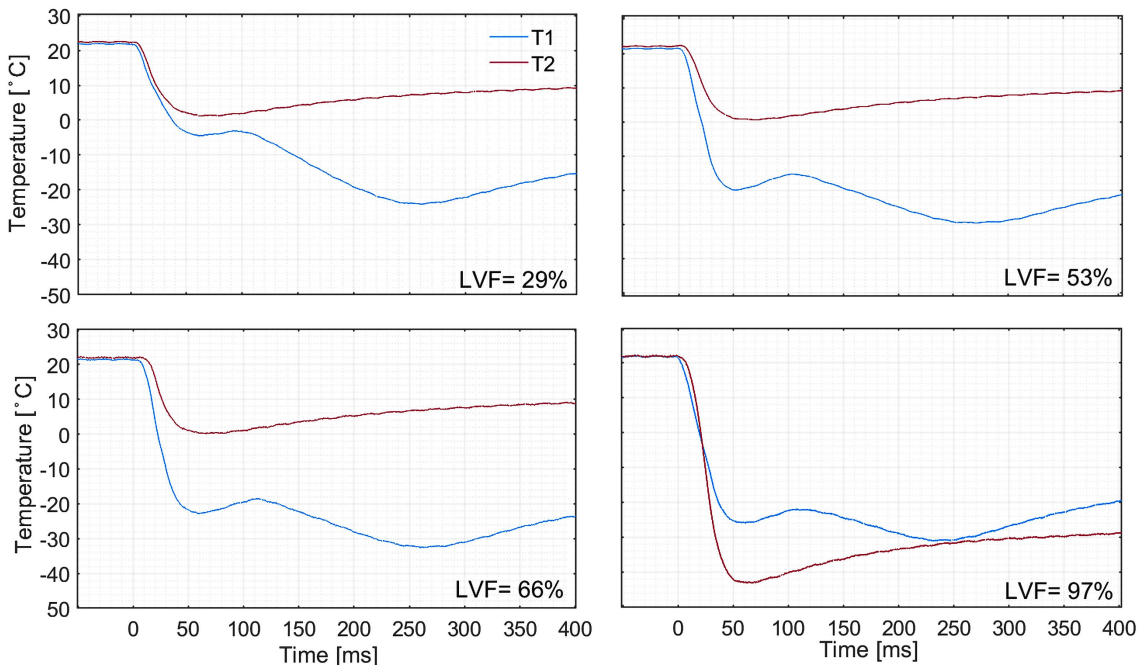
Hki 06<"Rtguuwtg"tcpuwgt"tgeqtf u'f wtkpi "62"o u'tgrgcug"qh'rks wkf "EQ4"htqo "vj g"dqwqo "qh"e" tgevpi wct"f wev'hqt"NXH"qh'4; .75."88."cpf "; 9' "lp"e+.%d+."e+."cpf "f +."tgr gevkgn{ 0"

Vj g'r tguuwtg"tgeqtf u'uj qy "c"f getgcug"chgt"vj g'o gvcucdrng"ucvg."eqttgur qpf lpi "vq"vj g'rks wkf )u" gxcr qtcvkqp0Vj g'r tguuwtg"tgeqtf u'uj qy "c"f getgcug"chgt"vj g'o gvcucdrng"ucvg."eqttgur qpf lpi "vq"vj g" rks wkf )u"gxcr qtcvkqp0K"vj g'rcuv'r ctv'qh'vj g'gzr gtko gpw."vj g'qdugt'xgf "r tguuwtg'f getgcug"y cu'f wg"vq" vj g"y q/r j sug"o kz wtg"qwhny 0Dgecwug"qh"vj g'rko kgf "rks wkf "o cuu'hny "cv"vj g"qwwgv."vj g'rks wkf " lpukf g"vj g'f wev'tgs wtkgf "o qtg"vko g"vq"gxcr qtcvg0Cnuq."hqt"vj g'NXH"qh'75' "cpf "j ki j gt."vj ku'v gpf "

ecp'dg'uggp'cu'cp'kpetgcug'kp'r'tguuwtg0Vj g'gxcrcqtcv'kqp/f'tkxgp'r'tguuwtg'kpetgcug'ku'hw'vj g't'r'tqhqwpf " hqt" vj g" j ki j gt "NXHu0'J qy g'xgt." cu" vj g" f gi tgg" qh" uwr gtj gcv'kpi " ku" g'zr ge'v'f " vq" dg" uo cm" vj g" gxcrcqtcv'kqp'r'tqegu'eqwf "cnuq'qeew'f wg"v'j" g'vgtqi g'p'g'q'w'u'p'weng'cv'kqp"cv'vj g'f we'v'u'y cm0"

Vj g'xgmek'k'gu'q'h'vj g"j gcf "qh'vj g'tctgh'cv'kqp'y cxg'y gtg'ecre'w'v'g'f "dcug'f "qp"vj g'tgeqtf u'htqo "vj g" vj tgg'r'tguuwtg'ugpuqtu0'Vj g'i tcr j kecn'r r tqcej "wug'f "v'q'f g'v'g'to k'p'g'vj g'xgmek'k'gu'ku'f guet'kd'g'f "k'p"cp" gctr'kgt "uwf { "J35\_0'Vj g'ecre'w'v'g'f "tctgh'cv'kqp'y cxg'xgmek'k'gu'y gtg'422"o lu'hqt" | qpgu'R4/R5"cpf " R4/R3'k'p"\*c+'y kj "c'NXH'q'h'4; ' 0Hqt'vj g'NXH'q'h'; 9' 'k'p'\*f '+'4; ; 'o lu'hqt" | qpg'R4/R5'cpf'4: 7'o lu' hqt"R4/R30'Vj g'xgmek'k'f "ecre'w'v'kqp"gttqtu'y gtg'gu'ko cv'g'f "cu"Ö. "o lu'0'hw'vj g'to qtg."vj g'ur g'g'f "qh" uqwpf "dcug'f "qp"vj g'Ur cp/Y ci pgt "Gs we'v'kqp"qh'U'cv'g'u'v'cd'w'v'g'f "f cv"J36\_'ku'ecre'w'v'g'f "v'q"dg"533" o lu'hqt'vj g'f'ks w'k'f "r j cu'g'cpf'3; 5'o lu'hqt'vj g'x'c'rc'q't'cv'70 9'O Rc"cpf "440'Æ0"

Hki 07'uj qy u'vj g'vgo r gtcwtg'tgeqtf u'hqt'vj g'htu'v'622"o u'ch'v'gt'vj g'f'k'cr j tci o 't'w'r w't'g'f 0'Vj g'NXHu" ctg"gs w'cn'l'v'q" vj g'r'r'tguuwtg'r'm'q'u'0'I tcr j u'k'p"Hki 0'7"htqo " \*g/i + "uj qy "c"urki j v't'g'f we'v'kqp"k'p"vj g" vgo r gtcwtg"\*V3+'cu'vj g'g'x'c'rc'q't'cv'g'f "f'ks w'k'f "x'q'm'o g'k'p'et'g'c'ug'f . 'y j k'g'vj g'v'g'o r gtcwtg"\*V4+'f't'qr 'y cu" p'g'c't'n'f "vj g'uc'o g."ctqwpf "2'Æ0"

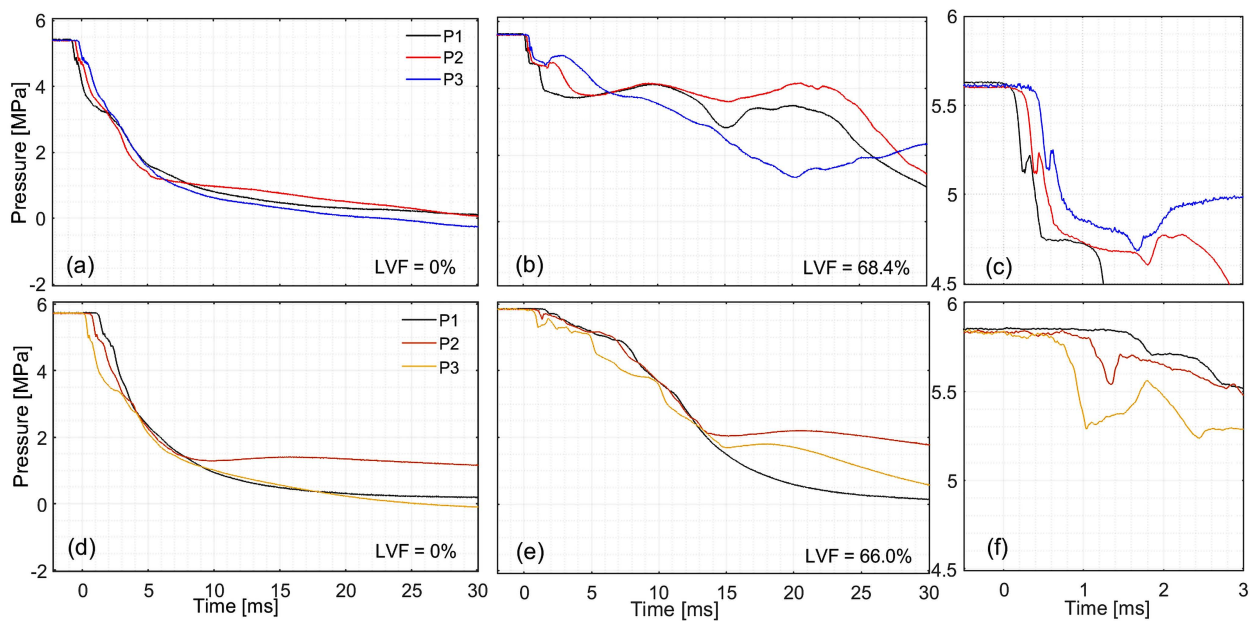


Hki 0'7<' Vgo r gtcwtg" ugpuqtu)" tgeqtf u" V3\*dq'w'q'o +" cpf " V4\*V'qr +" f w't'k'pi " 622" o u" qh' EQ4 f gr'tguuwt'k'cv'kqp'hqt'NXH'q'h'4; .75.'88'cpf"; 9' 'k'p'vj g'i tcr j u'g'+'\*h'+'i '+'cpf'vj g'+'eq'tt'g'ur q'p'f'k'pi n'f 0' k'p'v'g't'g'uk'p'i n'f . 'vj g'f't'qr 'k'p'v'g'o r gtcwtg"\*V4+'k'p'Hki 07'vj g'+'y cu'o qtg'uki p'k'h'ec'p'v'j cp'vj g'v'g'o r gtcwtg" f'gen'k'p'g'f w't'k'pi "72"o u'f'gr'tguuwt'k'cv'kqp'0'Cu'vj g'f'ks w'k'f "r'g'x'g'n'y cu'cd'q'x'g'vj g'y q'ug'p'q'tu."vj g'f'ks w'k'f "

gxr cpukqp"cpf "gxcr qtcvkqp"o c{ 'j cxg'dggp'guugpvkcnhcevqtu'lp"vj ku'vgo r gtcwtg'tgf wevkqp0Hqt 'NXH' ?'; 9' . 'vj g'f tqr 'lp"vgo r gtcwtg'y cu'/6406ÅE0E qo r ctkpi 'vj g'vgo r gtcwtg'tgeqtf u'y kj 'vj g'r tguwtg' ugpuqtu'o gcuwtgo gpw.'hqt 'NXH'qh'; 9' . 'vj g'cvo qur j gtle'r tguwtg'ku'tgcej gf "crr tqzko cvgn{ "chgt" 72"o u"\*pqv'uj qy p"lp"Hki wtg"6+0'Vj ku'ej cpi g"qh'ucv"ko r rkgu'f t{ "leg"hqto cvkqp0J qy gxgt."vj g' vgo r gtcwtg'ugpuqt"V4"f qgu'pqv'tgcej "vj g'tkr rg'r qkp v\*/7806ÅE+0'Vj ku'ku'cuwo gf "vq'dg"fg"vq"vj g' tgrvkggn{ 'urqy 'tgur qpug'qh'vj g'vgo r gtcwtg'ugpuqtu"

5040E qo r ctkuqp"qh'Vqr "cpf "Dqwqo "f wev'tgrgcugu"

Vj g'tguwtg'htqo "vj g'dqwqo 'tgrgcug"\*DT+'gxr gtko gpw'y gtg'eqo r ctgf "vq"vj qug'cej kxgf 'r tgxkqun{ " d{ 'J cpugp"j37\_'htqo "vqr 'tgrgcug"\*VT+'vguu'lp"vj g'uco g'f wev'0'Vj g'cko 'ku'vq'f guetkdg'vj g'f khtg'pgegu" lp"vj g'f { pco le"hrqy "ej ctcevgtknku'dgy ggp"vj g'dqwqo "\*"DT+'cpf "vqr "\*"VT+'tgrgcugu"qh'rks wkhgf " EQ40Hki 08"eqo r ctgu'vj g'r tguwtg'tgeqtf u'lpukf g'vj g'tgevcpj wrct" f wev'htq"VT"\*c"cpf "d+'cpf "DT"\*f " cpf "g+'gxr gtko gpw'0'Gprcti gf "ugi o gpw'qh'5"o u'htqo "\*"d+'cpf "\*"g+'ctg'uj qy p"lp"Hki 08"\*e"cpf "h'0R4" cpf "R5'y gtg'dgrqy "vj g'rks wk'ngxgn'lp"VT"cpf "DT"vguu'0'



Hki 08<E qo r ctkuqp"qh'r tguwtg'j kuqtkgu'f wtkpi "52"o u'qh'EQ4" f gr tguwtk cvkqp'lp"vj g'tgevcpj wrct" f wev'u'tgrgcug'htqo "vj g'vqr "\*"c"cpf "d+'cpf "vj g'dqwqo "\*"f"cpf "h'0"\*e"cpf "h+'ctg'emug/wr u'eqxgtkpi "5" o u'qh"\*d"cpf "g+0'Vj g'NXHu'ctg'2' 'lp"\*c"cpf "f+""8: 06' 'lp"\*d+"cpf ""88' 'lp"\*g+0'

Vj g'r tguwtg'f genkpg'f wtkpi "EQ4" f geqo r tguukqp'y cu'hcugt'lp"DT"vguu'vj cp'lp"VT0Cu'uggp'lp"Hki 0' 8"\*d+."k'tgs wktgf "cdqw'39"cpf "48"o u'htq"R4"cpf "R5"vq'tgcej "4"O Rc."y j kng'k'tgs wktgf "cdqw'350" o u'htq"DT"lp"Hki 08"\*g+0'Vj g'o quv'rkngn{ "ecwug"ku'vj cv'vj g'f qy pwtgco "vy q/r j cug"o kzwatg'y cu"

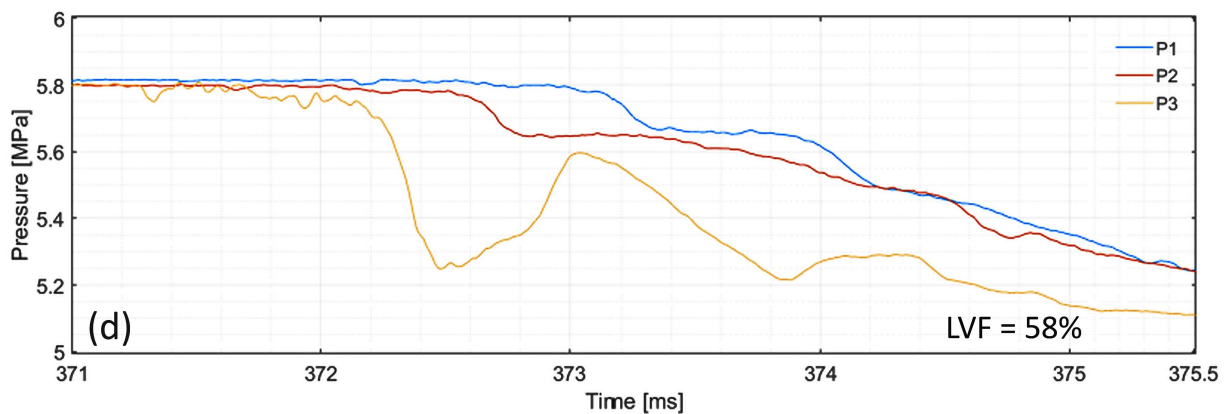
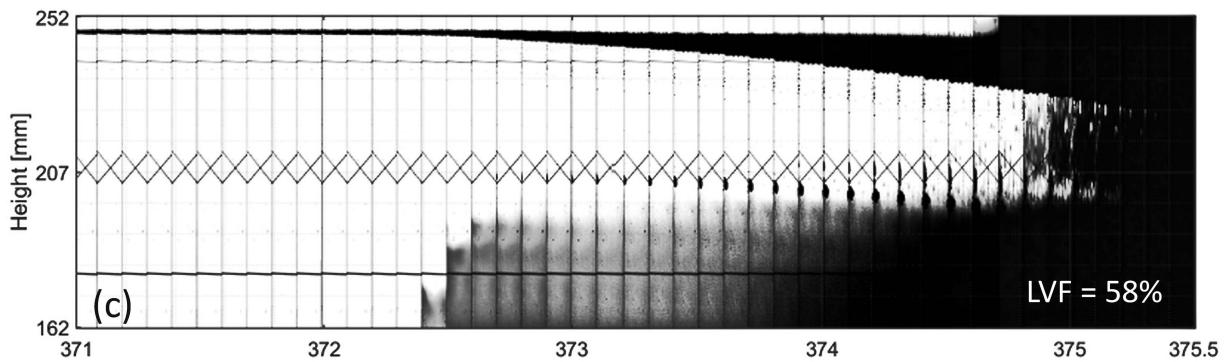
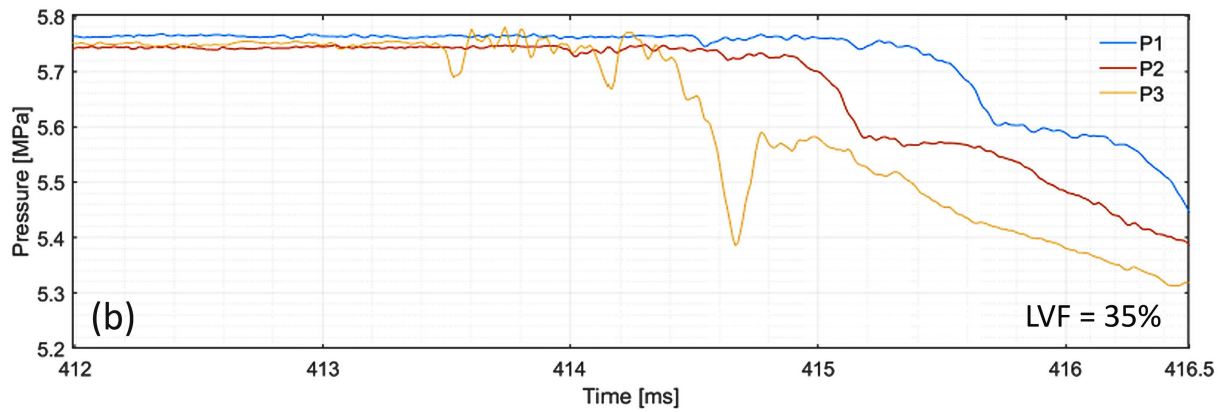
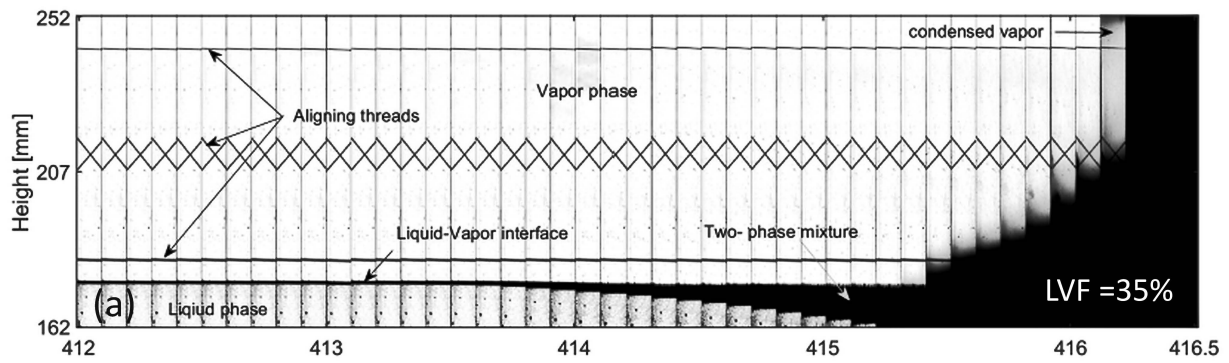
ej qnkpi "cv'vj g'f wev'qr gp kpi 'f wt kpi 'vj g'VT"vguu0'Vj g'r tguuwtg'f get gcug'f wt kpi "DT"vguu'tguuwtg'f  
htqo 'vj g'f ker j tci o 'twr wt kpi "cpf 'vj gp 'vj g' rks wkf "o cuu'qwhmry 'htqo 'vj g'dqwqo 0'k'VT"vguu. 'vj g'  
rks wkf "o quu' "gxcr qtcvgf "kpkf g'vj g'f wev'J qy gxgt. "gxcr qtcvkqp"qeevttgf "kpkf g'cpf "qwu'kf g'vj g'  
f wev.'cpf "gxcr qtcvkqp'y cu'hcuvgt'f wt kpi "DT"vguu0"

Cff kkpem{. "Uko ı gu/O qtgkc": \_"f ghkpgf "vj g'f gi tgg"qh'uwr gtj gcvkpi "\*F QU+"cu'vj g'o czko wo "  
gzr cpukqp'kp'vj g'o gvcucdng'tgi kqp0'K'ku'f guetkdgf 'd{ 'r tguuwtg'f tqr 'htqo 'r tg/twr wtgf 'r tguuwtg'vq"  
vj g'r tguuwtg'qh'vj g'uwr gtj gcvgf "rks wkf "kp'vj g'o gvcucdng"ucv'g0'Vj g'htuv'uj ctr 'f get gcug'kp'rks wkf "  
r tguuwtg"\*R4"cpf "R5+'kp'Hki 08"\*e"cpf "h+'ku'cdqw'2078'O Rc'hqt"DT"cpf "20 'O Rc'hqt"vj g'VT0'Vj g'  
hcev'vj cv'c'r qtvkqp'qh'vj g'gzr cpf gf "rks wkf "hmry gf "qwf'wt kpi "DT"eqwf "gzr rckp'vj g'uo cm'f gi tgg'qh"  
uwr gtj gcvkpi "\*F QU+"cwkpgf "eqo r ctgf "vq'vj g'VT"gzr gtko gp0'

500Uj cf qy i tcr j 'ko ci gu'cpcn{ uku"

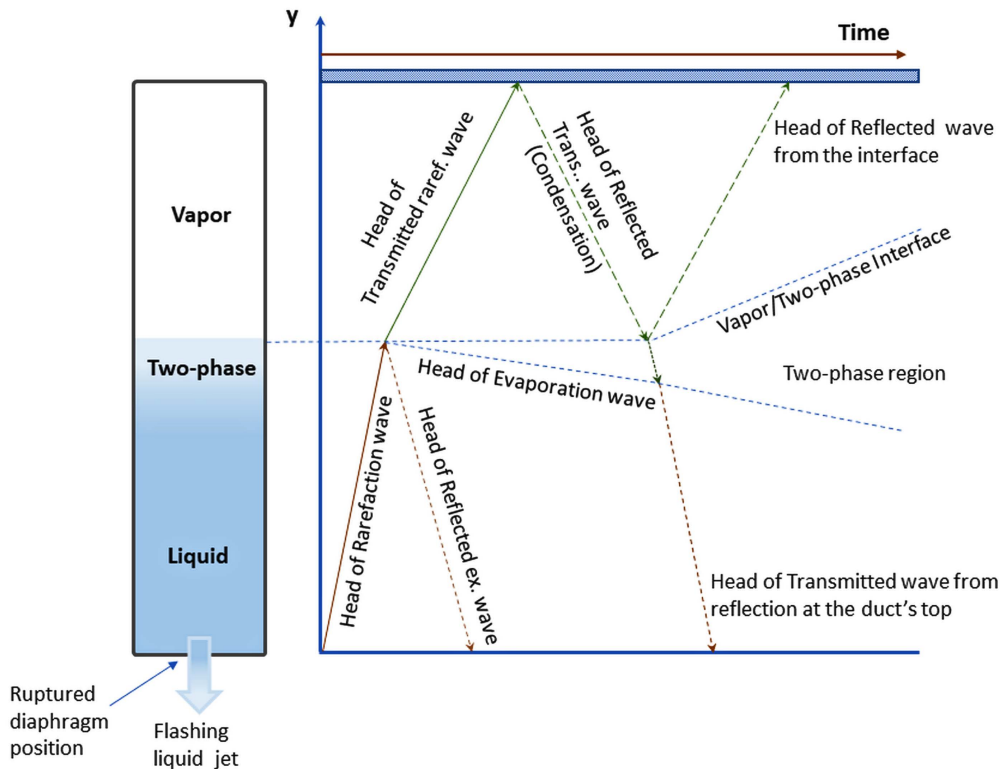
Hki 09"uj qy u'c'ugs wgpeg'qh'etqrr gf "ko ci gu'htqo "uj cf qy i tcr j "xkf gq'htco gu'cpf "eqttgur qpf kpi "  
r tguuwtg'tgeqtf u'f wt kpi "60'o u'qh'E Q4'rks wkf "gxcr qtcvkqp'y kj "NXH'qh'57' "kp"\*c"cpf "d+'cpf "7: ' "  
kp"\*e"cpf "f +0'Vj g'vko g'uwr "dgy ggp'htco gu'kp'dqj 'ko ci g'ugs wgpegu'ku'208'o u0'K ci gu'uj qy "vj g'  
qpugv'qh'vj g'gxcr qtcvkqp'r tqegu'cv'vj g'uwthceg. 'ugr ctkvpi 'vj g'rks wkf 'htqo "xcr qt'kp'vj g'f ctm'gi kqp"  
qh'uj cf qy i tcr j u'y j kej "kpetgcukpi n{ "gzr cpf gf "kpvq"vj g'gpvktg"i gqo gvt{ 0'Vj ku'f ctm'| qpg'y cu"  
i gw kpi "vj lengt "f wg'vq'rks wkf "gxcr qtcvkqp"cpf "vy q/r j cug'o kz wtg'htqo cvkqp0'Vj g'f ctm'| qpg'eqwf "  
j cxg"ctkugp'htqo "f kvqt vkqp"cpf "dmqenci g'qh'vj g'rki j v'tc{ u0'Ku'go gti gpeg'eqttgur qpf u'vq'f gpukv{ "  
i tcf kpvu. 'r tko ctkn{ "dgecwug'vkp{ "dwdrgu'o cng'vj g'hwkf "wptcpur ctgp0'"

Vj g'uy kej "kp'vj g'kpv'pukv{ "qh'vj g'i tc{ uecrg'r cwgtp"eqkpek'gf "y kj "vj g'ej cpi gu'kp'vj g'r tguuwtg"  
r tqh'ku0'ht'gzco r ng. 'kp'Hki 09"\*e+. 'vj g'r tguuwtg'f get gcug'f "cdtwr v{ "dgy ggp'594"cpf "5940'o u'cpf "  
vj gp'r gcmgf "cv'cdqw'595'o u0'Vj g'f ctngt'ctgc"dgvy ggp'594"cpf "595'o u'eqkpek'gu'y kj "c'r tguuwtg"  
f tqr "qp"R5"\*kpu'cngf "cv'j ""? "378"o o +0'Vj g'f ctngt'ctgc"ku'cuwo gf "vq'dg"j gvg'qi gpg'qwu'y cm'  
pwergcvkqp0'Vj gp'k'vqpgf "f qy p'cpf "hvt'vj gt'kpv'pukv'gf "cu'vj g'r tguuwtg'f ger'kpgf 0'"



Hi 0'90' Ugs wpgpeg" qh' etqrr gf" ko ci gu" r tqeguugf" htqo " uj cf qy i tcr j " xkf gqu" \*c" cpf" e+" cpf" u{pej tqpk gf "r tguwtg" tgeqtf u\*d"cpf "f +f wtkpi "hs wkf "EQ4" tgrgcug" htqo "yj g" f we\ u' dqwqo 0'

Vj g'y cxg"eqphki wtckqp" f wt kpi "vj g" r j cug" tcpuokkqp" ku" s wkg" eqo r r g z" f w g" v q" y cxg" kpvgtcev kpu" dgwy ggp" vj g" r tko ct { . "tcpuo kwgf "vj tqwi j "vj g" rks wkf l xcr qt" kpvgt hceg. "cpf " tghrgev g" y cxgu" Hki 0: "ku" c" vko g/ f kucpeg" f kci tco "uj qy kpi "vj g" j gcf "qh" tctghcev kpu" y cxgu. "vj g" g xcr qtcv kqp" y cxg. "cpf "vj g" y q/ r j cug" kpvgt hceg" kpu k f g' vj g' f we0"

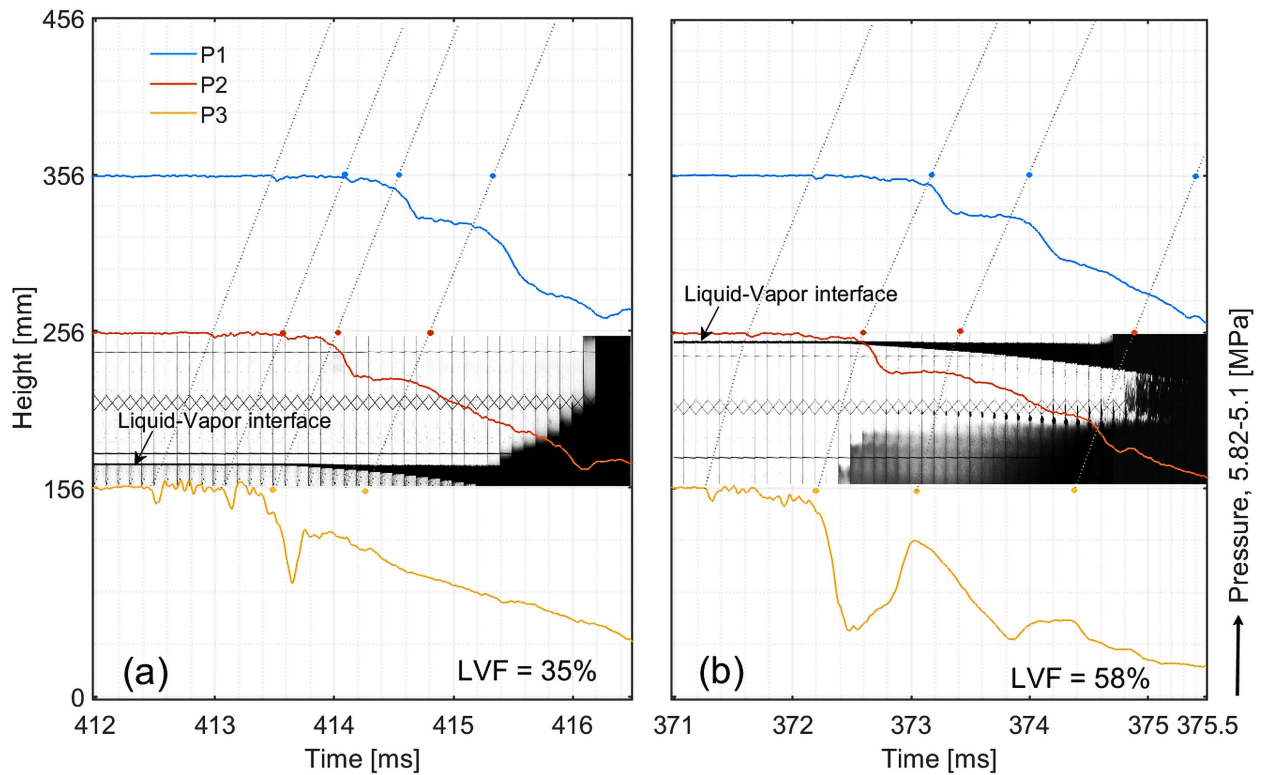


**Hki 0: 0** Vko g/ f kucpeg" f kci tco "uj qy kpi "vj g" j gcf "qh" tctghcev kpu" y cxgu. "vj g" g xcr qtcv kqp" y cxg. "cpf " vj g" y q/ r j cug" kpvgt hceg" kpu k f g' vj g' f we0" \*vj g" xgmek kgu" qh" vj g" y cxgu" ctg" pqv" f tcy p" v q" uecrg+ "

Cu" vj g" f kcr j tci o " twr wtgf. " cp" g z r c p u k q p" y cxg" r t q r c i c v g f " w r y c t f " k p u k f g" v j g" f w e 0" k p u c p w c p g q w u n { . " c" u j q e m" y c x g" r t q r c i c v g f " f q y p y c t f u" k p v" v j g" c v o q u r j g t g. " h q m y g f " d { " c p" g z r c p f g f " o w m k r j c u g" l g v" \* p q v" u j q y p" k p" v j g" h k i w t g- 0" V j g" t c t g h c e v k p u" y c x g" r t q r c i c v g f " w r y c t f u" v j t q w i j " v j g" r k s w k f " c p f " x c r q t" j g c f u r c e g 0" Y j k r g" k" t c p u o k w g f " v j t q w i j " v j g" r k s w k f l x c r q t" k p v g t h c e g" k p v" v j g" x c r q t" r j c u g. " k" y c u" c n u q" t g h r g e v g f " d c e m" k p v" v j g" r k s w k f 0" V j g" g z r c p f g f " r k s w k f " d g e c o g" u w r g t j g c v g f " h q t" c" y j k r g" d g h q t g" v j g" g x c r q t c v k p p" u c t v g f 0" Y j g p" v j g" t c t g h c e v k p p" t c p u o k w g f " y c x g" t g c e j g f " v j g" f w e v u" v q r . " k" y c u" t g h r g e v g f " k p v" g z r c p f g f " u c w t c v g f " x c r q t 0" V j g p" r c t v q h" k" y c u" t g h r g e v g f " c v" v j g" y q/ r j c u g l x c r q t" k p v g t h c e g" y j k r g" t c p u o k w g f " k p v" v j g" y q/ r j c u g" o k z w t g 0" F w t k p i " x c r q t" g z r c p u k q p. " k" r c t v k m { " e q p f g p u g u" f w g" v q" v j g" j g c f " q h" v j g" t c p u o k w g f " t c t g h c e v k p u" y c x g" r t q r c i c v k p p 0" E c r e w r v k p u" d c u g f " q p" v j g" U r c p/ Y c i p g t" G Q U" ] 3 8 \_" f g o q p u t c v g f " v j c v" c h g t" v j g" u c w t c v g f " x c r q t"

lugptqr ke" gZr cpukqp." yj g" gZr cpf gf "hwkf " j cf "c" xcr qt "s wcrk\{ "qh"2Q 50 Vj ku" tguwn" xgt hkgu" yj g" cdqXgo gpvkqpgf "qdugtXcvkqp" cdqwr' ctvcn' xcr qt "eqpf gpucvkqp" lp "Hki 09"%. "e+0

Vj g'r tguuwtg'tgeqt f u'y gtg'f tcy p"qp" yj g'f wev'j gki j v'ko g'uecrg"vq"uj qy "yj g'y cxg"v'clgevtkgu0Vj g" r qkpw"qp" yj g'r tguuwtg"ewtXgu"qh"qdugtXcdrg" kpenkpgu"uki pkh\ ("y cxgu)"r cy u"yj cv'hqmqy "yj g'f ghkpgf" vko g'r qkpw'cv"yj g'hZgf 'r tguuwtg'ugpuqtu)"r qukkkpu"]35\_0Hki 0; kmwutcvgu'r tguuwtg'j kuvtkgu'dgy ggp" 70 "cpf "70" "O Rc" f tcy p"qp" yj g'f wev'j gki j v'uecrg" f wtkpi "60" "o u"qh'ns wkhgf "EQ4" f gr tguuwtk cvkqp" hqt "NXHu"qh'57' "lp" %c+ "cpf "7: " "lp" %d+0"



Hki 0; 0J gki j v'ko g'f kci tco "f go qpuctvkpi "r tguuwtg"v'cpuf wegt "tgc f kpi u"qp" xguugr' j gki j v'czku" f wtkpi "60" "o u"qh'ns wkhgf "EQ4" tgrgcug" hqo "yj g'f wev'u" dqwqo "ukf g0Hqt "NXHu"qh'57' "lp" %c+ "cpf "7: " "lp" %d+0Vj g'uj cf qy i tcr j "ko ci gu'y gtg'f kur r\{ gf "cv" yj g'eqtgur qp f kpi "j gki j v'r qukkkqp0

Vj g'i tcr j u"lp" Hki 0; "kpenw" g" yj g'etqr r gf "uj cf qy i tcr j "ko ci gu'hqt" yj g'uev'gf "NXHu0Rqkpv"2"qp" yj g" j gki j v'czku" tghgtu"vq" yj g'f kcr j tci o "r qukkkqp" \*ugg" Hki 0'5+0Vj g" o gcp" ecn'wrcv'gf "xgrqek\{ "hqt" yj g" tctghcvcv' yj cxg" chgt" yj g' hktu'wuf gp" r tguuwtg' f tqr "hqt" yj g'NXH"qh'57' "y cu"42204" o lu. y j krg' hqt" 7: " "y cu"48804" o lu0"



Vj g'ns wkf . "cpf "vj g'xcr qt. "y gtg'cv'gs wkrkdkwo "dghqtg"vj g'f lcr j tci o "twr wtgf 0'Kp'Hki 09. "k'ecp"dg" qdugt xgf " vj cv' vj g' kpvgt hceg" y cu" pgctn{ " gs wcdng0' Y j gp" vj g' f lcr j tci o " twr wtgf ." kpvgt hcekn" r gt wtdcvkqpu"go gti gf "f wg"vq"vj g'r tguuwtg" f tqr "cpf "vj g'tctghcevkqp"y cxg'r tqr ci cvkqp"r gpgt cvkpi " vj g'kpvgt hceg0'Kp"vj g'htuv"r j cug" chgt "vj g'f lcr j tci o "twr wtg. "kpuvcdkrlkku"kp"uqo g"ur quu"cv"vj g' kpvgt hceg"y gtg" c'r cwgt p"qh"vkp{ "ur kngu"vj cv'f gxgnr gf "qxgt"vko g0'Vj ku"r j gpqo gpqp"ku" f guetkdgf "d{ " J km"]; \_."y j gtg" c"eqrf gt "ns wkf "rc{ gt "y cu"vgo r qtctkn{ "uj cr gf "cv"vj g'uwthceg"cpf "dgeco g'f gpugt "vj cp" vj g'ns wkf "wpgt gpgcvj 0'Vj gp"kv'y cu" f kur mceg" d{ "c"y cto gt "ns wkf "y j krg"vj g'ns wkf )u'rgxgnf getgcugf " f wg"vq"vj g'j ki j "b cuu"cpf "j gcv'tcpuhgt "tcvg"cv'vj g'kpvgt hceg0'Vj g'uj cf qy i ter j "ko ci gu"kp'Hki 09"uj qy " vj cv' vj g' g'zr cpf gf " xcr qt" ceegr gtcvgf "kp"vq" vj g' f gpugt " ns wkf ." etgc vki " c" dwddn{ " o kzwatg" vj cv' r tqr ci cvgf "f qy py ctf u0'Vj g'vj kempgu"qh"vj g'vy q/r j cug" kpvgt hceg"rc{ gt "y cu"cuq "kpetgcugf "f wg"vq" vj g'dwddrgu"ctkukpi "htqo "j gvgqi gpgqu"pwengcvkqp"qp"vj g'f wevu"y cm0'K'ku"wpengct "htqo "vj g'r ncpct" uj cf qy i ter j "ko ci gu"y j gvj gt "vj g'vy q/r j cug"rc{ gt "g'zr cpukqp"ku" f wg" vq" vj g' uwthceg. "dwm" qt" dqwpf ct{ "rc{ gt "ghgeu0'J qy gxgt. "vj g'ko ci gu"uj qy gf "vj cv'vj g'ns wkf lcr qt" kpvgt hceg" f gxgnr gf "kp"vq" c"vy q/r j cug" o kzwatg" cpf "tgo ckpgf "pgctn{ "eqpuvcp0'Y j krg" c"ugeqpf "ns wkf ly q/r j cug" o kzwatg" kpvgt hceg"y cu"htqo gf . "f gxgnr kpi "f qy py ctf "kp"vj g'ns wkf 0'Vj ku"ku"qr r qugf "vq"VT" g'zr gtko gpwu" y j gtgkp"vj g'kpklcn"ns wkf lcr qt" eqpvev"uwthceg" \*cpf "f qy putgco "vy q/r j cug" o kzwatg" +r tqr ci cvgf " wry ctf u"ko o gf kvgn{ "chgt"vj g'f lcr j tci o "twr wtg0"

Vj g'uj cf qy i ter j "ko ci gu"qh" vj g' DT" g'zr gtko gpwu"uj qy gf "hwtvj gt" f gxgnr o gpv" d{ " kpvgt hceg" dtgcnkpi "w" cpf "r tqr ci cvkpi "tr kfn{ "wry ctf u0'Cu"vj g'g'zr cpukqp"y cxg'r tqr ci cvgf "wry ctf u"vj tqwi j " vj g'xcr qt"cpf "tghngvgf "htqo "vj g'vqr . "c"eqpf gpucv"vq"y cxg'y cu"qdugt xgf "vq"r tqr ci cvg"dgj kpf 0'Vj ku" vtgpf "ecp"dg"uggp"chgt "63804"o u"kp"Hki 09" \*c-0'Chgty ctf . "vj g'vy q/r j cug" hmwk "kpetgcugf "wpvki"kv" qeewr kgf "vj g'gpvtg" f wevu"xqno g0'

**60 Eqpenwkqpu**

Uo cm'uecrg" g'zr gtko gpwu"y gtg"r gthqto gf "kp" c"tgevcpi wrc" f wev"vq" wpgt uvcpf "r j cug" vtcpukqp" f wtkpi " vj g' tgrgcug" qh" ns wkkgf "EQ40' K' ku" j ki j n{ " tgrgxcpv" vq" c" DNGXG" uegpctkq" eqpukf gtkpi " ceekf gpvcn'xguugn"qt" r kr g"twr wtg0'Eqo r ctkpi "vj g'tguwmu"htqo "vj g'ewtgpv"dqwqo "tgrgcug" \*DT+ g'zr gtko gpwu"y kj "vj g'r tgxkqu"vqr "tgrgcug" \*VT +tguwmu"]37 \_"tgxgcu"vj cv"

- Vj g'uj cf qy i ter j "ko ci gu"htqo "DT"vguu"uj qy gf "vj cv'vj g'kpklcn"ns wkf lcr qt" eqpvev"uwthceg tgo ckpgf "hrcwpgf ."cmo quv"j qtk qpvcn{ . "ht" c"tgrcvkgn{ "rpi "r gtkqf "dghqtg"dtgcnkpi "wry . "vj gp f gxgnr kpi "kp"vq" c"vy q/r j cug"htqpvtckkpi "vj g'g'zr cpukqp"y cxg0

- Ákp'vj g'VT'vguu.'vj g'fks wkf lxcr qt'eqpcev'uwthceg'ku'ko o gf kcvgn{ 'uwengf 'qwd{ 'vj g'gizr cpukqp" y cxg0'
- ÁVj g'f gi tgg'qh'uwv gtj gcvkpi 'kp'vj g'DT'vguu'y cu'mqy gt'vj cp'kp'VT0'
- ÁVj g'r tguuwtg'f tqr 'y cu'cr r tqzko cvgn{ 'vy q'vko gu'hcuvgt'f wtkpi 'DT'vj cp'VT'vguu.'ko r n{ kpi " hcuvgt'gxcv qtcvkqp'qh'vj g'fks wkf 0'

Vj ku'gizr gtko gpv'uj qy u'vj cv'vj g'gxcv qtcvkqp'tcv'f gr gpf u'qp'y j gyj gt'vj g'twr wvgt'ctgc'ku'dgrqy "qt" cdqxg'vj g'fks wkf 'hgxgr0Vj ku'y knikngn{ 'chhgev'vj g'dmuv'wtgpi vj 'cpf 'htci o gpv'htqto cvkqp'kp'ceekf gpvcn' gxcv'w'lxqxv'kpi 'twr wvgt'qh'xguugn'eqpv'kpi 'fks wkf 'EQ40''

"  
"

**Tghgt gpegu''**

13\_ ""EERU.'I wkf grkpgu'hqt'Xcr qt'Emwf 'Gzr m'ukqp. 'Rt guuwtg'Xguugn'Dwtuv.'DNGXG.'cpf ""Hrcuj " Hktg'J c| ctf u0'Ugeqpf 'gf 0'Egpvt'ht' 'Ej go kecn'Rtqeguu'Uchgv{.'CkEj G/Y kg{.'P [ .'4232.'r r 0' 533/5820'

"

14\_ """"[ 0\ j cpi .'L0'Uej qtm'M0'Nwf y ki . ""Tgxkuk'kpi "vj g'eqpf k'kpu'hqt" c"EQ4"vcpm'gizr m'ukqp. " Rtqeggf kpi u'qh'vj g'; 'I m'dcnEqpi tguu'qp'Rtqeguu'Uchgv{.'CkEj G.'Ucp'Cpvqpkq.'Vgzcu.'4235.' r r 032; /3420'

15\_ ""G0'Cpi grq.'L0'T0'U0O qtgktc.'F 0'D0'Dcttkqu.'Vj ggt { "cpf "Qeewt'gpeg'qh'Gxcv qtcvkqp"Y cxgu. "" Rtqeggf kpi u'qh'vj g'3: vj 'k'vgt'pcvkqpcnEqpi tguu'qh'O gej cplecn'Gpi kpggtkpi . 'Qwtq'Rtgvq.'O kpcu' I g'cku.'Dtc| kn'42270'

16\_ ""R0T'gk'ng.'Uwt'ceg'dq'k'kpi 'qh'uwv gtj gcvf 'fks wkf .'Rj F 'vj guku.'O gej cplecn'Gpi kpggtkpi 'GVJ .' \ w'lej . Uy k'j g'gtr'pf . 3; ; 9. RUK/; 9/23. ["j vr <lkpku0cgc0ti lugctej lugctej 0ur zAqtki as?TP <: 252842""""""](#)

17\_ ""O 0'O 0'Xl'gktc.'L0'T0'Uko ; gu/O qtgktc.'Nqy /r tguuwtg'hrcuj kpi "o gej c'pkuo u'kp'kuq/q'evcp'fks wkf " l'gu.'Lqwt'pcn'qh'Hw'kf 'O gej cpleu"794"\*4229+, pp.'343/366.'f qk<320239IU22443342282256520'

18\_ ""R0O 0J cpugp.'C0X0I ccv'cwi . 'F 0'Dlgt'ng'x'gf v.'M0'Xcci ucgyj gt.'Tcr kf 'f gr tguuwt'k' cvkqp'cpf " r j cug"v'cpuk'kqp'qh'EQ4"kp"xgt'k'ecn'f w'eu'ó"Uo cm'uecn'g'zr gtko gpw'cpf "T'cpnk'p'g/J wi q'pk'q'v' cpcn'ugu.'Lqwt'pcn'qh'J c| ctf qwu'O cvgt'k'cu'587 \*423; +; 'pp. 38/47." [f qk<"j vr u<lf qk0ti B20238 l0j c| o cv023: 020; 40'](#)

19\_ " M0' M0' F gy cpi cp." R0' M0' F cu." Gzr gtko gpvcn' cpcn'uku" qh' hrcuj kpi " ht'qpv' r tqr ci cvkqp" kp" uwv gtj gcvf " y cvgtô 'Gh'gewu" qh' f gi tgg" qh' uwv gtj gcv." wdg" k'p'ek'cvkqp." cpf " ugeqpf ct { " p'weng'cvkqp.'Rj { u'ku'qh'Hw'kf u'54 \*9+\*4242+'f qk<320285I702228: 620'

]: \_ " L0'T0'Uko ; gu/O qtgktc.'Cf k'cd'v'k' gxcv qtcvkqp"y cxgu. ""Rj F 'vj guku.'T'g'puugr'gt'Rqn'v'ej ple" k'p'uk'w'wg.'Vt'q{.'P Q . '3; ; 60'["j vr u<ldqgm0 qqi m0p0 ldqgm0Af ?o lli vi CCECCL'](#)

- ] ; \_ "NOI OJ km" Cp"gzr gtlo gpvcn'uwf { "qh'gxcr qtcvkqp'y cxgu'lp'c'uwv gtj gcvgf "rks wkf . "Rj F "vj guku " Ecrkhtpke" kpukwg" qh" Vgej pqm { ." Rcuuf gpc." Ecrkhtpke' 3 ; ; 30' [j wr u<lt guqmg t@cngej Qf wEcngej GVF <gv /32464227/3254460](#)'
- ]32\_"L0G0Xgpctv" I 0C0T wrngf i g. "MOUwo cvj kr em. "MOUqmvy u. "Vq"DNGXG"qt"pqv"vq"DNGXG" Cpcvqo { "qh'c'dqkpi "rks wkf "gzr cpf kpi "xcr qt "gzr mqkqp. "Rtqegu"Uchgv { "Rtqi tguu"34"\*4+\*3 ; ; 5+; pp. 89/92. "f qk"320224 lr tu0: 23424240'
- ]33\_"U0Vãaug."MOXcci ucgy gt. "F 0Dlgtngwxf v."Cp"Gzr gtlo gpvcn'kpxguki cvkqp"qh'Tcr kf "Dqkpi " qh'EQ4. "Uj qeni"Y cxgu"47"\*4236+; pp. "499/4: 4. "f qk"320229 lu223; 5/236/2745/80'
- ]34\_"S kpi twk'Uj cpi .\ j gpi nwp"Vlcp. "Uwr cp"Y cpi . "O kp"J wc. "Z wj ck'Rcp. "Uj lej gpi "Uj k'Lxpej gpi " lkpi . "Gzr gtlo gpvcn'tgugctej "qp"vj g'vy q/r j cug"gzr mqkxg"dqkpi "o gej cpkuo "qh'uwv gtj gcvgf " rks wkf "wpf gt "f khgt gpv'rgcni g'eqpf kkpqu. "Cr r rkgf "Vj gto cn'Gpi kpggtkpi "438"\*4244+\*33; 2: 2." [j wr u<lf qkQti B20238 llQr r mj gto cnpi 0424403; 2: 20'](#)
- ]35\_"Q00 0Kktcj ko ."R00 OJ cpugp. "F 0Dlgtngwxf v."MOX°i uâ vj gt. "Gxcr qtcvkqp"ej ctcevgtkukcu" f wtkpi "f geqo r tguukqp"qh'rks wkhgf "EQ4"htqo "c"eqplecn'uj cr gf "xguugn"Tuwwu'lp"Gpi kpggtkpi " 34"\*4243+; pp. "3/: . "f qk" [j wr u<lf qkQti B20238 llQkpgpi 042430225260](#)'
- ]36\_"T0Ur cp. "Y 0Y ci pgt. "C" P gy "Gs wcvqp"qh'Ucvg'ht' Ectdqp" F kqz kf g'Eqxgtkpi "vj g'Hwkwf "T gi kqp" htqo "vj g" Vtkr ng Rqkp" Vgo r gtcwtg" vq" 3322" M' cv' Rtguwtgu" wr "vq" : 22" O Rc. "Lqwtpen' qh' Rj { ukecn'cpf "Ej go kecn'Tghgtgpeg" F cvc"47"\*8+\*3 ; ; 8+; "r r 0372; /37; 8. "3 ; ; 8 B3 l23." f qk" [j wr u<lf qkQti B20285 B077; ; 30'](#)
- ]37\_"R0J cpugp. "Gzr gtlo gpvcn'cpf "vj gqtg'kecn'uwf kgu"qh'tcr kf "r j cug"t'cpukkp'lp'ectdqp" F kqz kf g. " Rj F "vj guku. "Wpkxgtukv { "qh'Uqwj /Gcvgtp" P qty c { ."423: 0' [j wr u<lqr gpctej kxg0wup0q lwupzo nklj cpf ng B347247: 9679Auj qy ? hwn'](#)
- ]38\_"C0'O lccxewgp. "Vj gto qf { pco ke"o qf gni"cpf "vqnu"ht" J 4Q. "J 4. "EQ4. "cpf "Ck. "I kJ wd0' [j wr u<li kj wd0eqo lctg/o lly gto qf { pco keul kJ wd0' ceeguugf "4243+0'](#)
- ]39\_"O "Kktcj ko ."Quco c"\*4245+.)T grgcug"qh'rks wkf "EQ4"htqo "vj g"dqvqo "qh'c'f wev). "O gpf grg { " "\*\*\*\*\*" F cvc. "X3. "f qk"32098541 { | ur 8; i r v f 0

## **Rcr gt '6''**

### **Blast Wave Overpressures from CO<sub>2</sub> Depressurization in a Conical-Shaped Vessel.**

This paper is published in the 10<sup>th</sup> International Seminar on Fire and Explosion Hazards conference proceedings, 2022, Oslo, Norway. p. 86-94.

<https://hdl.handle.net/11250/3030345>



# Blast Wave Overpressures From CO<sub>2</sub> Depressurization In A Conical-Shaped Vessel

M. brahim O.<sup>1,\*</sup>, Hansen P.M<sup>1</sup>, Bjerketvedt D.<sup>1</sup>, Vågsæther K.<sup>1</sup>

<sup>3</sup>Vj g'Wpkxgtuks' qh'Uqwj /Gcigt p'Pqty c f. 'Hcewn' qh'Vej pqrqi { . 'Pcwt cn'Uekpegu 'cpf' " O ctkko g'Uekpegu 'F gr ctvo gpv'qh'Rt qeguu 'Gpgti { "cpf "Gpxkt qpo gpw'n'Vej pqrqi { ." 'Māp'gu'Tkpi '78. '5; 3: . 'Rqt iū twpp. 'Pqty c f' "0" , Eqt t gur qpf lpi 'c'wj qt u'go ckr<"[guco c0t0dt c j ko B wup0q](#)

## ABSTRACT

The primary hazards arising from boiling liquid expanding vapor explosion (BLEVE) during liquid CO<sub>2</sub> transport are the pressure waves, flying fragments, and sizeable CO<sub>2</sub> discharges to the surroundings. Risk assessment and process safety analyses are crucial aspects to tackle these hazards. This paper studies release of liquid CO<sub>2</sub> from a double-membrane conical apparatus to a tube opened to atmospheric conditions. It aims to characterize the effects of a blast wave arising from the phase transition process in the existing test geometry. Results from measured peak overpressures and calculated impulses indicate that the rapid liquid evaporation significantly impacts the leading overpressure positive phase. Besides, they increase with an increase in liquid volume fraction (LVF). Based on analysis of high-speed videos, the estimated fragments' velocity and their corresponding kinetic energy increase with an increase in LVF, and observed velocity up to 112 m/s for LVF of 73.6%. Comparison of estimated fragment velocity from the test with LVF of 52.7% and calculated velocity based on the initial fragment velocity model at the same initial conditions show a difference of about 16 m/s.

**KEYWORDS:** Peak overpressure, Impulse, Expansion, Fragment velocity.

## INTRODUCTION

In increasingly developing Carbon Capture and Storage (CCS) technologies, there are growing apprehensions over unintended release during CO<sub>2</sub> transport and storage. A container carrying liquid CO<sub>2</sub> at a temperature significantly above its atmospheric boiling point might be exposed to harmful conditions, resulting in its breaking. Such conditions include exposure to higher temperatures, projectile impact, or corrosion. The Boiling Liquid Expanding Vapor Explosion ( BLEVE) is a primary hazard, wherein a storage tank filled with liquified CO<sub>2</sub> could fail catastrophically, and a sizeable mass of saturated liquid and vapor exploded into the surroundings. Besides, it is instantaneously generating destructive pressure loads on adjacent structures, and perilous rocketed fragments [1]. The discharge of large CO<sub>2</sub> volumes also represents a major health threat as it is toxic at high concentrations, causing suffocation and frostbite burns. Several CO<sub>2</sub> BLEVE accidents have been reported, including the 1988 CO<sub>2</sub> tank BLEVE in Worms, Germany. Where three people died, eight suffered frost burns, and nearby buildings crumbled. An investigation report concluded that the leading causes were overheating and fracturing [2]. There were two casualties, and the sinking of two ships carrying chemicals resulted from a catastrophic rupture of the CO<sub>2</sub> ship tank in 2008, Yuhang, China. The reasons were believed to be overfilling and technical faults [3]. The presented CO<sub>2</sub> BLEVE examples clearly show its strength and seriousness. Therefore, process safety analyses and risk assessment are the essential elements to ensure the detection, prevention, and mitigation of such disastrous events.

Key parameters that characterize the shock wave strength and evaluate its impact on the surrounding structures and living beings include overpressure and the wave's positive impulse [4]. Birk et al. [5] described overpressure results from BLEVE tests conducted in tanks filled with propane at various levels. The study concluded that liquid energy content had an insignificant effect on generated shock overpressure. However, in the case of tank disintegration, the energy of expanded multiphase flow generated powerful dynamic overpressure loads on the surrounding surfaces. Based on the contained

energy in the vessel and energy released in the explosion, several models have been proposed to estimate the overpressures during the BLEVE incident [6, 7, 8]. Van der Voort et al. [9] tested overpressures during CO<sub>2</sub> BLEVE utilizing 40-l CO<sub>2</sub> cylinders. The experimental results were applied to validate the inertia-limited prediction model proposed by Van den Berg [8], and good agreement was reported. Hansen et al. [10] studied the effects of liquid volume fraction and the vent size on originated overpressures during CO<sub>2</sub> depressurization in a rectangular duct. The obtained results were compared with simulations of one-phase gas dynamics in a confined chamber, and they showed good correspondence.

This paper demonstrates the results of the laboratory-scale experiments on blast waves consequences during CO<sub>2</sub> decompression into an atmospheric vented cylindrical tube. It analyzes overpressure and impulse resulting from rapid CO<sub>2</sub> liquid evaporation in a conical-shaped vessel for different liquid levels. Additionally, it determines the velocity and kinetic energy of the flying fragments in four explosion experiments. This study also evaluates a model for calculating initial fragment velocity and compares it with the experimental results.

## EXPERIMENTAL SETUP AND PROCEDURE

Laboratory-scale experiments were conducted in a double-membrane arrangement comprising a conical-shaped vessel as a high-pressure driver section (HPS). A slip-on flange is designed as a medium-pressure section (MPS) set between the HPS and another slip-on flange on the top. Furthermore, The three sections are separated by two membranes that seal the HPS and the MPS. The upper flange is connected to a tubular duct opened to atmospheric conditions. Fig. 1 shows an experimental setup sketch and an image.

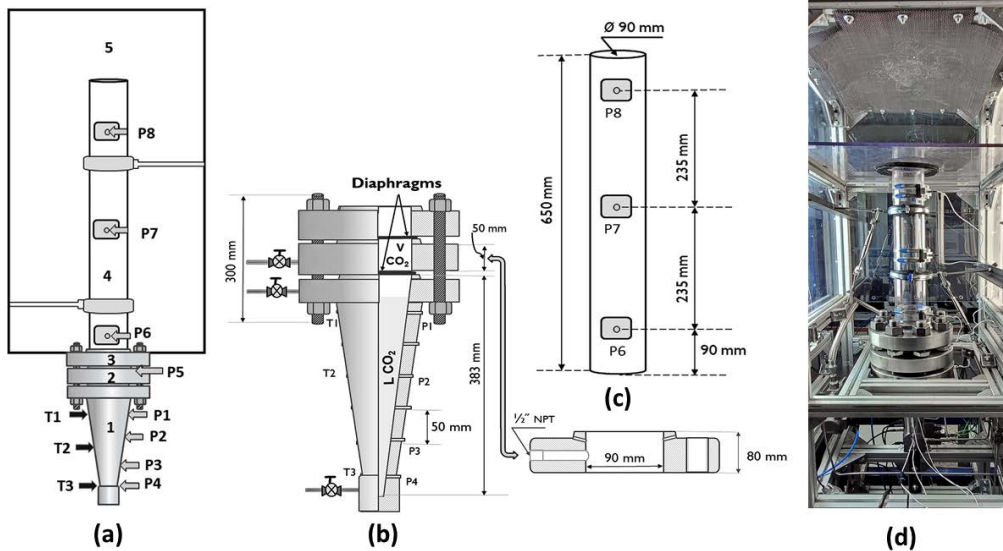


**Fig. 1.** Schematic drawing of the setup: (a) main installed parts: 1- HP conical vessel, 2- MP slip-on flange, 3- upper flange opened to atmospheric pressure, 4- polycarbonate tube, 5- chamber. (b) Conical shaped vessel's detail with the MPS slip-on flange closed up. (c) polycarbonate tube dimensions. (d) An image of the installation.

The conical vessel and the two slip-on flanges are fabricated from stainless steel AISI 316 and installed on an aluminum frame. The HP vessel has an inner volume of  $480 \cdot 10^3 \text{ mm}^3$ , while the MP slip-on flanges' cylindrical section volume is  $510 \cdot 10^3 \text{ mm}^3$ . The HP vessel wall has an angle of  $4^\circ$  to

the central axis and a top diameter of 90.7 mm, similar to the MP slip-on flange and polycarbonate tube diameters. Besides, it has a flat bottom diameter of 9.37 mm. Two industrial graded cylinders separately supplied the HP vessel with liquid CO<sub>2</sub> up to 5.2-5.6 MPa, and the MP section with gaseous CO<sub>2</sub> up to 2.6-2.8 MPa. Before vessel's and duct's filling, they were flushed by 1 MPa vapor CO<sub>2</sub>. All experiments were carried out at ambient temperature. The vessel has unsighted walls. Therefore the vessel filling to the desired level is achieved with the help of an auxiliary HP duct with glass windows. The atmospherically opened tube is made of transparent polycarbonate and has a height of 650 mm and a cross-section area of about 0.184 m<sup>2</sup>. The inner cylindrical rim of the upper atmospheric flange was excavated to place in the polycarbonate tube at a depth of 60 mm. Grooves were carved on its side to prevent potential leaks during the multiphase release. A detailed description of the HP vessel, MPS slip-on flange, and the release mechanism is provided in a previous study [11]

The tests were initiated by increasing the pressure in the medium pressure section by triggering a three-way valve. As a result, the MP diaphragm ruptured, and the pressure fell to atmospheric. Following the increase in the pressure difference between the HP and MP sections, the second diaphragm burst. Subsequently, a multiphase mixture spurted out in the atmospherically vented tube. HP vessel is equipped with four Kulite XTM-190-2000G transducers to record the pressure during the decompression process. The distance between pressure transducers' positions is 100, 100, and 50 mm from top to bottom. Besides, The resulting overpressures from the explosion were measured with three transducers types Kulite XTM-190-100G and Kulite XTM-190-50G. They attached to the cylindrical tube's sidewall at an equal distance of 235 mm and 90 mm from the bottom. The temperature inside the HP vessel is measured using three K-type thermocouples assigned as T1-T3 in Fig. 1 (a). However, this study excluded their records because they have a slow response time. Diaphragm rupturing and erupted multiphase mixture evolution captured by a high-speed camera (Photron Fastcam SA-1). A digital pulse generator unit (Quantum Composers 9500) simultaneously triggered the three-way valve, data acquisition system, and high-speed camera at the test start.

## RESULTS AND DISCUSSION

### Overpressure and impulse

Overpressure description required knowledge about the factors influencing the processes in the HP test section. Fig. 2. shows pressure records inside the HP conical vessel during depressurization of liquid CO<sub>2</sub> with 35.2% liquid volume fraction (LVF). Time zero signifies the HP diaphragm rupture. The MP diaphragm ruptured by increasing the medium section pressure to about 3.7 MPa. As a result, the HP diaphragm responded with bulging seen as oscillations that faded out through about 18 ms, and the pressure stabilized before the HP diaphragm was ruptured. The duration between the two ruptures was 109 ms, while the pressure decreased from pre-ruptured 5.4 MPa to 5 MPa.

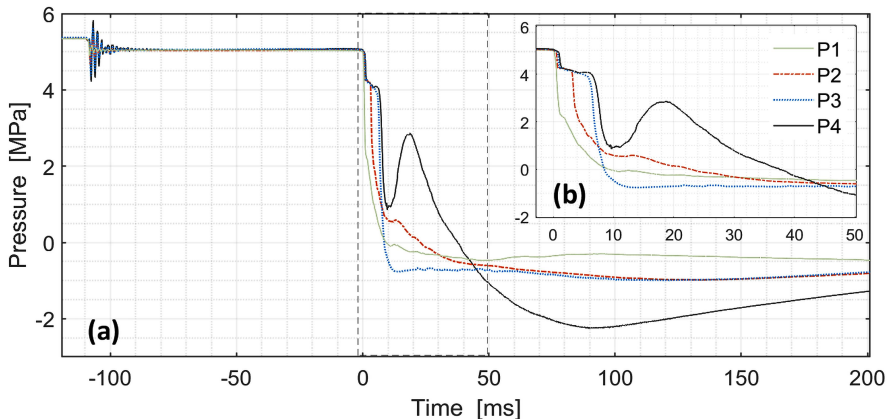


**Fig. 2.** (a) Pressure sensors record P1-P4 (top to bottom) during 200 MS of CO<sub>2</sub> depressurization for LVF of 35.2%. (b) a close-up Graph covers 50 ms after the rupture of the HP diaphragm



After the HP diaphragm ruptured, a rarefaction wave moved downward through the saturated liquid resulting in isentropic expansion with reduced temperature and pressure. The calculated rarefaction wavefront average velocity is 358.7 m/s. Whereas the local speed of sound is determined from SW-EOS tabulated data is 350.5 m/s for the liquid phase and 197.5 m/s for the vapor phase. The liquid was kept temporarily in the metastable state when the pressure reached about 4.3 MPa. The evaporation wave required roughly 6 ms to pass across the liquid volume. The first shock wave was generated once the MP diaphragm ruptured, releasing the vapor from the MP section. The second shock followed the HP diaphragm rupture and release of multiphase flow. The observed decrease in pressure reading P3 below zero while the two-phase mixture was expanding could be attributed to the drift due to the rapid temperature drop.

Fig. 3. shows measured peak overpressure (MPO) in the tube at 180/100 mm (bottom) and 650/570 mm (top) from the HP/MP diaphragms, respectively. Also, it illustrates overpressure records during explosive CO<sub>2</sub> depressurization from a conical vessel filled with 15 (a), 35.2 (b), and 52.7 % (c) LVF. Time zero signalizes the HP diaphragm rupture. Graphs (a'), (b'), and (c') in Fig.3. are corresponding enlarged segments covering 100 ms from the upper raw graphs. The first peak overpressure indicates the blast wave produced by vapor decompression in the MP section. While the second denotes the waves followed the depressurization in the HP vessel. As the blast signals are measured parallel to the direction of pressure waves, there is no account for reflected pressures from impinging on any surface except the tube wall and the champer's ceiling. The MPOs in Fig. 3. specify two peaks of overpressure in the leading positive phase with a higher second peak following the first lower peak. The expanded headspace vapor produces the first pressure wave, while the second peak results from the expansion due to liquid evaporation.

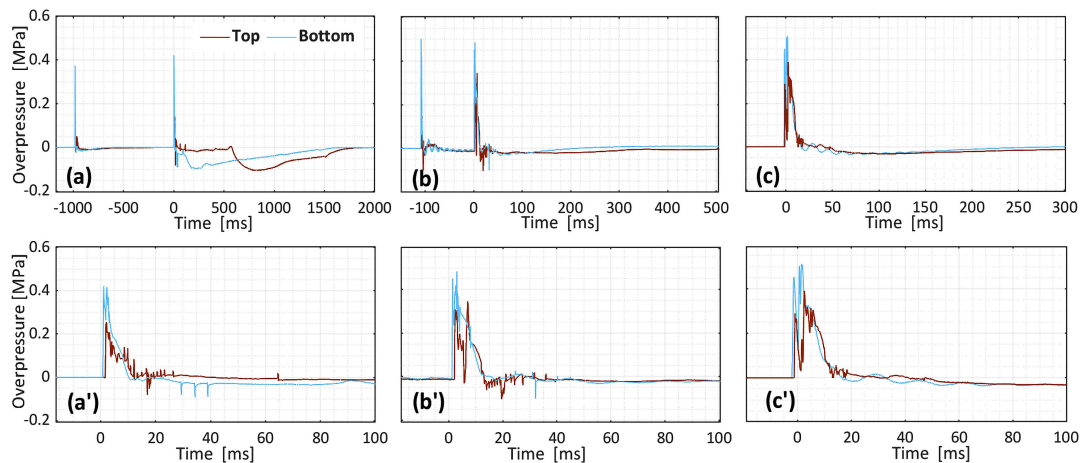


**Fig. 3.** Measured overpressures at the top and bottom alongside the tube at 180 and 650 mm from the HP diaphragm. For LVF of 15 (a), 35.2 (b), and 52.7% (c). graphs (a'), (b'), and (c') are the corresponded enlarged segments.

The graphs above show that the period between MP and HP diaphragm ruptures decreases as the LVF increases. Similarly, the measured peak overpressure from the top and bottom sensors increases with an increase in LVF. These overpressures peaked at 0.42, 0.48, and 0.51 MPa from the bottom sensor's records and 0.25, 0.35, and 0.38 MPa from the top sensor's histories. The blast wave signal shape primarily depends on the expansion development, particularly the evaporation process pace [12]. Ciccarelli et al. [13] have measured overpressures generated from CO<sub>2</sub> decompression in a polycarbonate tube. The signals are typified by a gradual increase in pressure at two different positions, while graphs in Fig. 3. show a steep increase. It is interesting to note that these results indicate a rapid evaporation process in this geometry as the downstream mixture flows towards a regularly increasing cross-section in the conical-shaped vessel. Additionally, the MPOs are much higher than those measured during CO<sub>2</sub> decompression in a constant cross-section duct done by

Hansen et al. [10]. The correlations between MPOs and the LVFs (0, 15, 20, 25, 35.2, 52.7, and 73.6 %) are presented in Fig.4.

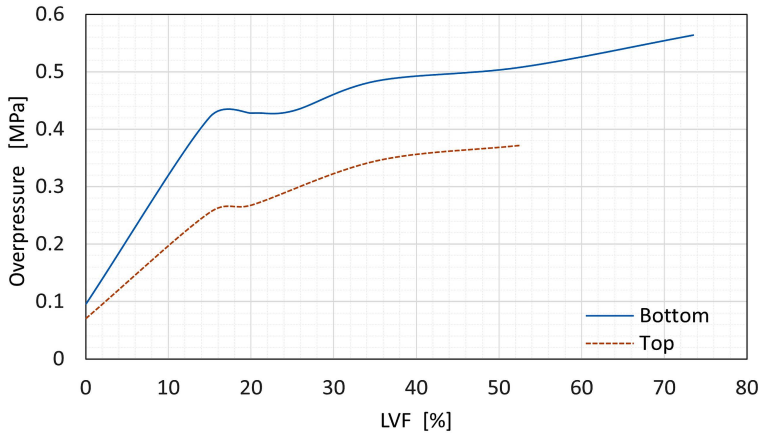


**Fig. 4.** Measured peak overpressure at the top (180 mm) and bottom (650 mm) of the atmospheric tube versus LVF during CO<sub>2</sub> depressurization in the conical-shaped vessel.

The energy quantity from the explosion potentially transferred to the structure is illustrated as a calculated impulse over 40 ms in Fig. 5. The impulse computations have been executed by integration of the pressure histories. Graph (a) represent the calculated impulse for pressure records at the bottom tube cite. In comparison, graph (b) shows them at the top transducer position. After 40 ms, all impulse curves fade out, and there is no positive phase. Besides, there are no significant differences in the lines' behavior during approximately 2 ms from the start

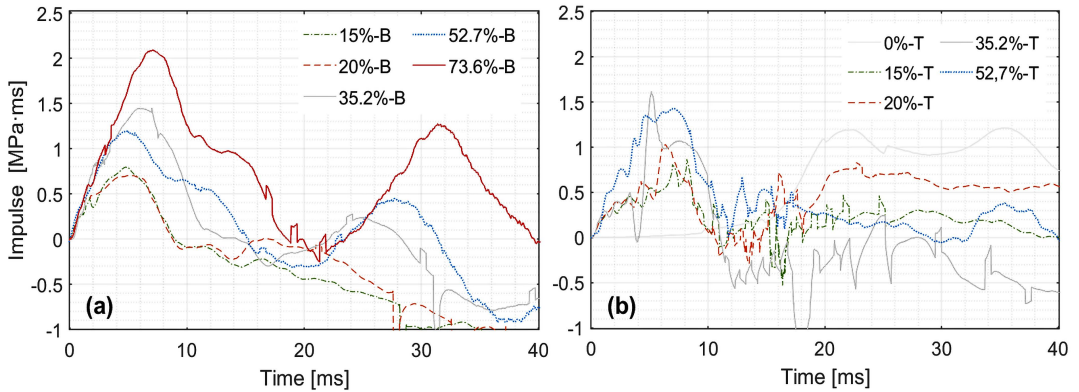


**Fig. 5.** The calculated impulse from the measured overpressure records at the tube's bottom (a) and top (b).

Interestingly, in Fig. 5. (a), the curve with 35.2 % LVF peaked higher than the one with 52.7%. Then the curves traversed twice before the latter curve peaked higher in the second positive phase. This behavior may be due to the expansion of higher vapor volume in the vessel's headspace and subsequent expansion of multiphase mixture after the evaporation wave has passed. The impulse curves in Fig. 5. (b) have inverse behavior, wherein the lines with lower LVF peak higher in the second positive phase. This trend can be observed from the 0% and 15% LVF curves pattern.

**Fragments' initial velocity and kinetic energy**

The analysis of flying fragments and missiles is essential in estimating BLEVE incident effects. The fragmentation of the pressure vessel constitutes a severe hazard to surrounding living beings and structures. Therefore, it is necessary to assess the consequences impacts of such risk for better safety

management. Generally, the explosion-released energy is an aggregate of pressure wave's energy, fragments' kinetic and potential energy, and the surrounding heating. The pressure wave energy has been suggested to be around 80% of the explosion energy in the case of fragile vessel fracture [14]. Several methods were proposed to quantify the fragments' hazard. Birk [15] has offered experimental data showing that the projectile hazard from shattering a tank filled with pressurized propane in terms of mass x range ( $\text{kg}\cdot\text{m}$ ) increased with an increase in average liquid temperature before the explosion. Baum [16] has measured the end-cap velocity during experiments with pressurized water in a horizontal vessel. According to obtained data, he proposed a formula to calculate the fragment's initial velocity ( $v_f$ ) as:

$$v_f = \left( \frac{2 \cdot k_q \cdot Q_{ex}}{m_f} \right)^{0.5} \quad (1)$$

$$Q_{ex} = m_l \cdot C_p \cdot (T_{rupt} - T_b) = (V_V \cdot \phi \cdot \rho_l) \cdot C_p \cdot (T_{rupt} - T_b) \quad (2)$$

where  $m_f$  is the fragment mass [kg],  $Q_{ex}$  is the excess heat stored in the liquid before the explosion [J], and  $k_q$  is the fraction of the excess heat transformed to the fragment kinetic energy, and the most suitable value noticed to be 0.00126.  $C_p$  is the pre-ruptured liquid specific heat at constant pressure [ $\text{kJ}/\text{kg}\cdot\text{K}$ ],  $T_{rupt}$  is superheated liquid temperature [K],  $T_b$  is the liquid boiling temperature at atmospheric pressure [K].  $V_V$  is the vessel volume [ $\text{m}^3$ ].  $\phi$  is liquid volume fraction.  $\rho_l$  is the Liquid density at the superheated state [ $\text{kg}/\text{m}^3$ ].

This section compares fragments' velocities analyzed based on experimental results with fragment velocity calculation results from the above relationship.  $\text{CO}_2$  properties at pre-ruptured saturation state were found from tabulated data built from the Span-Wagner equation of state (SW-EOS) and NIST [17, 18]. Based on Baum's equation, the fragment velocity from the rupture of a vessel containing  $\text{CO}_2$  with 52.7% LVF at pre-ruptured conditions 5.58 MPa and 292 K is:

$$Q_{ex} = 0.25 \cdot 4.0145 \cdot (292 - 194.69) = 97.66 \text{ kJ} \quad (3)$$

$$v_f = \left( \frac{2 \cdot 0.00126 \cdot 97660}{0.0282} \right)^{0.5} \approx 93.4 \text{ m/s} \quad (4)$$

During the explosion experiments in the HP conical vessel, the flying fragment is a circular diaphragm consisting of three aluminum layers with 0.8, 0.5, and 0.3 mm thicknesses. Fragments velocities were estimated by processing the high-speed videos from four experiments of  $\text{CO}_2$  depressurization in the conical vessel filled with LVF of 25, 35.2, 52.7, and 73.6%. The videos were captured at 7200 frames per second (fps) and a 256 x 1024 pixels resolution. Velocity calculations have been done along two equal tube heights, each covering 235 mm, by tracking the diaphragm trajectories with a height to pixel conversion of 0.94 mm/pixel. Fig. 6 (on the top) shows cropped images from the sequence of video frames during 10.4 ms covering the evolution of the ruptured HP diaphragm through the atmospheric tube. The images are cut from the video captured in the test with 35.2 % LVF. The cropped images resolution was minimized to 119 x 901 pixels, and the variance between one image and the followed image is three frames (about 0.42 ms). A light line is drawn underneath the trajectory of the diaphragm movement. In addition, Fig. 6. (on the bottom) shows the pressure records corresponding to the duration of the image sequence.

From the data in Fig. 6., the emergence of the diaphragm in the tube required about 1 ms and took nearly 7 ms to propagate through the tube length. The liquid remained in a metastable state during this period, as shown in Fig. 6. (bottom). This trend reveals that the ruptured diaphragm is propelled mainly by the expanded vapor in the vessel's headspace

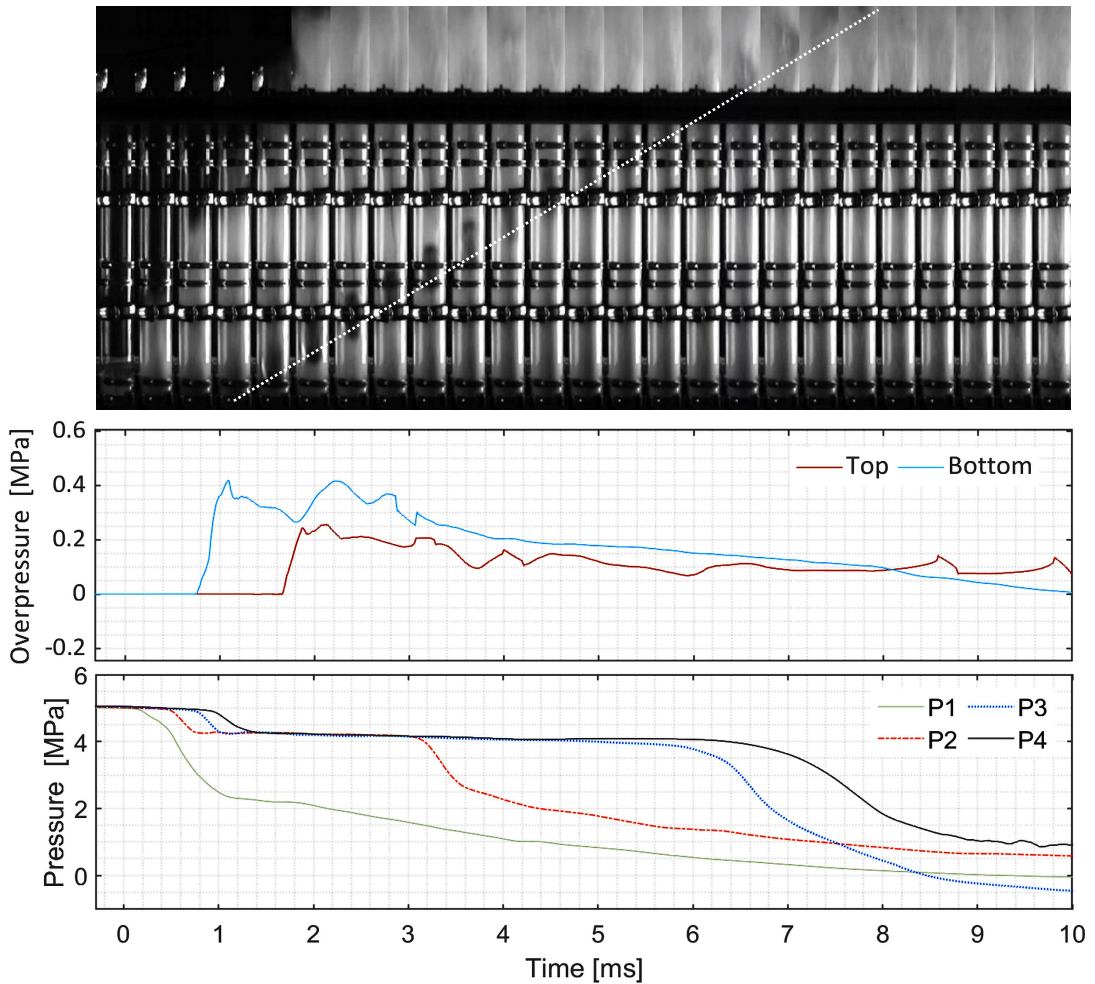


**Fig. 6.** Top: sequence of cropped images from a high-speed video of CO<sub>2</sub> depressurization test with LVF of 35.2% (time step of 0.416 ms). Middle: synchronized overpressure records on the top and bottom of the polycarbonate tube. Bottom: corresponding pressure histories from HP vessel during 10.4 ms.

Interestingly, the force of the released expanded multiphase mixture acting on the diaphragm should likely result in parabolic path motion. However, its movement is described by a constant velocity ( as the linear trajectory shows in Fig. 6). It could be argued that it moves with about the same velocity as the released multiphase mixture, but further research might explore its movement without net force.

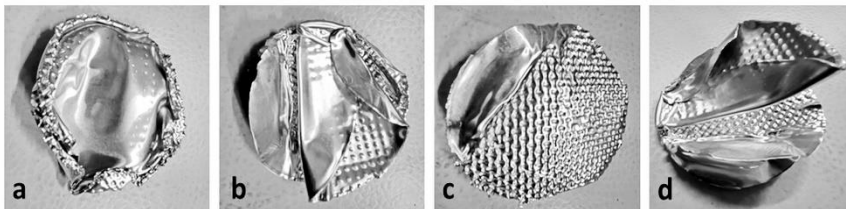


**Fig. 7.** Fragments' (HP diaphragm layers) shape after they are propelled through the tube and hit the protective mesh at the chamber's ceiling. The VLF in the vessel was 73.6 in (a), 52.7 in (b), 35.2 in (c), and 25% in (d).

The rocketed fragments from four experiments with different LVFs were collected, classified, and weighed (see Table 1). Pictures showing the diaphragms' shape after hitting the protective mesh at the chamber ceiling are presented in Fig. 7. After the propelled diaphragms' weights were determined, their kinetic energy was calculated, and the results are set out in Table 1.

**Table 1. Characteristics of the fragments from HP diaphragm rupture**

LVF, %	Weight, g	Velocity, m/s	Kinetic energy, J
73.6	27.9	121.1	204.9
52.7	28.2	109.3	168.6
35.2	28.5	112.0	177.1
25	28.5	94,6	127.4

## CONCLUSION

Laboratory-scale experiments have been conducted to study the release of liquified CO<sub>2</sub> from a conical-shaped vessel sealed with double-membrane apparatus to an atmospherically vented tube. The research goal is to describe the blast wave consequences during the CO<sub>2</sub> depressurization in such geometry. Analysis of measured overpressure at the top and bottom of the tube shows that rapid evaporation significantly influences the leading overpressure positive phase. This positive phase combines a second higher peak from expansion due to liquid evaporation and an initial lower peak driven by the expanded headspace vapor content. The peak overpressure increases with an increase in LVF. The measured peak overpressures in the tests with LVF of 15, 35.2, and 52.7% are 0.42, 0.48, and 0.51 MPa, respectively.

In addition, this research estimates the flying diaphragms' velocity and their kinetic energy by analyzing high-speed videos. Results indicate that the propelled diaphragm's velocity and the corresponding kinetic energy increase with increasing LVF. The highest values obtained from the test with 73.6% LVF are about 121 m/s and 205 J. Comparing the obtained velocity from the test with LVF of 52.7% with the calculated model for initial fragment velocity at the same initial conditions indicates conservative divergence. It is 109.3 m/s for the former and 93.4 m/s for the latter.

## REFERENCES

- [1] CCPS, Guidelines for Vapor Cloud Explosion, Pressure Vessel Burst, BLEVE, and Flash Fire Hazards. AIChE-Wiley, pp. 311-360, 2010.
- [2] W. E. Clayton, M. L. Griffin, Catastrophic failure of a liquid carbon dioxide storage vessel. Process Safety Progress. vol. 13, no. 4, (1994) pp. 202-209, doi: doi.org/10.1002/prs.680130405.
- [3] Y. Zhang, J. Schork, K. Ludwig, Revisiting the conditions for a CO<sub>2</sub> tank explosion. Proceedings of the Ninth Global Congress on Process Safety, San Antonio, Texas: AIChE, pp. 109-120, 2013.
- [4] A. C. Van den Berg, M. M. Van der Voort, J. Weerheijm, N. H. A. Versloot, BLEVE blast by expansion-controlled evaporation. Process Safety Progress. vol. 25, no. 1, (2006) pp. 44-51, doi: 10.1002/prs.10116.

- [5] A. M. Birk, C. Davison, M. Cunningham, Blast overpressures from medium-scale BLEVE tests. *Journal of Loss Prevention in the Process Industries.*" vol. 20, no.3, (2007) pp.194-206, doi: doi.org/10.1016/j.jlp.2007.03.001.
- [6] R. W. Prugh, Quantitative Evaluation of "Bleve" Hazards. *Fire Protection Engineering*, "vol. 3, no. 1, (1991) pp. 9-24, doi: 10.1177/104239159100300102.
- [7] E. Planas-Cuchi, J. M. Salla, J. Casal, "Calculating overpressure from BLEVE explosions. *Loss Prevention in the Process Industries.*" vol. 17, no. 6, (2004) pp. 431-436, doi: doi.org/10.1016/j.jlp.2004.08.002.
- [8] A. C. van den Berg, Blast charts for explosive evaporation of superheated liquids. *Process Safety Progress*, vol. 27, no. 3, (2008) pp. 219-224, doi: [doi.org/10.1002/prs.10252](https://doi.org/10.1002/prs.10252).
- [9] M. M. van der Voort, A. C. van den Berg, D. J. E. M. Roekaerts, M. Xie, P. C. J. de Bruijn, Blast from explosive evaporation of carbon dioxide: experiment, modeling, and physics. *Shock Waves*, "vol. 22, no. 2, (2012) pp. 129-140, doi: 10.1007/s00193-012-0356-0.
- [10] P. M. Hansen, A. V. Gaathaug, D. Bjerketvedt, K. Vaagsaether, "Blast from pressurized carbon dioxide released into a vented atmospheric chamber" *Uj qem'Y cxgu*" vol. 28, no. 5, pp. 1053-1064, Art no., doi: 10.1007/s00193-018-0819-z.
- [11] O. M. Ibrahim, P. M. Hansen, D. Bjerketvedt, and K. Vågsæther, "Release mechanisms and waves interaction during liquified CO<sub>2</sub> depressurization in a double-membrane conical vessel," *SN Applied Sciences*, vol. 4, no. 4, p. 89, 2022/03/02 2022, doi: 10.1007/s42452-022-04975-4.
- [12] J. C. A. M. v. Doormaal and R. M. M. v. Wees, 2005 , Rupture of vessels. in *Methods for the calculation of physical effects: due to releases of hazardous materials (liquids and gases)*, The Hague: Min. VROM, ch. 7, 2018, pp. 7.1 - 7.78.
- [13] G. Ciccarelli, J. Melguizo-Gavilanes, J. E. Shepherd, Pressure field produced by the rapid vaporization of a CO<sub>2</sub> liquid column. 30th International Symposium on Shock Waves, Tel-Aviv, Israel, 2015.
- [14] J. Casal, J. Arnaldos, H. Montiel, E. Planas-Cuchi, J. A. Vi'lchez, Modeling and understanding BLEVEs. in *The Handbook of Hazardous Materials Spills Technology*. NY: McGraw-Hill, pp. 22.1-22.27, 2002.
- [15] A. M. Birk, Hazards from propane BLEVEs: An update and proposal for emergency responders. *Loss Prevention in the Process Industries.*" vol. 9, no. 2, (1996) pp. 173-181, doi: doi.org/10.1016/0950-4230(95)00046-1.
- [16] M. R. Baum, Failure of a horizontal pressure vessel containing a high temperature liquid: the velocity of end-cap and rocket missiles. *Loss Prevention in the Process Industries.*" vol. 12, no. 2, (1999) pp. 137-145, Art no., doi: doi.org/10.1016/S0950-4230(98)00051-5
- [17] R. Span, W. Wagner, A New Equation of State for Carbon Dioxide Covering the Fluid Region from the Triple - Point Temperature to 1100 K at Pressures up to 800 MPa. *Physical and Chemical Reference Data*. vol. 25, no. 6, (1996) pp. 1509-1596, doi: [doi.org/10.1063/1.555991](https://doi.org/10.1063/1.555991).
- [18] Eric W. Lemmon, Mark O. McLinden, D. G. Friend. Thermophysical Properties of Fluid Systems. in *NIST Chemistry WebBook, NIST Standard Reference Database Number 69*, Eds. P.J. Linstrom and W.G. Mallard, National Institute of Standards and Technology, Gaithersburg MD, 20899, <https://doi.org/10.18434/T4D303> (accessed, 2021).

## Regrt '7'

### **Modeling of the two-phase flow during depressurization of liquified CO<sub>2</sub> in a pipe.**

This paper is published in the Proceedings of the 63<sup>rd</sup> International Conference of Scandinavian Simulation Society, SIMS, NTNU, Trondheim, Norway, No. 192, pp. 226.

doi: <https://doi.org/10.3384/ecp192>.





y kj " r t g x k w u " u j q e m ' w d g " g z r g t k o g p v e n ' f c v c 0 ' O w p n g l q t f " g v ' c i f 0 [ 6 . 7 ] c x g ' c r r r k e f " y q " o q f g n ' v q " u w f { " y j g " k p h w g p e g " q h ' k o r w t k l u " c p f " y j g " k p k l c n ' v g o r g t c w t g " q p " y c x g " x g n e k f " f w t k p i " E Q 4 / t k e j " o l z w t g " f g e q o r t g u k q p 0 ' V j g " j q o q i g p g q w u " g s w k k d t k w o " o q f g n ' J G O - f c p f " y j g " v y q / h w k f " o q f g n ' \* V H O - f y g t g ' h q t o w e v g f " d { ' l o r r g o g p v k p i " y j g ' o w n k ' u c i g " e g p v g t g f " u e j g o g " \* O W U V C - f u k o w n c p g q w u n { " y k j " U q c x g / T g f r e j / M y q p i " c p f " R g p i / T q d k p u q p " G Q U " v q " e c r e w r c v g " y j g " v j g t o q f { p c o k e c n ' r t q r g t v g u 0 ' V j g " o q f g n u ' e c r e w r c v k p " h k p f k p i u " y g t g " e q p t c u v g f " y k j " u j q e m ' w d g " v g u v ' t g u w u . " y j k e j " f g o q p u t c v g f " o k p o c n ' g p j c p e g o g p v ' k p " V H O " r t g f k e v k p u " c i c k p u v " J G O 0 ' D q t q u " g v ' c i f 0 [ 8 ] c x g ' r g t h q t o g f " u j q e m ' w d g " g z r g t k o g p w ' q p " r w t g ' E Q 4 " c p f " e q o r t c t g f " y j g " t g u w u u " y k j " " g u k o c v k q p u " h t q o " " o q f g n u ' c p f " q p " y j t e g g " g s w c k q p u " q h ' u c v g < I G T I / 4 2 2 : . " R g p i / T q d k p u q p . " c p f " D Y T U 0 V j g f { ' e q p e n w f g f " y j c v ' a p n f " I G T I / 4 2 2 : " e q t t g u r q p f g f " y k j " g z r g t k o g p v c i f c v c 0 J q y x g t . " y j g " k p e q p u k n g p e { ' k p e t g c u g f " y k j " v g o r g t c w t g ' t g f w e v k p o 0 ' O q t k p " g v ' c i f 0 [ 9 ] c x g " r t g u g p v g f " c p " c r r t z k o c v g " T l g o c p p " u q r x g t " q h ' T q g " h q t " y j g " r k r g u " E Q 4 " f g r t g u u w t k c v k p o ' U k o w r e v k p " t g u w u " f g o q p u t c v g f " y j c v ' y j g ' e g p t c n ' u e j g o g " w p f g t g u k o c v g f " y j g ' r t g u u w t g " r w u g u " o c z k o w o " c o r r k w f g 0 ' Y j k e g " y j g " j k j / t g u n w k q p " T q g " u e j g o g " c e e w t c v g n f " f g u e t k d g f " y j g " r w u g 0 ' C " j q o q i g p g q w u " t g r e z c k v p " o q f g n ' \* J T O + " y k j " e w d k e " G Q U " y c u ' k p t q f w e g f " d { " D t q y p " g v ' c i f 0 : \_ v q " f g u e t k d g " y j g " t g n g c u g f " h u y " t g u w n k p i " h t q o " f g p u g " r j c u g " E Q 4 r k r g ' t w r w t k p i 0 ' V j g " o q f g n ' y c u ' t g u i x g f " d { " e q p l w i c v k p i " c " u g o k f k u e t g v g " H k p k g " X q n w o g " O g j q f " c p f " J N N " \* J c t g p / N c z / x c p " N e g t - f c r r t z k o c v g " T l g o c p p " u q r x g t 0 ' K ' c n q " u j q y g f " t g c u p c d n g " c i t g g o g p v " y k j " y j g " t g e n ' f e v e " h t q o " t w r w t k p i " y j g " E Q 4 r k r g r k p g 0 ' k p " y j k u ' r e r g t " c f ' t k h ' h w z " / \* J G O + " k u ' d w k n ' w k k k k p i " e g p t c n ' w r y k p f / y g l i j v g f " g u u g p v k m f " p q p / q u e k m v q t { " \* Y G P Q + " p w o g t k e c n ' u e j g o g u ' v q ' k n w u t c v g ' y q / r j c u g ' h u y " h u y " h u y k p i " E Q 4 " f g e q o r t g u k q p ' k p " c ' r k r g 0 ' "

400 g y j q f q u j i { "

V j k u " o q f g n ' k p e q r t c v g u " y j g " f t k h / h w z " o q f g n ' \* j q o q i g p g q w u " g s w k k d t k w o + . " U r c p / Y c i p g t " G s w c v k p " q h ' U c v g . " c p f " e g p v g t g f / w r y k p f / Y G P Q " u e j g o g . " k p e n w f k p i " y j g " T w p i g / M w w c " h q w t v j / q t f g t " o g y j q f " v q " f g u e t k d g " y j g " v t c p u k g p u " e j c t c e v g t k u k e u " f w t k p i " n s w k f " E Q 4 " f g e q o r t g u k q p 0 ' V j g " o q f g n ' k n w u t c v g u " q p g " e q o r q p g p v ' \* E Q 4 + " y k j " y q / r j c u g " h u y " k p u k f g ' c ' j q t k k q p v c i r k g ' c p f " k u ' c u u w o g f " v q ' d g ' k p " y j g t o c n ' o g e j c p k e c n ' c p f " e j g o k e c n ' g s w k k d t k w o 0 k 0 " y j g i c u ' c p f " n s w k f " r j c u g u j c x g ' v j g ' u c o g ' g o r g t c w t g " \* V + : r t g u u w t g \* R + : c p f " e j g o k e c n ' r q v g p v c i n \* μ - 0 "

$$T_l = T_g = T; P_l = P_g = P; \mu_l = \mu_g = \mu \quad (1)$$

400' H w k f ' f { p c o k e u ' k p ' y j g ' r k r g ' h u y " o q f g n ' "

W p r k n g " y j g " F t k h ' H w z " O q f g n ' \* F H O + " k p " y j g " J G O " o q f g n ' y j g " i c u ' c p f " n s w k f " x g n e k f " c t g " k f g p v k e c n \* p q " u r k r + 0 ' k p ' c f f k k q p . " y j g ' o q f g n ' k u ' q p g / f k o g p u k p c n f w e " v q " h u y " k p " q p g " f k g e v k p p " c m p i " y j g " r k r g 0 ' V j g " h u y " x c t k c d r g u ' c t g ' c x g t c i g f " q x g t ' y j g ' r k r g u ' e t q u u / u g e v k p o 0 ' V j g " i q x g t p k p i " g s w c v k p u " c t g " k p " y j g " h q t o " q h ' j { r g t d q r k e " r c t v c n ' f k h g t g p v c i n ' g s w c v k p u " u k o k e c t " v q " G w g t ' u ' g s w c v k p u / h q t ' e q o r t g u k d r g ' k p x k u e k f " h u y " q h ' c " u k p i n g ' h w k f " c p f " e c p ' d g ' f g u e t k d g f " c u " "

$$\frac{\partial}{\partial t} U + \frac{\partial}{\partial x} F = 0 \quad (2)$$

y j g t g " U " k u " y j g " x g e v q t " y j c v ' e q p v k p u " y j g " e q p u g t x g f " x c t k c d r g u ' c p f " F ( U ) k u ' y j g ' h w z ' h w p e v k p c "

$$U = [\rho, \rho v, E]; F = [\rho v, \rho v^2 + P, v(E + P)] \quad (3)$$

E q t t g r c v g f " e n q u w t g ' r c y u ' h q t " y j g " J G O " e q p u k w g g " y j g " v y q / r j c u g " o k z w t g " f g p u k f " ρ . " y j g ' v q v c n ' g p g t i { " E . " y j g " e q t t g u r q p f k p i " o k z w t g k u " u r g e k k e " k p v g t p c n ' g p g t i { e\_{mix} , c p f " y j g ' x q n w o g ' h c e v k p p ' t g r e v k p p ' c u ' h u y " u " "

$$\begin{aligned} \rho &= \alpha_g \rho_g + \alpha_l \rho_l; \\ E &= \rho(e + 0.5v^2); \\ e &= (\alpha_g \rho_g e_g + \alpha_l \rho_l e_l) / \rho; \end{aligned} \quad (4)$$

"α<sub>g</sub> + α<sub>l</sub> = 1"

y j g t g " ρ " f g p q v g u " f g p u k f . " v " / " x g n e k f " E " - " y j g ' v q v c n ' g p g t i { . e " - " u r g e k k e " k p v g t p c n ' g p g t i { . " P " - " r t g u u w t g " α<sub>i</sub> - volume fraction of the phase i . " c p f " u w d u e t k r u " g " c p f " l " c t g " i c u " c p f " n s w k f " r j c u g u " t g u r g e v x g n f 0 ' h q t ' u k o r n e k f . " y j g ' u w t e g ' v g t o u ' c t g ' p q v ' k p e n w f g f . k 0 0 ' y j g j g e v t c p u h g t ' y j t q w j ' y j g ' r k r g y c m " y c m ' h k e v k p . " c p f " y j g " i c t x k c v k p c n ' h q t e g u " c t g " p g i n g e v g f 0 " G s w c v k p " \* 4 + " e c p ' d g " y t k w g p ' k p " c " s w e u k r k p g c t ' h q t o " c u "

$$U_t + A(U)U_x = 0 \quad (5)$$

y j g t g " A ( U ) = \frac{\partial F}{\partial U} " k u " y j g " l c e q d k c p " o c v t k " q h " y j g " u { u g o 0 "

400' V j g t o q f { p c o k e u " "

C " h w p e v k p " P ( e , ρ ) " y j c v ' t g r c v g u " y j g " r t g u u w t g " v q " y j g " k p v g t p c n ' g p g t i { " c p f " f g p u k f { " k u " t g s w t g f " v q " e q o r n g v g " y j g " o q f g n 0 ' V j k u " y q t n f " w u g u " y j g " U r c p / Y c i p g t " G s w c v k p " q h ' U c v g " \* U Y " G Q U + 0 ' K ' k u ' e q p u k f g t g f " y j g " o q u v ' c e e w t c v g " G Q U " h q t " E Q 4 " c p f " k u ' d c u g f " q p " J g m j q n f u " h g g " g p g t i { " \* J H G + " c u " c " h w p e v k p " q h ' v g o r g t c w t g . " x q n w o g . " c p f " y j g ' p w o d g t " q h 0 ' q r g u < A ( T , V , N ) ' V j g " o q r c t " r t q r g t v g u " q h ' y j g " J H G " c p f " y j g " x q n w o g " c t g "

$$a = \frac{A}{N}; v = \frac{V}{N} \quad (6)$$

"  
 K'lo r rkgu'vj cv'"a(T, v)0'Vj g'tgrvkvq"qh'"a"vq"vj g"  
 qvj gt'vj gto qf { pco le'r tqr gt'vku'ecp'dg'g'zr tguugf "kp"  
 vto u" qh' r ctvkn' f gtxcvkxgu" qh' 'vj g' kpf gr gpf gpv'  
 xctkcdrg'(T, v). Vj g'tgrvkvq"vj'vj g't' tguuwtg. k'pvtgpcn'  
 gpgti { ".cpf"gpvtqr { "ctg"cu'hqmqy u<"

$$P = -\frac{\partial a}{\partial v};$$

$$e = a + Ts = a - T \frac{\partial a}{\partial T};$$

$$s = -\frac{\partial a}{\partial T};$$

Cu'vj g'r j cug'vcpukvq"qewtu'hqmqy kpi "cf kcdvle"  
 r tguuwtg'tgf wekvq. "Vj g'o qrc't'gpvtqr { "ku'eqpugt'xgf 0'  
 Vj g'vgo r gtcwtg"ku'wpnpy p. "cpf"kv'ku'tgs wktgf "vq"  
 uqrxg"qpg"qt"o qtg'h'pogct"gs wekvqpu'kpxqmkpi e and  
 v' vq" f gvgto kpg"ku'xcnwg0'UY "GQU" f go qpvtcvgu"  
 g'zr riek' g'zr tguukvqpu" hqt" J HGU" cr r tqr tlcvg" r ctvkn'  
 f gtxcvkxgu. cmqy kpi "hqt"pwo g'kcn' (uqrxkpi "hqt"vj g"  
 vgo r gtcwtg" wulpi " P gy vqpu" o gvj qf 0' Vj g' kpkkn'  
 o qrc't'xqno g'cpf "k'pvtgpcn'gpgti { " (v0, e0)"ecp'dg"  
 f gvgto kpgf " cu" c" h'pvekvq" qh' 'vj g' npqy p" kpkkn'  
 ucwtcvf "vgo r gtcwtg'cpf 't' tguuwtg' T0, P0 +0'Vj gp'vj g"  
 gs wekvq" kpxqmkpi " o qrc't' k'pvtgpcn' gpgti { " cu" c"  
 h'pvekvq"qh'vgo r gtcwtg'cpf "o qrc't'xqno g'lj qwf "dg"  
 uqrxg" d { "pgy vqpu" o gvj qf "k'g'cvkvq" "

$$G(X) = [e(X) - e_0] = 0;$$

$$X_{i+1} = X_i - J^{-1} \cdot G(X) \tag{8}$$

J gtg"X"uki p'kku'vj g'xgevt(T, v)^T. "cpf" J = \frac{\partial e}{\partial T} "ku"  
 vj g' l'ceqdkcp'qh'G0Vj gp'vj g'vj gto qf { pco le'v'cvg"ku"  
 f gvgto kpgf "cu" c' h'pvekvq"qh'T"cpf "v" "O l'ccxcwgp."  
 4244+0'  
 Vj g'ur ggf "qh'uqwpf "kp'vj g'o kzwg'ku'i kxgp"cu<"

$$C_m = \sqrt{\frac{v^2}{M_W} \cdot \left( \frac{\partial a^2}{\partial v^2} - \frac{\partial a^2}{\partial v \partial T} \right)} \tag{9}$$

K'cf f k'kq. "p = \frac{M\_W}{v} "y j gtg" M\_W "ku"vj g'o qrgewrt"  
 y gki j v' hqt"EQ4. "66023i lo qn0'

4050" Pwo g'kcn'0 gvj qf "

Gs wekvq" \*4+ "ecp'dg"uqrxgf "wulpi "vj g'h'p'kg/xqno g"  
 uej go g. " y j gtg'p' "vj g' f qo clp" ku" f kuetg'k'gf "kp'vq"  
 uwdf qo clpu" \*eqpvtqn' xqno gu+0' Vj g' ugo k'f kuetg'g"  
 hqto wr" \*ur cvkn' qr gtcvt" f kuetg'k' cvkvq+ "ecp" dg"  
 qd'cvkpgf "d { "Gs 0\*4+ k'p'gi tcvkq<"

$$L(U) = -\frac{1}{\Delta x} \left( F_{i+\frac{1}{2}} - F_{i-\frac{1}{2}} \right) \tag{10}$$

y j gtg" L(U) "f kuetg'k' cvkvq"qh'vj g'ur cvkn'qr gtcvt=" "  
 F\_{i+\frac{1}{2}} " " "vj g' h'wz" dgwy ggp"egmi" i" cpf "i + 10' Vlo g"  
 k'g'cvkvq" hqt"vj g' ugo k'f kuetg'g" hqto wr" ku" gzgewgf "  
 wulpi "vj g'v'cn'xctkcvkq" f lo k'pkuj kpi " \*VXF +T wpi g/  
 M'wv" o gvj qf " \*TMO +0' C'ceqtf kpi "vq" I q'wk'gd" gv'cn'

\*3; ; : + "vj ku'b gvj qf "h'ggr u'VXF" r tqr gt'vku'uc'vuh' kpi "  
 vj g'EqwcpvH'k'gf tlej u'Ngy { " \*EHN+ "eqpf k'k'p'0'Vj g"  
 v'lo g' k'g'cvkvqpu" d { " h'qwt'vj / qtf gt" VXF" TEO" ctg"  
 g'zr tguugf "cu" \*Uj w'cpf "Quj gt. "3; ; : +<"

$$U^{(1)} = U^{(0)} + \frac{1}{2} \Delta t L(U); \tag{11.1}$$

$$U^{(2)} = \frac{1}{2} U^{(0)} + \frac{1}{2} U^{(1)} - \frac{1}{4} \Delta t L(U^{(0)}) + \frac{1}{4} \Delta t L(U^{(1)}); \tag{11.2}$$

$$U^{(3)} = \frac{1}{9} U^{(0)} + \frac{2}{9} U^{(1)} + \frac{2}{3} U^{(2)} - \frac{1}{9} \Delta t L(U^{(0)}) - \frac{1}{3} \Delta t L(U^{(1)}) + \Delta t L(U^{(2)}); \tag{11.3}$$

$$U^{(4)} = \frac{1}{3} U^{(1)} + \frac{1}{3} U^{(2)} + \frac{1}{3} U^{(3)} + \frac{1}{6} \Delta t L(U^{(1)}) + \frac{1}{6} \Delta t L(U^{(3)}); \tag{11.4}$$

y j gtg" U^{(0)} "cpf" U^{(4)} "ctg" r tqr gt'vku'cv'vj g'v'lo g'p'cpf "  
 p- 3. "t'gur gev'k'gn' 0'E'q'p'k'f gt kpi "vj g'EHN" rko k'cvkvq."  
 vj g'v'lo g'v'ng' "ku'ur gek'k'gf "cu<"

$$\Delta t \leq c \cdot (\Delta x / \max\{\lambda_i\} \forall i) \tag{12}$$

y j gtg" c" ku" vj g' EHN" pwo dgt" cpf " \lambda\_i ctg" vj g"  
 gki g'p'xcn'wgu'qh'vj g' l'ceqdkcp" o cvtkz < A(U) = \frac{\partial F}{\partial U}.

K' ku" ej cngpi kpi "vq" f kuetg'k' g' r t'g'k'gn' { "vj g' egmi"  
 k'p'v'g'g'eg" h'wz" h'pvekvq'0' k'g'0' Vj g' h'wz" " F\_{i+\frac{1}{2}} " ku"

ej cngpi kpi "vq" f gvgto kpg'cv'vj g' egmi'k'p'v'g'g'eg" i' kxgp"  
 vj g' xcn'wgu" qh' U\_i. " U\_{i+1}. U\_i^n, and U\_i^{n+1}. Mcp { "  
 pwo g'kcn' cr r t'q'cej gu" j cxg' dggp" uwi i' g'v'gf " vq"  
 eqo r w'g' F\_{i+\frac{1}{2}}' Vj ku" y qtm' cr r r'kgu" vj g' egp'v'g'f /  
 wr y kpf / Y GP Q" uej go g' \*E W / Y GP Q+ " f g'x'gn' r gf "  
 d { " \*Y g'ncj g'wki g' gv' cn' 4244+ " hqt" vj g' J GO " vq"  
 ec'v'w'v'g' vj g' h'wz" h'pvekvqpu" d { " vj g' egp'v'cn' wr y kpf "  
 uej go g' y j k'g' vj g' egmi'k'p'v'g'g'eg" r tqr gt'vku'd { " Y GP Q"  
 t'geq'p'ut wekvq'0' Vj ku" h'qto wr v'kvq" u'ggmi" vq" k'p'v'gi t'cvg"  
 vj g' egp'v'cn' wr y kpf 'h'g'c'w'g' u'k'p'v'g' vj g' Y GP Q' uej go g. "  
 y j lej " eqwf " lo r t'q'xg" vj g' t'guu'wu' ceewtce { " cpf "  
 u'cd'k'k'v'0'

Vj g' egmi'k'p'v'g'g'eg" h'wz" ku" eqo r w'g'f "ceeqtf kpi "vq" vj g"  
 egp'v'cn' wr y kpf " g'zr t'guukvq" r t'g'ug'p'v'g'f " d { " M'w'i cpq'x "  
 gv'cn'0' 4223+0' Vj g' uej go g' ur gek'k'gu' vj g' h'q'ec'n' ur ggf u"  
 qp" vj g' uk'f g' qh' y cxg" r tqr ci cvkvq" u' f k'g'ev'kvqpu"  
 \*f k'ueq'p'v'p'v'k'v' { " r tqr ci cvkvq" ur ggf u+0' Vj g' k'x'cn'wgu'ctg"  
 gs w'k'x'c'ng'p'v' vq" vj g' o cz'lo wo " cpf " o k'plo wo " qh' vj g"  
 l'ceqdkcp" o cvtkz" u' gki g'p'xcn'wgu' Vj g' r q'uk'k'xg" cpf "  
 p'gi cvk'xg" f k'ueq'p'v'p'v'k'v' { " r tqr ci cvkvq" ur ggf u" ctg "  
 f g'h'k'p'gf "cu"

$$a_{i+\frac{1}{2}}^{n+1} = \max \left\{ \begin{array}{l} \max \left\{ \lambda \left( U_{i+\frac{1}{2}}^{n-} \right) \right\}, \\ \max \left\{ \lambda \left( U_{i+\frac{1}{2}}^{n+} \right) \right\}, 0 \end{array} \right\} \tag{13.1}$$

$$a_{i+\frac{1}{2}}^{n,-} = \min \left\{ \begin{array}{l} \min \left\{ \lambda \left( U_{i+\frac{1}{2}}^{n,-} \right) \right\}, \\ \min \left\{ \lambda \left( U_{i+\frac{1}{2}}^{n,+} \right) \right\}, 0 \end{array} \right\} \quad (13.2)$$

where  $\lambda$  denotes the eigenvalues of HEM:

$$\lambda = \{v + c_m, v, v - c_m\} \quad (13.3)$$

Then, for the central-upwind scheme, the high-resolution numerical flux is expressed as:

$$F(U)_{i+\frac{1}{2}}^n = \frac{a_{i+\frac{1}{2}}^{n,+} \cdot F \left( U_{i+\frac{1}{2}}^{n,-} \right) - a_{i+\frac{1}{2}}^{n,-} \cdot F \left( U_{i+\frac{1}{2}}^{n,+} \right)}{a_{i+\frac{1}{2}}^{n,+} - a_{i+\frac{1}{2}}^{n,-}} - \frac{a_{i+\frac{1}{2}}^{n,+} \cdot a_{i+\frac{1}{2}}^{n,-}}{a_{i+\frac{1}{2}}^{n,+} - a_{i+\frac{1}{2}}^{n,-}} \cdot \left( U_{i+\frac{1}{2}}^{n,+} - U_{i+\frac{1}{2}}^{n,-} \right) \quad (14)$$

The cell interface properties are calculated by applying a fifth-order WENO reconstruction based on a third-order ENO stencils approach; for (r)-order ENO, (2r-1)-order WENO can be constructed. The cell averages calculate the cell interface properties in each stencil. So, the negative direction value at the cell interface  $i + \frac{1}{2}$  is given as:

$$U_{i+\frac{1}{2}}^- = \omega_0 U_{i+\frac{1}{2}}^{-,0} + \omega_1 U_{i+\frac{1}{2}}^{-,1} + \omega_2 U_{i+\frac{1}{2}}^{-,2} \quad (15)$$

Here,  $\omega$  is a weight function. The sum of weight functions is one ( $\omega_0 + \omega_1 + \omega_2 = 1$ ), and they are calculated as:

$$\omega_0 = \frac{\alpha_0}{\alpha_0 + \alpha_1 + \alpha_2}; \omega_1 = \frac{\alpha_1}{\alpha_0 + \alpha_1 + \alpha_2}; \omega_2 = \frac{\alpha_2}{\alpha_0 + \alpha_1 + \alpha_2} \quad (16)$$

Where  $\alpha_i$  are given as:

$$\alpha_0 = \frac{1}{10 \cdot (\epsilon + \beta_0)^2}; \alpha_1 = \frac{6}{10 \cdot (\epsilon + \beta_1)^2}; \alpha_2 = \frac{3}{10 \cdot (\epsilon + \beta_2)^2} \quad (17)$$

Where setting  $\epsilon = 10^{-6}$  aims to avoid division by zero.  $\beta$  - is a smoothness indicator that involves (r-1)-order polynomial function

$$\beta_0 = \frac{13}{12} (U_{i-2} - 2U_{i-1} + U_i)^2 + \frac{1}{4} (U_{i-2} - 4U_{i-1} + 3U_i)^2; \quad (18.1)$$

$$\beta_1 = \frac{13}{12} (U_{i-1} - 2U_i + U_{i+1})^2 + \frac{1}{4} (U_{i-1} - U_{i+1})^2; \quad (18.2)$$

$$\beta_2 = \frac{13}{12} (U_i - 2U_{i+1} + U_{i+2})^2 + \frac{1}{4} (3U_i - 4U_{i+1} + U_{i+2})^2 \quad (18.3)$$

The positive direction value  $U_{i+\frac{1}{2}}^+$  at the cell interface  $i + \frac{1}{2}$  can be calculated by symmetry.

### 3. Results and discussions

Numerical simulations analyzing the transient pipe flow behavior during the evaporation of the CO<sub>2</sub> dense phase are presented. The CU-WENO numerical schemes resolve hyperbolic conservation equations. The fluid dynamics part is combined with SW EOS to determine the variations in thermodynamic properties. The release incident involves the decompression of liquified CO<sub>2</sub> in a pipe length of 100 m. The initial conditions are: pressure ( $P_0$ ) = 7.27 MPa, temperature ( $T_0$ ) = 303.5 K and velocity ( $v_0$ ) = 0 m/s. The simulation sets out at  $x = 50$  m,  $t = 0$  s after the pipe end ruptures, and the liquid CO<sub>2</sub> depressurizes to a pressure of 3.67 MPa. As a result, a rarefaction wave travels through the liquid, causing its expansion to superheated liquid. Then, the evaporation wave moves through the superheated liquid, leading to its evaporation and generating an expanded two-phase mixture propagating toward the pipe's end with high velocity.

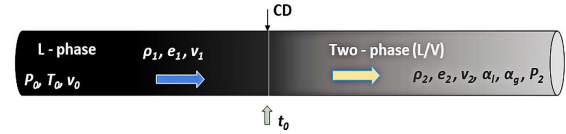
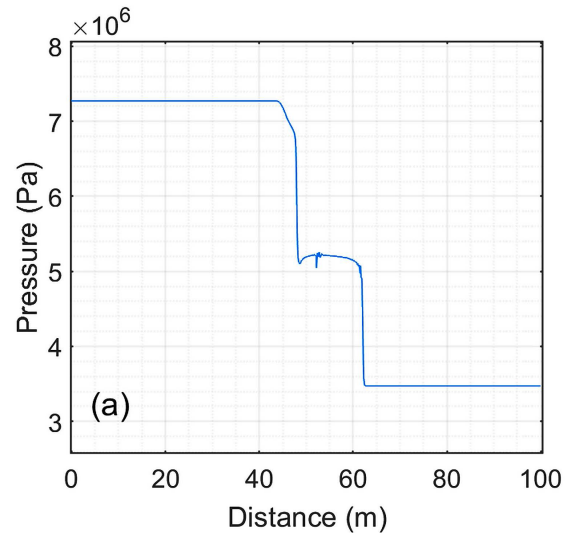


Figure 1: Schematic drawing shows CO<sub>2</sub> depressurization in a pipe.

Figure 2 shows the pressure, mixture velocity, and vapor/liquid volume fraction variations along the pipe's length. The plots demonstrate calculations for 1000 cells and 90 ms after the pipe ruptures. The passage of the rarefaction wave begins with the gradual liquid expansion corresponding to a pressure decrease from about 7.3 to 6.9 MPa and then a steep decline to almost 5.1 MPa (Figure 2(a)). The expanded superheated liquid remains in a metastable state at nearly constant pressure (slightly convex route), passing about 12.6 m before the pressure decreases sharply, indicating rapid evaporation.



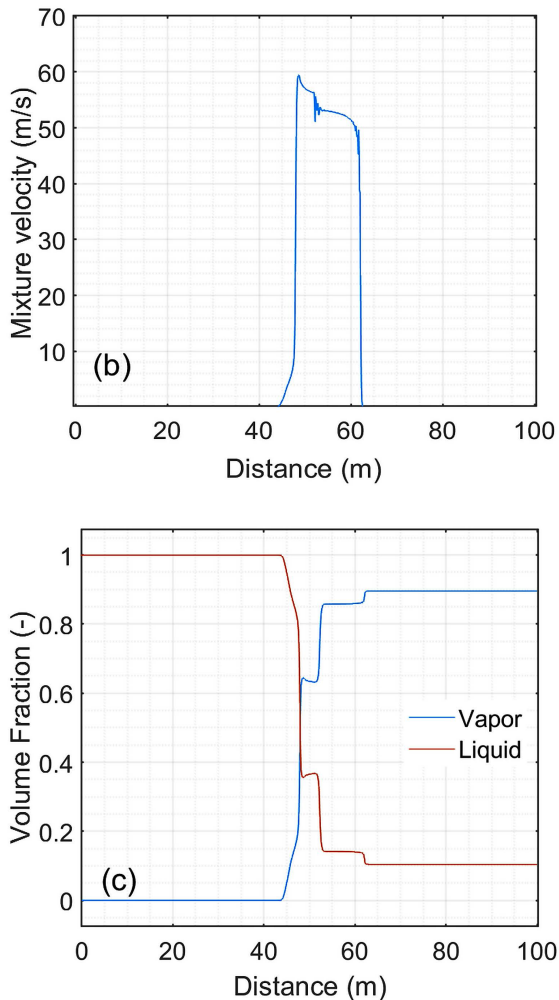


Figure 2: Change in pressure (a), mixture velocity (b), and vapor/liquid volume fraction (c) along the pipe's length during 90 ms of liquified CO<sub>2</sub> depressurization.

In addition, the rapid pressure drop results in the propagation of expanded fluid with increased velocity up to 59.3 m/s. Subsequently, the velocity decreases with small fluctuations before its abrupt drop once the evaporation wavefront has passed.

The vapor volume fraction (VVF) has risen in steps following the change in the thermodynamic state described by the pressure route. As seen in Figure 2 (c), complete evaporation has not been attained, and the third (last) jump in VVF seems to be related to the contact discontinuity wave.

Particular difficulties were encountered in the model implementation when depressurization was chosen to lower pressure near the atmospheric conditions. The temperature and subsequent calculated pressure showed unphysical behavior and may have been affected by the simplifying assumptions used in the model. In particular, the two-phase mixture velocity calculations can be vulnerable in contrast to the two-fluid model. The small rapid fluctuations seen in pressure and velocity profiles at about 52 and 61 m

(Figure 2 (a) and (b)) are likely caused by numerical computation of the temperature as a function of molar internal energy and volume. The intermittent fluctuations sites corresponded with the beginning of the rapid change in the internal energy (see Figure 4 (c)), which may produce transient instability in temperature calculations.

Computations have been implemented on grid cells between 200 and 2000 to evaluate the convergence of the CU-WENO numerical schemes. An appropriate numerical method should not create additional unreal oscillations as the cells' number increases. Figure 3 illustrates the convergence results for mixture density (a) and pressure (b) after 60 ms, implementing various cells' numbers on the CU-WENO schemes. As seen in Figure 3, the solution converges well as the grid is refined, i.e., as the size of the cells shrinks.

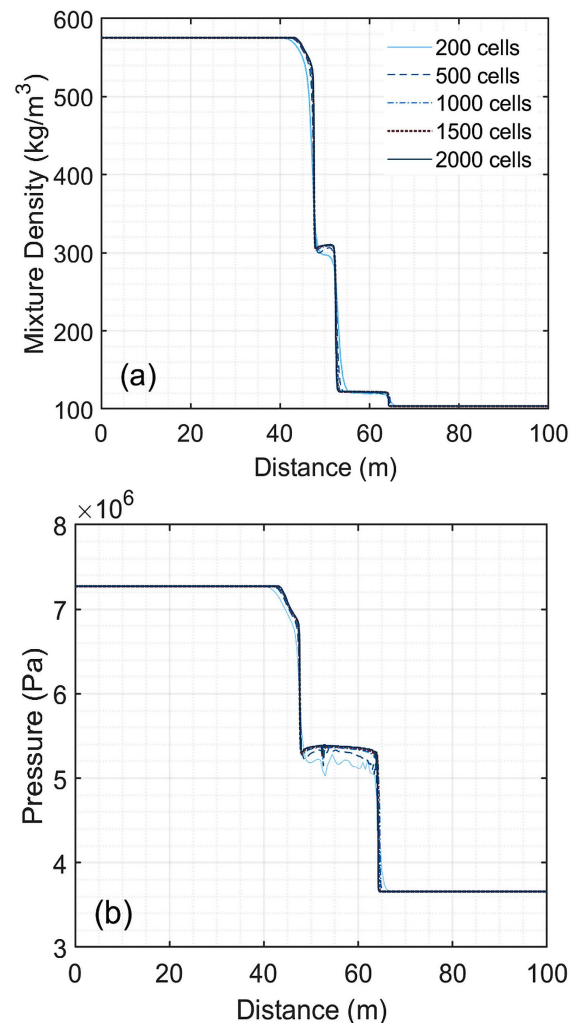


Figure 3: Grid refinement results for CU-WENO numerical schemes' convergence after 60 ms of CO<sub>2</sub> depressurization. (a) for mixture density, and (b) for the pressure.

There are no extra oscillations observed in either plot. Instead, the observed small fluctuations on the

pressure lines in Figure 3 (b) are flattened due to the grid refinement. The diffusivity of results reduces with grid refinement, and a grid size of 1500 can be recommended for the simulation.

Figure 4 shows vapor volume fraction (a), mixture density (b), and mixture internal energy (c) profiles along the pipe's length at different time stamps of 30, 50, 70, and 100 ms after the rupture. The waves' behavior can be described by tracing the changes in property profiles. The initial pressure gradient promotes the generation of three waves: shock and contact discontinuity, traveling in the right direction. Besides, an expansion wave moves in the opposite left direction.

In Figure 4 (a), the second and third sharp increases in VVF signifies the evaporation wavefront and the contact discontinuity, respectively. Additionally, the evaporation wavefront propagates towards the left as time runs, while the shock and contact surface propagate in the right direction.

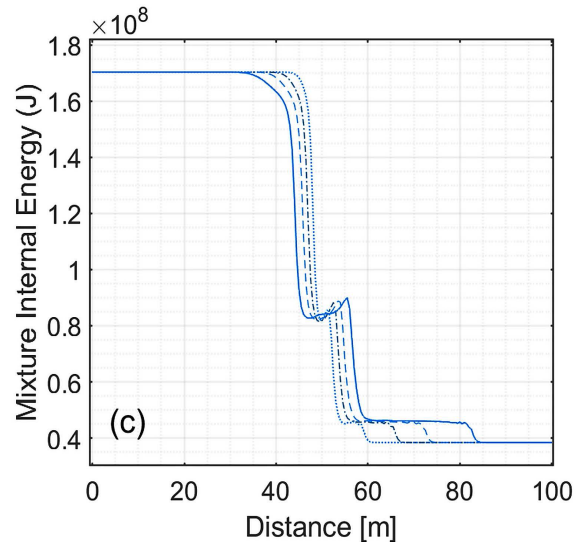
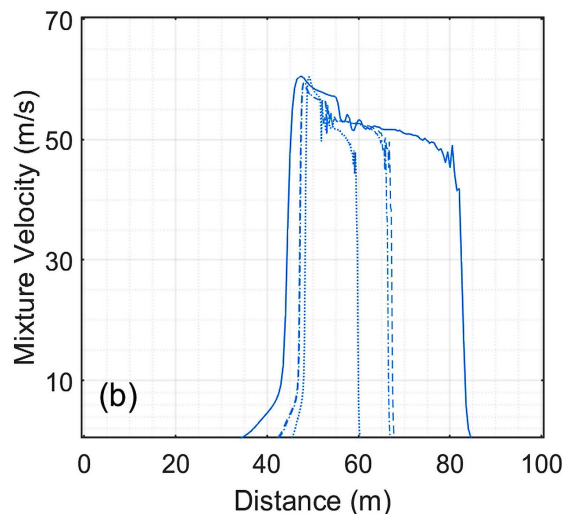
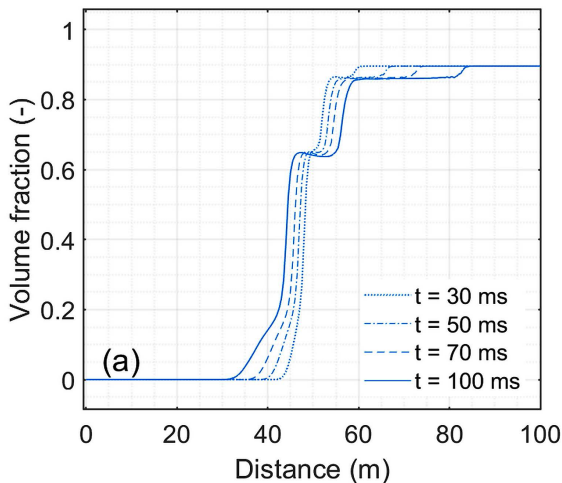


Figure 4: The behavior of vapor volume fraction (a), mixture density (b), and mixture internal energy (c) along the pipe's length during various time intervals and for 1000 grid cells.

The velocity profile in Figure 4 (b) demonstrates the two-phase mixture movement along the pipe towards the vented end. At the same time, the velocity peak increases while it moves in the reverse direction. However, the pressure wave behavior affects the two-phase mixture velocity after the evaporation starts due to the expansion waves' sequence propagation with different speeds (see Figure 4 (b) and Figure 2 (b)).

Figure 4 (c) shows that the mixture's internal energy rises in the metastable state following the rarefaction wave. This trend could be attributed to the liquid state transition from saturated to superheated, whereby the liquid stores the gained energy during its expansion as long as it remains in the metastable state. Then the energy is released during the phase change process providing the required latent heat of vaporization.

#### 4. Conclusions

A homogeneous equilibrium model (HEM) for two-phase flow during CO<sub>2</sub> depressurization in a pipe has been developed. The model considers equilibrium in pressure, temperature, and chemical potential, using SW EOS to calculate fluid properties in different thermodynamic states. Additionally, the method integrates two numerical schemes to use the CU-WENO scheme, wherein the numerical flux is calculated from central-upwind flux and the cell interface values from the third-order WENO reconstruction. The aim is to fit the central-upwind features in the WENO scheme, which can enhance accuracy and stability. The model is able to trace the

pressure, two-phase mixture density, and vapor volume fraction patterns during the rapid phase transition. In addition, the simulation results demonstrate the model's ability to predict the rarefaction and evaporation waves' dynamic characteristics and the convergence of the CU-WENO scheme. The numerical method well captured the moving discontinuity without blurs, and they have a similar pattern as in works done, for instance, by Munkejord et al. (2010) and Morin et al. (2010). However, the CU-WENO scheme illustrated the shock and expansion waves with less sharp edge transitions compared to the mentioned studies.

It is important to mention that the presented model does not consider the slip between phases during the compression and describes it as a uniform mixture pattern inside the pipe. However, the pipe rupture could result in a stratified flow pattern whereby the phase slip velocities should be considered. Additionally, the choice of initial pressure is dictated by the depressurization model's characteristics, as good predictions have been achieved close to the critical point. Further study may consider the mentioned remarks in developing pipe CO<sub>2</sub> accidental release models.

## References

- Aursand E. *et al.* (2016) 'Fracture propagation control in CO<sub>2</sub> pipelines: Validation of a coupled fluid-structure model', *Engineering Structures*, vol. 123, pp. 192-212, doi: 10.1016/j.engstruct.2016.05.012.
- Botros K. *et al.* (2015) 'Measurements of Decompression Wave Speed in Pure Carbon Dioxide and Comparison With Predictions by Equation of State' *Journal of Pressure Vessel Technology*, vol. 138, no. 3, doi: 10.1115/1.4031941.
- Brown S. *et al.* (2013) 'A homogeneous relaxation flow model for the full bore rupture of dense phase CO<sub>2</sub> pipelines', *International Journal of Greenhouse Gas Control*, vol. 17, pp. 349-356, doi: 10.1016/j.ijggc.2013.05.020.
- Elshahomi A *et al.* (2015) 'Decompression wave speed in CO<sub>2</sub> mixtures: CFD modelling with the GERG-2008 equation of state', *Applied Energy*, vol. 140, pp. 20-32, doi: 10.1016/j.apenergy.2014.11.054.
- Gottlieb S. and Shu C.W. (1998) 'Total variation diminishing Runge-Kutta schemes' *Mathematics of Computation*, vol. 67, no. 221, pp. 73-85, doi: 10.1090/S0025-5718-98-00913-2.
- Kurganov A., Noelle S., and Petrova G.(2001) 'Semidiscrete Central-Upwind Schemes for Hyperbolic Conservation Laws and Hamilton--Jacobi Equations SIAM' *Journal on Scientific Computing*, vol. 23, no. 3, pp. 707-740, doi: 10.1137/S1064827500373413.
- Mjaavatten A. (2022) 'thermodynamic models and tools for H<sub>2</sub>O, H<sub>2</sub>, CO<sub>2</sub>, and Air', <https://github.com/aremj/thermodynamics/releases/tag/v2.1>, GitHub.
- Morin A. *et al.* (2010) 'Numerical Resolution of CO<sub>2</sub> Transport Dynamics', *Proceedings of the 2009 SIAM Conference on "Mathematics for Industry" The Art of Mathematics for Industry (MI)*, doi:10.1137/1.9781611973303.13
- Munkejord S. *et al.* (2010) 'Thermo- and fluid-dynamical modelling of two-phase multi-component carbon dioxide mixtures' *International Journal of Greenhouse Gas Control*, vol. 4, no. 4, pp. 589-596, doi: 10.1016/j.ijggc.2010.02.003.
- Munkejord S. T. and Hammer M. (2015) 'Depressurization of CO<sub>2</sub>-rich mixtures in pipes: Two-phase flow modelling and comparison with experiments' *International Journal of Greenhouse Gas Control*, vol. 37, pp. 398-411, doi: 10.1016/j.ijggc.2015.03.029.
- Shu C.-W. and Osher S. (1988) 'Efficient implementation of essentially non-oscillatory shock-capturing schemes' *Journal of Computational Physics*, vol. 77, no. 2, pp. 439-471, doi: 10.1016/0021-9991(88)90177-5.
- Welahettige P. *et al.* (2022) 'Development of central-upwind-WENO scheme for two-phase 1-D drift flux model in pipe flow', Submitted to the 63<sup>rd</sup> Conference on Simulation and Modelling (63<sup>rd</sup> SIMS),.

## Proceeding A

**Expansion waves behavior during liquified CO<sub>2</sub> depressurization in a divergent cross-section vessel.**

An extended abstract in the Proceedings of the 28<sup>th</sup> International Colloquium on the Dynamics of Explosions and Reactive Systems (ICDERS), Napoli, Italy, June 2022.

# Expansion Waves Behaviour during Liquefied CO<sub>2</sub> Depressurization in a Divergent Cross-Section Vessel

Osama M Ibrahim, Per Morten Hansen, Dag Bjerketvedt, Knut Vågsæther  
University of South-Eastern Norway  
Porsgrunn, Telemark, Norway

## 1 Abstract

Recent developments in carbon capture and storage have led to an increased concern about the safety of CO<sub>2</sub> transport systems. Hazards that arise from the accidental release of liquid CO<sub>2</sub> during its transportation include rapid phase change with explosive evaporation and expansion. Therefore, it is essential to research the mechanisms and the dynamics affecting these process developments. The presented work investigates the phase transition mechanisms occurring during liquefied CO<sub>2</sub> depressurization from a double-membrane installation with a high-pressure conical vessel. It provides experimental results and analysis describing the effect of the divergent cross-section and liquid volume fraction on expansion wave behavior. Results indicate a considerable pressure increase at the vessel's bottom after the evaporation wave has passed due to the over-expansion effect. Its peak values were proportional to the increase in liquid volume fraction (LVF). Besides, the rarefaction wave velocities were nearly constant in all vessel height regions. In contrast, they were varied for evaporation wavefront. Velocities increased as the evaporation wave propagated towards a constantly reducing cross-section area.

## 2 Introduction

Transport and storage of liquefied CO<sub>2</sub> involve serious hazards associated with pressure container malfunction due to different detrimental situations such as heating, a projectile hit, or corrosion [1, 2]. The catastrophic container failure due to explosive evaporation proceeded from rapid decompression of a liquefied gas which, in certain conditions, may characterize as boiling liquid expanding vapor explosion (BLEVE) [3]. If the pressure of a pure liquefied substance decreases below its saturation pressure, it potentially develops into a superheated or metastable liquid. This state encompasses the region between the liquid saturation and spinodal curves. The phase transition occurs when the liquid approaches or surpasses its superheat limit temperature (SLT). The depressurization rate controls the degree of superheat. When it is low, heterogeneous nucleation develops at the container's surface or liquid's impurities. Consequently, the possibility for severe explosion is dwindled.

According to Reid [4], a BLEVE occurs once the liquid expands to its SLT, and the phase change is governed by homogeneous nucleation. However, Zhang et al. [5] pointed out that BLEVE may be developed without the liquid temperature exceeding its SLT. They also mentioned that explosive



evaporation could be promoted due to the formation of solid-phase nuclei as liquid CO<sub>2</sub> pressure falls rapidly to the atmospheric pressure. During CO<sub>2</sub> depressurization in a vertical vessel, the phase transition occurs in a narrow zone symbolizing the evaporation wavefront. It moves into metastable liquid downwards, and its propagation is strictly dependent upon the degree of superheat.

Several experimental studies have examined the dynamics influencing evaporation wave's emergence and propagation during decompression of different liquified substances. Das et al. [6], Hill [7], and Reinke et al. [8] are among the studies that have observed the evaporation wave and measured its front velocity. The research group for process safety, combustion, and explosion laboratory at the University of South-Eastern Norway, for many years, investigated liquid CO<sub>2</sub> depressurization. Small-scale experiments on BLEVE have been conducted on cylindrical test tubes by Bjerketvedt et al. [9] and Wei Ke [10]. Tosse et al. [11] and Hansen et al. [12] have analyzed the development of the evaporation wave intensively during liquified CO<sub>2</sub> depressurization. Most of the stated research described an evaporation wave propagating with almost steady velocity. However, the mentioned studies and most experimental research on liquified gas depressurization have been performed in constant-area ducts or tubes. Therefore, this small-scale experimental study aims to provide results and analysis of rarefaction and evaporation wave features during liquified CO<sub>2</sub> decompression in a conical-shaped vessel. It focuses on the effect of divergent cross-section on expansion waves behaviour and determination of their velocities.

### 3 Experimental configuration and procedure

A stainless steel (AISI 316) vertical conical-shaped vessel and two slip-on flanges constituted the central assembly parts of a double-diaphragm installation. These components are reinforced on an aluminum structure and opened to an atmospherically vented chamber. The vessel has a volume of  $480 \cdot 10^3 \text{ mm}^3$  and each of the flanges' cylinder volumes is  $510 \cdot 10^3 \text{ mm}^3$ . The high-pressure reservoir (the conical vessel) was filled with liquid CO<sub>2</sub>, whereas the medium-pressure MP section (mid flange) with vapor. Industrial-grade liquid and gaseous cylinders were independently provided CO<sub>2</sub> to HP and MP sections. A high-pressure HP diaphragm was pressed between the high-pressure reservoir and the medium-pressure MP section. A second diaphragm separated the MP section from the upper flange and opened to chamber pressure. The initial pre-ruptured condition in the HP vessel was 5.2-5.8 MPa, while it was 2.6-2.9 MPa in the MP section. The temperature was ambient in all sections. Figure 1 shows the setup components and a close-up image of the conical vessel and slip-on flanges fixed above it.

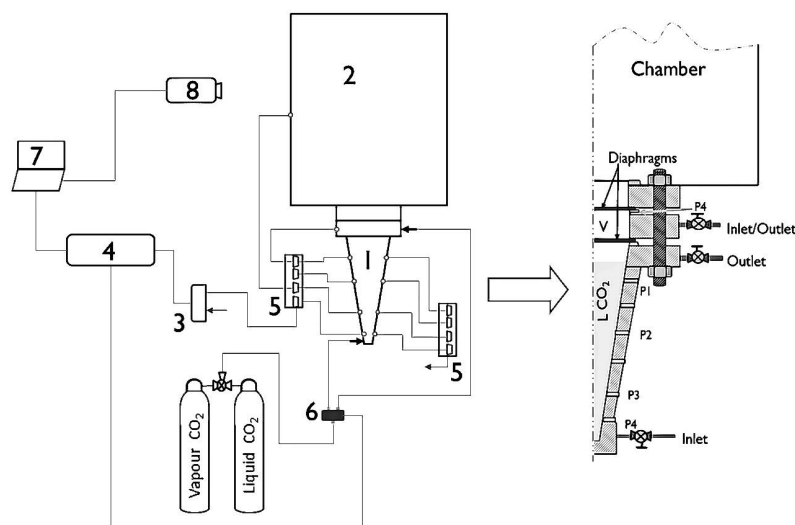


Figure 1: Schematic drawing of the experimental setup: 1. conical vessel, 2. chamber space, 3. hub, 4. Triggering unit, 5. data acquisition system, 6. 3-way valve, 7. PC, 8. Photron camera. An enlarged segment of the conical vessel and flanges on the right-hand side.

A Quantum composers 9500 series pulse generator initiated the experiments by triggering a three-way valve to increase the pressure in the MP section. As a result, the MP diaphragm ruptured, and the MP section's pressure fell to atmospheric in milliseconds. Subsequently, the HP diaphragm burst due to the grown pressure difference between its sides. Pressure and temperature histories during the expansion inside the vessel were recorded with Pressure sensors Kulite XTM-190-2000G (P1-P4) and k-type thermocouples (T1-T3 ). Besides, a pressure sensor P5 of the same type was attached to the MP section. One Kulite XTM-190-100G sensor was attached in the middle of the chamber. Besides, a high-speed camera (Photron Fastcam SA-1) captured the evolution of the released multi-phase mixture through the chamber's transparent polycarbonate walls.

## 4 Results and Discussion

A series of experiments were performed with different liquid volume fractions (LVF): 0, 35, 52, and 73%. Diaphragm thickness for the set separating HP vessel from MP flange was 1.6 mm, and the set pressed between flanges was 1.5 mm. The pre-ruptured state in the vessel was saturated  $\text{CO}_2$  at the temperature range of 19-21 °C. Figure 2 illustrates 65 ms of pressure histories inside the conical vessel (a), in the MP section (b), and overpressure in the chamber (c) during the depressurization of 73% LVF  $\text{CO}_2$ .

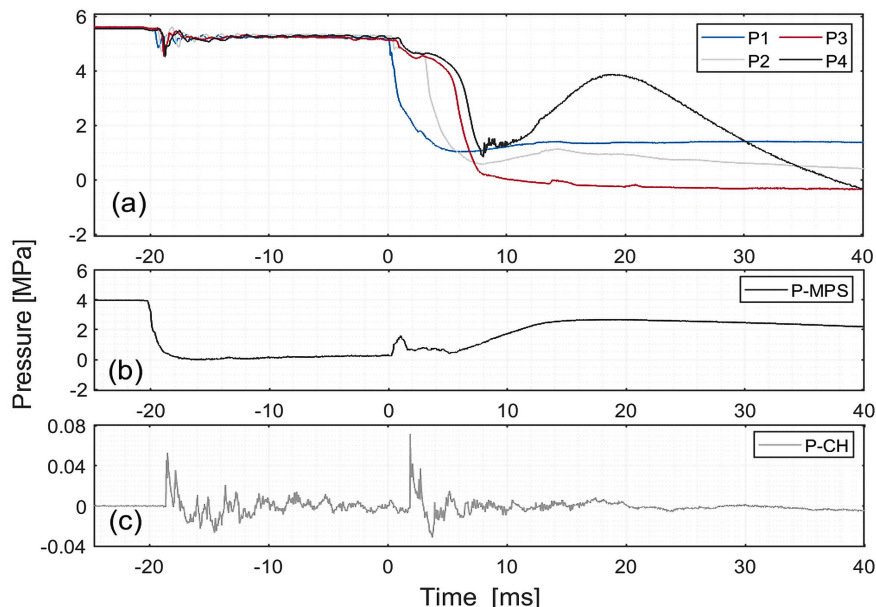


Figure 2: Pressure records during 65 ms of  $\text{CO}_2$  depressurization in a conical vessel for 73% LVF, (a) inside the vessel, (b) in the MP section, and (c) overpressure in the chamber space.

A shock wave has arisen due to the MP diaphragm rupturing and proceeding upwards in the chamber space. Wherein the recorded overpressure was 0.051 MPa. While a rarefaction wave moved downwards, it hit the HP diaphragm and reflected into the chamber. After the MP diaphragm has ruptured, about 20 ms was required for the HP diaphragm to destabilize. Meanwhile, the diaphragm underwent bulging and cracks due to increased pressure difference and the waves hitting its surface. When it burst, a second shock wave initiated and traveled upwards. It passed through the MP section, raising the pressure to about 1.6 MPa. Besides, the recorded overpressure in the chamber was 0.072 MPa. The shock wave was followed by the contact surface that primarily divided vapor and liquid. Simultaneously, a rarefaction wave propagated downwards through the vapor headspace and the liquid. As a result, the liquified  $\text{CO}_2$  went through isentropic expansion. The phase transition ensued during the passage of the evaporation wave behind the rarefaction wave towards the vessel's bottom. Figure 3 presents the pressure histories inside the vessel during 30 ms of  $\text{CO}_2$  decompression for different LVFs (0, 35, and

52%). Time 0 indicates the HP diaphragm rupture. The first steep pressure drop corresponds to the rarefaction wave traveling through the liquid. Subsequently, the CO<sub>2</sub> liquid became superheated.

The pressure lines in the metastable state fluctuated slightly and nearly plateaued. Metastable state duration depended on the LVF. It varied from about 4.1ms for 35% to 4.7 ms for 73% LVF.

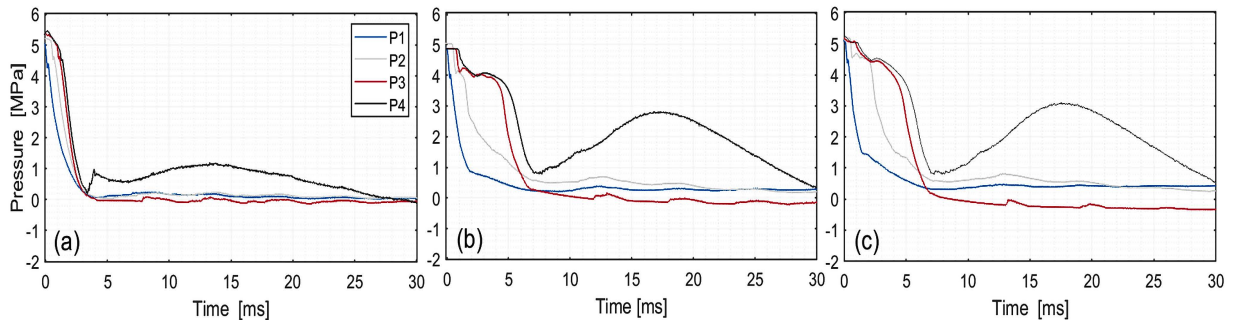


Figure 3: Pressure-time diagrams of CO<sub>2</sub> depressurization in the HP vessel for LVFs 0, 35, and 52% in (a), (b), and (c), respectively.

Figures 2 (a) and 3 show that the bottom sensor P4 has distinctive reading lines with pressure rise after reaching about 1 MPa. Then it started rising along with an onset fluctuation. It peaked and then dropped to atmospheric pressure. Figure 4 compares P4 readings for the above-indicated LVFs. The pressure peak value increased with the LVF, so it was around 1.2, 2.8, 3.1, and 3.9 MPa for 0, 35, 52, and 73%, respectively. The observed fluctuation on P4 lines is due to the reflection of the expansion wave on the vessel's bottom. It also intensified with increasing LVF, as shown in Figure 4.

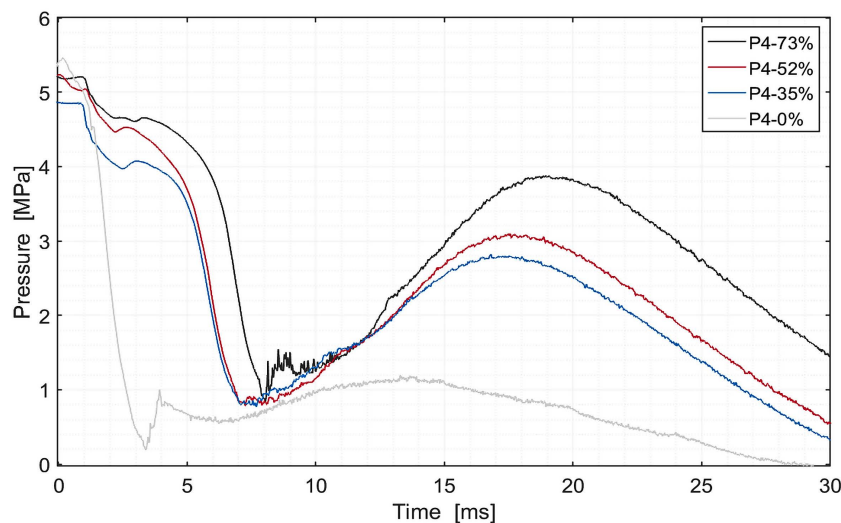


Figure 4: comparison of pressure transducer P4 recordings during 30 ms of CO<sub>2</sub> depressurization in the conical vessel for LVFs 0, 35, 52, and 73%.

The pressure surge in P4 signifies a dramatic phenomenon resulting from the potential consequence of over-expansion. After the evaporation wave had rapidly passed through and the pressure fell to about 1 MPa, the formed two-phase mixture moved upwards. Then, a heavier part of this mixture was drawn back towards the bottom with high velocity due to low pressure. While its movement decayed at the vessel's bottom, the pressure rose again. As the pressure increased, reaching its peak and falling to atmospheric, the expanded two-phase mixture flowed toward the vessel's exit.

The expansion wave velocities were determined graphically by analyzing the pressure records along the length between sensors' positions (zones P1-P2, P2-P3, and P3-P4). For this purpose, The pressure

readings were illustrated on the height-time diagram, as shown in Figure 5. The rarefaction and evaporation waves' path went through the sites where the pressure sharply decreased. The exact time turning points were defined by drawing tangent lines on both sides of the turning curves. Then, connecting the tangent lines' junction to the mid-point on the line passed through the tangency points. The locus of intersection of these connecting lines with the pressure curves demonstrated the time turning points at which pressures change.

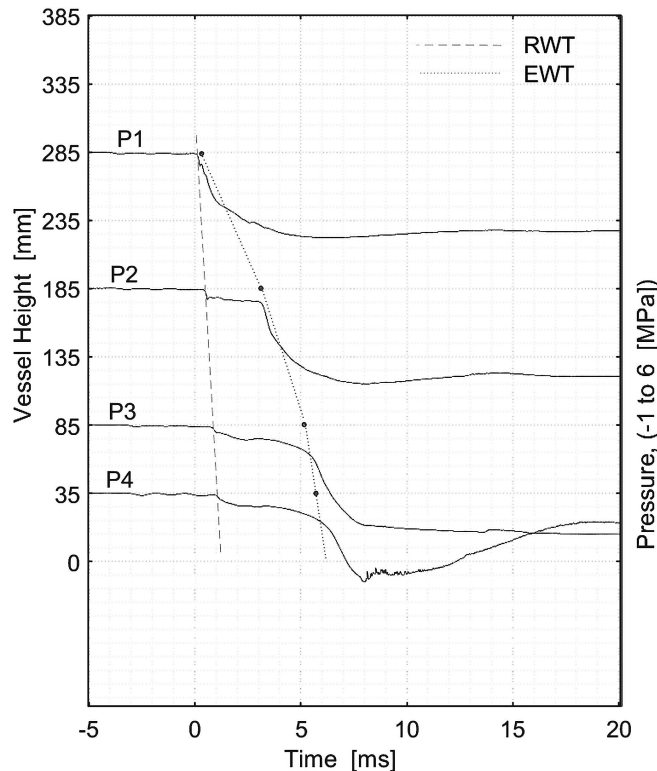


Figure 5: Synchronized pressure transducer recordings plotted on vessel's height axis during 25 ms of CO<sub>2</sub> depressurization in the conical vessel for 73% LVF. The diagram illustrates wave trajectories of rarefaction (RWT) and evaporation (EWT).

Results from calculated rarefaction wave velocities have slightly differed in the various height zones. So, the average rarefaction wave velocities were 246.7, 271.7, and 293.3 ms<sup>-1</sup> for the LVFs 35, 52, and 73%, respectively. However, the evaporation wave velocities varied along the three vessel's regions. For the LVFs 35, 52, and 73%, the corresponding calculated wavefront velocities in the region P3-P4 were about 89, 92.6, and 106.8 ms<sup>-1</sup>. There were about 37.8, 56, and 73 ms<sup>-1</sup> in the region P2-P3. The wavefront velocity for 73% VLF in zone P1-P2 was 36.8 ms<sup>-1</sup>. The presented numbers signify that the rarefaction waves propagated inside the vessel with nearly constant speed. However, differing from the previously mentioned studies, the evaporation wavefront swiftness increased as it propagated downwards. This trend implies that the wavefront speeded up as the vessel's cross-section area diminished. In addition, it decreased with LVF reduction. The highest evaporation wavefront velocities were in the region close to the vessel's bottom (zone P3-P4) and for LVF of 73%. The observed trend of the pressure at the vessel's bottom is different from the results of the previous experiments conducted in ducts with a constant cross-sectional area, for instance, in experimental studies by Ciccarelli et al. [13], Reinke [14], Chaves [15], and Hansen et al. [12]. This difference could be attributed to the nearly steady evaporation wave velocity in constant cross-section ducts. In contrast, the velocity increased as the cross-sectional area decreased in the conical-shaped vessel. Simultaneously, the subsequent expanded two-phase mixture propagated towards a regularly increasing cross-sectional area.

## 5 Conclusion

The small-scale experimental investigation of the expansion waves during CO<sub>2</sub> decompression in a conical vessel has shown that the rarefaction wave velocities were nearly constant over the vessel's height for various LVFs. While the evaporation wavefront velocities increased as it propagated toward the vessel's bottom with reducing cross-section area and LVF. One of the more significant findings from this study is the pressure rise after the evaporation wave reached the vessel's bottom. This occurrence arose from the over-expansion effect when the pressure at the bottom fell sharply, and subsequently, the downstream two-phase mixture was drawn down. After its inertia at the vessel's bottom, the pressure rose gradually, and the two-phase mixture propagated upwards to the vessel exit.

## References

- [1] Abbasi T, Abbasi SA (2007). The boiling liquid expanding vapour explosion (BLEVE): Mechanism, consequence assessment, management. *Journal of hazardous materials*. 141: 489-519.
- [2] Heymes F, Aprin L, Birk AM, Slangen P, Jarry JB, François H, Dusserre G (2013). An experimental study of an LPG tank at low filling level heated by a remote wall fire. *Journal of Loss Prevention in The Process Industries*. 26:1484-91,.
- [3] Birk AM, Heymes F, Eyssette R, Lauret P, Aprin L, Slangen P (2018). Near-field BLEVE overpressure effects: The shock start model. *Process Safety and Environmental Protection*. 116:727-736.
- [4] Reid RC (1979). Possible Mechanism for Pressurized-Liquid Tank Explosions or BLEVE's. *Science*. 203:1263-5.
- [5] Zhang Y, Schork J, Ludwig K (2013). Revisiting the conditions for a CO<sub>2</sub> tank explosion. Proc. 9<sup>th</sup> G. C. on Process Safety. AIChE. San Antonio, Texas.
- [6] Das PK, Bhat GS, Arakeri VH (1987). Investigations on the propagation of free surface boiling in a vertical superheated liquid column. *International Journal of Heat and Mass Transfer* 30(4):631-38.
- [7] Hill LG (1991). An experimental study of evaporation waves in a superheated liquid. PhD Th. California Institute of Technology. Pasadena, California.
- [8] Reinke P, Yadigaroglu G (2001). Explosive vaporization of superheated liquids by boiling fronts. *International Journal of Multiphase Flow*. 27:1487-1516.
- [9] Bjerketvedt D, Egeberg K, Ke W, Gaathaug A, Vaagsaether K, Nilsen SH (2011). Boiling liquid expanding vapour explosion in CO<sub>2</sub> small scale experiments. *Energy Procedia*. 4: 2285-92.
- [10] Ke W (2009). CO<sub>2</sub> BLEVE (Boiling Liquid Expanding Vapor Explosion). M.Sc thesis Telemark University College. Norway.
- [11] Tosse S, Vaagsaether K, Bjerketvedt D (2015). An experimental investigation of rapid boiling of CO<sub>2</sub>. *Shock Waves*. 25(3):277-82.
- [12] Hansen PM (2018). Experimental and theoretical studies of rapid phase transitions in carbon dioxide. PhD Th. 13. Process, Energy and Automation Engineering, University of South-Eastern Norway. Porsgrunn, Norway.
- [13] Ciccarelli G., Melguizo-Gavilanes J., Shepherd J. E. (2015). Pressure field produced by the rapid vaporization of a CO<sub>2</sub> liquid column. 30th International Symposium on Shock Waves, Tel-Aviv, Israel.
- [14] Reinke P. (1997). Surface boiling of superheated liquid. PhD Th. Paul Scherrer Inst. (PSI). Villigen, Switzerland.
- [15] Chaves H. (1984). Changes of phase and waves on depressurization of liquids with high specific heat, PhD Th. Max-Planck-Institut für Strömungsforschung. Göttingen, Germany.

## Proceeding B

### **Modeling the effect of phase transition on the blast wave in BLEVEs.**

An extended abstract, under review, submitted to the 29<sup>th</sup> International Colloquium on the Dynamics of Explosions and Reactive Systems (ICDERS), SNU Siheung, KOREA, July 2023.



# Modelling the effect of phase transition on the blast wave in BLEVEs

Knut Vaagsaether, Osama Kabbashi Mohammed Ibrahim, Per Morten Hansen, Dag Bjerketvedt  
University of South-Eastern Norway  
Porsgrunn, Norway

## 1 Introduction

The main interest in this work is the rapid expansion of fluid due to phase transition that will contribute to a blast wave in a BLEVE scenario. The study uses saturated liquid CO<sub>2</sub> as a medium. The use of carbon dioxide as a medium is a practical one since it is relatively safer to use in experiments than other liquefied gasses like propane or ammonia. The downside of using CO<sub>2</sub> is that the fluid will cross the triple point during depressurization, leading to solid/gas two-phase flow at lower pressures. However, in the present work, this process is assumed slow and is not included since it is doubtful that it will impact the blast wave caused by the initial fast phase transition. Figure 1 shows the isentropic expansion path of liquid CO<sub>2</sub> into the metastable region. The kinetic spinodals are limits for expansion where a significant generation rate of critical bubbles is reached. The kinetic spinodal for heterogeneous nucleation assumes that the critical work to generate bubbles in the liquid is half the critical work for the bulk. The thermodynamic states are calculated by using an equation of state (EOS) based on Helmholtz free energy [1] and [2].

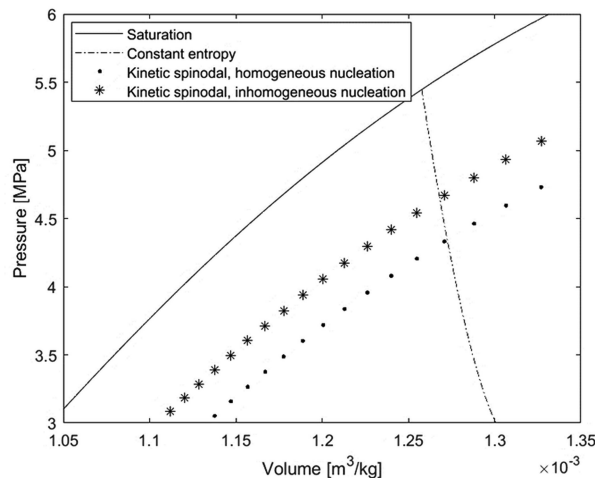


Figure 1: Pressure-volume diagram for CO<sub>2</sub> showing an isentropic expansion path from saturated liquid at 291 K and the kinetic spinodals for homogeneous and inhomogeneous nucleation.



## 2 Method

The present simulation method is based on Classical Nucleation Theory [3] and uses the production rate of critical bubbles as a source in a two-fluid multiphase equation set. The most important equations from the Classical Nucleation Theory are included here for completeness.

The rate of creation of a number of critical size bubbles pr. volume is calculated as equation 1.

$$dJ = J_0 \exp\left(-\frac{W_{cr}}{kT_0}\right), \quad (1)$$

The critical work is here simplified to eq. 2 by assuming the Poynting factor to be unity.

$$W_{cr} = \frac{16\pi\sigma^3}{3(p_{sat}(T)-p(T))^2}, \quad (2)$$

Where  $J_0$  – initial possible nucleation sites,  $k$  – Boltzmann constant,  $T_0$  – critical temperature,  $\sigma$  – liquid/gas surface tension.

The critical work needed during the inhomogeneous nucleation at the wall is assumed to be half of the critical work in the bulk. This reduction in critical work will be dependent on surface roughness, and the value of 0.5 assumes a 90° contact angle between droplet and wall.

### 2.1 Computational Fluid Dynamics

A two-fluid model for CFD simulations of the process uses mass, momentum, and energy conservation of two immiscible fluids (liquid and gas phases) [4]. One assumption in using this model is that the momentum of each phase is given by a common velocity, leading to a six-equation model in 2D. Equations 3 and 4 are equations for mass conservation of the two phases, equation 5 is the equation for the common momentum, and equations 6 and 7 are the energy equations for each phase.

$$\frac{\partial \rho_1 \alpha_1}{\partial t} + \nabla \cdot (\rho_1 \alpha_1 \vec{u}) = -\dot{R}, \quad (3)$$

$$\frac{\partial \rho_2 \alpha_2}{\partial t} + \nabla \cdot (\rho_2 \alpha_2 \vec{u}) = \dot{R}, \quad (4)$$

$$\frac{\partial \rho u_i}{\partial t} + \nabla \cdot (\rho \vec{u} u_i) + \frac{\partial p}{\partial x_i} = 0, \quad (5)$$

$$\frac{\partial \alpha_1 E_1}{\partial t} + \nabla \cdot (\alpha_1 \vec{u} (E_1 + p)) = -\dot{R} Q_{vap}, \quad (6)$$

$$\frac{\partial \alpha_2 E_2}{\partial t} + \nabla \cdot (\alpha_2 \vec{u} (E_2 + p)) = \dot{R} Q_{vap}, \quad (7)$$

Where  $\alpha_1$  is the volume fraction of liquid and  $\alpha_2$  is the volume fraction of the gas. The volume fractions are related as  $\alpha_1 + \alpha_2 = 1$  and  $\rho_1 \alpha_1 + \rho_2 \alpha_2 = \rho$ . The energies of each phase are calculated as equation 8.

And,  $p$  – pressure,  $u$  – fluid velocity,  $\rho$  – fluid density,  $Q_{vap}$  – the heat of evaporation.

$$E_i = e_i + \frac{1}{2} \rho_i |\vec{u}|^2, \quad (8)$$

For the liquid phase, a stiffened gas equation of state is used to model the dependence of internal energy to pressure (see equation 9).

$$e_1 = \frac{p + \gamma_1 p_\infty}{\gamma_1 - 1}, \quad (9)$$

Ideal gas law is used for the gas phase (phase 2), equation 10.

$$e_2 = \frac{p}{\gamma_2 - 1} + e^*, \quad (10)$$

The constant  $e^*$  is an energy term to set the correct difference in internal energy between the gas and liquid phase. Since the modelled internal energy is based on changes in internal energy, this term must be added to model the correct change of energy between the phases. The Flux Limiter Centered Scheme (FLIC) is used to solve the equations' hyperbolic parts, while a Newton-Raphson iterative solver is needed to isolate volume fraction and pressure from the conserved mass and energies.

The phase transition mass rate,  $\dot{R}$  in equation 11, is modeled using the nucleation rate in eq. 1.

$$\dot{R} = \rho_{g,sat}(T)V_{cr}dJ, \quad (11)$$

Where  $V_{cr}$  is the volume of a critical bubble and  $\rho_{sat}$  is the gas density of the critical bubbles. The radius of a critical bubble is calculated as equation 12.

$$r_{cr} = \frac{2\sigma}{p_{sat}(T) - p}, \quad (12)$$

The mass and energy sources are solved using Godunov splitting so that the hyperbolic part is solved using the FLIC scheme, and the sources are solved by a simple first-order Euler method. Table 1 shows the model constants used in the present work. The constants are obtained by fitting the internal energy and sound speed from the model to values from the Helmholtz free energy-based EOS along a constant entropy process from saturated liquid at 291 K into the metastable region. The choice of the fitting region is small but relevant for the expansion process of the liquid before the onset of nucleation.

Table 1: Model constants for CO<sub>2</sub>

Variable	Value
$\gamma_1$	1.066
$\gamma_2$	1.32
$p_\infty$	$7.3 \cdot 10^7$ Pa
$e^*$	$1.62 \cdot 10^6$ J/kg
$\sigma$	$2.0 \cdot 10^{-3}$ N/m
$Q_{vap}$	$1.8 \cdot 10^5$ J/kg

The experiments used as validation data have been published [5], but a short description is provided here. Figure 2 shows the experimental setup where saturated liquid CO<sub>2</sub>, with a saturated vapor head, is filled into a conical vessel. A double membrane release system is placed on top of the conical vessel. The double membrane system separates the high-pressure, conical vessel from the surroundings by two membranes, where the volume between the membranes will have a medium pressure of CO<sub>2</sub> before rupture. The rupture procedure is done by increasing the pressure in the separating volume up until the top membrane ruptures. The subsequent pressure drop leads to the rupture of the lower membrane initiating the depressurization of the CO<sub>2</sub> in the conical vessel. The conical vessel has an angle of 4° to the center axis and is ID 90 mm at the top. A polycarbonate pipe of ID 90 mm is fitted above the membrane system to be able to measure the blast wave from the depressurization of the fluid.

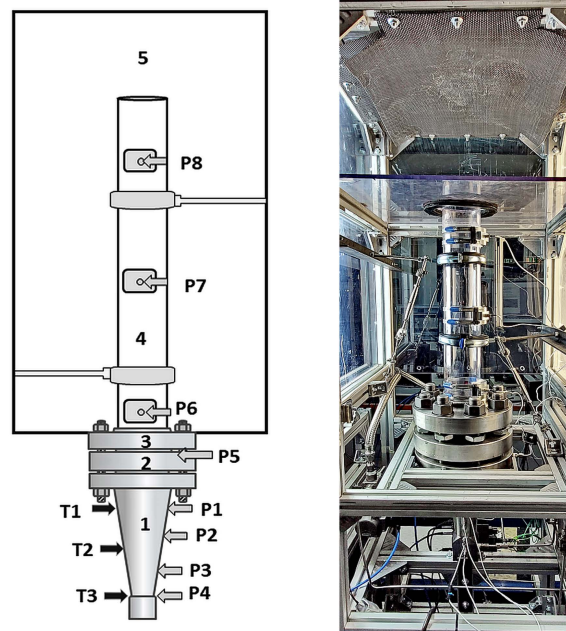


Figure 2: Schematic drawing of the setup on the left-hand side: 1- HP conical vessel, 2- MP slip-on flange, 3- upper flange opened to atmospheric pressure, 4- polycarbonate tube, 5- chamber. An image of the installation is on the right-hand side.

### 3 Results and discussion

The simulations were done in 2D axis symmetry, where the center axis of the geometry follows the conical vessel's center axis. The simulation also includes the rupture of the top diaphragm before the depressurization of the conical vessel is initiated. The timing of the rupture of the bottom diaphragm will be off in the simulation compared to the experiments since the response time of the material will not be simulated. The rupture of the top diaphragm and subsequent blast from the compressed CO<sub>2</sub> in the medium pressure volume will be seen as a shock wave propagating through the polycarbonate pipe. Figure 3 shows the pressure history of pressure sensor P2 located 185 mm from the "bottom" of the conical vessel for 35 and 73 % liquid volume fraction. The sensor is initially in the liquid phase. The first pressure drop after about 3 ms is the first rarefaction wave due to the sudden opening of the diaphragm. The state behind the rarefaction wave will be metastable liquid as the pressure is held at the kinetic spinodal pressure due to the pressure increase of the phase transition. A phase transition front follows the rarefaction wave as is seen as a sudden pressure drop at about 5-6 ms. The timing of the simulated phase transition front compared to the experimental results is somewhat delayed. The simulations will behave very ideally compared to an experiment as no stresses in the fluid, except from pressure, are simulated. The assumption of lower critical work at the wall by a factor of two is also not justified here. This factor may be significantly higher due to wall surface roughness, and further work is needed to determine this effect. The linear equations of state used in the simulations will lead to erroneous speeds of sound and fluid expansion in the metastable region as the compressibility will be handled as an ideal gas.

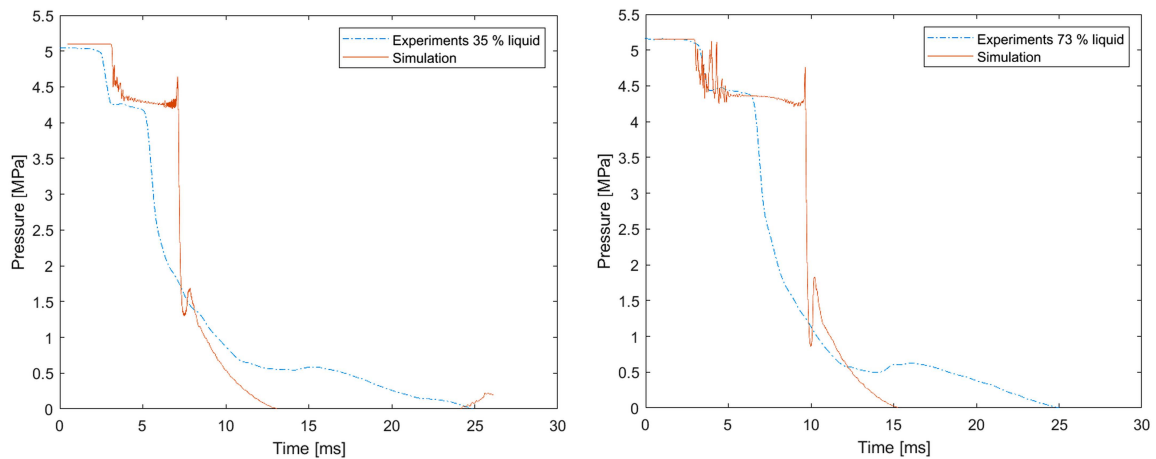


Figure 3: Experimental and simulated pressure history at pressure sensor P2 located 185 mm from the "bottom" of the cone. Left: 35 % liquid volume fraction in the vessel. Right: 73 % liquid volume fraction in the vessel.

Figure 4 (P6) and 5 (P8) shows the experimental and simulated blast waves propagating in the polycarbonate pipe. The activation of the double membrane is done by increasing the pressure in the medium pressure volume up until the rupture of the top membrane. The blast wave from this initiation is seen as a pressure peak at about -115 ms in Figure YX (Left) and -15 ms in (Right). The initiation is also included in the simulation, but the time delay is not simulated. The pressure peak from the simulated initiation is seen at about 0 ms for both liquid volume fractions. The reason for including the initiation was to ensure that the polycarbonate pipe had expanded CO<sub>2</sub> in it since this will influence the blast wave propagation. The simulated blast from the conical vessel with a liquid volume fraction of 35 % is closer to the experimental results than for 73 %. The blast wave for the 35 % case is dominated by the expansion of the vapor head, while for the 73 % case, the phase transition will significantly impact the blast wave. Since the simulated pressure drop over the phase transition front in Figure 3 is much steeper than the experimental one, it might indicate that the simulated phase transition rate is faster, leading to the higher blast pressures seen in the closest pressure transducer (270 mm).

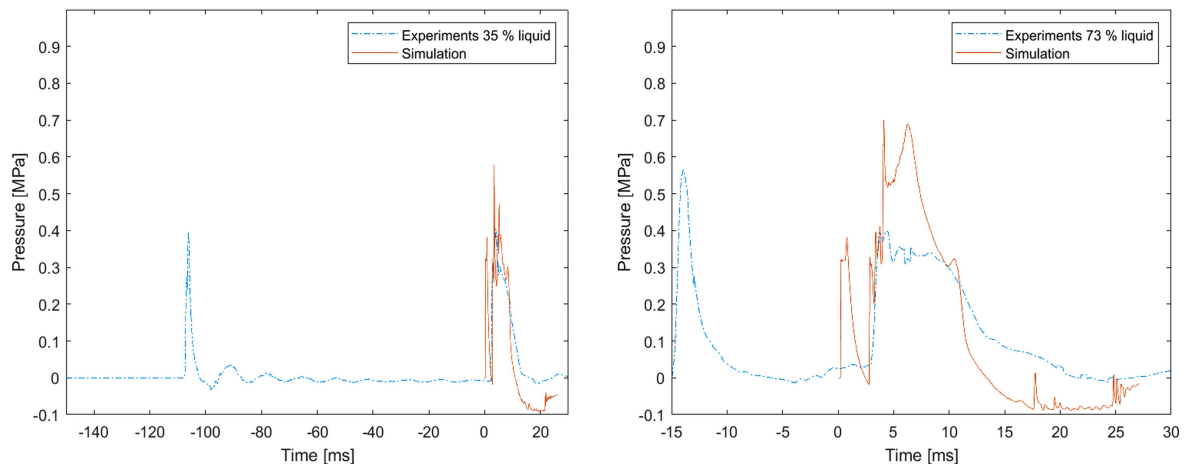


Figure 4: Experimental and simulated pressure history at pressure sensor P6, placed in the polycarbonate pipe at 270 mm above the bottom diaphragm. Left: 35 % liquid volume fraction in the conical vessel. Right: 73 % liquid volume fraction in the conical vessel.

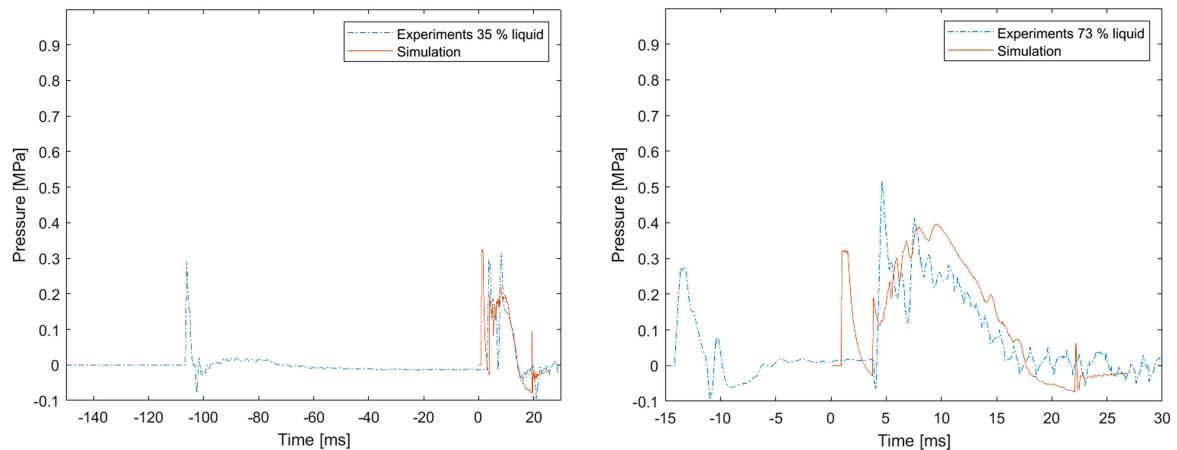


Figure 5: Experimental and simulated pressure history at pressure sensor P8, placed in the polycarbonate pipe at 740 mm above the bottom diaphragm. Left: 35 % liquid volume fraction in the conical vessel. Right: 73 % liquid volume fraction in the conical vessel.

## 4 Conclusion

The proposed simulation method recreates the main features of the fast depressurization that occurs during a BLEVE scenario. The liquid expansion into a metastable state is captured, and the following phase transition rapidly produces gas to generate a blast wave. The simulated blast wave pressure closest to the source is overestimated by the present method due to a too rapid modelled phase transition rate. This overestimation of the phase transition rate is believed to be due to missing dampening effects from the earlier onset of nucleation at the wall.

## References

- [1] Mjaavatten, A. H<sub>2</sub> and CO<sub>2</sub> thermodynamics. <https://www.github.com/are-mj/thermodynamics>
- [2] Span, R. and Wagner, W. A new equation of state for carbon dioxide. *Journal of Physical and Chemical Reference Data*, **25**, 1996, pp. 1509-1596.
- [3] Blander, M. and Katz, J. L. Bubble nucleation in liquids. *AIChE Journal*, **21(5)**, 1975, pp. 833-848.
- [4] Ishii, M. Thermo-fluid dynamic theory of two-phase flow. *Collection de la Direction des Etudes et Recherches d'Electricite de France*, No. **22**, 1975 pp. 275
- [5] Ibrahim, O.M., Hansen, P.M., Bjerketvedt, D., Vaagsaether, K. Blast Wave Overpressures from CO<sub>2</sub> Depressurization in a Conical-Shaped Vessel. *10th International Seminar on Fire and Explosion Hazards*, Oslo, Norway, 2022 pp. 86-94. <https://hdl.handle.net/11250/3030345>





## Errata

1. Page VI, Abstract: "rarefaction, evaporation, and blast wave in the existing setup" should be "rarefaction, evaporation, and blast waves in the existing setup."
2. Page 2, Background: "the fragments which flew approximately 300 meters" should be "the fragments that flew approximately 300 meters".
3. Page 3, Background: "That caused two death casualties and three injured from fragments hit" should be "That caused two death casualties and three injuries from fragments hit."
4. Page 19, Subsection 2.4.2: "The blast strength increases as the evaporated liquid fraction increase." should be "The blast strength increases as the evaporated liquid fraction increases."
5. Page 31, Setup 3.1: "The solid walls HP vessel" should be "the solid walls of the HP vessel."
6. Page 40, Setup 3.2: ". Its cylindrical upper rim was machined as the tube could precisely fit in at a depth of 60 mm." should be "Its cylindrical upper rim was machined so the tube could precisely fit in at a depth of 60 mm."
7. Page 52, Subsection 4.2.2: "The pressure sensor (P1–P4)" should be "The pressure sensors (P1–P4)."
8. Page 76, Section 5.2: "96,4%" should be "96.4%"



**Accidental release of liquid CO<sub>2</sub> from  
transport and storage**

Osama Kabbashi M. Ibrahim

**Doctoral dissertations at the  
University of South-Eastern Norway  
no. 174**

ISBN: 978-82-7206-805-8 (print)  
ISBN: 978-82-7206-806-5 (online)

**usn.no**